

AD-A173 490

PHYSICAL TECHNIQUES FOR THE STUDY OF SORPTION DIFFUSION 1/4

ELECTRICAL PROPER (U) VIRGINIA UNIV CHARLOTTESVILLE

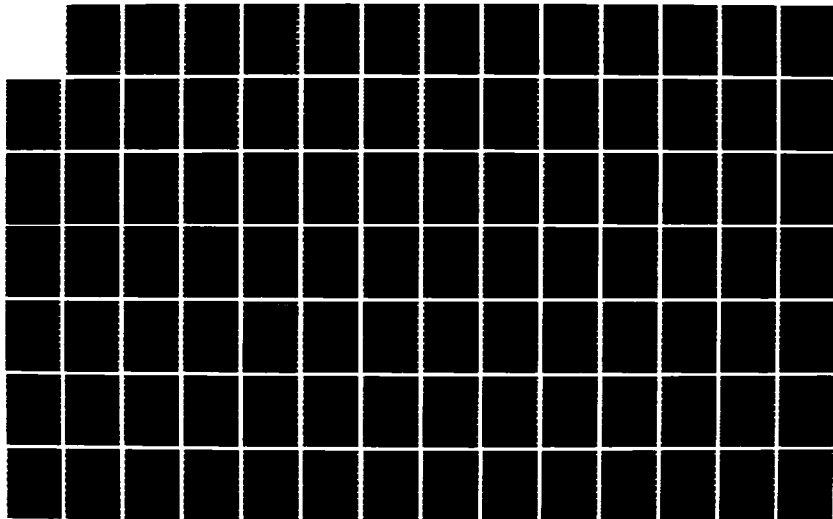
DEPT OF MATERIALS SCIENCE R E BARKER ET AL 26 JUL 86

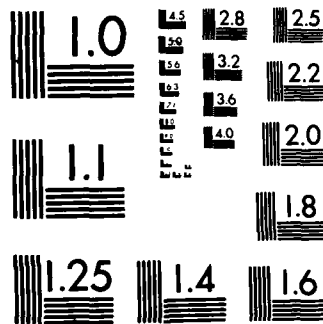
UNCLASSIFIED

UVA/525646/MS87/101 AFOSR-TR-86-0831

F/G 11/9

NL





MICROCOPY RESOLUTION TEST CHART
NATIONAL BUREAU OF STANDARDS-1963-A

AFOSR-TR- 86-0891

AUG 4 1986

Technical Report

Grant No. 82-0290C

PHYSICAL TECHNIQUES FOR THE STUDY OF SORPTION,
DIFFUSION, ELECTRICAL PROPERTIES, AND INTERFACIAL
EFFECTS IN ORDERED POLYMERS: CHARGE TRANSPORT
AND CONDUCTION MECHANISMS IN POLYMER FIBERS

Submitted to:

U. S. Air Force Office of Scientific Research
Bolling Air Force Base
Washington, D. C. 20332-6448

Attention: Dr. Donald R. Ulrich
Building 410 NC

Submitted by:

R. E. Barker, Jr.
Professor

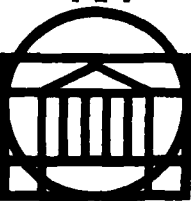
J. A. Hawk
Research Assistant

Report No. UVA/525646/MS87/101
July 1986

This document has been approved
for public release and sale; its
distribution is unlimited.

OCT 23 1986

A



SCHOOL OF ENGINEERING AND
APPLIED SCIENCE

DEPARTMENT OF MATERIALS SCIENCE

UNIVERSITY OF VIRGINIA
CHARLOTTESVILLE, VIRGINIA 22901

DTIC FILE COPY

AD-A173 490

UNCLASSIFIED

SECURITY CLASSIFICATION OF THIS PAGE

AD-A173 490

REPORT DOCUMENTATION PAGE

1a. REPORT SECURITY CLASSIFICATION UNCLASSIFIED			1b. RESTRICTIVE MARKINGS NONE		
2a. SECURITY CLASSIFICATION AUTHORITY			3. DISTRIBUTION/AVAILABILITY OF REPORT Distribution Unlimited		
2b. DECLASSIFICATION/DOWNGRADING SCHEDULE					
4. PERFORMING ORGANIZATION REPORT NUMBER(S) UVA/525646/MS87/101			5. MONITORING ORGANIZATION REPORT NUMBER(S) AFOSR-82- AFOSR-TR. 86-0831		
6a. NAME OF PERFORMING ORGANIZATION University of Virginia Dept. of Materials Science		6b. OFFICE SYMBOL (If applicable) MS/SEAS	7a. NAME OF MONITORING ORGANIZATION U. S. Air Force Office of Scientific Research Air Force Systems Command Directorate of Chemical & Atmospheric Science		
6c. ADDRESS (City, State and ZIP Code) Thornton Hall Charlottesville, VA 22901			7b. ADDRESS (City, State and ZIP Code) ATTN: Dr. D. R. Ulrich Bolling Air Force Base Building 410 NC Washington, D. C. 20332-6448		
8a. NAME OF FUNDING/SPONSORING ORGANIZATION AFOSR See 7a		8b. OFFICE SYMBOL (If applicable) BCAS NC	9. PROCUREMENT INSTRUMENT IDENTIFICATION NUMBER AFOSR-82-0290		
8c. ADDRESS (City, State and ZIP Code) See 7b			10. SOURCE OF FUNDING NOS.		
			PROGRAM ELEMENT NO. 6102F	PROJECT NO. 2303	TASK NO. A3
			WORK UNIT NO.		
11. TITLE (Include Security Classification) Charge Transport in Polymer Fibers (See Block 15)					
12. PERSONAL AUTHOR(S) R. E. Barker/J.A. Hawk					
13a. TYPE OF REPORT Technical Report		13b. TIME COVERED FROM 09/09/84 TO 09/08/85		14. DATE OF REPORT (Yr., Mo., Day) 07/26/86	
15. PAGE COUNT					
16. SUPPLEMENTARY NOTATION The Grant Title was: "Physical Techniques for the Study of Sorption, Diffusion, Electrical Properties, and Interfacial Effects in Ordered Polymers"					
17. COSATI CODES			18. SUBJECT TERMS (Continue on reverse if necessary and identify by block number)		
FIELD	GROUP	SUB. GR.	Ordered Polymers Fibers		
			Conductivity BBL (poly benzimidazo benzophenanthroli		
			Transport Properties PPBT (poly phenylene benzobisthiazole)		
19. ABSTRACT (Continue on reverse if necessary and identify by block number) Electrical conduction in several types of polymer fibers has been investigated under a vareity of environmental conditions. The configuration and circumstances of these experiments are quite different from the ordinary types of measurements reported in the literature dealing with the conductivity of thin films. Methods for separating the surface component of the total conductivity from the volume component are developed and experiments are performed on both doped and undoped samples. Experimental results indicate that the surface is the major region of current flow for some fibers. In this work, special techniques and instrumentation previously utilized by Chen and Barker have been further developed to measure electrical conductivities of small diameter polymer fibers (as small as 10 μ m). The fibers studied included the					
20. DISTRIBUTION/AVAILABILITY OF ABSTRACT UNCLASSIFIED/UNLIMITED <input checked="" type="checkbox"/> SAME AS RPT. <input type="checkbox"/> DTIC USERS <input type="checkbox"/>			21. ABSTRACT SECURITY CLASSIFICATION		
22a. NAME OF RESPONSIBLE INDIVIDUAL Ulrich			22b. TELEPHONE NUMBER (Include Area Code)		22c. OFFICE SYMBOL NC

DD FORM 1473, 83 APR

EDITION OF 1 JAN 73 IS OBSOLETE.

SECURITY CLASSIFICATION OF THIS PAGE

Item 19. Abstract (continued)

✓ Air Force ordered polymers PPBT (polyparaphenylene benzobisthiazole) and BBL (benzimidazo-benzophenanthrolin). For comparison nylon6, nylon6,6, polypropylene, and polyethylene also were included in the study.

Several types of dopants were used in this research; these included metal-salt solutions (e.g., LiCl, NaCl, etc.), organic liquids (e.g., n-pentane, phenol, etc.) and charge transfer complex forming dopants (e.g., I₂). The effect on fibers of this doping produced variations in the electrical conductivity which sometimes were surprising. For example, in the case of BBL, the main mode of conduction was electronic and the presence of certain dopant ions actually reduced the overall conductance. For some dopants, non-ohmic conduction appears at surprisingly low electric field strengths, suggesting significant electrochemical processes and space charge limited conduction in the surface layers. The energy of thermal activation was found to depend on the dopant.

Technical Report

Grant No. 82-0290C

PHYSICAL TECHNIQUES FOR THE STUDY OF SORPTION,
DIFFUSION, ELECTRICAL PROPERTIES, AND INTERFACIAL
EFFECTS IN ORDERED POLYMERS: CHARGE TRANSPORT
AND CONDUCTION MECHANISMS IN POLYMER FIBERS

Submitted to:

U. S. Air Force Office of Scientific Research
Bolling Air Force Base
Washington, D. C. 20332-6448

Attention: Dr. Donald R. Ulrich
Building 410 NC

Submitted by:

R. E. Barker, Jr.
Professor

J. A. Hawk
Research Assistant

Approved for public release;
distribution unlimited.

Department of Materials Science
SCHOOL OF ENGINEERING AND APPLIED SCIENCE
UNIVERSITY OF VIRGINIA
CHARLOTTESVILLE, VIRGINIA

AIR FORCE OFFICE OF SCIENTIFIC RESEARCH (AFOSR)
MEMPHIS, TENNESSEE 38117
This report is approved and is
approved for release under E.O. 13526-12.
Distribution is unlimited.
MAURICE L. KATZ
Chief, Technical Information Division

Report No. UVA/525646/MS87/101
July 1986

Copy No. _____

FOREWORD

The research described in this report was initiated under Grant AFOSR-82-0290 entitled "New Physical Techniques for the Study of Large Molecular Diffusion, Sorption, and Interfacial Effects in Ordered Polymers," (Proposal No. MS-AFOSR-2408-82, May 1982). On occasion, certain documents related to the work have had other file designations (83 NC 204, and 82-0209C).

Some of the research covered in this report was the outgrowth of previous research supported under Grant AFOSR 80-0014B. This report was prepared at the Department of Materials Science of the University of Virginia. The research was administered under the direction of the Air Force Office of Scientific Research (Chemical Structures Program) Dr. D. R. Ulrich, Project Manager, Bolling Air Force Base, Washington, D. C. 20332-6448.

Due to the relevance of portions of the research to the ordered polymers interests of the Air Force, we have continued to have cooperation from a number of Air Force personnel and other U.S. AFOSR and U.S. AFWPL grantees who supplied us with various samples and advice. Especially, we thank Dr. E. C. Chenevey and Dr. J. R. Leal of the Celanese Research Company for supplying us with PPBT samples and helpful information about them, Dr. T. E. Helminiak (AFWPL) for loaning us the "world's supply" of BBL fiber and for his encouragement and keen advice, and to Dr. D. R. Ulrich (AFOSR) for his perceptive recommendations; and we express appreciation to Dr. D. Bhaumik, Prof. J. E. Mark and Dr. W. J. Welsh of the University of Cincinnati; Profs. S. L. Hsu, F. E. Karasz, and E. L. Thomas of the University of Massachusetts, Dr. J. F. Wolfe of Stanford Research Institute and Prof. G. C. Berry of Carnegie-Mellon University.

Accession For	6
NTIS G-01	
DTIC TAB	
Unannounced	
Justification	
by	
or	
through	
the	
NTIS	
System	
Accession	
Number	
1	
2	
3	
4	
5	
6	
7	
8	
9	
10	
11	
12	
13	
14	
15	
16	
17	
18	
19	
20	
21	
22	
23	
24	
25	
26	
27	
28	
29	
30	
31	
32	
33	
34	
35	
36	
37	
38	
39	
40	
41	
42	
43	
44	
45	
46	
47	
48	
49	
50	
51	
52	
53	
54	
55	
56	
57	
58	
59	
60	
61	
62	
63	
64	
65	
66	
67	
68	
69	
70	
71	
72	
73	
74	
75	
76	
77	
78	
79	
80	
81	
82	
83	
84	
85	
86	
87	
88	
89	
90	
91	
92	
93	
94	
95	
96	
97	
98	
99	
100	

A-1



TABLE OF CONTENTS

List of Tables	x
List of Figures	xi
List of Symbols	xix
Chapter	
I. INTRODUCTION	1
II. CONDUCTION IN POLYMERS	8
2.1. Introduction to Conduction in Disordered Solids	8
2.1.1. Overview of Factors Affecting Theoretical Study of Conduction in Disordered Solids	8
2.1.2. Charge Carriers in Polymers	15
2.1.3. Localized Electronic States in Polymeric Materials	22
2.1.4. General Equation for Conduction ..	29
2.2. Ionic Conduction in Polymers	34
2.2.1. Introduction to Ionic Conduction: General Concepts	34
2.2.2. Equations Used in Describing Ionic Conductivity in Polymers	45
Weak Electrolyte Model	45
Field Dependence of Ionic Conductivity	47
Free Volume Model for Ionic Conductivity	56

<u>Chapter</u>	<u>Page</u>
Diffusion Mechanism of Ionic Carriers Using Free Volume Model .	58
Summary	65
2.2.3. Local Structure Hypothesis	65
2.3. Electronic Conduction Mechanisms in Disordered Materials	73
2.3.1. Introduction to Electronic Conduction	73
2.3.2. Bulk Limited Mechanisms	75
Ohmic Conduction	78
2.3.3. Non-Linear Effects	85
Space-Charge-Limited Current (SCLC)	85
Poole-Frenkel and Onsager Enhancement	87
2.3.4. Electrode-Limited Mechanisms	93
Schottky Emission	93
Tunneling	94
2.3.5. Steady-State Behavior: A Perspective	96
2.4. Generalized Theory of Conductivity in Organic Polymers (Cotts and Reyes)	98
Introduction to Model	98
Model for Conductivity	99
Functional Dependence of Conductivity	101
III. EXPERIMENTAL CONSIDERATIONS	105
3.1. Introduction	105
3.2. Formalism for Describing the Conductivity Measurements	106
3.3. General Principles of Electrode Geometry .	109

<u>Chapter</u>	<u>Page</u>
3.4. Experiments Performed and Selection of Materials	115
3.5. Doping of Polymer Samples	117
3.6. Instrumentation	122
Electrical Instrumentation	124
Conductivity Cell Design	126
3.7. Separation of Surface and Volume Conductivity in Fibers	129
3.8. Conduction by Thin Surface Layers	137
3.9. Current Transients in Dielectrics	140
IV. RESULTS AND DISCUSSION	151
4.1. Introduction	151
4.2. Current Versus Time	152
4.3. Relative Humidity Experiments	178
4.4. Activation Energy Calculation	186
4.5. Current Versus Voltage Measurements	198
4.6. Surface-to-Volume Condition Determination.	203
4.7. Effects of Doping of Polymer Fibers	210
4.8. Summary of Results	216
V. CONCLUSIONS	229
References	231
Appendix A	241
Appendix B	245
Appendix C	249
Appendix D	252
Appendix E	255

<u>Chapter</u>	<u>Page</u>
Appendix F	258
Appendix G	262

LIST OF TABLES

<u>Table</u>	<u>Page</u>
2.1 Carrier Concentration for Given Conductivity Values for $\mu = 10^{-5}$ cm ² /V-sec and Unit Electronic Charge	33
3.1 Properties for Selected Polymers	118
3.2 Diffusants Used in Doping Polymer Fibers	123
3.3 Calculation of δ Based on Model for PPBT at Typical Room Conditions	140
3.4 Outline of Transient Current Behavior.....	144
4.1 Comparison of Conductivities of Polymers in Undoped State	217
4.2 Comparison of Conductivities of Polymers in Iodine Vapor	218
4.3 Comparison of Conductivities of Undoped and Doped BBL Fibers	219
4.4 Comparison of Conductivity of BBL Soaked in Distilled H ₂ O and NaI (1 molar) Versus Length of Time in Soaking Medium	220
4.5 Comparison of Conductivities of Doped and Undoped PPBT Fibers	222
4.6 Comparison of Conductivities Doped and Undoped Nylon Fibers	223
4.7 Comparison of Differential Current ($\Delta I/I_{\min}$) for Various Doped and Undoped Polymers	224
4.8 Activation Energies for Doped and Undoped BBL Fibers	225
4.9 Activation Energies for Other Polymers: Doped and Undoped	226
G.1 Value of Hall Voltage for Different Values of Mobility	265

LIST OF FIGURES

<u>Figure</u>	<u>Page</u>
2.1 Conductivity of Materials, Both Polymeric and NonPolymeric	9
2.2 Schematic Representation of Band Structure and Band Gap for (a) Metal, (b) Semiconductor and (c) Insulator	12
2.3 Highly Schematic Representation of Some of the Structural Features of a Partially Crystalline Polymer	14
2.4 Schematic Representation of Soliton in Polyacetylene, Emphasizing the Shift in the Direction of the Double Bond	21
2.5 Schematic Representation of a Semicrystalline Polymer, after Flory, Showing Crystalline Regions Embedded in an Amorphous Matrix	23
2.6 Hypothesized Molecular Crankshaft Motion of Chain Segments in Polymers (a) Schatzki and (b) Boyer	26
2.7 Surface Resistivity of Groups of Polyelectrolytes as a Function of Relative Humidity. The Particular Anions and Cations Also Play Important Roles	35
2.8 Proton Conduction Mechanism in Dissociation of Hydrogen Bonded Amide Group: (a) Self Ionization; (b) Proton Transfer; and (c) Transfers of Proton and Electron. (Mechanism Proposed by Seanor to Account for Ionic Conduction in Nylon 6,6)	36
2.9 Free Ion Mobility, Carrier Density, and Conductivity as a Function of %H ₂ O by Weight for Ag ⁺ Counterion Sample at 300K. (•) High Voltage (> 2.0 V) dc Measurements; (x) low voltage (< 2.0 V) dc Measurements; (□) ac Measurements; (Δ) Mobility Measurements Requiring the Low-Water-Content Technique	38

<u>Figure</u>	<u>Page</u>
2.10 Effect of Rhodamine Doping on Polyester Polymer: (a) Electrical Conductivity Changes (•) Undoped Polymer, (x) Polymer with 0.5 w/o Rhodamine 6G, (1) T = 333K, (2) T = 313K (E = 6×10^4 V/cm); (b) Temperature Dependence of the Electrical Conductivity and Thermal Expansion-- $\sigma = J$ (10 min)/E, E = 10^4 V/cm; (c) Temperature Dependence of Cation Mobility	39
2.11 Activation Energy for Conduction in Dry Membranes as a Function of the Cube of the Hydrated Radius of the Counter Ion	41
2.12 Activation Energies for Ionic Conduction of Alkali-Chloride Impregnated Cellulose Acetate (a) Above T_g and (b) Below T_g vs. Alkali Ion Volumes. For the Undoped CA, $E_a \approx 29.3$ kcal/mole and $E_b \approx 11-16$ kcal/mole	42
2.13 Three Probe Variable Temperature Electrical Resistivity of Lithium Containing Polyimide Film Measured in Air () and Vacuum (+). Region "a" Attributed to Evolution of H ₂ O From Polyimide Film During Test Due to Increasing Temperature .	44
2.14 (a) Log R Versus 1/T for Wet (72% RH) and Dry Epoxy Impregnated Polyester/Polyamide Fiber Mat. (b) Log R Versus 1/ ϵ T for Dry and Wet Composite of (a) Showing Linear Relationship	48
2.15 (a) Effect of Temperature on the Dry Dielectric Constant of Epoxy Impregnated Polyester/Polyamide Fiber Mat. (b) Effect That Humidity has on the Dielectric Constant of (a) Over a Range in Temperature	49
2.16 Two Potential Well Mode of Ion Migration (a) Ordinary Case and (b) With Application of an External Electric Field	50
2.17 Current Density as a Function of Electric Field of Unplasticized Polyvinyl Chloride Below and Above the Glass Transition Temperature. λ is an Apparent Jump Distance of the Ion	54
2.18 Replot of Data from Figure 2.17 in log J/E Versus log E format	55

<u>Figure</u>		<u>Page</u>
2.19	(a) Arrhenius Plots of Electrical Conductivity and (b) Plots of $\log \sigma + \gamma V_i^*/2.303 V_f$ Versus Reciprocal Temperature. Plot in (b) is Linear Over Entire Temperature Region and Slope of Line Corresponds to a Hybrid Activation Energy-Ionic Jump Energy and Ionic Dissociation Energy (O : PMMA; \odot : Unsaturated Polyester (UP); and \bullet : PS)	59
2.20	Change in Current With Time After Application of dc 2.5 V for 15-60 Minutes in One Direction and the Reversal of the Applied Voltage Polarity for the Poly(propylene Oxide)(PPO) Lithium Perchlorate (LiClO_4) Complex ($[\text{LiClO}_4]/[\text{PO unit}] = 0.076$) at Various Temperatures	61
2.21	(a) Temperature Dependence of Ionic Mobility for PPO- LiClO_4 Complexes and (b) Temperature Dependence of Ionic Diffusion Coefficient for PPO- LiClO_4 Complexes	62
2.22	Schematic Representation of Chains in a Non-crystalline Polymer. In (a) Note the Chains A and B Where no Ions are Present. In (b) an Ion Pair has Reduced the Number of Configurations Available to A and B	67
2.23	Coulombic Interaction Energy Between Monovalent Ions Separated by a Distance r_{ij} in Media of Different Dielectric Constant	70
2.24	Distance From a Monovalent Ion Corresponding to a Given Electric Field Strength E. Curves Represent Range at Which the Ion's Field Will Cancel the Opposing Component, E, of the Applied Field	71
2.25	Notation Used for One-Dimensional Carrier Flow of a Polymer Slab or Film Held Between Two Metal Electrodes	76
2.26	(a) Electron Transfer Mechanism Between Adjacent Sites Via Hopping Over a Potential Energy Barrier or by Tunneling Through the Barrier. (b) Hopping Between Localized States	82
2.27	Overlap of Impurity (Traps) Potentials Due to High Concentrations	84

<u>Figure</u>		<u>Page</u>
2.28	Possible Regimes for a Single Carrier Space-Charge-Limited Current With a Single Set of Traps. (i) Ohm's Law Region; (ii) Trap Free Child's Law; (iii) Child's Law With Trapping ...	88
2.29	High Field Models for Bulk Conduction. (a) A One Center Poole-Frenkel System; (b) Multiple Overlap Poole-Frenkel System; and (c) Tunneling System Showing Both Simple Tunneling and Partial Thermal Excitation (Mixed Mode Operation)	90
2.30	High Field Effects at the Contacts: (a) Schottky Emission; (b) Tunneling; and (c) Tunneling Out From Valence Band	95
3.1	(a) Schematic Representation of Two Probe Resistivity Measurement; (b) Circuit Diagram of Two Probe Method	107
3.2	(a) Schematic Representation of Four Probe Resistivity Measurement; (b) Circuit Diagram of Four Probe Method	110
3.3	Measurement of High Volume Resistivity: Three Terminal or Guarded Electrode System	112
3.4	Schematic Representation of System for Measuring Surface Resistivity	114
3.5	Comparison of Observed Current Levels Before and After Washing PPBT Samples in Ethyl Alcohol	122
3.6	Schematic Representation of Conductivity Cell Used In Fiber Research	128
3.7	Theoretical Technique to Separate σ_{vol} and σ_{sur} . (a) Experimental Technique; (b) Case Where $\sigma_{vol} > \sigma_{sur}$ and Case Where $\sigma_{sur} > \sigma_{vol}$; (c) Advantages and Disadvantages of Method	131
3.8	Equivalent Circuit Model for Determining Surface and Bulk Conductivity by Making Two Measurements on a Single Fiber	133
3.9	Special Technique to Separate σ_{vol} and σ_{sur} by Varying Effective Length of Fiber	135
3.10	Schematic Representation of Conduction by a Surface Layer of Thickness δ	139
3.11	Schematic Representation of Current Versus Elapsed Time Showing Transient Current Regimes .	141

<u>Figure</u>		<u>Page</u>
3.12	Cole-Cole Plots of Current Versus Time with $\alpha = \frac{1}{2}$. The Values of $\tau = 0.01, 1$ and 100 Correspond to High, Intermediate and Low Temperatures Respectively. At Long Times, the Apparent Activation Energy is Negative. Asymptotic Limits for $\tau = 1$ are Shown as Dashed Lines	146
4.1	Transient Charge and Discharge Curves for Undoped, Stretched Polypropylene Fiber	154
4.2	Transient Charge and Discharge Curves for Nylon 6,6 Fiber Soaked in NaI Solution	155
4.3	Variation in Transient Charging Curves With Temperature for Undoped, Stretched Polypropylene Fiber	157
4.4	Variation in Transient Charging Curves With Temperature for $\text{Fe}(\text{NO}_3)_3$ Doped PPBT (30-1) Fiber	158
4.5	Variation in Transient Charging Curves With Temperature for Nylon 6 Fiber Soaked in Dimethyl Sulfoxide	160
4.6	Transient Charge and Discharge Curves at High Temperature for Nylon 6 Fiber Soaked in Dimethyl Sulfoxide	161
4.7	Steady-State Current Curves for Nylon 6,6 Fiber Soaked in Ethyl Alcohol. Note Decrease in Observed Current, Possibly Due to the Sweeping Out of Ions	166
4.8	Current Versus Time Curves for Nylon 6,6 Fiber Doped With Iodine Vapor (I_2) Showing the Steady-State Current Observed in Dry Atmosphere and Resulting Change in Current From Exposure to a Moist Atmosphere	168
4.9	Current Versus Time Curves for Nylon 6,6 Fiber Soaked in NaI Solution Showing the Steady-State Current Observed in Dry Atmosphere and Resulting Change in Current From Exposure to a Moist Atmosphere	169
4.10	Current Versus Time Curves for Nylon 6 Fiber Doped With Iodine Vapor (I_2) Showing the Steady-State Current Observed in Dry Atmosphere and Resulting Change in Current From Exposure to a Moist Atmosphere	170

<u>Figure</u>	<u>Page</u>
4.11 Current Versus Time Curves for Polypropylene Fiber Doped With Iodine Vapor (I_2) Showing the Steady-State Current Observed in Dry Atmosphere and Resulting Change in Current From Exposure to a Moist Atmosphere	171
4.12 Current Versus Time Curves for Polyethylene Fiber Doped With Iodine Vapor (I_2) Showing the Steady-State Current Observed in Dry Atmosphere and Resulting Change in Current From Exposure to a Moist Atmosphere. The Second Graph Shows the Steady-State Current for Polyethylene Soaked in Ethyl Alcohol	172
4.13 Current Versus Time Curves for PPBT (30-1) Fiber Soaked in LiCl Solution Showing the Steady-State Current Observed in Dry Atmosphere and Resulting Change in Current From Exposure to a Moist Atmosphere	173
4.14 Current Versus Time Curves for PPBT (30-1) Fiber Doped With Iodine Vapor (I_2) Showing the Steady-State Current Observed in Dry Atmosphere and Resulting Change in Current From Exposure to a Moist Atmosphere	174
4.15 Current Versus Time Curves for BBL Fiber Soaked in Ethyl Alcohol Showing the Steady-State Current Observed in Dry Atmosphere and Resulting Change in Current From Exposure to a Moist Atmosphere	175
4.16 Current Versus Time Curves for BBL Fiber Soaked in NaI Solution Showing the Steady-State Current Observed in Dry Atmosphere and Resulting Change in Current From Exposure to a Moist Atmosphere .	176
4.17 Differential Current, $\Delta I/I_{min}$, Versus Time, Showing Relative Current Increase With Moisture Sorption for Various Doped Polymer Fibers	180
4.18 Differential Current, $\Delta I/I_{min}$, Versus Time, Showing Relative Current Increase With Moisture Sorption for Various Doped Polymer Fibers	181
4.19 Differential Current, $\Delta I/I_{min}$, Versus Time, Showing Relative Current Increase With Moisture Sorption for Various Doped Polymer Fibers	183
4.20 Differential Current, $\Delta I/I_{min}$, Versus Time, Showing Relative Current Increase With Moisture Sorption for Various Doped Polymer Fibers	184

<u>Figure</u>		<u>Page</u>
4.21	Differential Current, $\Delta I/I_{\min}$, Versus Time, Showing Relative Current Increase With Moisture Sorption for Various Doped Polymer Fibers	185
4.22	Arrhenius Plots of Conductivity Versus $10^4/T$ for BBL Fibers--Untreated and Soaked in Distilled Water and Ethyl Alcohol	187
4.23	Arrhenius Plots of Conductivity Versus $10^4/T$ for BBL Fibers Treated With Iodine Vapor (I_2) and NaI Solution	188
4.24	Arrhenius Plot of Conductivity Versus $10^4/T$ for BBL Fiber Soaked in an Indigo and Distilled Water Solution (0.2497 gms Indigo in 40 ml of Distilled Water)	189
4.25	Arrhenius Plot of Current Versus $10^4/T$ for PPBT (29022-30-1) Fiber Soaked in $Fe(NO_3)_3$ Solution .	190
4.26	Arrhenius Plot of Current Versus $10^4/T$ for Untreated PPBT (29022-17-9) Fiber. Upper Curve is First Test of the Fiber, While Lower Curve was Generated 29 Hours Later	191
4.27	Arrhenius Plot of Current Versus $10^4/T$ for Nylon 6 Fiber Soaked in Dimethyl Sulfoxide	192
4.28	Arrhenius Plot of Current Versus $10^4/T$ for Nylon 6 Fiber Soaked in $Fe(NO_3)_3$ Solution	193
4.29	Arrhenius Plot of Current Versus $10^4/T$ for Stretched and Untreated Polypropylene Fiber	194
4.30	Current Versus Voltage Curve Showing Linear Dependence for Untreated PPBT (29022-17-9) Fiber	199
4.31	Current Versus Voltage Curve Showing Linear Dependence for BBL Fibers Soaked in Ethyl Alcohol and Distilled Water	200
4.32	Current Versus Voltage Curve for a BBL Fiber Soaked in an Indigo/Water Solution. There is a Bend in the Curve at Around 0.8 Volts	201
4.33	Current Versus Voltage Curves at Various Temperatures for a BBL Fiber Soaked in Acetone. A Slight Downward Curvature Exists in the Low Voltage Region	202
4.34	Non-Ohmic Electronic Processes	204

<u>Figure</u>	<u>Page</u>
4.35 Non-Ohmic Ionic Processes	205
4.36 Current Versus Length for BBL Fibers Used in Determining the Portion of the Surface or Volume Conductivity of the Total Observed Conductivity	208
4.37 Mass Uptake for Long Cylindrical Fibers in an Infinite Bath, From Eq. (4.3)	212
B.1 Densities of States for Free Electrons and Free Holes, $N(E)$, and Densities of Electron Traps, $N_t(E)$, and Hole Traps, $P_t(E)$, as a Function of Energy	246
D.1 Capture (A_1 Process) and Excitation (A_2 Process) of an Electron at a Trap Site	253
E.1 Measured and Calculated Relative Conductivities at Various Field Strengths, According to Several Formulae, of (a) Polyethylene Terephthalate at 80°C and (b) Polyimide at 250°C	257
F.1 Contactless Electrodes	259
G.1 Origin of Hall Field and Hall Effect	263

LIST OF SYMBOLS

A'	constant
A	constant; electrode area
a_{π}	parameter [= $(\gamma^{\nu+} \cdot \gamma^{\nu-}) / \gamma_0$]
a_0	Bohr radius (0.529 Å)
a^*	molecular diameter of ion
A_1, A_2	rate constants
B	constant; bulk modulus of polymer
B_m	containing energy and entropy terms
b	sample thickness
C_p	heat capacity constant pressure
C_1, C_2	parameter in W-L-F Equation (Eq. 2.60)
C_3	constant (three-dimensional case)
D	diffusion coefficient
D^*	parameter (= ga^*u)
D	electric displacement
d	thickness of dielectric
d_e	combined thickness of layer (= $d_0 - d$)
d_0	separation between electrodes
E_a	energy in conduction equation
E_b	energy term in conductivity equation
E_F	Fermi energy
E_H	Hall field
E_t	local electric field
ΔE	incremental change in energy between initial and final states

E	electric field
e	unit of electronic charge
F_e	force due to electric field
F_H	Hall Force
F_L	Lorentz force [= $e(\underline{V} \times \underline{B})$]
F_v	viscous force acting on an ion
f_g	free volume fraction at T_g
ΔG	incremental change in Gibbs free energy
g	geometric factor
ΔH_j	potential energy barrier overcome by ion jumping into a hole of critical volume
ΔH_o	energy barrier height to ion migration
I	current (A)
J_c	convection current density (defined by Eq. 2.80)
J_{COND}	electrical conduction current density
J_{DIFF}	diffusion current density
J	current density (A/cm ²)
$K, K_{1:1}$	dissociation constant and related coefficients
k_B	Boltzmann's constant
l	specimen length; hop length
m	variable; effective mass of charge carrier
N	concentration of charge scattering centers
N_A	concentration of acceptors
N_a	Avogadro number
N_c	effective density of state for conduction bands
$N(E)$	density of localized states
N_t	concentration of shallow trapping levels
N_{total}	negative charge concentration

N_v	effective density of state for valence bands
n	number of carriers, concentration, or carrier density
n_i	concentration of carriers of species i
n_0	number of salt molecules per unit volume when $\phi = 0$
P_H	probability of finding a hole
P_j	probability of jumping into a vacant hole
P_n	hopping probability
p	pressure; free positive carrier concentration
p_t	trapped positive carrier concentration
p_0	thermal carrier concentration
q	amount of charge a carrier possesses (ze)
q_i	charge of i th species
R	gas constant (8.314 J/mole K)
r	radius
r_D	effective radius of the domain for monovalent ion
r_i	ionic radii based on x-ray data for crystals
r_{ij}	distance between two ions ($= r_i + r_j$)
r_s	effective radius of an ion of spherical shape
S	scattering cross-section
ΔS	incremental change in entropy
s	sum of ionic radii
T	absolute temperature (measured in Kelvin)
T_g	glass transition temperature
T'_g	a glass transition point indicated by the intersection of extrapolated portions of $\log \sigma$ vs. $1/T$ plots
t	time

U_{ij}	Coulombic interaction energy
U_0	crystal lattice energy
U'_0	effective dissociation energy
ΔU	incremental change in internal energy
u	gas kinetic velocity of ion confined to a cage
V	volt; volume of n polymer segments; volume
V_f	free volume
V_g	specific volume at T_g
V_H	Hall voltage
V_i	interaction volume of the impregnating ion
V_0	mean or most probable value of V ; barrier
V^*	holes with volume larger than critical value
V_i^*	volume of hole
ΔV	incremental change in volume
v_{drift}	average drift velocity
v_{th}	thermal carrier velocity
\bar{v}	mean velocity
v	drift velocity; mean velocity of electrons
W	energy separation
W_I	trap ionization energy
W_p	polaron binding energy
w_{ads}	moisture content (i.e., weight of water per unit mass of polymer)
X^+	alkali or other positive ion
x	parameter ($= e\lambda E/k_B T$); distance into sample
Y^-	halogen or other negative ion
y	variable
z, z_i	valence number of ion; valence of i th species

α	coefficient of thermal expansion; constant
α_f	expansion coefficient of the free volume
α_0	correlation factor ($0 < \alpha_0 < 1$)
β	$1/B$ - compressibility
β_S	Shottky coefficient
β_{PF}	Poole-Frenkel coefficient
Γ, Γ_{AB}	jump probability
Γ_c	critical jump probability
Γ^*, Γ_{\pm}^*	frequency of transition (in positive or negative directions with respect to applied field)
γ	fall off in wave function (cm^{-1}); geometric mean of the activity coefficients $(\gamma_+ \gamma_-)^{1/2}$
γ_{\pm}	activity coefficient
γ^*	numerical factor correcting free volume overlap
δ_0	measure of the free volume
ϵ	permittivity
ϵ_{dry}	permittivity in dry state
ϵ_{wet}	permittivity in wet state
ϵ_0	permittivity of free space
ϵ'	dielectric constant
ϵ'_{eff}	effective dielectric constant (defined in Eq. 2.26)
ζ	parameter ($= s/za_0$); parameter ($= \beta_{PF} E^{1/2}/k_B T$)
η	viscosity
η'	effective local viscosity
Λ	capture cross-section
λ	jump distance; mean free path
μ	mobility ($\text{cm}^2/\text{V-sec}$)
$\underline{\mu}$	mobility tensor

μ_{\pm}	ion mobilities
μ_0, μ'_0	constants
μ_{eff}	effective mobility
μ_i	mobility of ith species
μ_l	local mobility
μ_m	ionic mobility
ν	vibrational frequency
Ξ	overlap parameter
ξ	constant (= 6.3)
π	constant
ρ	average hopping distance between sites (\AA)
ρ_l	local density
σ	electrical conductivity (S/cm or S/m)
$\underline{\sigma}$	electrical conductivity tensor
σ_0	constant
σ_3	constant (three-dimensional case)
τ	time of flight of carriers; time constant
Φ	volume fraction of occupied sites in percolation model
Φ_c	percolation threshold
Φ_D	parameter including frequency of electron impinging upon potential barrier and its probability of escape
ϕ	fractional dissociation; constant

CHAPTER I

INTRODUCTION

There are a number of reasons for studying conduction processes in polymers aside from the principal reasons associated with such directly practical ones as the insulation of electrical devices and power loss in electric cables. Applications where larger values of conductivity in polymers would be useful include static electrification of clothing, carpeting, phonograph records, and satellite antenna bushings. Additionally, precise knowledge of conduction mechanisms would aid in electrostatic recording (xerography), electret applications (electroacoustic, pyroelectric and biomedical), capacitor dielectrics and films formed by glow discharge polymerization (switching devices and passivation of semiconductors). These latter applications have an important function in the electronics and electrophotographics industries. Reviews on new conductive polymers and the applications of these polymers in industry can be found in the literature.¹⁻⁸

Experiments are underway in many organizations to determine the possibility of using carbon- and metal-filled polymers (i.e., composite systems) as moldable "semiconductors".^{9,10} (Although the term semiconductor is often misused from the solid state physics point of view, these materials are of industrial importance.) Other

studies are in progress in many laboratories to determine the influence on the electrical conductivity that strong oxidizing agents (e.g., AsF_5) and strong reducing agents (e.g., Na) have on certain polymers.¹¹⁻¹⁴ These polymers have unsaturated chemical bonds along the chain "backbone" (e.g., polyacetylene) and initially exhibit semiconducting electrical properties. After treatment with the proper oxidizing/reducing agent, metallic conduction is ultimately observed.

For example, polyacetylene films, first synthesized by Shirakawa¹⁵ and later modified with oxidizing agents by MacDiarmid and Heeger,¹⁶ possess conductivities of 2000 S/cm when doped with iodine. (The symbol S is called the Siemen and is equivalent to ohm^{-1} , and 1 S/cm is equal to 100 S/m). Another conducting polymer, polypyrrole, exhibits a conductivity of only 100 S/cm. These values fall far short of the conductivities of 10^6 S/cm achieved by good metallic conductors like copper. Even though the goal of replacing metallic conductors is not realistic, there are applications where the lower than metallic conductivities achieved by conductive polymers are sufficient.

In the case of antistatic equipment, conductivities in excess of 10^{-8} S/cm are necessary in materials which are suited for avoiding electrostatic charge buildups. This value is easily achieved by the electrically conducting polymers already mentioned. These polymers are also useful in shielding against electromagnetic interference. By

increasing the film thickness of polypyrrole, its shielding efficiency reaches values comparable with the shielding properties of metals. Another use for these polymers is for switchable contact bridges. These switching devices are only suitable for uses where small currents are generated. The advantage of the conductive polymers, as opposed to that of thin metal layers on a polymer substrate, can be seen in their low sensitivity with regard to mechanical damage of their surface. Destruction of the metal layer seriously degrades the function of the metallized polymer film contact bridge. Mechanical scratches on a polypyrrole film leaves its electrical properties nearly unchanged due to the inherent conductivity of the bulk material.¹⁷

In one sense, the number and scope of applications of polymeric materials is extensive due to their flexibility, strength and lightness, but such applications are limited in another sense by the electrical properties. An important collective goal of research into the electrical properties of polymers in the broadest sense is to be able to develop polymeric systems not only as insulators, but also as semiconductors and conductors. From the scientific point of view, further careful investigations on the effects of additives and dopants which modify a polymer's conductivity appear to be quite significant and collectively may be reasonably expected to lead to additional uses in the electronics industry.

The present work builds on research started by Chen.¹⁸ That research centered on conductivity measurements of polyparaphenylene benzobisthiazole (PPBT) films and fibers and included effects due to moisture, changes in temperature, and certain metal-salt dopants. The present research has concentrated on conduction mechanisms and the overall electrical conductivity of several different types of polymers, with special emphasis on conduction in fibers.

The standard methods of resistivity and/or conductivity measurements use large samples, usually in sheet form, with standard cells.¹⁹ When faced with unusual sample size or geometry or both, new methods of performing the experiments and interpreting the results must be found. For example, some of the fibers examined are only 20 μm in diameter and pose a number of problems in cell design. To aid in the interpretation of the results on conductivity in fibers where the distribution of space charge and microstructure gradients were expected to play an important role, data from bulk samples obtained from standard testing procedures need to be used as a reference whenever possible. A number of types of conduction measurements were performed to get some idea of the differences between bulk and surface conductivity in fibers. According to a hypothesis of Barker,²⁰ small strongly charged ions modify the local structure of the polymeric material in such a way that the relatively small volume fraction in which the ions reside is atypical of the average structure for the material.

Conductivity measurements are presumed to probe the perturbed structure. Hence, another area of interest centered on the role that organic and metal-salt diffusants of various charge-to-size (z/r) ratios had on the overall electrical conductivity. In this regard, the role of sorbed water in the conduction process is of great interest. Measurements as a function of temperature were also made to determine activation energies for conduction for various polymers in both the doped and undoped states.

When investigating the electrical conductivity of fibers, the contribution of the surface conduction to the total should be a matter of concern. Given that the geometry of fibers is cylindrical, the question arises as to how much current flows along or very near the outer surface as opposed to the interior of the fiber. This becomes of particular significance when it is realized that a process used to make fibers usually produces a substantially modified morphology near the surface. If, at some point in the future, it is deemed desirable to use polymer fibers as current-carrying agents, then morphological and/or chemical surface modification of the polymer may be all that is necessary to enhance the fiber's overall conductivity. Therefore, methods were devised to relate observed conductivity data on fibers to the cylindrical fiber geometry and thus separate the volume and surface conductivity components.

This dissertation is divided into three major parts. Part one consists of an examination of the differences between ionic and electronic conduction and provides a short introduction to the types of carriers that are thought to exist in polymers which account for the transport of charge. Also included in this part is an overview of the various models of the conduction process with emphasis on the role that polymer morphology may have in the process. In particular, the role of the "local structure" is examined. The experimental details of the research are contained in part two. Instrumentation, cell design, and the principles of conductivity measurements are discussed. Polymer selection, doping schemes and the details of the individual experiments are also found in this section. Also included in this section is a discussion on transient current phenomena as well as the effect of cylindrical geometry on the conduction process. Part three contains the results of the research with analyses and discussion of the data, including that related to transient current phenomena.

Any research into the electrical properties of polymers necessarily presents certain problems, chief among them is the reproducibility of results. This arises from the many ways that a given polymer is manufactured, and to the sensitivity of certain electrical properties to additives and contaminants. Not only do polymer samples vary from manufacturer to manufacturer, but they also sometimes vary from batch to batch within the same company. Thus, it

should be remembered that the figures presented in this dissertation, although measured and represented in precise terms, should not be construed to represent uniquely definitive values for the types of polymers studied. This research has investigated certain representative classes of polymers with samples of specific geometry and certain conclusions, hopefully of broad validity, are drawn from these results.

CHAPTER II

CONDUCTION IN POLYMERS

2.1 Introduction to Conduction in Disordered Solids

2.1.1 Overview of Factors Affecting Theoretical Study of Disordered Solids

The range of electrical conductivity σ observed in materials spans 25 orders of magnitude, making this one of the largest variations of any materials property. Polymers tend to be recognized primarily as insulating materials; however, recent discoveries of highly conducting graphite intercalation compounds,²¹ graphite superconductivity, metallic polysulfur nitrogen,²² and doped polyacetylenes,²³ that can be made to exhibit metallic conductivity as well as p-type or n-type semiconductor response,²⁴ illustrate that a similar range of electrical conductivity also exists for carbon-based polymers and compounds. This wide range of electrical conductivities of both polymeric and non-polymeric materials is shown in Figure 2.1.

Probably the foremost problem in studying polymers of any type is the uncertain knowledge of their structural order. Polymeric materials are unique in that they can be synthesized into a large number of structural forms. Polymers can exist as amorphous materials or as crystalline materials. On another level, polymers are molecular materials where the basic structural unit is an individual polymer chain. Interaction with other polymer chains is

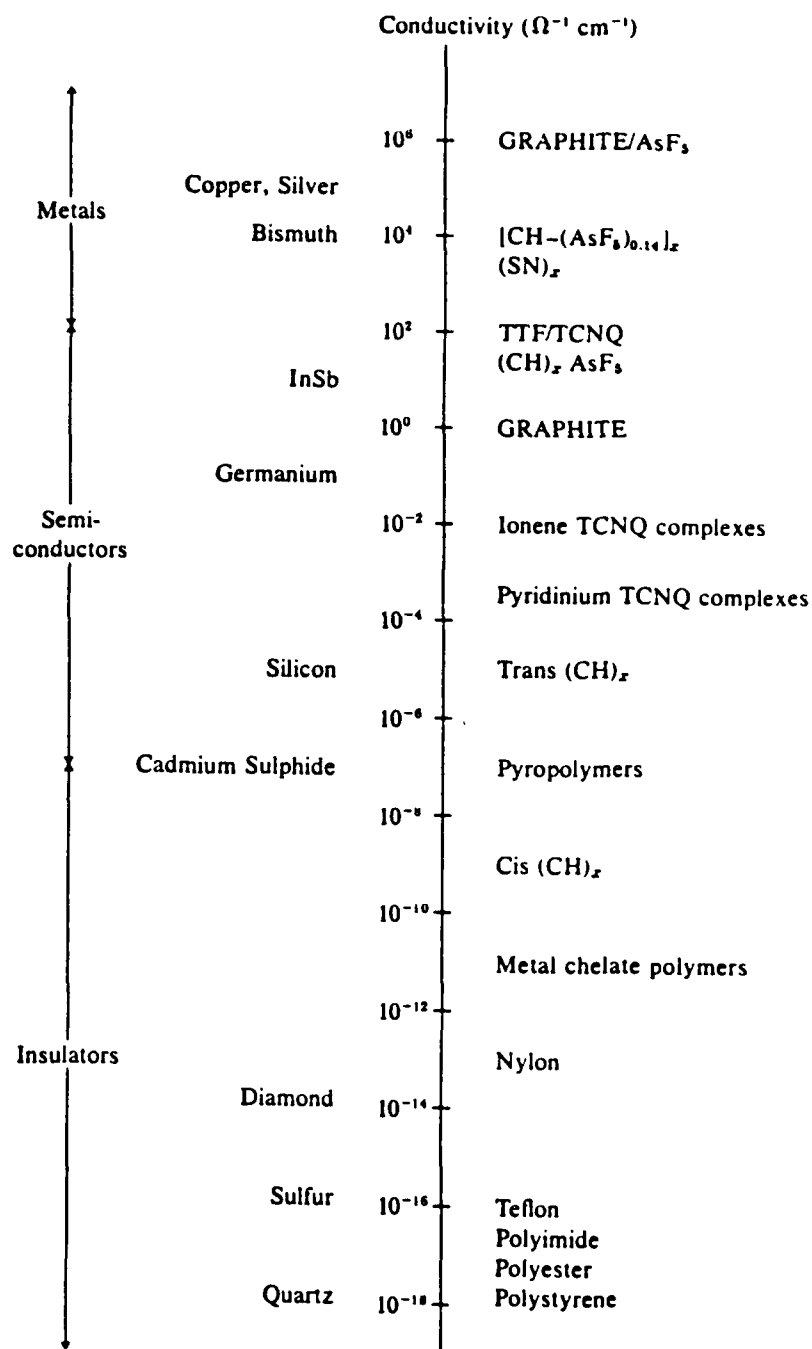


Figure 2.1. Conductivity of Materials,²⁵ Both Polymeric and Nonpolymeric.

usually through secondary chemical forces (such as van der Waals bonds) which allow the individual chains to assume different conformations. Mechanical reorientation of the chains is thus possible. Proceeding to yet another structural level, the chemical units within the polymer chain need not have a unique spatial arrangement. One chemical unit can be rotated about its bond with another chemical unit as long as there is enough energy to overcome intramolecular steric hindrances and intermolecular space into which it can move. Additionally, polymeric materials are characterized by a distribution of molecular weights about a mean, known as the weight average molecular weight. Thus, thermoplastic polymeric solids are relatively disordered, with weak intermolecular bonding, when compared to well ordered, covalent or ionically bonded inorganic crystals.²⁵

When studying electrical conductivity mechanisms for which good theoretical models exist, we have two extremes--inorganic crystalline lattices²⁶ and amorphous semiconductors.²⁷ The long-range periodic order present in crystalline lattices allows the electronic configuration of individual atoms to combine and form long-range delocalized bands of discrete energies. The observed conductivity is due to the population of charge carriers in the valence and conduction bands. Thus, whether a material will be an insulator or an intrinsic conductor can be explained in terms of the mobilities of the carriers and the "energy gap"

between the conduction and valence bands. These cases are shown in Figure 2.2. For semiconductors, the jumping of electrons from the valence to the conduction band is achieved by thermal activation or by some other form of activation such as photoactivation. The doping of semiconductors with species of differing electronic structures aids the conductivity by a modification of the activation energy by distorting the lattice (interstitially) or by providing conduction band electrons (valence band holes) in occupying lattice sites substitutionally.

Amorphous semiconductors lack long range order and conduction occurs because the band edges are smeared. This leads to a "mobility gap" rather than an energy gap and charge carriers are highly localized at sites of structural disorder. The energy difference from site to site is small, so conduction is limited by the mobility of the charge carriers instead of the total number of charge carriers. Thus charge carriers hop from site to site by way of a weak thermally activated process. Typically, polymers fall into that large gap that lies between these two extremes.

Polymers can be viewed as composite materials--on many levels--consisting of both amorphous and crystalline material with many possible defect structures. In viewing a polymeric material, there may be an array of molecular states and molecular ion states with many localized dipole states associated with the inherent disorder of the polymer.

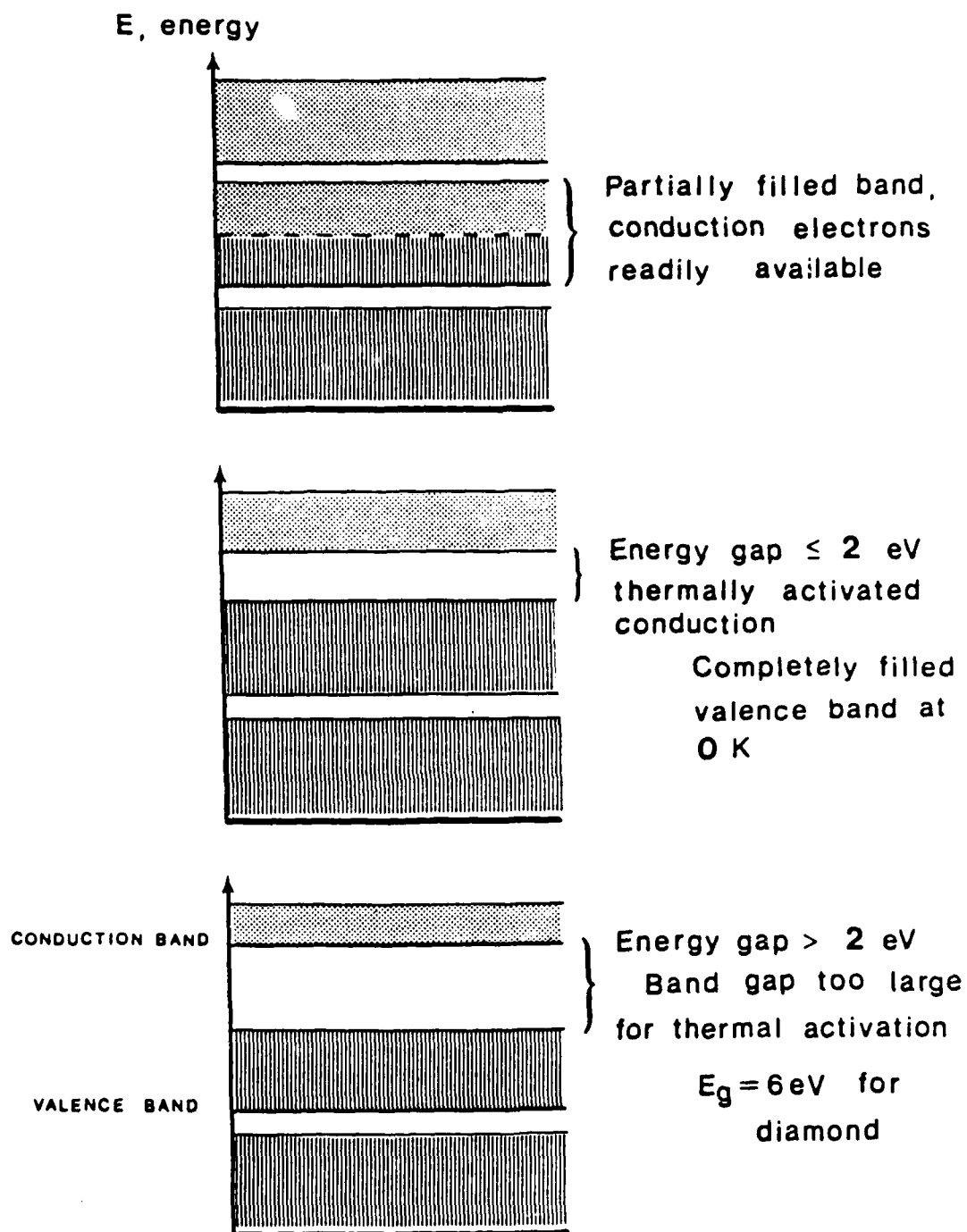


Figure 2.2. Schematic Representation of Band Structure and Band Gap for (a) Metal, (b) Semiconductor and (c) Insulator.

In most polymers, i.e., not single crystals, a band structure is not clearly evident.

The nature of polymers places great importance on the chemical structure of the monomer units which determines the behavior of the polymer. A correlation also exists between the position of one repeat unit and its two covalently bonded nearest neighbors. This spatial arrangement of the basic chemical units within the individual polymer molecules determines the microstructure. Differences in entropic and kinetic conditions preclude the formation of evenly spaced microscopic lattices out of the highly entangled chains. The formation of the types of crystalline arrays necessary for the application of band theory typically do not exist in polymers except on a limited and small scale. In addition, residual products from the polymerization process, deeply sorbed water in sites along the polymer chain or in microvoids of the polymer interior, and specifically introduced dopant species further complicate any attempt to formulate a theoretical basis of electronic conduction in polymers. The status of models for ionic conductivity will be discussed later. All these considerations must be kept in mind when trying to interpret experimental results of electrical conductivity measurements.

Figure 2.3 is a highly schematic representation of some of the structural features of a partially crystalline polymer. This figure provides some indication of the complexities associated with polymer research when

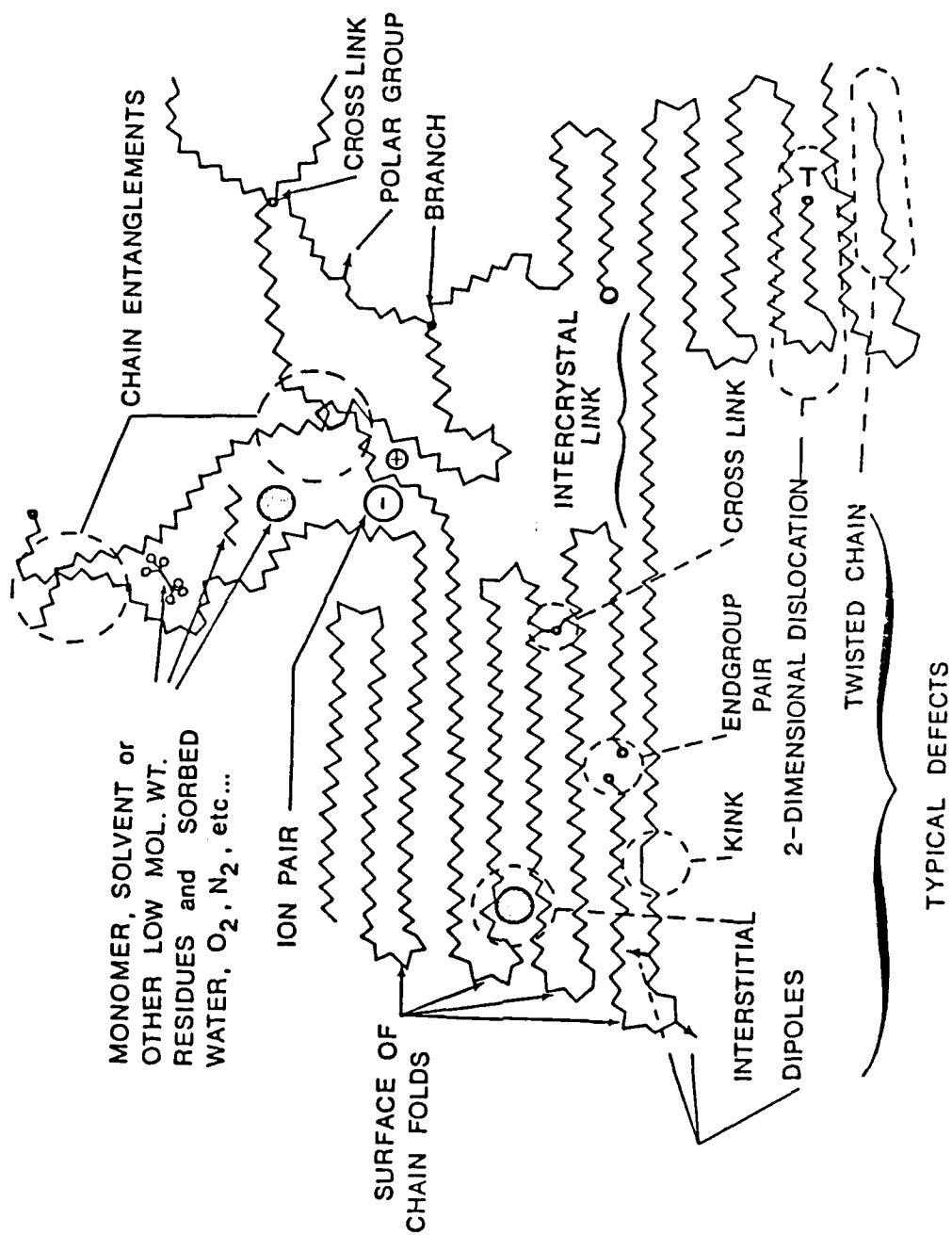


Figure 2.3. Highly Schematic Representation of Some of the Structural Features of a Partially Crystalline Polymer.

investigating any transport properties. The local environment presents many obstructions to transport of a certain kind, e.g., interface between crystalline and amorphous regions acts as a barrier to ion transport. Ions are freer to move in the less densely packed amorphous material. The crystalline regions with tight packing and a regularity of structure tend to impede ion movement. In general, as the charge carriers move through an amorphous region, they experience spatial and possibly temporal fluctuations in local density, orientation, and energy of side groups and dipoles associated with the polymer. Furthermore, the very strong electric field near the charge carriers may actually modify the local properties. In order to get a better understanding of conduction in disordered solids, it is necessary to examine the charge carriers hypothesized to exist in polymers.

2.1.2 Charge Carriers in Polymers

In this section, the charge carriers thought to be responsible for electrical conduction in polymers are considered. It is generally accepted that in polymers as a class of materials, both electrons and ions contribute to the total observed conductivity. Depending upon the case, it is likely that one type of conductivity will predominate. Also, as the intensive variables of the system change, it is entirely possible that the predominant mode will shift to another type.²⁰

Electrons and holes are considered to be the majority carriers in the case of electronic conduction. The electronic conduction process may be intrinsic, a property of the pure materials such as in silicon, or extrinsic, depending on the trace impurities needed to obtain higher levels of conduction, as in the case of silicon doped with arsenic. Although the detailed mechanisms for ionic conductivity are quite different, ionic conduction can also be thought of as intrinsic, where the ions originate in a self-dissociating manner, or extrinsic, where the ionic species have been introduced in the form of impurities arising from the polymerization process or deliberately in the case of impurity dopants. The total current may be due predominantly to mobile cations, as in the case of sodium salt in poly (methacrylic acid), or to mobile anions, as for secondary amine derivatives of polystyrene.²⁰

Phenomenologically, electrical conductivity in polymers usually increases rapidly with increasing temperature. Many researchers feel that classical semiconductor theory indicates intrinsic charge carrier creation of electrons and/or holes occurs as described by solid-state physics.^{28,29} This implies that charge carriers and the generation step are intrinsic to the polymer. However, certain non-linear and non-ohmic behavior in polymers have been attributed to ionic conductivity,²⁵ and in many cases the response of the conductivity to changes in moisture content is certainly strong evidence for an ionic mechanism.

Ionic carriers³⁰ are distinct, ionically charged chemical entities--originating from acids, bases, salts, and organometallic impurities due to residual catalysts or species intended to be electronic dopants, but which end up as mobile ionic species.³¹ Conduction by hydronium ions and protons is an important and rather special case of ionic conductivity. In principle, ionic conduction occurs in both amorphous and crystalline regions and requires actual mass transport. As in the case of chemical diffusion, the transport in the amorphous regions usually exceeds that in the crystalline region by several orders of magnitude. Not surprisingly, ionic conduction is extremely sensitive to pressure (i.e., the available free-volume in the polymer) and humidity (i.e., directly due to the dissociation of H_2O into H^+ and OH^- ions and indirectly due to the enhanced dissociation of other ionic components).

Another type of charge carrier, proposed first by Frenkel,³²⁻³⁴ is the intramolecular exciton. An exciton is a neutral excitation consisting of an electron and the positive hole it leaves behind. The "neutral"³⁵ or "tightly bound" exciton represents one limiting case whereby both charges are distributed over one molecule in the lattice. The other limiting case is the "loosely bound" or "ionized"³⁵ exciton in which the electron and hole are separated by a distance as large or larger than the lattice spacing of the crystal. In molecular crystals, the "ionized" excitons in which the electron moves around the

hole in one or another of a series of bound states, resemble the states observed in the hydrogen atom and converge towards a series limit at which the electron becomes independent of the hole, thus dissociating into separate charge carriers. The exciton as a unit can diffuse throughout the crystal as well as separating into an electron and a hole.²⁹

Neutral excitons are uncharged and do not enter into the steady state conduction phenomena, but they appear to account for energy transport.^{36,37} The elementary excitations of isolated repeat units are coupled by bond overlap, and are treated as dipole-dipole interactions. This gives rise to a band of states, the exciton band, capable of propagating the excitation along the polymer chain. Transport occurs with the cooperative polarization of the lattice, both for a periodic atomic lattice and a molecular lattice found in organic single crystals. The exciton contributes to bulk conduction when the neutral species becomes "ionized" by an applied electric field.

Analogous to the concept of the exciton as charge carriers is the electron/hole pair associated with the band theory of conduction.²⁶ Application of an electric field allows these species to migrate. The electron and/or hole is the charge carrier responsible for conduction in band theories of amorphous semiconductors. For the charge carrier to be able to contribute to the conductivity in a crystalline semiconductor, an electron must be promoted

across the band gap from the valence to the conduction band through an energy transfer such as direct photon absorption or by an increase in temperature. In an amorphous semiconductor, the tails of the distribution functions of the valence holes and conduction electrons overlap, and the concept of an energy gap is replaced, to some extent, by that of a "mobility gap."

The concept of localized ionic states^{38,39} is another concept through which charge carriers can be visualized. Localized ionic states, particularly anions, are truly ionic in nature although the transport mechanism for conduction is electronic. The species involved is usually a discrete molecule or some type of molecular residue which possesses a high affinity for electrons. These anions may be formed through electron transfer that is photoinitiated, chemically driven as in a donor:acceptor complex, or caused by an electrochemical redox reaction.³¹ In systems where these carriers are responsible for conduction, the carrier movement occurs through a random hopping mechanism.

There are two other hypothesized charge carriers according to Cotts and Reyes.³¹ The first is the localized electronic excited state.⁴⁰ These energy states are localized on a single molecular residue or repeat unit and hence do not participate in conduction. They can contribute to electron spin resonance (ESR) signals if their spins are unpaired.

The last charge carrier centers on the concept of the "soliton", and is controversial. The concept of the soliton comes from solutions of non-linear differential equations that apply to a variety of physical phenomena.⁴¹ This type of mechanism is thought to be responsible for conduction in quasi-one-dimensional models for polyacetylene. The simplest way to visualize a soliton is in terms of a surge wave in a canal. On one side of the "crest", the polyacetylene double bonds are oriented in a particular direction. On the other side of the crest, the double bonds point in the opposite direction. The charge carrier exists somewhere in the "crest" region. It is delocalized in that the soliton may be spread out over an area consisting of as many as 15 carbon-carbon double bonds. This is illustrated in the following way in Figure 2.4. The soliton sweeps along the molecular chain, changing the electronic configuration as it propagates. It is hypothesized that the soliton may conduct electricity by transferring electrons to other solitons on nearby polymer chains. This concept applies only to polymers that can be modeled as one-dimensional conductors, e.g., polyacetylene. Thus, it is easiest to think of the soliton as a type of defect or kink. The controversy over the existence of solitons is readily apparent. Su et al.⁴² hypothesize its existence in polyacetylene, while Tomkiewicz et al.⁴³ suggest that solitons play no role in charge transport in doped

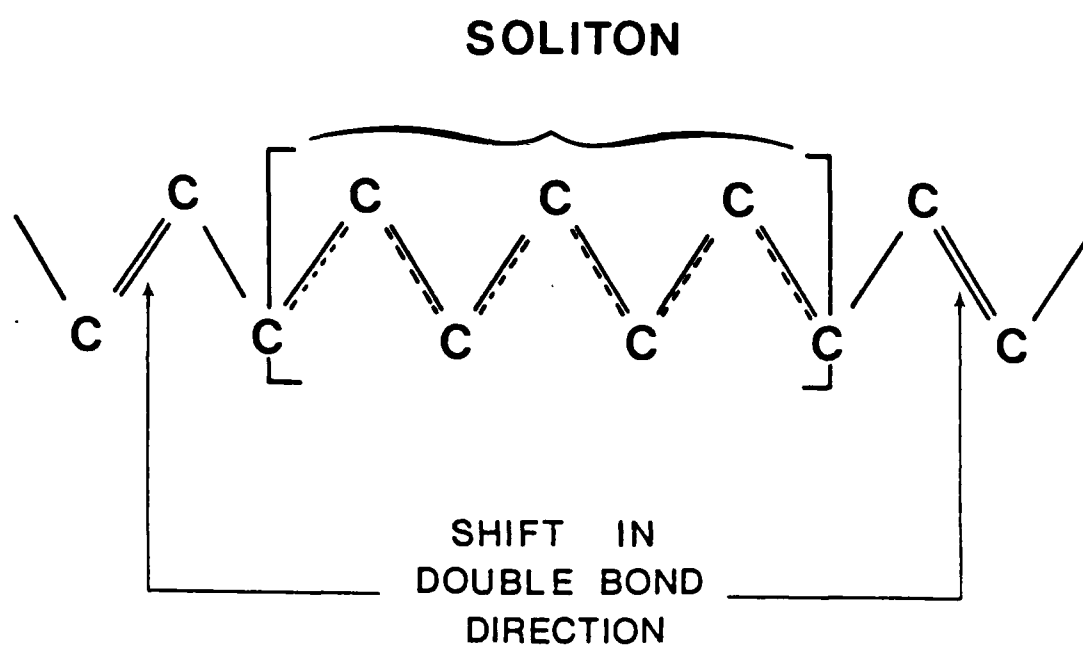


Figure 2.4. Schematic Representation of Soliton in Polyacetylene, Emphasizing the Shift in the Direction of the Double Bond.

polyacetylene. Certainly the case for or against solitons is still open to debate.

2.1.3 Localized Electronic States in Polymeric Materials

When working with polymers, the application of band theories to electrical conduction is a dubious procedure because polymers tend to be considerably more disordered than metals are. Band theories work best when regular arrays of similar atoms, preferably on lattice sites, are available. Polymers, even in single crystal form usually contain a higher concentration of defects than metals do, and band theories work only as approximations. The kind of order that provides regular spacing of like atoms occurs for quasi-one-dimensional polymers, for example, polymethylene $(-\text{CH}_2-)_n$, polyenes, polyacetylenes, etc. The order occurs along the chain axis. So it is apparent that polymer morphology, especially variations in the local structure of the polymer is of great importance in studying conduction processes.

Figure 2.5 is a schematic representation of a semicrystalline polymer. It is presented to show that even polymers considered to be highly crystalline have amorphous regions separating the crystalline regions. The most highly crystalline polymers seldom have a crystallinity greater than 90% and even the crystalline regions will be disordered to some extent. Carrier trapping occurs at the interfaces between the crystalline and amorphous material. Polar

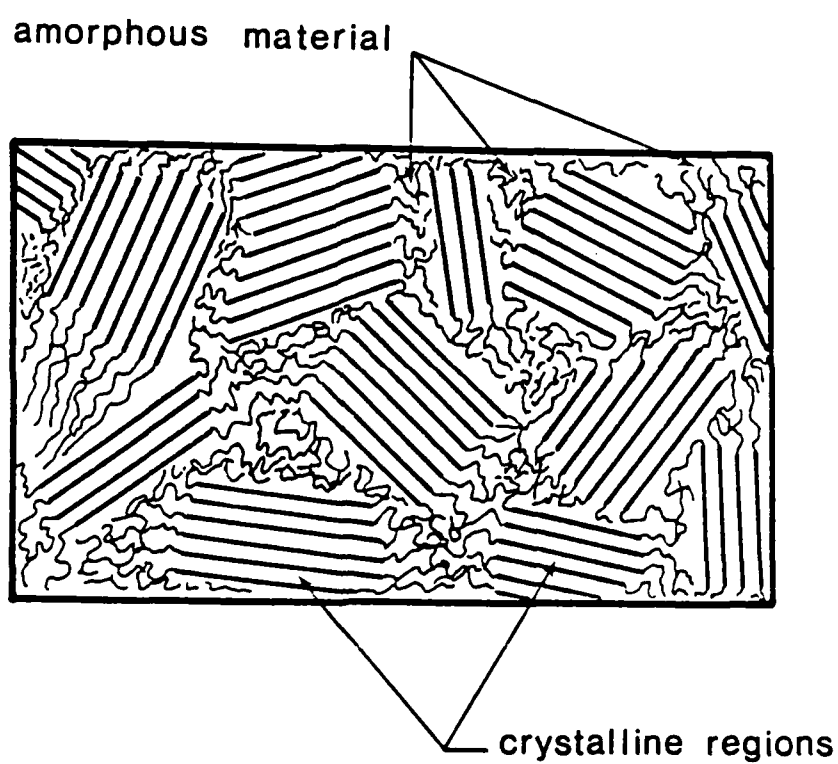


Figure 2.5. Schematic Representation of a Semicrystalline Polymer, after Flory,⁴⁵ Showing Crystalline Regions Embedded in an Amorphous Matrix.

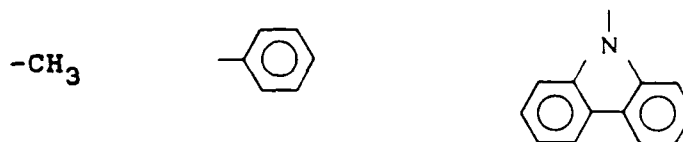
groups also exist in many polymers and can act as electron or hole traps. At room temperature, a dipole of 1.65D is capable of binding an electron.⁴⁴ Additionally, dielectric relaxation occurs around the trapped charge carrier. Semicrystalline polymers can be thought of as a composite material--a continuous matrix of amorphous polymer in which the properties are modified by crystalline regions that act as reinforcing agents for the amorphous matrix. One effect of crystallinity is to reduce the electrical conductivity of the polymer. For ionic conduction, the mobility of the ion is lower in crystalline regions of the polymer. Electronic conduction through crystalline regions may be somewhat faster than in the amorphous regions, but the crystalline-amorphous interface acts as a good trapping region--a phenomenon similar to the Maxwell-Wagner interfacial polarization.⁴⁶⁻⁴⁹

Amorphous polymers can exist in two states depending upon whether they are above or below their glass transition temperature, T_g . Below the glass transition temperature, the wholly amorphous polymer is in the glassy state while once T_g is exceeded, the rubbery state is reached. The glass-rubber transition has many features of a second-order transition with no discontinuities for enthalpy or volume but c_p , α , and mechanical properties (e.g., β) do have discontinuities.

As T_g is passed in going from the glassy to the rubbery state, there is a "freeing-up" of gross molecular modes of

motions of the polymer chain. Five types of motion appear possible in amorphous materials and are listed in order of increasing temperature. (Figure 2.6 also shows two models of molecular motions.),

- (a) side chain motions, e.g., rotation of



- (b) motion of two four-carbon moieties in the main chain (the Schatzki crankshaft⁵¹ effect),
 (c) motion of moieties containing hetero-atoms in the polymer chain,
 (d) reptation motion of segments containing 50-100 backbone atoms (corresponding to T_g),
 (e) motion of the entire chain as a unit and Zimm-Rouse modes in the molten state.

In crystalline polymers, additional possibilities exist:

- (a) crystal melting,
 (b) change in crystalline structure,
 (c) motion of side chains in the crystallite,
 (d) crystalline-amorphous interactions including interfacial friction, and crystallite thickening,
 (e) intracrystallite interactions, including the propagation of Reneker kink defects.

Thus, localized electronic energy states, i.e., those states not forming extended bandlike states, can be associated with the following molecular features:

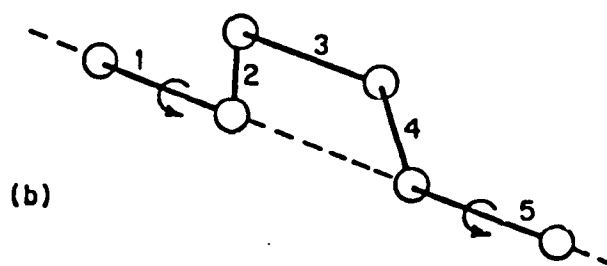
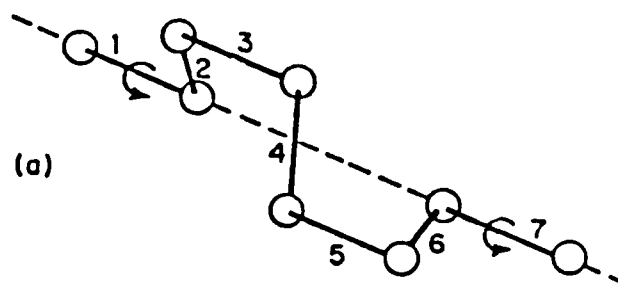


Figure 2.6. Hypothesized Molecular Crankshaft Motion of Chain Segments in Polymers (a) Schatzki and (b) Boyer.⁵⁰

- (a) surface states induced by strain or chemical reactions,
- (b) surface dipole states,
- (c) bulk dipole states,
- (d) bulk molecular ion states,
- (e) impurities (different chemical groups, polar groups, ionic groups),
- (f) chain ends,
- (g) chain branches,
- (h) chain folds,
- (i) kinks, two-dimensional dislocations, and twisted chains,
- (j) changes in tacticity or stereochemistry,
- (k) crystalline-amorphous boundaries,
- (l) broken bonds,
- (m) polaron states (trapped charge and its surrounding polarized dielectric), and
- (n) local density fluctuations.

Most of these defect states can be seen in schematic form in Figure 2.3. Escape from these localized states may require the input of energy and thus depends on the local environment and specific molecular motions. The local electric field may also aid in the detrapping of charge carriers from these sites. A trapped charge in a localized state can also act as a recombination center for charges of opposite sign. If the lattice around the trapped charge becomes polarized, transport becomes more difficult;

polarization tends to increase trap depth and thus the time spent in the trap. Density fluctuations, especially in amorphous regions, create localized states and possibly mobility bands.⁵²⁻⁵⁴

In dipole-containing polymers, it is not clear that energy bands can be derived, even in concept, in the crystalline regions. Duke and Fabish⁵⁵ propose that side groups act as traps to create ion-radical states. Local differences in the environment may have energy level variations of as much as 1 eV, thus reducing the hopping probability. This leads to the hypothesis that the localized states which reside deep within the energy gap are an inherent property of the polymer and related directly to its chemical structure. Thus this hypothesis does not need the inclusion of impurities or defects to explain traps. Lack of long range order does contribute to the range of energy associated with a particular chemical group. Consequently, in the equation describing hopping probability (i.e., from one site to an adjacent site)

$$P_n \propto \exp\left(\frac{-\Delta E}{k_B T}\right) \exp(-\gamma\rho) \quad (2.1)$$

both the distance ($\gamma\rho$) and energy ($\Delta E/k_B T$) terms will be small. This is due to energy differences ΔE between adjacent sites. The average hopping distance is ρ (in units of Å), while γ describes the fall-off in the wave function with distance measured in reciprocal centimeters.

Alternatively, disorder provides a range of energetically different environments for each chemically different group in the polymer. Once a charge carrier becomes trapped, the resulting polaron states are spread over a broad range of energy.⁵⁶ In addition to these bulk states, there can also be surface and interfacial states.

2.1.4 General Equation for Conduction

Direct electric current conduction in either solids, liquids, or gases requires the existence of mobile charge carriers. The conductivity is defined as the charge transported across a unit cross-sectional area per second per unit electric field applied.²⁹ The conductivity is thus proportional to the amount of charge, q , in units of e , the electronic charge, so that each carrier possesses (ze) of electronic charge, which may be either positive or negative. If the concentration, or density, of charge carriers is assumed to be n carriers per cubic centimeter, the total charge transported is (nze) . The velocity with which the charge carrier moves under a constant, unit electric field, i.e., under a potential gradient of 1 V/cm, is called the mobility, μ --with dimensions of $\text{cm}^2/\text{V-sec}$. The conductivity σ in units of S/cm, can thus be written for a single type of charge carrier as

$$\sigma = z e n \mu. \quad (2.2)$$

The conductivity is the reciprocal of the resistivity, which is the resistance per unit cube in ohm-cm.

The charge carriers need not be restricted to electrons. For instance, impurity ions can be, and often are, the charge carrying entities.⁵⁷ For an ion, the ionic mobility, μ_m is defined as the drift velocity, \underline{v} , per unit electric field, \underline{E} :

$$\underline{v} = \mu_m \underline{E} . \quad (2.3)$$

If n is the concentration of charge carriers, each transporting a charge, q , then the current density vector \underline{J} is given by

$$\underline{J} = q n \underline{v} \quad (2.4)$$

which becomes, upon substitution of $\underline{v} = \mu_m \underline{E}$

$$\underline{J} = q n \mu_m \underline{E} . \quad (2.5)$$

This is equivalent to Eq. (2.2), since by definition the conductivity, σ , is expressed as the ratio of the current density, J , to the electric field, E , then

$$\sigma = q n \mu_m . \quad (2.6)$$

If μ_m and n are independent of E , then Ohm's law applies. Equation (2.6) is the same as Eq. (2.2), but in this case, μ_m is the mobility of ions as opposed to electrons.

It is evident that more than one species of charge carriers may be present--electrons, holes, and positive or negative ions of several types may all contribute to the conductivity. To formulate a general equation, let i different species of carriers be present, each species in a concentration of n_i . The charge of each species is designated as q_i which is also equivalent to $z_i e$ where z_i is the valence of the i th species of charge carrier. Each species, i , also possesses a mobility μ_i . Assuming that the law of independent migration holds, i.e., there is negligible interaction between different carrier species so that each carrier species moves as if the others were absent, the total conductivity of the medium can be written as

$$\sigma = \sum_{i=1}^m [q_i n_i \mu_i] = \sum_{i=1}^m [z_i e n_i \mu_i] \quad (2.7)$$

where the summation is extended over all species of carriers. This equation holds only as long as the law of independent migration holds. The validity of this law is mainly determined by carrier densities, and in fact, would be ultimately a consideration even for a single type of charge carrier.

The mobility, μ , may be different for different spatial directions in an anisotropic medium. This leads to anisotropy in the conductivity. Thus, the mobility and conductivity may have to be expressed in tensor form.

$$\sigma_{\approx} = \sum_{i=1}^n [q_i n_i \mu_{\approx i}] \quad (2.8)$$

For just one species of carrier this can be written as

$$\underline{\sigma} = qn \begin{pmatrix} \mu_{11} & \mu_{12} & \mu_{13} \\ \mu_{21} & \mu_{22} & \mu_{23} \\ \mu_{31} & \mu_{32} & \mu_{33} \end{pmatrix} \quad (2.9)$$

where

$$\underline{\sigma} = \begin{pmatrix} \sigma_{11} & \sigma_{12} & \sigma_{13} \\ \sigma_{21} & \sigma_{22} & \sigma_{23} \\ \sigma_{31} & \sigma_{32} & \sigma_{33} \end{pmatrix} \quad (2.10)$$

The axial conductivity is designated as σ_{11} while σ_{22} and σ_{33} are the transverse conductivities. Usually a principal conductivity coordinate system is assumed, so that only the diagonal elements are needed to describe the conductivity.

Physical insight into the conductivity of polymers can be gained from the following calculations by using Eq. (2.6). A mobility value of 10^{-5} cm²/V-sec is used which is found for ionic carriers in hydrocarbon liquids at room temperature. The values of mobilities in solid polymers would surely be smaller, but by no more than a factor of 10^3 or so for small ions. For conductivities ranging from 10^{-8} S/cm to 10^{-16} S/cm and where the ions carry a unit electronic charge, i.e., 6×10^{-19} C, the carrier densities can be calculated and are listed in Table 2.1.

Table 2.1
Carrier Concentration for Given Conductivity
Values for $\mu = 10^{-5} \text{ cm}^2/\text{V-sec}$
and Unit Electronic Charge

<u>Conductivity (S/cm)</u>	<u>Carrier Concentration (cm^3)</u>
10^{-8}	6×10^{15}
10^{-10}	6×10^{13}
10^{-12}	6×10^{11}
10^{-14}	6×10^9
10^{-16}	6×10^7

A polymer with a molecular weight of 10^6 has approximately 12×10^{18} end groups per cubic centimeter.²⁵ Thus, we see that even for a conductivity of 10^{-8} S/cm , the concentration of charge carriers necessary for conduction is still less than the number of possible ion sources, i.e., $6 \times 10^{15} - 12 \times 10^{18} \approx 5 \times 10^{-4}$, presuming that the number of ion sources is the same as the number of end groups. Thus, ions as a source of charge carriers is not only possible, but probable. When taken in conjunction with any electronic charge carriers, it is seen that the overall conductivity can be easily accommodated. The question then becomes what is happening in the polymer that causes the conductivity to be low when compared to the number of charge carriers available.

2.2 Ionic Conduction in Polymers

2.2.1 Introductuion to Ionic Conduction: General Concepts

There are a number of reasons for assuming that at least some of the electrical conduction in polymers is due to ionic movement. For example, in the most highly insulating polymers, electrons are tightly bound to individual atoms and molecules and yet there exists a measurable current flow in these materials. Deviations from Ohm's law have also been rationalized as evidence for ionic conductivity, however, deviations from Ohm's law can arise from other causes as well.

There are some polymeric systems where ionic conductivity is fairly well substantiated. Such polymers contain ions (ionomers, polyelectrolytes), or possess groups capable of ionizing or have ionic materials already added to them. Water plays an important role in electrical conduction by acting as a source for ions, as a high-dielectric constant impurity, as a plasticizer, or as a local structure modifier (see Figure 2.7).

The most definitive evidence for ionic conduction is detecting electrolysis products formed on the discharge of ions upon arrival at the electrode. This was the method Seanor⁵⁸ used in determining that a form of ionic conduction occurred in nylon 6,6. It was found that at temperatures in excess of 120°C, the quantity of gas evolved was about half that calculated for protonic conduction alone. Figure 2.8

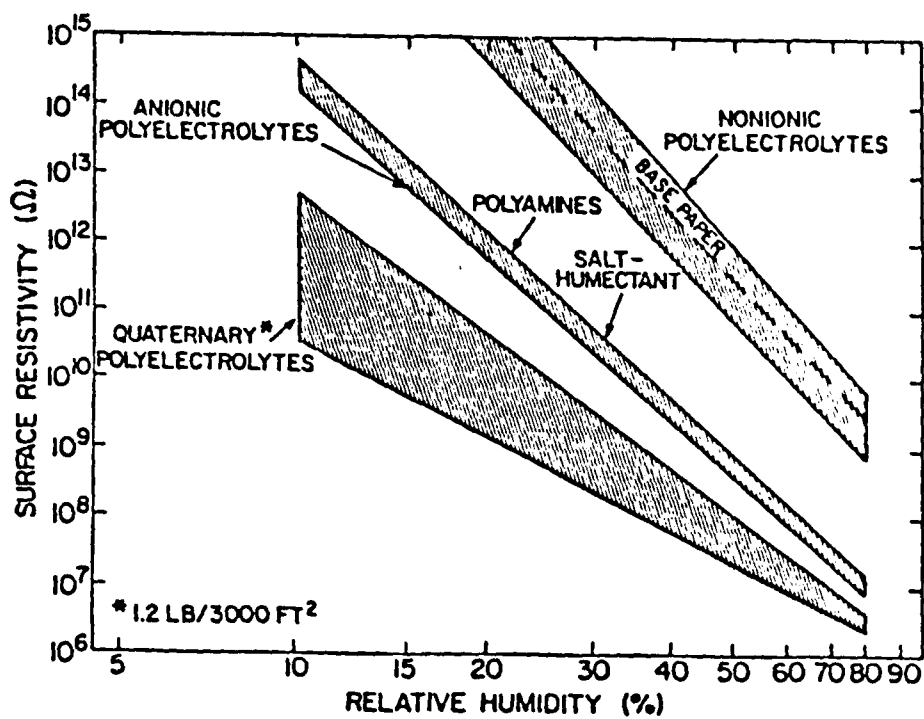
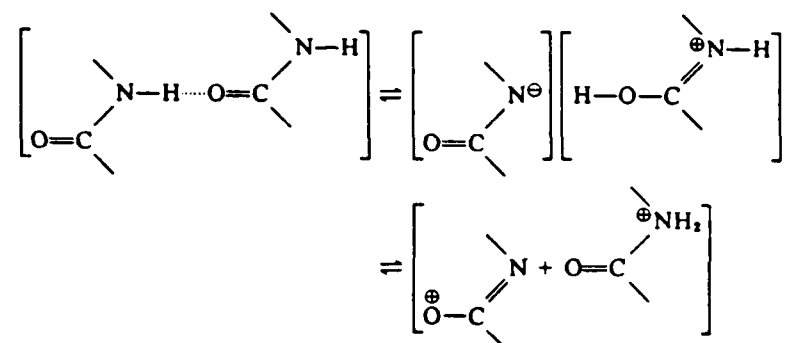
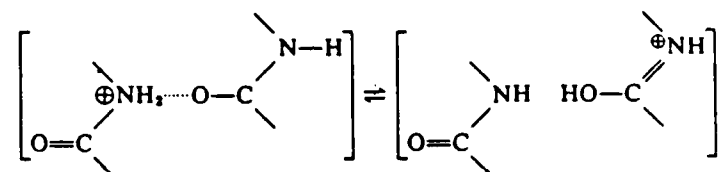


Figure 2.7. Surface Resistivity of Groups of Polyelectrolytes as a Function of Relative Humidity. The Particular Anions and Cations Also Play Important Roles.⁵⁹

Self-ionization:



Proton transfer:



Transfer of proton and electron:

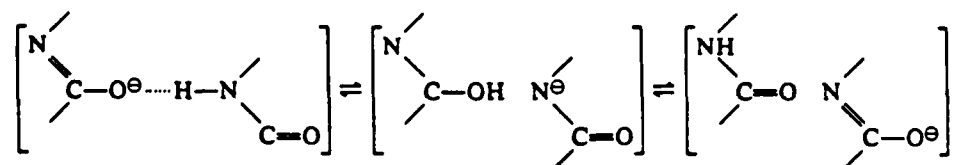


Figure 2.8. Proton Conduction Mechanism in Dissociation of Hydrogen Bonded Amide Group: (a) Self Ionization; (b) Proton Transfer; and (c) Transfers of Proton and Electron. (Mechanism Proposed by Seanor to Account for Ionic Conduction in Nylon 6,6).⁵⁵

illustrates the proton-conduction mechanism proposed involving the self-dissociation of hydrogen bonded amide groups followed by bond rearrangement. Unfortunately, the low levels of electrical conduction makes gas detection difficult. At a conductivity of 10^{-11} S/cm, a relatively high value for insulating polymers, 100 V applied across a specimen 1 cm^2 in area and 0.1 cm thick would only produce about 10^{-5} cm^3 of gas at NTP per hour.³⁰

Crowley et al.⁶⁰ studied silver ion (Ag^+) migration in ion exchange sulfonated polystyrene. Figure 2.9 presents data on conductivity, Ag^+ mobility and Ag^+ concentration as a function of water concentration. Above 2% by weight of water, ion mobility increases suggesting plastification of the polymer is important.

Sodolski^{61,62} has studied ionic conduction in a polyester polymer doped with 0.5 w/o of rhodamine 6G. As a result of rhodamine dissociation, the Cl^- anion and the colored cation are generated. The movement of the colored cation can be followed under certain conditions more easily above T_g and is found to accumulate at the proper electrode. The doping of the polyester with rhodamine also increases the conductivity over the undoped polyester. This is shown in Figure 2.10.

Additionally, Wallace^{63,64} has studied the conductivity of sulfonated polystyrene and has related ion content, ion mobility and water content in this material. Water aids the dissociation process, as well as increasing ion mobility at

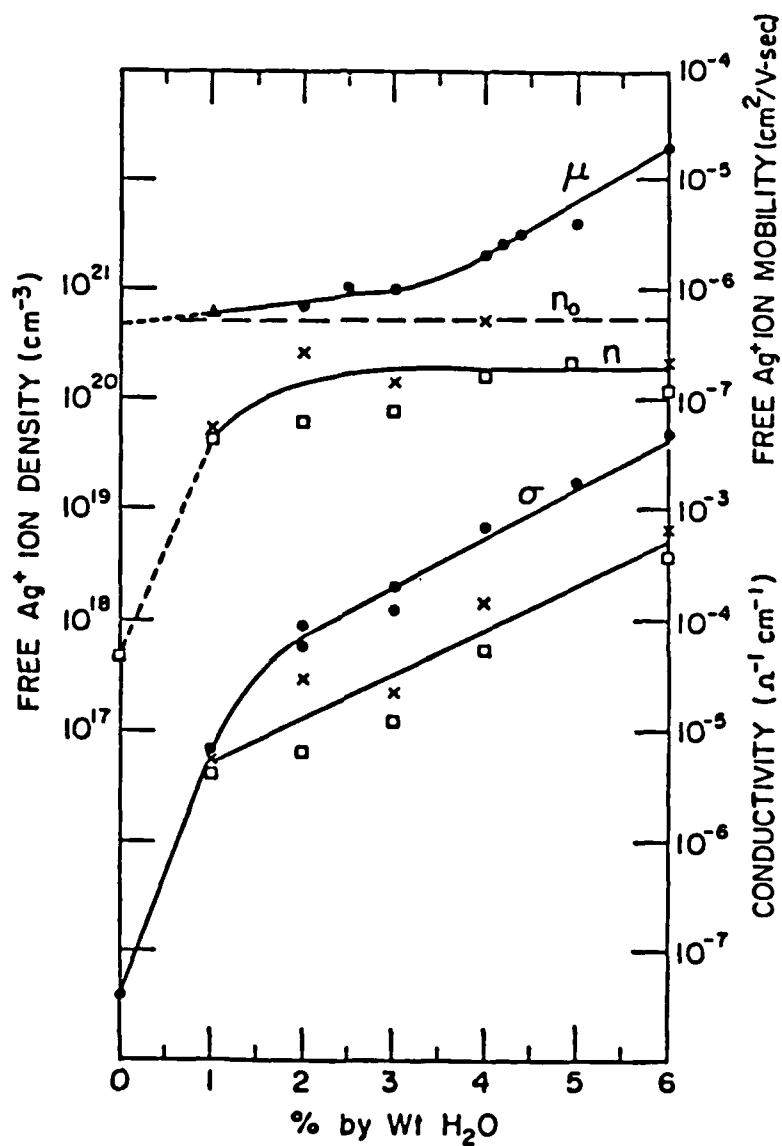


Figure 2.9. Free Ion Mobility, Carrier Density, and Conductivity as a Function of %H₂O by Weight for Ag⁺ Counterion Sample at 300K. (●) High Voltage (> 2.0 V) dc Measurements; (x) low voltage (< 2.0 V) dc Measurements; (□) ac Measurements; (Δ) Mobility Measurements Requiring the Low-Water-Content Technique.⁶⁰

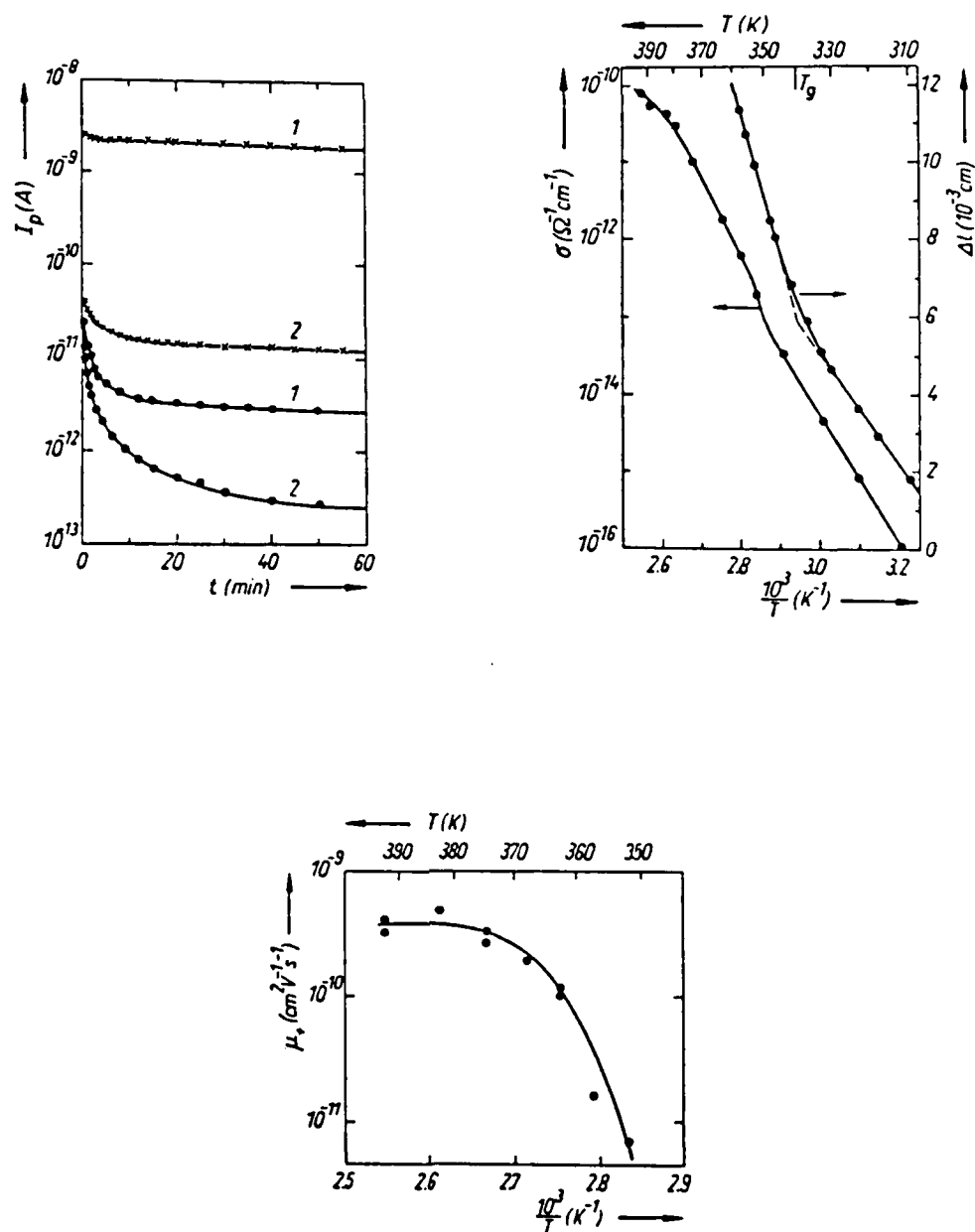


Figure 2.10. Effect of Rhodamine Doping on Polyester Polymer: (a) Electrical Conductivity Changes (●) Undoped Polymer, (x) Polymer with 0.5 w/o Rhodamine 6G, (1) $T = 333K$, (2) $T = 313K$ ($E = 6 \times 10^4$ V/cm); (b) Temperature Dependence of the Electrical Conductivity and Thermal Expansion -- $\sigma = J$ (10 min)/ E , $E = 10^4$ V/cm; (c) Temperature Dependence of Cation Mobility.^{61,62}

higher levels of moisture content. Figure 2.11 compares activation energy for conduction in dry polystyrene membranes as a function of the cube of the hydrated radius of the counter ion. The values of activation energy and the hydrated ion radius are shown in the accompanying table included in the figure. The figure shows that a linear relation exists between activation energy and ionic volume. The activation energy increases with increasing ionic size. Such a relationship was also found to exist in cellulose-acetate.⁶⁵

Barker and Thomas⁶⁵⁻⁶⁸ studied various aspects of moisture, ion sorption, and electric field strength on the conductivity and glass-transition of alkali-halide-doped cellulose acetate. Some general conclusions reached included the following ones. A moderate increase of moisture in the polymer resulted in a substantial increase in conductivity and an increase in the dielectric constant. Also, they reported a linear relationship between the activation energy for ionic conduction and the ionic volume. This is shown in Figure 2.12. It was hypothesized that ions also influenced the local structure of the polymer, thereby decreasing the available free volume. This leads to a relative decrease in conductivity as well as an increase in the local (but not macroscopic) glass transition in the cellulose acetate.

Moisture sorption plays an important role in the conduction process. A general relationship between moisture

Counterion	E_a (eV)	Hydrated Radius, Å
H ⁺	1.0	2.44
Li ⁺	1.06	2.50
Na ⁺	0.88	2.17
K ⁺	0.80	1.75
Rb ⁺	0.78	1.53
Cs ⁺	0.77	1.47
Ag ⁺	0.73	1.26

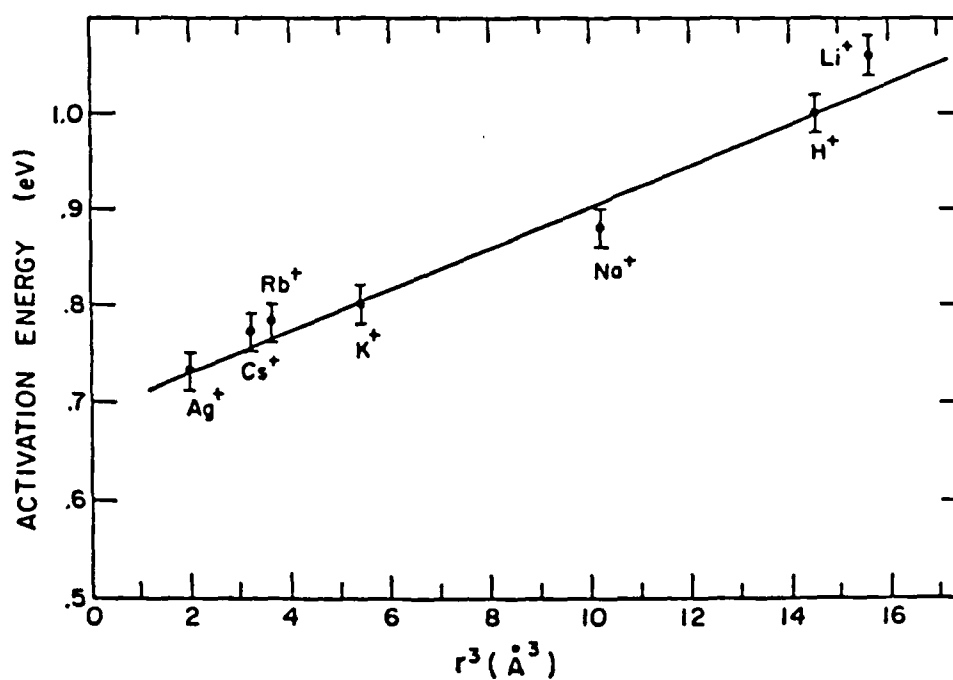


Figure 2.11. Activation Energy for Conduction in Dry Membranes as a Function of the Cube of the Hydrated Radius of the Counter Ion.⁶⁰

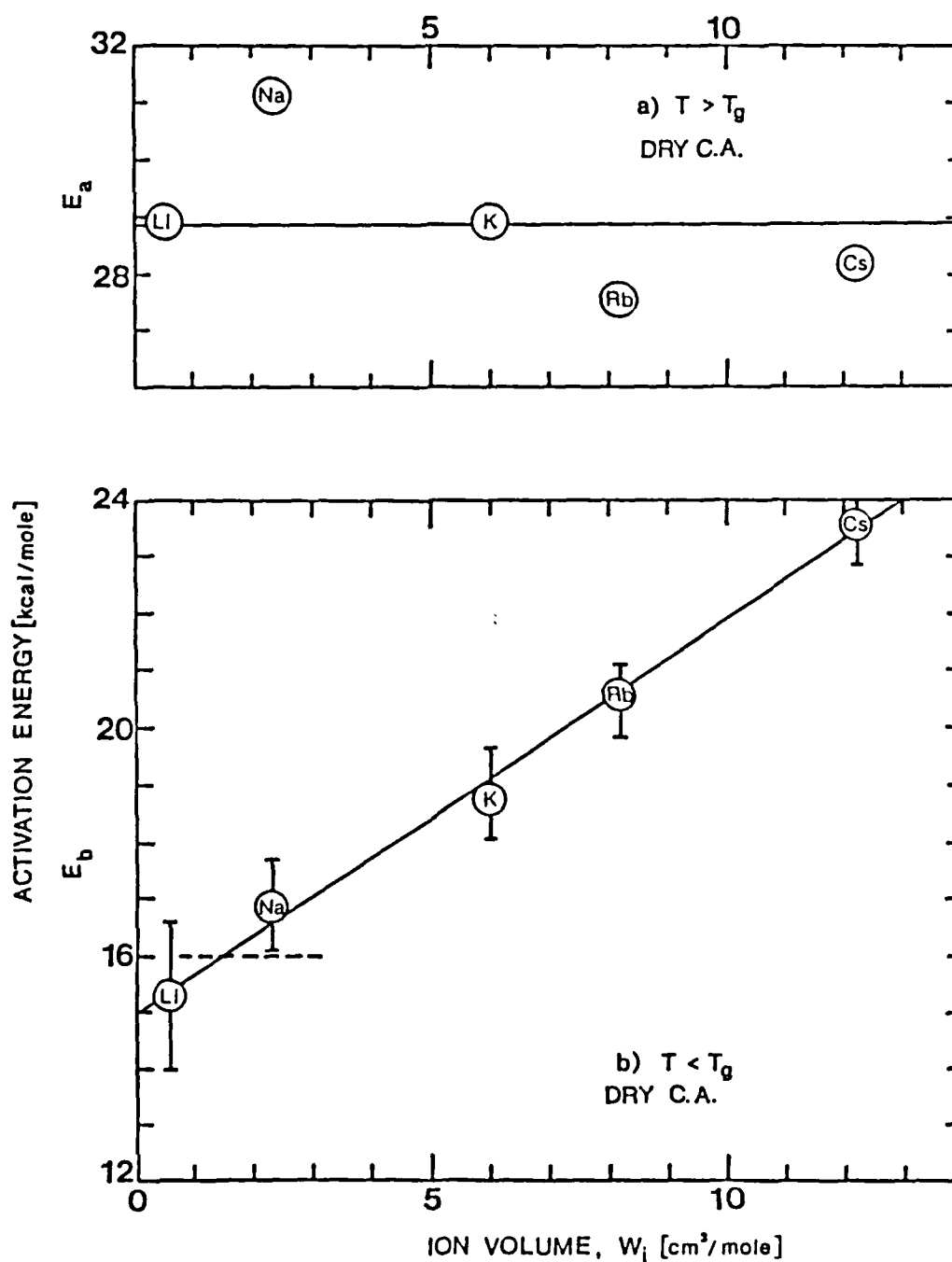


Figure 2.12. Activation Energies for Ionic Conduction of Alkali-Chloride Impregnated Cellulose Acetate, (a) Above T_g and (b) Below T_g vs. Alkali Ion Volumes. For the Undoped CA, $E_a \approx 29.3$ kcal/mole and $E_b \approx 11-16$ kcal/mole.^{65a}

content w_{ads} and conductivity proposed by Rosenberg⁶⁹ can be written as

$$\ln \sigma = \ln \sigma_{\text{dry}} + \alpha w_{\text{ads}} . \quad (2.11)$$

This relation is widely observed, where the dielectric constant is related to the water uptake when using an equation of the form

$$\alpha w_{\text{ads}} = A \left(\frac{1}{\epsilon_{\text{dry}}} - \frac{1}{\epsilon_{\text{wet}}} \right) . \quad (2.12)$$

Once again, α and A are constants and w_{ads} is the weight of the water per unit mass of polymer. The dielectric constant is given by ϵ . It should be noted that not all results agree with the form of Eq. (2.12). Data generated by Barker and Thomas⁶⁶ for wet and dry cellulose acetate did not fit the relationship in Eq. (2.12) although an equation similar to Eq. (2.11) was used.

One general conclusion of the effect of water on the conduction process is an increase in the effective dielectric constant. Moisture effects on the mechanical properties of most polymers indicate that some degree of plasticization occurs. One result of this may be that the charge-carrier hopping distance or mean path length increases. Water is also capable of acting as an electron donor and a source of charge carriers.²⁵ The complicated effect of moisture is illustrated by the data of Rancourt et al.⁷⁰ in Figure 2.13. Lithium-doped polyimide

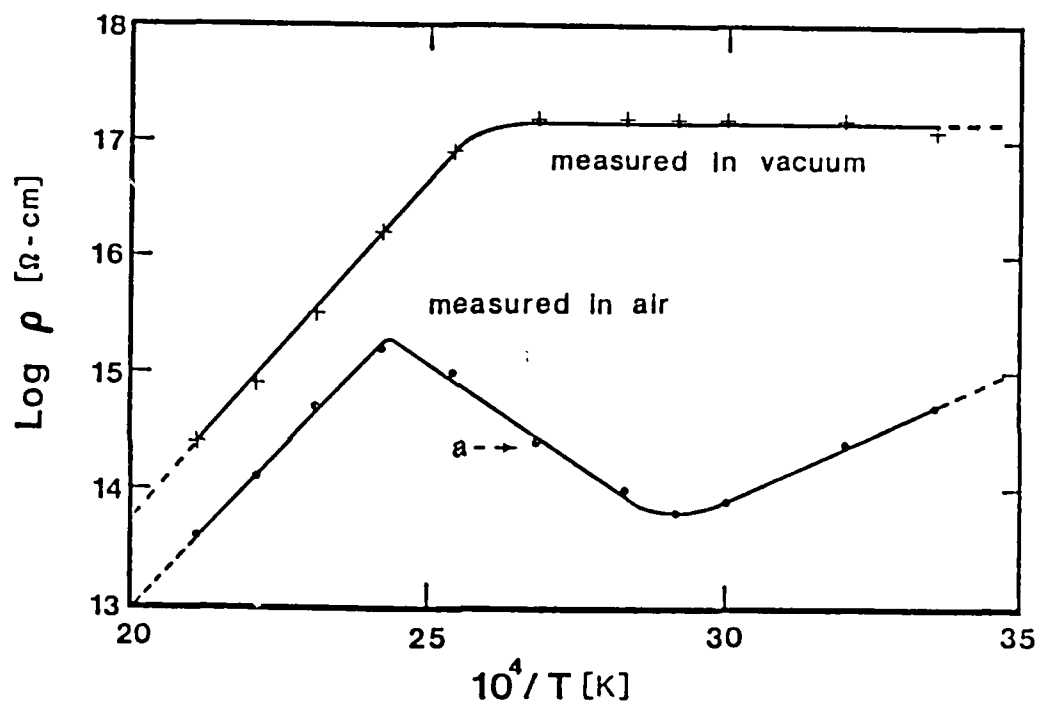


Figure 2.13. Three Probe Variable Temperature Electrical Resistivity of Lithium Containing Polyimide Film Measured in Air (\odot) and Vacuum (+). Region "a" Attributed to Evolution of H_2O From Polyimide Film During Test Due to Increasing Temperature.⁷⁰

conditioned in air exhibits a larger conductivity than the vacuum conditioned film.

Usually, the intentional addition of ions to polymers enhance the conductivity over and above that observed for the undoped polymer. This would probably be the general case if completely pure ion-free polymers were available for the reference states. Studies have verified that there is actual mass transport by the motion of ions. In addition, these effects are enhanced to a greater extent if moisture is available.

2.2.2 Equations Used in Describing Ionic Conductivity in Polymers

Weak Electrolyte Model

Evidence favoring ionic conduction is provided by a strong correlation between dielectric constant and conductivity. This is explained by the reduction of Coulombic forces between ions in a high dielectric constant medium. Barker and coworkers have looked into the dissociation process of "weak electrolytes" both in solid polymers^{66,71} and liquids.⁷² Following the theoretical development of Barker,^{66,71,72} most possible ionic contaminants (in the parts per million range) in polymers are expected to be 1:1 type electrolytes. There are also a number of multivalent ions which might occur including Ca^{2+} , Cu^{2+} , SO_4^{2-} . A general form of the mass action relation is useful and can be written as

$$X_{v+}^{2+} \cdot Y_{v-}^{2-} = [\nu_+] X^{2+} + [\nu_-] Y^{2-} \quad (2.13)$$

which also may be represented as

$$n_0 (1-\phi) = [\nu_+] n_0 \phi + [\nu_-] n_0 \phi \quad (2.14)$$

When $\nu_+ = \nu_- = 1$ and $z_+ = z_- = 1$, the equilibrium coefficient $K_{1:1}$ becomes

$$K_{1:1} = \frac{\gamma^2 \phi^2 n_0}{(1-\phi)} \quad (2.15)$$

where $\gamma = (\gamma_+ \gamma_-)^{1/2}$ and is the geometric mean of the activity coefficients and ϕ is the fractional dissociation of n_0 associated pairs per unit volume. By assuming an approximation where $\phi \ll 1$, the result

$$K_{1:1} \approx \phi^2 \gamma^2 n_0 \quad (2.16)$$

is obtained, which upon rearrangement, becomes

$$\phi \approx \left(\frac{K}{\gamma^2 n_0} \right)^{1/2} \quad (2.17)$$

This allows the conductivity to be written as

$$\sigma = e n_0^{1/2} \left(\frac{K}{\gamma^2} \right)^{1/2} (\mu_+ + \mu_-) \quad (2.18)$$

This is equivalent to

$$\sigma = e \left(\frac{n_0}{\gamma^2} \right)^{1/2} (\mu_+ + \mu_-) \exp \left(\frac{-e^2}{2\epsilon_{eff} s k_B T} \right) \exp \left(\frac{-B_m}{2k_B T} \right) \quad (2.19)$$

when the chemical equilibrium constant K is replaced by

$$K = \exp \left(\frac{-\Delta G}{k_B T} \right) = \exp \left(\frac{-\Delta U}{k_B T} \right) \exp \left(\frac{-p\Delta V}{k_B T} \right) \exp \left(\frac{\Delta S}{k_B} \right) \quad (2.20)$$

Another way of expressing Eq. (2.20) is by

$$\Delta G \approx \frac{e^2}{S\epsilon_{\text{eff}}} + B_m \quad (2.21)$$

where the pressure-volume and entropy terms are contained in B_m . To a first approximation, let $\epsilon'_{\text{eff}} = \epsilon'$ and $U'_0 = e^2/s$. U'_0 is the energy required to completely dissociate ions in a vacuum. Thus,

$$\sigma = e \left(\frac{n_0}{\gamma^2} \right)^{1/2} (\mu_+ + \mu_-) \exp \left(\frac{-U'_0}{2\epsilon' k_B T} \right) \exp \left(\frac{-B_m}{2k_B T} \right) \quad (2.22)$$

It follows that $\ln \sigma$ is a linear function of $1/\epsilon'$ and also of $1/T$, and that σ is proportional to the square root of the "salt" concentration. Link⁷³ has shown (see Figure 2.14) that $\ln R$ versus $1/\epsilon T$ is a linear function. The empirical relation used by Link also incorporates the effect of moisture in an indirect manner through changes in the dielectric constant. Figure 2.15 shows the change in dielectric constant with temperature and relative humidity. Thus, the presence of ϵ' in the exponent of Eq. (2.22) means that it can exert a strong influence on the conductivity.

Field Dependence of Ionic Conductivity

From other studies on the dependence of current on applied voltage, further evidence of ionic conduction may be obtained. Mott and Gurney⁷⁴ have derived a theoretical expression from a simple model of two ions in adjacent potential wells separated by a distance λ ; Figure 2.16(a) depicts this condition. The unit motion of an ion in the

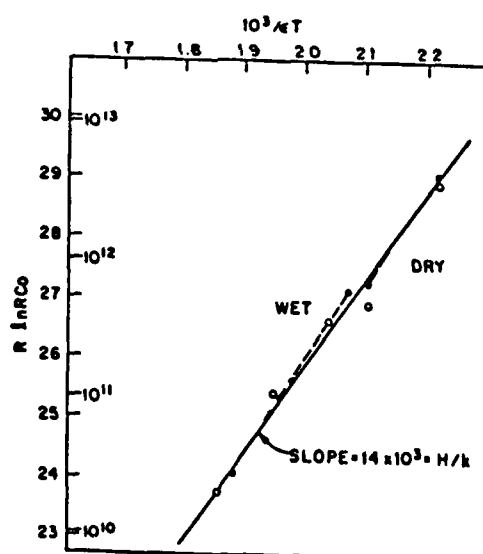
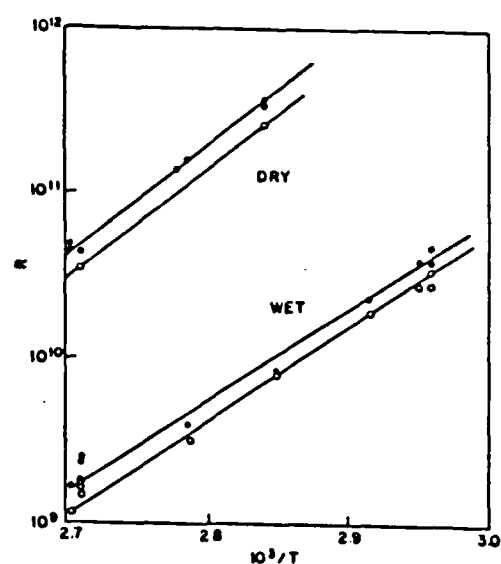


Figure 2.14. (a) $\log R$ Versus $1/T$ for Wet (74% RH) and Dry Epoxy Impregnated Polyester/Polyamide Fiber Mat. (b) $\log R$ Versus $1/\epsilon T$ for Dry and Wet Composite of (a) Showing Linear Relationship.⁷³

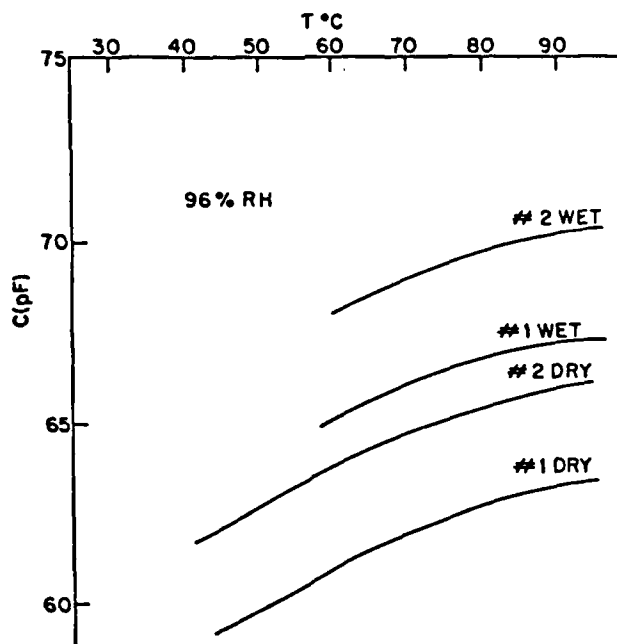
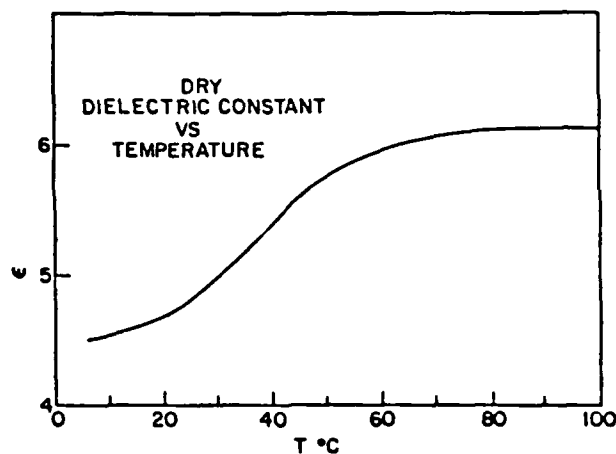


Figure 2.15. (a) Effect of Temperature on the Dry Dielectric Constant of Epoxy Impregnated Polyester/Polyamide Fiber Mat. (b) Effect That Humidity has on the Dielectric Constant of (a) Over a Range in Temperatures.⁷³

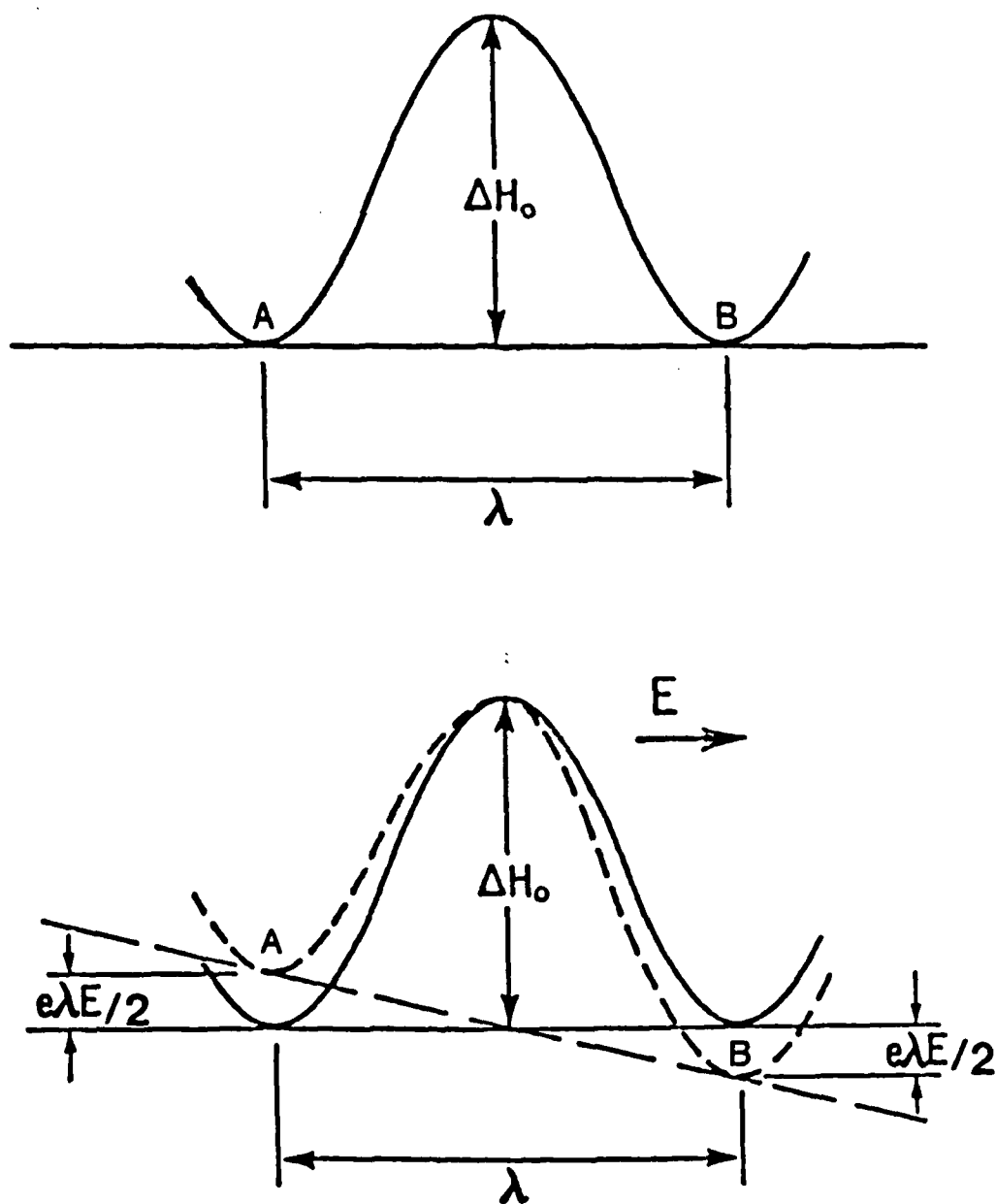


Figure 2.16. Two Potential Well Model of Ion Migration (a) Ordinary Case and (b) With Application of an External Electric Field.

absence of an applied electric field is a jump within the matrix of polymer molecules. The energy of sites A and B is equal so that the number of ions contained in each site is the same. Now in order for the ions to move from one well to the other, there must be sufficient thermal energy available from the surrounding environment for the ion to jump the energy barrier of height ΔH_0 . In accordance with Boltzmann statistics, the probability per second that an ion jumps from site A to B can be written as

$$\Gamma = \nu \exp\left[\frac{-\Delta H_0}{k_B T}\right] \quad (2.23)$$

where ν is the vibrational frequency of the ions within their potential energy wells. Under equilibrium conditions and in the absence of an external electric field, ions jump continuously between A and B.

Figure 2.16(b) illustrates the case where an external electric field is applied. The ions in site A will now see a potential barrier of $(\Delta H_0 - \frac{1}{2}e\lambda E)$, whereas those in B face a larger barrier equal to $(\Delta H_0 + \frac{1}{2}e\lambda E)$ assuming that the charge on the ions equals the electronic charge, e . Subsequently, the ions will prefer to locate themselves in site B. The resultant probability of an ion moving from A to B is now given as

$$\Gamma_{AB} = \nu \exp\left[-\frac{(\Delta H_0 - e\lambda E/2)}{k_B T}\right] \quad (2.24)$$

or in terms of Eq. (2.23)

$$\Gamma_{AB} = \Gamma \exp\left[\frac{e\lambda E}{2k_B T}\right] \quad (2.25)$$

The net probability for a jump in the direction of the applied field is given as

$$\Gamma_{AB} = 2\nu \left[\exp\left(\frac{\Delta H_0}{k_B T}\right) \sinh\left(\frac{e\lambda E}{2k_B T}\right) \right] \quad (2.26)$$

The average drift velocity, v_{drift} , is just $\lambda \Gamma_{AB}$ or

$$v_{\text{drift}} = 2\nu\lambda \exp\left(\frac{\Delta H_0}{k_B T}\right) \sinh\left(\frac{e\lambda E}{2k_B T}\right) \quad (2.27)$$

and the mobility, μ , is

$$\mu = \frac{v_{\text{drift}}}{E} = \frac{2\nu\lambda}{E} \exp\left(\frac{\Delta H_0}{k_B T}\right) \sinh\left(\frac{e\lambda E}{2k_B T}\right) \quad (2.28)$$

At small fields, $\sinh(e\lambda E/2k_B T) \approx e\lambda E/2k_B T$, and the mobility can be written as

$$\mu \approx \frac{\nu\lambda^2 e}{k_B T} \exp\left(\frac{\Delta H_0}{k_B T}\right) \quad (2.29)$$

Thus, at low fields, the mobility is very nearly independent of the applied field. Letting $x = e\lambda E/k_B T$, the limitation $x \ll 1$ implies that fields be less than 10^4 V/cm, since λ is on the order of the size of the microstructure (≈ 10 nm). At higher fields, the mobility becomes non-linear and it is conceivable that the potential wells will be distorted. The top of the barrier may be shifted significantly from the midpoint, thus requiring quantitative adjustment to the previous equations.⁷⁵

With the concentration of the ions proportional to $\exp(-U_0'/2\varepsilon'k_B T)$, the current density, J , flowing through a

specimen, across which an electric field has been applied, is given by

$$J \propto A' \sinh\left(\frac{X}{2}\right) \exp\left[\frac{1}{k_B T} \left(\frac{\Delta U_0}{2\epsilon'} + \Delta H_0 \right)\right] \quad (2.30)$$

or more simply as, at constant temperature,

$$J \propto A \sinh\left(\frac{X}{2}\right). \quad (2.31)$$

A similar expression for Ohm's law can be written as

$$J \approx A \left(\frac{X}{2}\right) \quad (2.32)$$

which applies in the low field approximation. For larger fields

$$J \approx \frac{A}{2} \exp\left(\frac{X}{2}\right). \quad (2.33)$$

Kosaki et al.⁷⁶ have measured electrical conduction in polyvinyl chloride and have applied this model to account for their experimental results. Figure 2.17 shows their results. Conclusions drawn from this plot suggest that ionic conduction dominates from low- to high-field regions. The ionic jump distance can also be deduced from this plot. The slope of the $\log J$ versus $\log E$ curves in the high-field region gives the value for λ . A more sensitive plot than the previous one is $\log J/E$ versus $\log E$ curve, and this is illustrated for the Kosaki data in Figure 2.18.

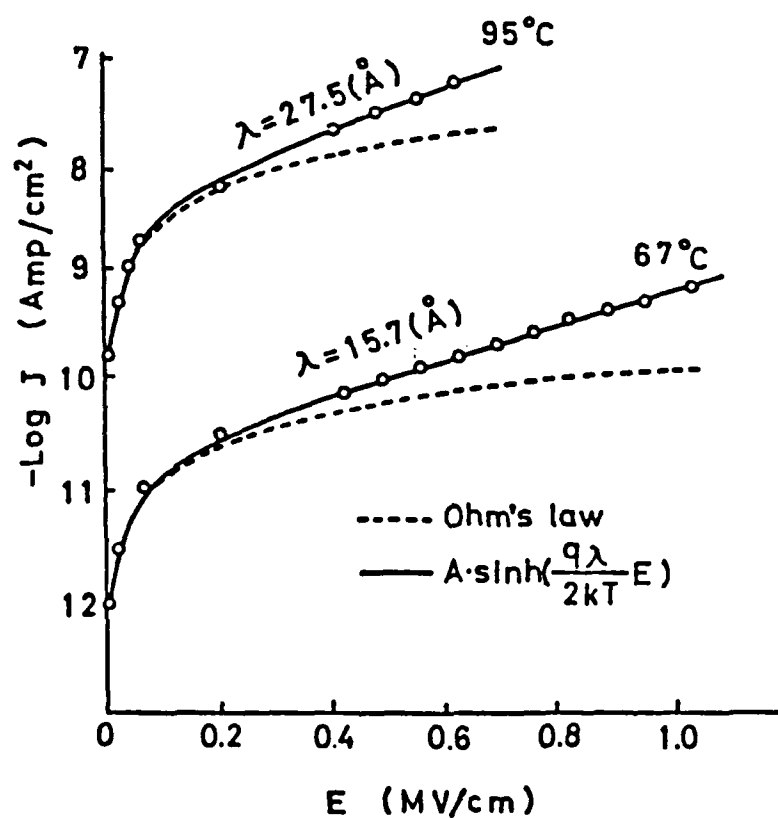


Figure 2.17. Current Density as a Function of Electric Field of Unplasticized Polyvinyl Chloride Below and Above the Glass Transition Temperature. λ is an Apparent Jump Distance of the Ion.⁷⁶

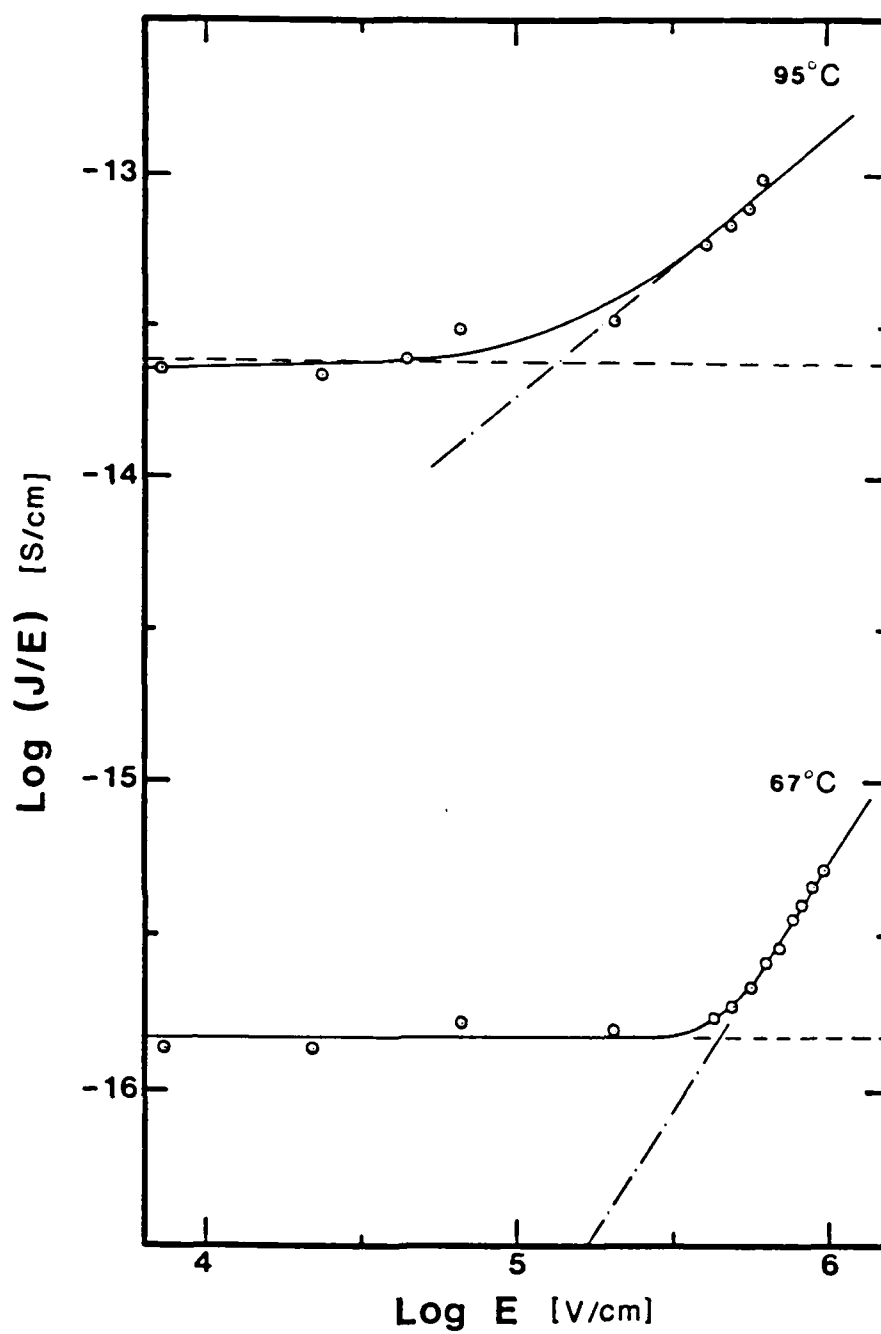


Figure 2.18. Replot of Data from Figure 2.17 in $\log J/E$ Versus $\log E$ format.

Free Volume Model for Ionic Conductivity

A feature which is common to most polymers is the change in the temperature dependence of conduction as the temperature is raised through the glass transition region. Miyamoto and Shibayama⁷⁷⁻⁷⁹ use the free volume concept to explain electrical conductivity based on the assumption that the movement of ions is regulated by the amount and distribution of free volume.

The frequency of transition of an ion from one equilibrium position to another depends on the probability of finding a hole produced by redistributing the free volume (i.e., P_h = probability of finding a hole) and also on the probability of jumping into the vacant hole (i.e., P_j = probability of jumping into a vacant hole). The frequency of transition Γ^* is given by

$$\Gamma^* = \nu \alpha_0 P_h P_j \quad (2.34)$$

where ν is the vibrational frequency of the trapped ion and α_0 is a correlation factor ($0 < \alpha_0 < 1$). At temperatures above T_g , it may be possible as an approximation to use the thermodynamic theory of liquids for the polymer. A theory attributed to Cohen and Turnbull⁸⁰ is used and based on the assumption that molecular transport in liquids occurs by the movement of molecules into holes with sizes greater than a critical value V^* formed by thermal fluctuations of the free volume without energy. Thus the probability of finding a hole with size greater than V_i^* is given by

$$P_h = \exp\left(-\frac{\gamma^* V_l^*}{V_f}\right) \quad (2.35)$$

where γ^* is a numerical factor which corrects for overlap of the free volume V_f .

The probability of a jump into V_l^* by surmounting a potential barrier of height ΔH_j can be expressed by

$$P_j = \exp\left(-\frac{\Delta H_j}{k_B T}\right) \quad (2.36)$$

The jump frequency, Γ^* , is given by

$$\Gamma^* = \nu \alpha_0 \exp\left(-\frac{\gamma^* V_l^*}{V_f}\right) \exp\left(-\frac{\Delta H_j}{k_B T}\right) \quad (2.37)$$

As discussed earlier, for positive ions the height of ΔH_j decreases in the direction of the applied field E (at the frequency Γ^*) and the apparent jump energy is equal to $\Delta H_j^0 - \frac{1}{2} e \lambda E$. Conversely, the height of the energy barrier for a positive ion increases in the reverse direction to the field (at frequency Γ^*) where the apparent jump energy is equal to $\Delta H_j^0 + \frac{1}{2} e \lambda E$. The mean velocity, \bar{v} , is given by

$$\bar{v} = \lambda (\Gamma_+^* - \Gamma_-^*) \quad (2.38)$$

thus allowing the current density, J , to be written as

$$J = n e \lambda (\Gamma_+^* - \Gamma_-^*) \quad (2.39)$$

where n is the concentration of ions as expressed in the Barker-Sharbaugh "weak electrolyte theory." With

$$n = \left(\frac{K_0}{\gamma^2}\right)^{1/2} n_0^{1/2} \exp\left(-\frac{U_0}{2\epsilon k_B T}\right) \quad (2.40)$$

the equation for current density, Eq. (2.39), can be rewritten using Eqs. (2.37) and (2.40) as

$$J = \frac{2\nu\alpha_0 e\lambda}{\gamma} [K_0 n_0]^{1/2} \sinh\left(\frac{x}{2}\right) \exp\left(-\frac{[(U_0/2\epsilon') + \Delta H_j^0]}{k_B T} - \frac{\gamma^* V^*}{V_f}\right). \quad (2.41)$$

The conductivity becomes

$$\sigma = \frac{2\nu\alpha_0 e\lambda}{\gamma E} [K_0 n_0]^{1/2} \sinh\left(\frac{x}{2}\right) \exp\left(-\frac{[(U_0/2\epsilon') + \Delta H_j^0]}{k_B T} - \frac{\gamma^* V^*}{V_f}\right). \quad (2.42)$$

Incorporated in the K_0 term is the contributions of entropy and pressure-volume.

Plots of data from Miyamoto and Shibayama⁷⁸ are shown in Figure 2.19 for $\log \sigma + \gamma^* V_f^*/2.303 V_f$ versus $1/T$ and $\log \sigma$ versus $1/T$. The apparent activation energy obtained from the slope of the curve in Figure 2.19(b) corresponds to the hybrid energy of the ionic jump energy and the ionic dissociation energy. They also concluded that transport of ions in the rubbery polymer is strongly affected by the free volume.

Diffusion Mechanism of Ionic Carriers Using Free Volume Model

Following Watanabe et al.,⁸¹⁻⁸⁴ suppose the charge carriers in a polymer are only generated from the incorporated salt complex (lithium perchlorate, LiClO_4 , in this instance). In the equation for conductivity

$$\sigma = n e (\mu_+ + \mu_-) \quad (2.43)$$

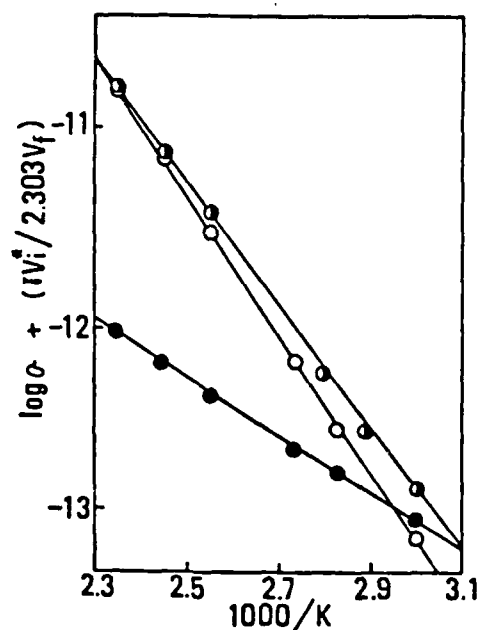
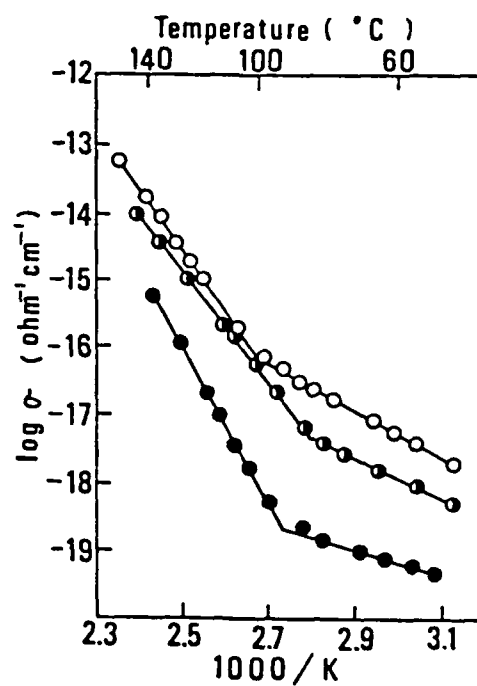


Figure 2.19. (a) Arrhenius Plots of Electrical Conductivity and (b) Plots of $\log \sigma + \gamma V_i^2 / 2.303 V_f$ Versus Reciprocal Temperature. Plot in (b) is Linear Over Entire Temperature Region and Slope of Line Corresponds to a Hybrid Activation Energy--Ionic Jump Energy and Ionic Dissociation Energy. (\circ : PMMA; \bullet : PS.)⁷⁸

μ_+ and μ_- correspond to the ionic mobilities of Li^+ and ClO_4^- respectively. Referring to Figure 2.20, if μ_+ and μ_- differ appreciably from each other, the time dependence of the current may have two peaks, corresponding to time of flight of carriers, τ , from one electrode to the other of cation and anion. However, as seen in Figure 2.20, only one current peak at each temperature was observed. Two interpretations of the observed result are readily apparent. One is based on the premise that μ_+ and μ_- are nearly equal. Thus, the peak appearing at τ reflects the combined mobility of μ_+ and μ_- . The second interpretation is that the value of τ corresponds to the time of flight of Li^+ only. Since solvation effects of ions may be negligible in the polymer matrix, the smaller radius of Li^+ makes its ionic mobility larger. (This assumes there is no hydration or similar phenomena affecting the ion.) Additionally, the peak based on the flight of the anion (ClO_4^-) may be hindered by the current of the cation (Li^+) migration. Thus, μ may be seen to represent either similar μ_+ and μ_- or only μ_+ . This is seen in Figure 2.21(a), a plot of the temperature dependence of ionic mobility for polypropylene oxide (PPO) - lithium perchlorate (LiClO_4) complexes. The mobility value of $10^{-6} - 10^{-5} \text{ cm}^2/\text{V-sec}$ is relatively high for ions in solvent-free polymers.

The ionic mobility, μ , is related to the ionic diffusion coefficient, D , by the Nernst-Einstein-Townsend (NET) relation by

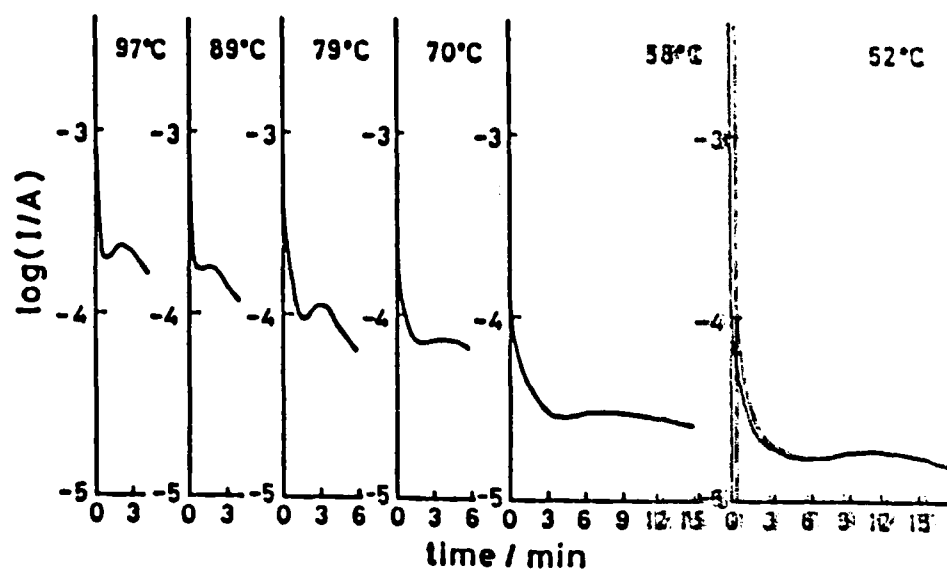


Figure 2.20. Change in Current With Time After Application of dc 2.5V for 15-60 Minutes in One Direction and the Reversal of the Applied Voltage Polarity for the Poly(propylene Oxide)(PPDO) Lithium Perchlorate (LiClO_4) Complex ($[\text{LiClO}_4]/[\text{PO unit}] = 0.075$) at Various Temperatures.⁸¹

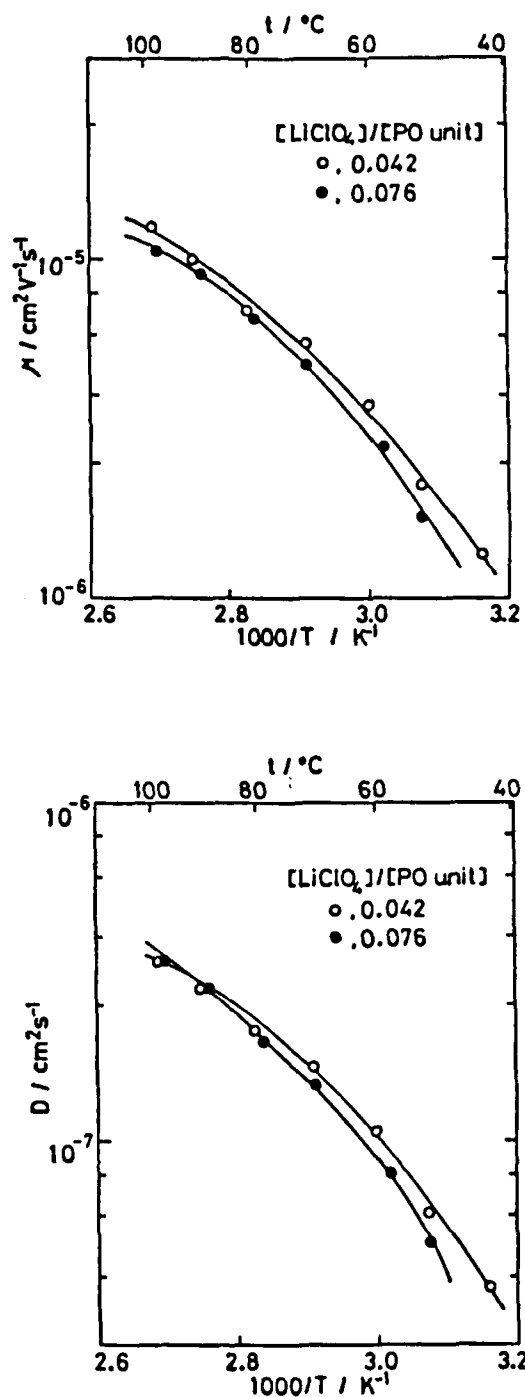


Figure 2.21. (a) Temperature Dependence of Ionic Mobility for PPO-LiClO₄ Complexes and (b) Temperature Dependence of Ionic Diffusion Coefficient for PPO-LiClO₄ Complexes.⁸¹

$$\mu = \frac{z e D}{k_B T} \quad (2.44)$$

Figure 2.21(b) shows the temperature dependence of D for PPO-LiClO₄. The diffusion of small particles in polymers at temperatures above T_g is expressed theoretically by the Cohen-Turnbull⁸⁰ equation. Thus

$$D(T) = D^* \exp\left(-\frac{\gamma V_i^*}{V_f}\right) \quad (2.45)$$

where D^* is a constant (i.e., $D^* = ga^*u$, where g is a geometric factor, a^* is approximately equal to the molecular diameter of the ion, and u is the gas kinetic velocity of an ion confined to a cage) and the other symbols have the same meaning as in Eq. (2.35). This equation increases with temperature above T_g which is seen by using the expansion coefficient of the free volume, α_f , as follows:

$$V_f = V_g[f_g + \alpha_f(T - T_g)] \quad (2.46)$$

where f_g is the free volume fraction at T_g and V_g is the specific volume at T_g . Substitution of Eq. (2.46) into Eq. (2.45) yields

$$\log\left(\frac{D(T)}{D(T_g)}\right) = \frac{C_1(T - T_g)}{C_2 + (T - T_g)} \quad (2.47)$$

which is the Williams-Landel-Ferry (WLF) equation⁸⁵ for D . The parameters C_1 and C_2 can be expressed as

$$C_1 = \frac{\gamma^* V_i^*}{2.303 V_g f_g} \quad (2.48)$$

$$C_2 = \frac{f_g}{\alpha_f} . \quad (2.49)$$

Watanabe⁸¹ found that Eq. (2.45) represented very well the change in D with temperature. He concluded that carrier ions in the PPO networks move from one site to another site when they find holes large enough to occupy. The formation of the hole depends upon the magnitude of V_f , since large V_f facilitates the micro-Brownian motion of the PPO chains and the probability of the redistribution of V_f is determined by the rate of segmental motion of the PPO chain. A correlation exists between ionic carriers and segmental motion.

Thus a temperature dependence of conductivity at temperatures above the critical temperature, i.e., in the rubbery state, can be developed from μ and n for polymers containing a monovalent salt. The diffusion mechanism of ionic carriers is based on the free volume theory represented by Eq. (2.45). The dissociation theory for weak electrolyte solutions is based on Eq. (2.40), and can be adopted for carrier generation. Combining Eqs. (2.43)-(2.45) and Eq. (2.40), the following result is obtained:

$$\sigma = \frac{ze^2 D^*}{\gamma k_B T} (K_0 n_0)^{1/2} \exp \left(\frac{-U_0}{2\epsilon k_B T} - \frac{\gamma V_i^*}{V_f} \right) . \quad (2.50)$$

This can be modified by replacing V_f with the expression obtained in Eq. (2.46). Thus

$$\sigma = \frac{ze^2 D^*}{\gamma k_B T} (K_0 n_0)^{1/2} \exp \left(\frac{-U_0}{2\epsilon k_B T} - \frac{\gamma V_i^*}{V_g [f_g + \alpha_f (T - T_g)]} \right) . \quad (2.51)$$

The first and second terms in the exponential of Eq. (2.51) correspond to the Arrhenius activation process for carrier generation and the free volume process for carrier mobility, respectively.

Summary

A number of equations have been developed to account for ion generation and mobility in polymers both above and below the glass transition. A number of variables have been considered, including the effects of an applied electric field as well as the case of available free volume in the polymer, which would affect the overall conductivity. The equation which provides the best results ultimately depends on the detailed information obtained about the polymer during the experiments and in the quality of the estimates of any unknown variables. Furthermore, some of the assumptions used in deriving these equations may be overly ambitious and minor corrections may be necessary to allow it to achieve broader validity. One problem in visualizing polymers as viscous fluids is dealt with in Appendix A. This is the failure (partial) of Walden's rule for solid amorphous polymers.

2.2.3 Local Structure Hypothesis

Although the discussion of Barker's²⁰ "local structure hypothesis is aimed mainly at the effect that ions have on a polymer's local environment, it is clear that this concept is important in the conduction process. Whenever ions are

introduced into a polymer, their relative concentration is so small and their local electric field is so large that they tend to probe regions of the polymer that are atypical of the polymer as a whole. Figure 2.22 is a schematic representation of polymer chains in a non-crystalline polymer. In (a) no ions are present and the chains approach conformations that minimize the total free energy. In (b) the introduction of an ion pair has reduced the number of configurations available to the polymer chains. The ion not only reduces the free volume available to the polymer (on a very small scale), but it also modifies the properties of the polymer in that local region.

So far, nothing has been said about the strong local field E_l about an ion (ze). It must be assumed that the ion's local field modifies the local properties of material, for example to first order,

$$\epsilon_{\text{local}} \approx \epsilon + \frac{\partial \epsilon}{\partial E} E_l \quad (2.52)$$

$$\rho_{\text{local}} \approx \rho + \frac{\partial \rho}{\partial E} E_l \quad (2.53)$$

where

$$E_l = \frac{2}{4\pi\epsilon_0\epsilon} \frac{ze}{r^2} \quad (2.54)$$

In the case of the mobility of an ion, the local mobility μ_l may not be as great as the NET relation might lead one to expect, based on the magnitude of diffusion coefficients of

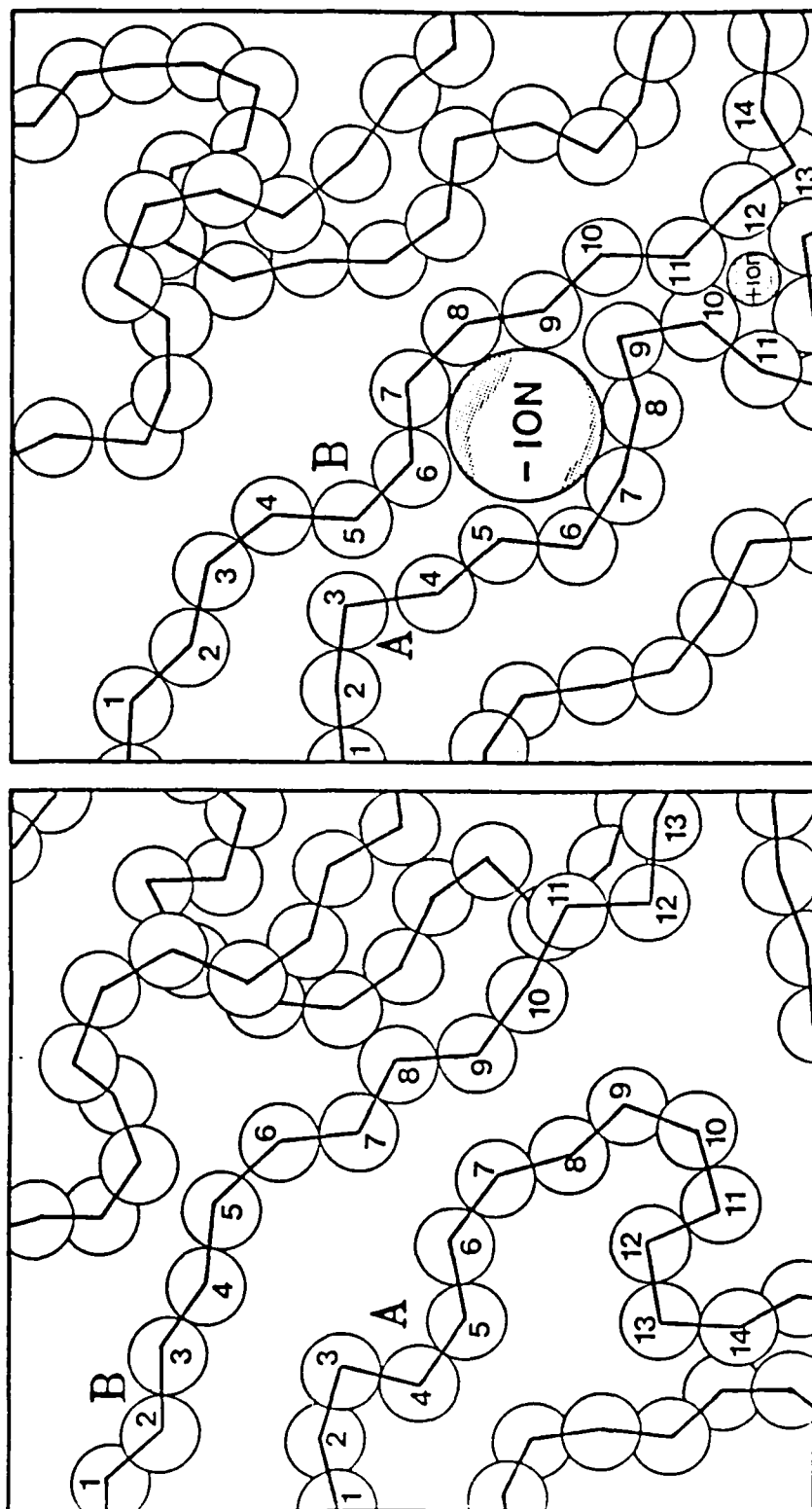


Figure 2.22. Schematic Representation of Chains in a Non-crystalline Polymer. In (a) Note the Chains A and B Where no Ions are Present. In (b) an Ion Pair has Reduced the Number of Configurations Available to A and B.²⁰

neutral molecules of the same dimensions. The electrostatic interaction between the ion and polymer chain (or an ion at some distance of same or opposite sign) may act as a shallow trapping site or as a means of slowing the movement of the ion through the polymer. This is similar to the formation of polarons in the case of electronic conduction.

A qualitative way of visualizing the effect of the ion's local field is to calculate an equivalent local pressure due to the ion field. Thus,

$$\begin{aligned} \rho_{\text{local}} &\approx \frac{1}{2} \epsilon_0 \epsilon' E_l^2 \\ \rho_{\text{local}} &\approx \frac{1}{2} \epsilon_0 \epsilon' \left(\frac{z e}{r^2} \frac{1}{4\pi \epsilon_0 \epsilon'} \right)^2 \\ \rho_{\text{local}} &\approx \frac{1}{32\pi^2} \frac{z^2 e^2}{\epsilon_0 \epsilon' r^4} \end{aligned} \quad (2.55)$$

Assuming some representative values: $z = 2$, $r = 5\text{\AA}$, $\epsilon = 4$, the pressure due to the local field of the ion is approximately $1.5 \times 10^8 \text{ N/m}^2$ ($\approx 1500 \text{ atm}$). This is indeed a significant change in an extremely localized region.

The range of interaction of two ions i and j separated by a distance $r_{ij} = r_i + r_j$ between centers is given by the Coulombic interaction energy U_{ij} . With energy in (eV) and distance in (\AA), the equation for z -valent ions is

$$U_{ij} = \frac{14.4 z_i z_j}{\epsilon' r_{ij}} \quad (2.56)$$

where ϵ' is the effective static dielectric constant of the medium. Figure 2.23 is a *log-log* plot of the interaction energy U_{ij} and the distance r_{ij} between the ions. Horizontal dashed lines give reference values of $k_B T$ at a number of different temperatures. This approach has one drawback--the polymer is treated as a continuum, i.e., a homogeneous infinitely divisible dielectric with ϵ' independent of E . Region A is of interest for bare ions. (In a vacuum, A would be moved up to $\epsilon' = 1$.) If the ion is hydrated, the area of emphasis shifts to B. Ions in a polymer will possess approximately 1 eV of Coulombic attractive energy, whereas the same ion pair in water would only have 0.05 eV. Therefore, substances that are normally considered as strong electrolytes now behave as weak electrolytes when in a low dielectric constant polymer.^{71,72} Region C corresponds, for typical polymers, to the size domain in which ionic attraction (or repulsion) exceeds that effect of thermal agitation. The domain of interaction is several hundreds of Angstroms in diameter. The effective radius of the domain for monovalent ions at 300K

$$r_D \approx \frac{14.4}{\epsilon' U} \sim \frac{14.4}{\epsilon' k_B T} \sim \frac{555 \text{\AA}}{\epsilon'} \quad (2.57)$$

The local electric field intensity around an ion is a good measure of its influence. The relation between electric field versus distance from the ion is shown in Figure 2.24 for the same four values of dielectric constant. The equation

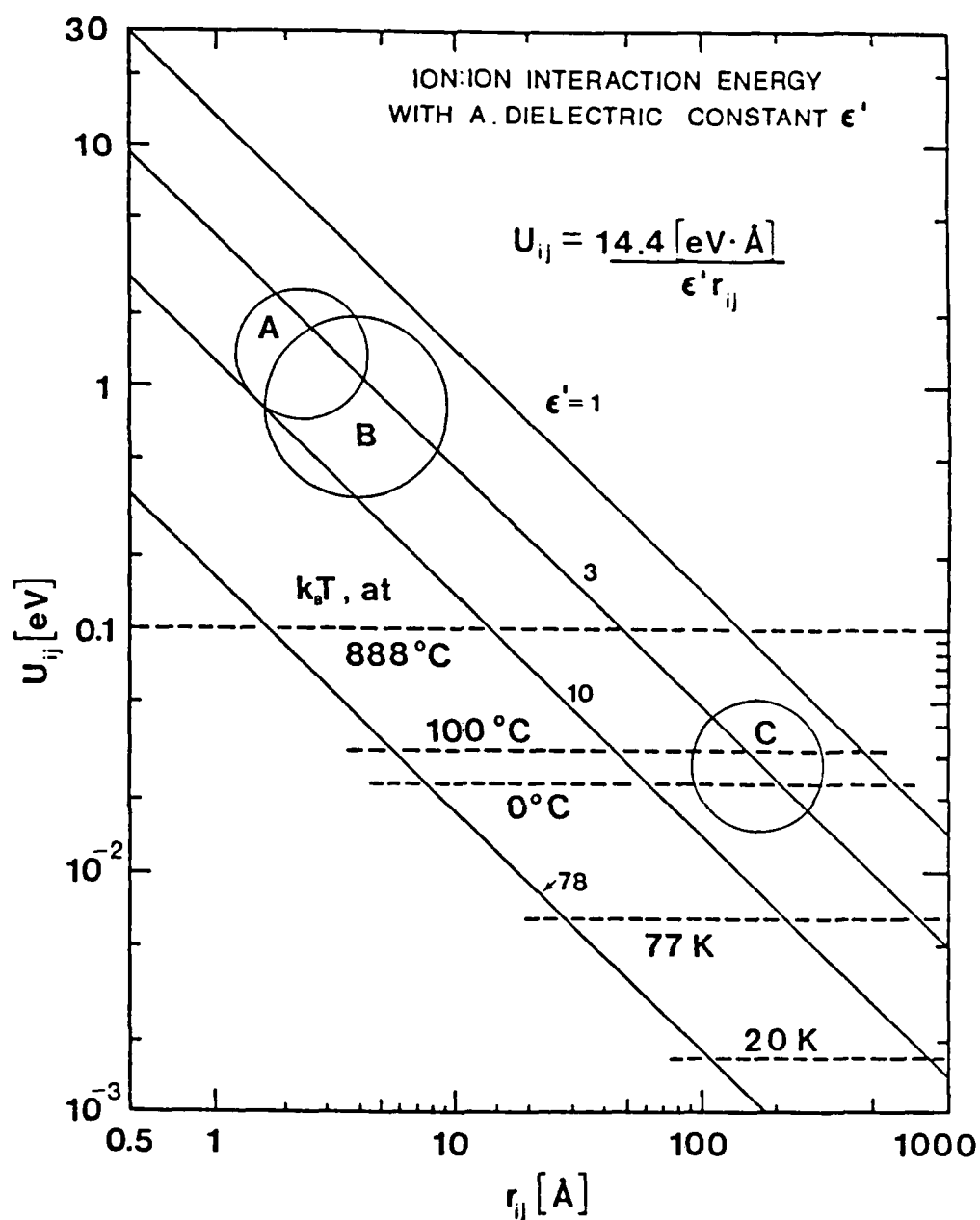


Figure 2.23. Coulombic Interaction Energy Between Monovalent Ions Separated by a Distance r_{ij} in Media of Different Dielectric Constant.^{20ij}

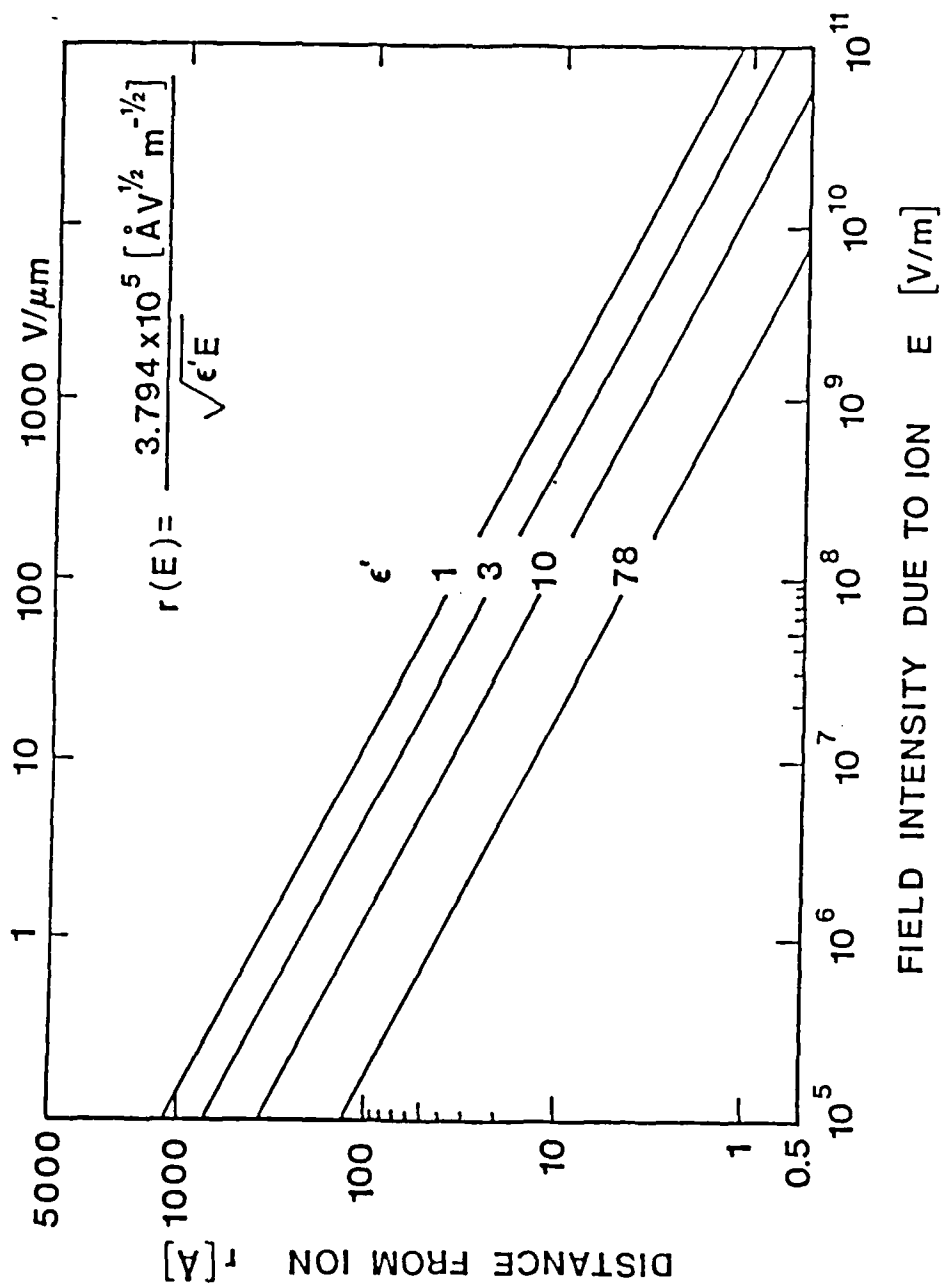


Figure 2.24. Distance From a Monovalent Ion Corresponding to a Given Electric Field Strength E . Curves Represent Range at Which the Ion's Field Will Cancel the Opposing Component, E , of the Applied Field.²⁰

$$r = (\epsilon'E)^{-1/2}[3.794 \times 10^5] \quad (2.58)$$

is merely $E = e/4\pi\epsilon_0\epsilon'r^2$ solved for r in (\AA) when E is in (V/m). For an external applied field of 10^5 V/m (positive towards the right), then the distance on the left side of the ion at which the resultant of the two fields is zero can be read from the graph as 700 \AA for a polymer with a dielectric constant of 3. On the right side of the ion at a distance of 700 \AA , the fields add to give a value of 2×10^5 V/m. At this value of applied external field, the ion's range of interaction dominates for close to 1000 \AA in all directions. To reduce the ion's range of dominance to about 3 \AA (for $\epsilon' = 3$), the applied external field would have to approach 10^{10} V/m. In most electrical conductivity tests the applied external field never approaches 10^{10} V/m. In most instances, $10^4 - 10^6$ V/m would be the range of the applied external field, so that the ion's field of dominance extends over millions of mers and could theoretically encompass small crystallites and other intermediate scale morphological features.

Thus, it is evident that ions influence the local structure of a polymer, modifying many properties in small localized regions. Especially important is the range of dominance of an ion's electric field. Taken in conjunction with Watanabe's⁸¹ supposition that large anions may be hindered in their movement by their size, the modification of the local structure by these ions thus serve as shallow

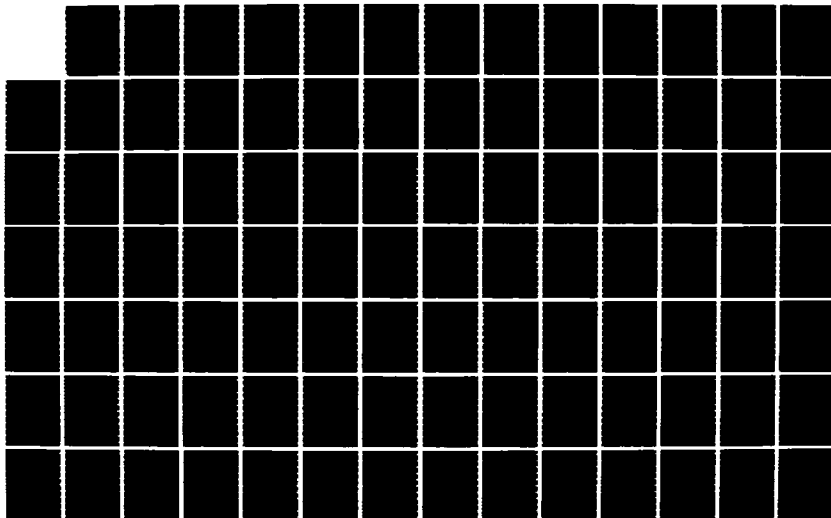
AD-A173 498

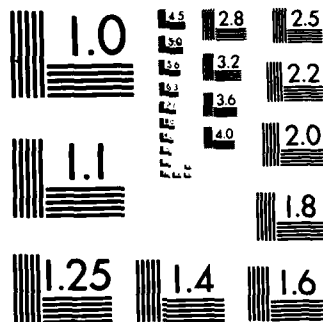
PHYSICAL TECHNIQUES FOR THE STUDY OF SORPTION DIFFUSION
ELECTRICAL PROPER (U) VIRGINIA UNIV CHARLOTTESVILLE
DEPT OF MATERIALS SCIENCE R E BARKER ET AL 26 JUL 86
UVA/525646/MS87/101 AFOSR-TR-86-0831 F/G 11/9

2/4

UNCLASSIFIED

NL





XEROCOPY RESOLUTION TEST CHART
NATIONAL BUREAU OF STANDARDS-1963-A

$$r = (\epsilon'E)^{-1/2}(3.794 \times 10^5) \quad (2.58)$$

is merely $E = e/4\pi\epsilon_0\epsilon'r^2$ solved for r in (\AA) when E is in (V/m). For an external applied field of 10^5 V/m (positive towards the right), then the distance on the left side of the ion at which the resultant of the two fields is zero can be read from the graph as 700 \AA for a polymer with a dielectric constant of 3. On the right side of the ion at a distance of 700 \AA , the fields add to give a value of 2×10^5 V/m. At this value of applied external field, the ion's range of interaction dominates for close to 1000 \AA in all directions. To reduce the ion's range of dominance to about 3 \AA (for $\epsilon' = 3$), the applied external field would have to approach 10^{10} V/m. In most electrical conductivity tests the applied external field never approaches 10^{10} V/m. In most instances, $10^4 - 10^6$ V/m would be the range of the applied external field, so that the ion's field of dominance extends over millions of mers and could theoretically encompass small crystallites and other intermediate scale morphological features.

Thus, it is evident that ions influence the local structure of a polymer, modifying many properties in small localized regions. Especially important is the range of dominance of an ion's electric field. Taken in conjunction with Watanabe's⁸¹ supposition that large anions may be hindered in their movement by their size, the modification of the local structure by these ions thus serve as shallow

traps to the movement of the cations. As the temperature is raised, the energy necessary to reinitiate cation movement is relatively small. At higher temperatures, near or above T_g , the free volume increases open channels between the polymer chains that allows movement of both anion and cation. However, this hypothesis need not be restricted to ionic conduction. When thinking of electronic conduction-mechanisms, it is evident that defects in the molecular structure produce local variations of wavefunction overlap between adjacent hopping sites (electrons) controlling the rate of exchange of charge carriers.⁸⁶ Ions trapped in the polymer with interaction ranges approaching 1000 Å can also influence the electronic conduction process.

2.3 Electronic Conduction Mechanisms in Disordered Materials

2.3.1 Introduction to Electronic Conduction

A number of conduction mechanisms have been hypothesized to account for the charge transport in polymeric dielectrics. One aspect of the problem is the diffusional motion of charge carriers in molecular solids. A difficulty arises in trying to quantify the effect on charge transport of disorder, i.e., spacial and temporal fluctuations of the intermolecular spacings in disordered organic solids. Bäessler⁸⁶ hypothesizes that disorder produces local variations of the wave function overlap between adjacent hopping sites. Another consequence of disorder is the interaction of an exciton located at a

hopping site with its local environment.⁸⁷ Thus, the general effect of disorder in molecular solids (polymers specifically) is to localize the electronic states. The electronic picture of polymeric materials is further complicated by chemical impurities and physical defects. Physical defects are associated with intermolecular conformations, causing deviations from the ideal molecular arrangement. This generates additional localized states outside of the distribution attributed to bulk states. An example of this is the formation of incipient dimers between adjacent planar aromatic substituents which act as traps for singlet excitons and charge carriers.^{88,89}

It is advocated by Scher and Montroll⁹⁰ that disorder renders the transport process dispersive, and reduces the effective mobility. The hopping of the charge carrier is no longer a constant, but becomes a time-dependent variable. The applicability of the Scher-Montroll theory to real systems is difficult because it is hard to assign a specific type of disorder to the observed time dependence of μ . Due to factors such as those mentioned, the identification of the conduction mechanisms for specific polymer systems is very difficult and many parameters will influence the final conduction equation.

Several mechanisms for modeling the charge transport through dielectrics have been proposed. These processes can be classified into two very general categories: bulk limited mechanisms (i.e., processes which occur in the

volume of the material), and electrode-limited mechanisms (i.e., processes which take place at the electrode-polymer interface). The following sections will summarize some of the important features of these conduction mechanisms. These mechanisms are discussed in depth in the literature.⁹¹⁻⁹³

2.3.2 Bulk Limited Mechanisms

Bulk limited conduction mechanisms characterize charge transport through the volume of the material. Figure 2.25 shows schematically a one-dimensional representation of a polymer held between two electrodes.⁷⁵ In this simple model, the lateral dimensions of the electrodes and specimen are much larger than the sample thickness, l . Current density is given by

$$\tilde{J} = \sigma \tilde{E} - eD_p \nabla p - eD_n \nabla n + \frac{\partial \tilde{D}}{\partial t} \quad (2.59)$$

$$\tilde{J} = \tilde{J}_{\text{COND}} + \tilde{J}_{\text{DIFF}} + \frac{\partial \tilde{D}}{\partial t}$$

D is the diffusion coefficient, \tilde{D} is the electric displacement, and p and n are the free positive and negative carrier concentrations, respectively. $\partial \tilde{D} / \partial t$ is the displacement current density. The particle current density is just $\tilde{J}_{\text{COND}} = \sigma \tilde{E}$, while the diffusion current is $\tilde{J}_{\text{DIFF}} = eD(\partial p / \partial x)$. The sum of these two terms give the current density attributed to charge transport. This sum is called

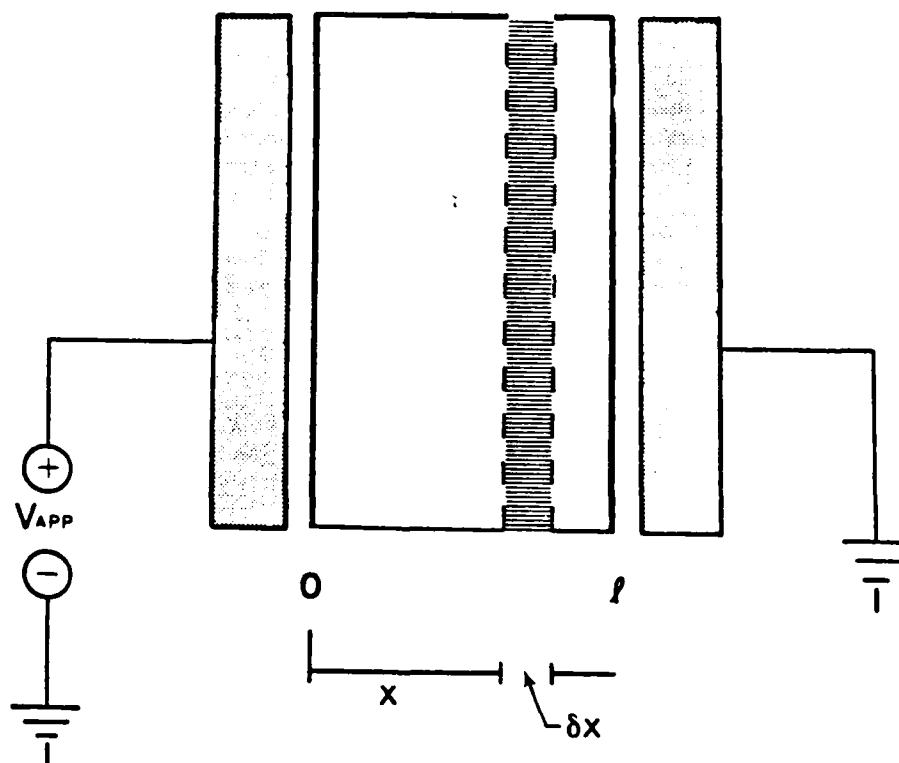


Figure 2.25. Notation Used for One-Dimensional Carrier Flow of a Polymer Slab or Film Held Between Two Metal Electrodes.⁷⁵

the convection current density, or particle current density, and is just

$$J_c = \sigma E - eD_p \frac{\partial p}{\partial x} - eD_n \frac{\partial n}{\partial x} . \quad (2.60)$$

In this model, $J=J(t)$ is independent of x , so that for time-varying conditions, particle current density and displacement current density are complementary.

Other equations that are useful in describing the terms of Eq. (2.59) are:

(1) Poisson's equation:

$$\text{div } \underline{D} = \rho = (p-n)e \quad (2.61)$$

(2) constitutive equation:

$$\underline{D} = \epsilon' \epsilon_0 \underline{E} = \epsilon \underline{E} \quad (2.62)$$

(3) field relations:

$$\underline{E} = - \text{grad } V \quad (2.63)$$

$$V_{\text{appl}} = \int_0^b \underline{E} \cdot d\underline{x} \quad (2.64)$$

(4) continuity equation:

$$\nabla \cdot \underline{J}_c + \frac{\partial \rho}{\partial t} = 0 \quad (2.65)$$

where $\rho [(p-n)e]$ is the net charge density, ϵ' is the dielectric constant and V is the potential difference as measured across the sample.

Ohmic Conduction

The most elementary behavior occurs during the steady state ($\partial D/\partial t=0$) for neutral materials ($\rho=0$). Assuming for simplicity, the case of positive carriers, p , with a constant carrier density ($\partial p/\partial x=0$). Thus, Eq. (2.59) becomes

$$J = \sigma E = pe\mu E . \quad (2.66)$$

This equation implies that the free carrier concentration, p , any trapped carrier concentration, p_t , are exactly balanced by an equal negative charge concentration, n_{total} . The moving carriers thus pass through a background countercharge. Since $(n_{\text{total}} - p_t) \equiv p$ is constant, the material is considered homogeneous where n_{total} and p_t are fixed. This is the normal situation for metals, and the condition of neutrality is a good approximation for homogeneous semiconductors. However, this model is not a good approximation for excellent insulating materials.

Deviations from the ohmic relation can be caused by both the barrier layers adjacent to the electrodes and inhomogeneities in the bulk. In general, this relation holds for most polymers in fields up to 10^4 V/cm, with the conductivity proportional to μp , or the equivalent expression $[\mu_{\text{eff}}(p+p_t)]$. Measurements of the electrical conductivity cannot separate these factors.

Free carrier concentrations n and p for the case of electronic conduction are given by the densities of states

at the specified temperature (see Appendix B for details). It is convenient to use the Fermi level concept when solving for n and p . Thus, N_v and N_c , the effective densities of states, can be estimated from band structure calculations. In disordered and impure materials (i.e., ones that are imperfect on an atomic scale as are polymers), numerous traps of varying levels are available. The number densities and energy depths of these traps are not well known or completely understood. The effective mobility, μ_{eff} , of charge carriers depends on the distribution of shallow trapping sites and cannot be calculated without a thorough knowledge of that distribution. Thus, estimates of carrier concentration are vague and there is no rigorous basis upon which to make accurate predictions of carrier densities.

Due to the problems and uncertainties in the theoretical methods for determining specific conduction parameters, it is instructive and useful to investigate experimentally those mechanisms which give rise to field independent conductivity.

For electronic charge carriers, the microscopic mobility is governed by scattering of the charge carriers by lattice vibrations.⁹⁴ The mean free path, λ , and the mean free time, τ , are defined as

$$\lambda \equiv \frac{1}{SN} \quad , \quad \tau \equiv \frac{1}{v_{\text{th}}SN}$$

where S is the scattering cross-section and v_{th} is the thermal carrier velocity. N is the concentration of charge

scattering centers. Assuming that any impulse received from the external field is destroyed upon impact,

$$eE\tau \cong mv_{\text{drift}} \quad (2.67)$$

where m is the effective mass of the charge carrier and v_{drift} is the mean velocity of drift of the charge carrier in the direction of the applied field. Thus the electronic mobility is deduced as

$$\mu_0 = \frac{v_{\text{drift}}}{E} = \frac{e\tau}{m} = \frac{e}{mv_{\text{th}}SN} \quad (2.68)$$

The microscopic mobility is controlled by electron lattice interaction through the quantities m and S , which are to be considered as effective values. Scattering cross-section, S , may change with the kinetic energy of the carrier, but since $v_{\text{drift}} \ll v_{\text{th}}$, S is effectively constant as an approximation. The mobility, μ_0 , is the main parameter which governs electron drift between trapping events.

Polaron motion and hopping between localized states are two other mechanisms which lead to ohmic conduction in amorphous materials.^{95,96} The polaron treatment of amorphous materials deals with the small polaron, which has an effective size comparable to atomic or molecular dimensions. This entity, which is constituted by the moving electron and the elastically distorted "lattice" it carries along with it, hops from site to site with an activation energy of $\frac{1}{2}W_p$, where W_p is the polaron binding energy. This mechanism is not usually associated with quasi-continuous

nonpolar or weakly polar solids. For polymers, this theory of charge transport is still in the developmental stages.

Of more interest is the hopping between localized states developed to explain conduction in amorphous semiconductors.^{54,96} The basic mechanism is shown in Figure 2.26, where a set of energy levels is distributed both in energy and position throughout the material. These levels may be due to impurities, associated with physical disorder (e.g., missing atoms, dislocations,), or the localized levels or band tails in the band gap resulting from a smearing of the band edges by the irregular nature of the molecular arrangement in the bulk material. When these levels encompass the Fermi level (or are close to it), an adequate population of electrons becomes available in these states. Transport thus occurs by the thermal excitation of an electron from a full state to an empty state. Thermal de-excitations must also occur with an equal frequency. The elementary process is similar to barrier hopping of ions, i.e., it exhibits a Boltzmann-like probability. However, in this case, the wave functions of the localized sites overlap, and as such, tunneling through the barrier is a possible occurrence. The probability, Γ , of a carrier executing a jump is

$$\Gamma = \nu \exp \left[- \frac{W}{k_B T} - 2\epsilon a \right] \quad (2.69)$$

where a corresponds to the separation between adjacent sites, ϵ is the overlap parameter, and W is the separation

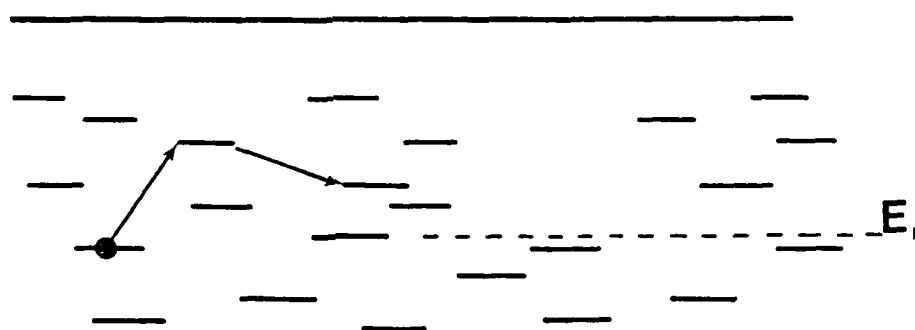
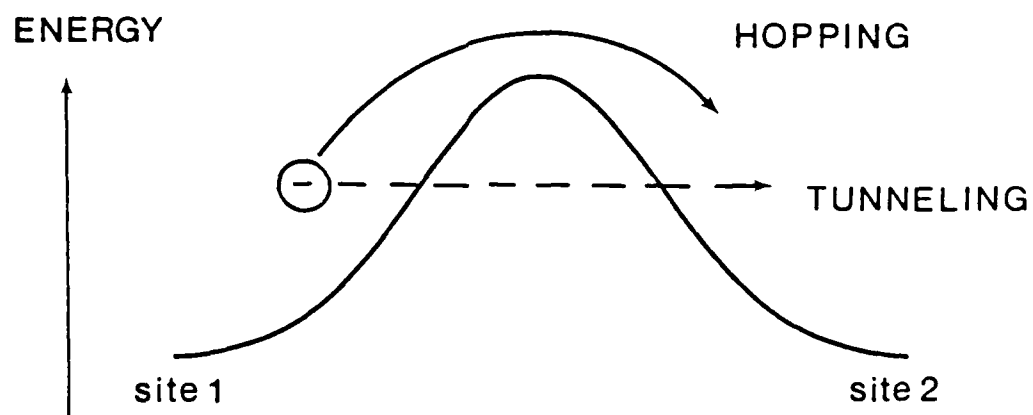


Figure 2.26. (a) Electron Transfer Mechanism Between Adjacent Sites via Hopping Over a Potential Energy Barrier or by Tunneling Through the Barrier. (b) Hopping Between Localized States.

in energy. For each carrier situated in a particular site, a number of adjacent sites, each with a value of W and a , are available into which the carrier may hop. This process is thus known as variable range hopping. The average result of the most probable jump displays a non-Arrhenius conductivity dependence with changing temperature.⁵⁴ For three dimensions,

$$\sigma = \sigma_3 \exp \left[-C_3 \left(\frac{N(E)k_3T}{E} \right)^{-1/4} \right] \quad (2.70)$$

where σ_3 and C_3 are constants and $N(E)$ is the density of localized states. This approach utilizes an optimum jump probability, whereas if all probabilities less than a critical value-- Γ_c --are ignored, then the conduction is controlled by the most resistive link and reduces to a percolation problem.⁹⁷

Another model of electronic conduction is "classical hopping" within the forbidden gap. With a sufficiently large trap density, the potential wells overlap and lead to the situation as depicted in Figure 2.27. The barrier height between successive traps is now less than the trap ionization energy, and hopping can take place with the carrier never entering the transport band. The barrier height is given by

$$\Delta H = W_I - \frac{e^2}{4\pi\epsilon\epsilon_0 a} \quad (2.71)$$

where W_I is the trap ionization energy and a is the separation between the centers. In the limit of high trap

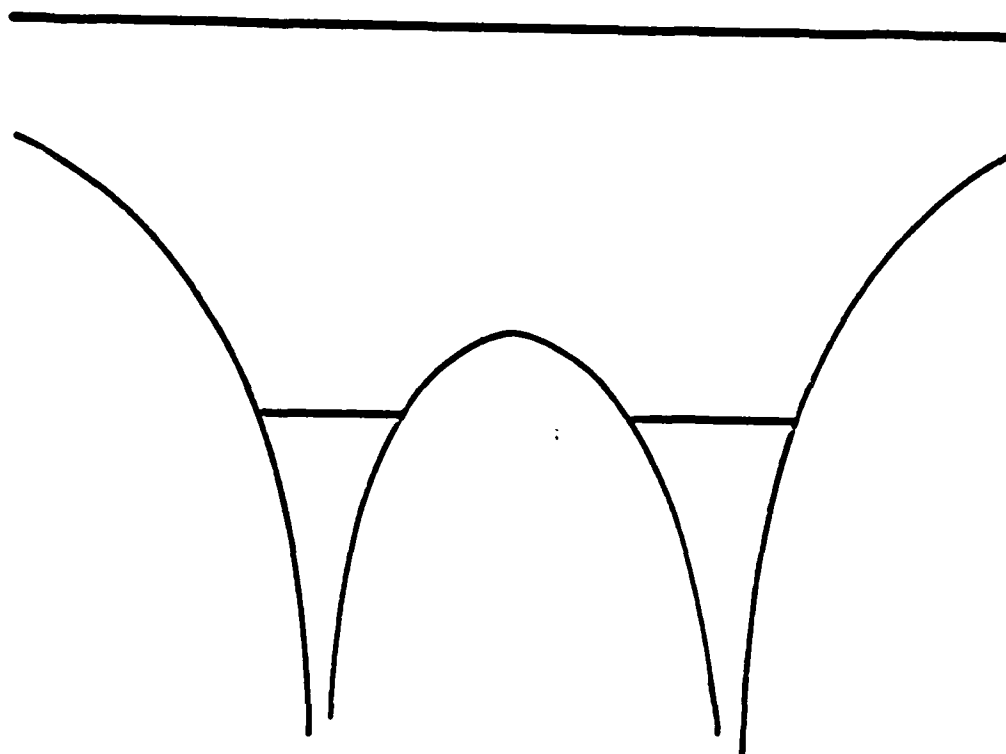


Figure 2.27. Overlap of Impurity (Traps) Potentials Due to High Concentrations.

concentration, tunneling may be possible or impurity band conduction may occur as ΔH approaches zero. If the value of a is replaced by some other type of probability distribution, a more complicated expression results even though the principles behind the model remain in force.

Arrhenius behavior is due to temperature variations of the carrier concentration and/or an activated change in the carrier mobility. A concentration-dependent activation energy implies hopping between localized states. Non-Arrhenius behavior may be due to the variable range hopping model. These divisions are not well defined in general. (It may be possible to get an Arrhenius-type behavior with an activation energy which depends on E . This is the essence of the Eyring rate model.)

2.3.3 Nonlinear Effects

Space-Charge-Limited Current (SCLC)

The easy injection of charge in one direction at the electrode polymer interface results (for a single type carrier) in space-charge-limited current (SCLC) flow. The carrier density is larger at the injecting electrode, thus enhancing the conductivity. This results in a smaller value of the electric field at the injecting electrode. In moving towards the collecting electrode, the electric field increases above its average value, while the charge carrier density falls off. This has the effect of keeping the total

current density constant under steady-state conditions. In SI units, the SCLC is given by^{74,98}

$$J = \frac{9\mu\epsilon'\epsilon_0 V^2}{8b^3} \quad (2.72)$$

where all variables are as previously defined and b is the specimen thickness. (For details on the derivation of Eq. (2.72), see Appendix C.) Diffusion currents are omitted in the derivation of this equation. Boundary conditions at the injecting electrode are $E=0$, $p=\infty$.^{93,99-101} Ohmic effects occur at low applied voltages; but as the voltage is increased, the voltage assumes a quadratic nature

$$V_x \cong \frac{ep_0 b^2}{\epsilon'\epsilon_0} \quad (2.73)$$

where p_0 is the thermal carrier concentration. At this point the mobility will be subject to

$$\mu_{eff} = \frac{\mu_0}{1 + \theta^{-1}} \cong \mu_0 \theta \quad (2.74)$$

where

$$\theta \equiv \frac{n}{n_t} = \frac{N_c}{N_t} \exp\left[-\frac{(E_c - E_t)}{k_B T}\right] \quad (2.75)$$

N_c is the number of carriers injected into the conduction band per cm^3 of solid and N_t is the concentration of shallow trapping levels which are all assumed to have equal energy. $(E_c - E_t)$ is the trap depth below the conduction band. (Definitions of these equations are found in Appendix B.) Large voltages induce strong injection at the electrode, thus filling the traps. Any further voltage increase leads

to a corresponding increase in charge carriers which cannot be trapped. This trap-filled limit occurs at a voltage V_{TFL} given by

$$V_{TFL} \cong \frac{eP_t b^2}{2\epsilon\epsilon_0} \quad (2.76)$$

These regimes are shown in Figure 2.28. As traps fill, the current approaches the trap-filled limit of the trap-limited Child's law region of the current voltage curve. At this point, a tremendous increase in the current occurs as the last traps are filled. The current rapidly approaches the trap-free Child's law current. This description is not adequate for a number of reasons, including distribution of traps in energy,¹⁰² the influence of carrier diffusion,¹⁰³ field-dependent mobilities,¹⁰⁴ velocity-dependent capture cross-sections of traps,¹⁰⁵ and field-enhanced release from traps (the Frenkel effect).¹⁰⁶ These effects round off the transition at V_x , yield a much higher power law for V and inverse power law for b than is given by Eq. (2.72), and obscure the transition at V_{TFL} .

Poole-Frenkel and Onsager Enhancement

Increasing the electric field distorts the potential wells in which the carriers are trapped. With mild fields, the depression of the barrier height is linear in the applied field and the escape probability is exponential in the field. (This is the case discussed for the movement of ions over potential barriers.) When the field is small enough, the exponential can be represented by a first-order

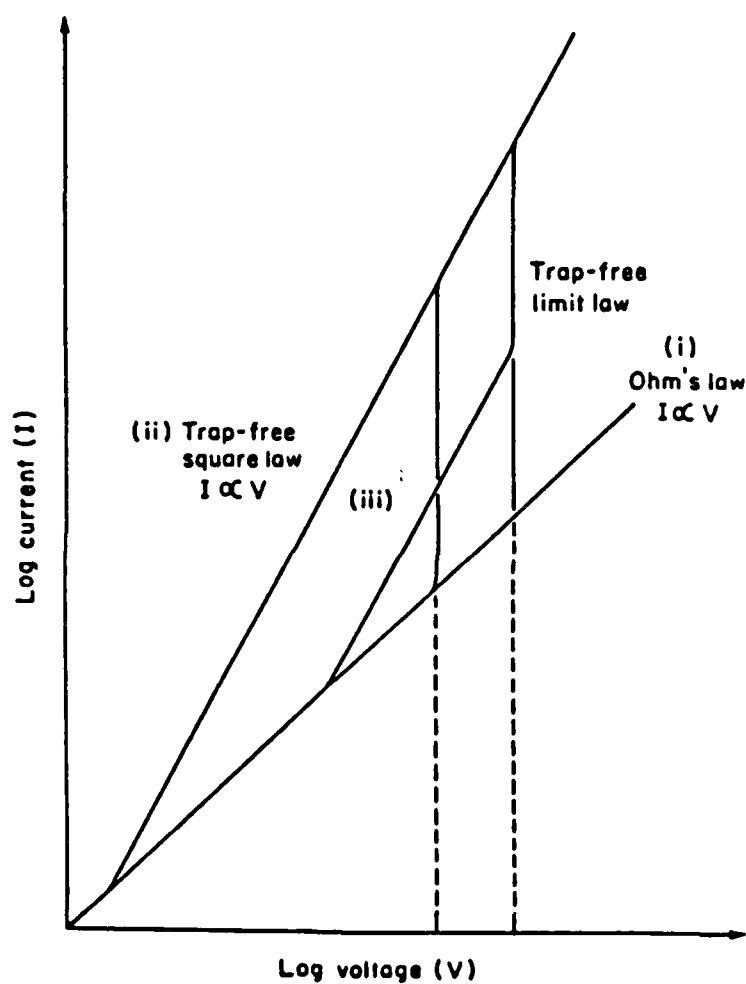


Figure 2.28. Possible Regimes for a Single Carrier Space-Charge-Limited Current With a Single Set of Traps. (i) Ohm's Law Region; (ii) Trap Free Child's Law; (iii) Child's Law With Trapping.

expansion. The resulting current is thus proportional to the difference between the forward and backward jump rates and is linear in the field.

In the case of high fields, the forward rate increases in the direction of the field while the backward rate is neglected as the probability of a jump in that direction is considered to be very small. The resulting expression is a temperature-dependent form of the Poole equation.¹⁰⁷

$$\sigma \propto \exp\left(\frac{eEa}{2k_B T}\right) \quad (2.77)$$

A drawback of this model is that the distortion of the barrier is not usually linear in field.

Consider the situation shown in Figure 2.29, which sets the stage for high field models for bulk conduction. The situation shown in (a) is the one-dimensional case of barrier lowering. Assuming a Coulombic trap, the potential energy of the carrier may be written as

$$W_{PE} = -\frac{e^2}{4\pi\epsilon_0\epsilon x} - eEx \quad (2.78)$$

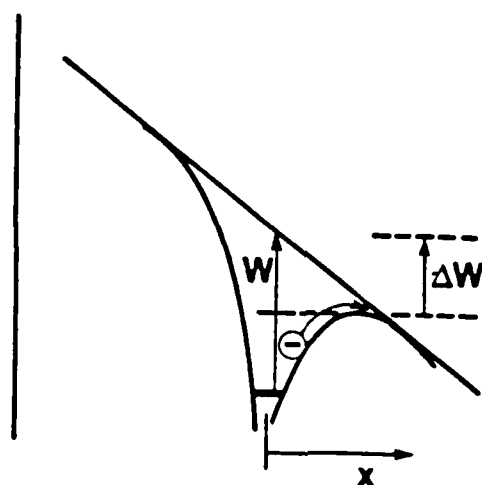
where x is measured from the trap site. This has a maximum at

$$x_{\max} = \left(\frac{e}{4\pi\epsilon_0\epsilon E}\right)^{1/2} \quad (2.79)$$

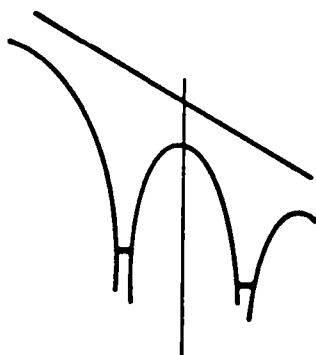
and the barrier height becomes

$$\Delta H = (W - \Delta W) = W - \left(\frac{Ee^3}{\pi\epsilon_0\epsilon}\right)^{1/2}$$

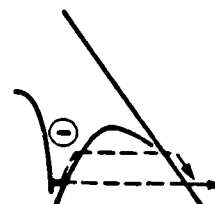
$$\Delta H = W - \beta_{PF} E^{1/2} \quad (2.80)$$



(a)



(b)



(c)

Figure 2.29. High Field Models for Bulk Conduction. (a) A One Center Poole-Frenkel System; (b) Multiple Overlap Poole-Frenkel System; and (c) Tunneling System Showing Both Simple Tunneling and Partial Thermal Excitation (Mixed Mode Operation).

Here, $\beta_{PF} = (e^3/\pi\epsilon'\epsilon_0)^{1/2}$ is the Poole-Frenkel coefficient. The probability per unit time of release of a carrier in the downfield direction is

$$\Gamma = \nu \exp\left(-\frac{W}{k_B T}\right) \exp\left(\frac{\beta_{PF} E^{1/2}}{k_B T}\right) \equiv A_2^* N_c \quad (2.81)$$

where A_2^* is the rate constant for excitation under the nonequilibrium dynamic steady state. The carrier density can be calculated as follows (see Appendix D for discussion of rate equations):

$$A_1 n (N_t - n_t) = A_2^* n_t (N_c - n) \quad (2.82)$$

and

$$A_2^* = A_2 \exp\left(\frac{\beta_{PF} E^{1/2}}{k_B T}\right) \quad (2.83)$$

This assumes that $n \ll N_c$ and that the traps are donor-like in that they are neutral when empty (i.e., $(N_t - n_t = n)$). Setting $n_t = N_t$ if the traps are only slightly ionized (low-temperature-deep trap limit), the carrier concentration and conductivity can be determined:

$$n^2 = N_t N_c \exp\left(\frac{\beta_{PF} E^{1/2}}{k_B T}\right) \quad (2.84)$$

and

$$\sigma = \sigma(0) \exp\left(\frac{\beta_{PF} E^{1/2}}{2k_B T}\right) \quad (2.85)$$

These equations are for the partially ionized, uncompensated state. The low field conductivity is given by $\sigma(0)$. When

the temperature is high enough for complete ionization, the Poole-Frenkel effect does not operate.

Other possibilities exist; consider the case where the donor-like states are partially compensated by a smaller concentration of acceptors, N_A , which will be wholly ionized. The neutrality condition becomes

$$n(N_A - p_A) = p + (N_t - n_t) \quad (2.86)$$

when p , n and p_A are small. This gives

$$n \propto \exp\left(\frac{\beta_{PF} E^{1/2}}{k_B T}\right) \quad (2.87)$$

and

$$\sigma = \sigma(0) \exp\left(\frac{\beta_{PF} E^{1/2}}{k_B T}\right) \quad (2.88)$$

for the case of partial compensation. Adamec and Calderwood¹⁰⁸ have developed a model for electrical conduction in dielectrics at high fields in three-dimensions. They have also included several other models (non-three-dimensional), including variations of the two developed in the preceding section. Basically, all the models are the same, except for slight changes in the pre-exponential and exponential terms (Appendix E lists several of these models for comparative purposes.)

Several details of the Poole-Frenkel model make this approach incomplete. The model ignores the three-dimensionality of the real center, and backward jumps are forbidden at all values of the applied field. In a proper

calculation, the long-range effect of the Coulomb potential must be considered so that thermalization of the excited carrier may take place within the well.¹⁰⁹ Thus, diffusion must be included in the model and the Onsager solution is more appropriate. This has the form

$$\frac{\sigma(\zeta)}{\sigma(0)} = \frac{2I_1(\zeta)}{\zeta} \begin{cases} \rightarrow 1 \text{ as } \zeta \rightarrow 0 \\ \rightarrow [2/\pi\zeta^3]^{1/2} \exp(\zeta) \text{ as } \zeta \rightarrow \infty \end{cases} \quad (2.89)$$

$I_1(\zeta)$ is a modified Bessel function and $\zeta = \beta_{PF} E^{\frac{1}{2}}/k_B T$. This model provides a consistent transition from the low field limit to the high field case which was one problem (i.e., low field description) of the Poole-Frenkel model. Because the simple Poole-Frenkel model is of the general form $\exp(\zeta)$, there is no great change in the form of the field dependence when compared to the Onsager approach.

If the Coulomb potential is screened, the conductivity ratio becomes^{110,111}

$$\frac{\sigma(\zeta)}{\sigma(0)} \approx \exp\left(\frac{\zeta}{(\zeta+2)^{1/2}}\right) \quad (2.90)$$

and the Schottky plot of J vs. $E^{\frac{1}{2}}$ will be curved at low fields. Also, the field dependence approaches a linear exponential rather than a square-root exponential of field at small fields.

2.3.4 Electrode-Limited Mechanisms

Schottky Emission

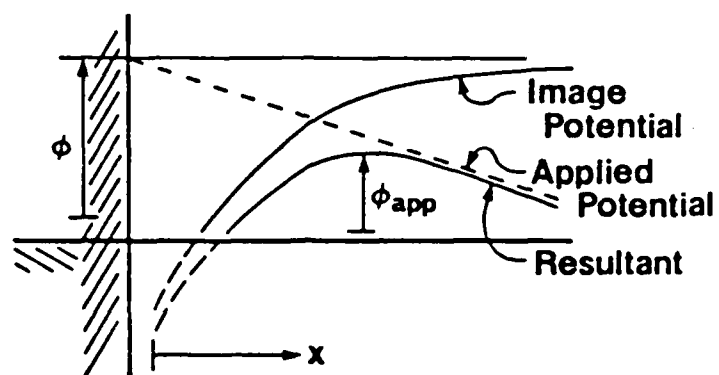
Theories of charge injection from a metal into an insulator encompass a large volume of literature. Only a brief outline of the mechanisms involved at the contacts will be provided. Barriers at the metal-insulator interfaces are quite high, thus the thermal injection of electrons (holes) is small. At medium fields, the most likely process is field-assisted thermionic emission (i.e., the Richardson-Schottky effect).¹¹² This is analogous to the Poole-Frenkel effect, except in this case, it takes place near the interface and the particle leaving the metal is retarded by its own image force in the electrode. This is shown in Figure 2.30(a). The force on the particle, a distance x from the interface, can be written as

$$F = eE - \frac{e^2}{4\pi\epsilon_0\epsilon'(2x)^2} \quad (2.91)$$

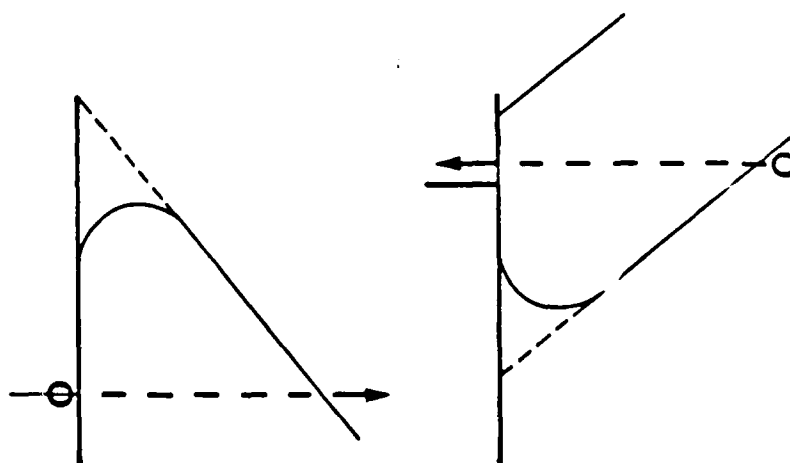
and this is equal to zero at the top of the effective potential curve. The amount of work done on the particle is

$$W = -\int F \, dx = -eEx - \left(\frac{e^2}{4\pi\epsilon_0\epsilon'} \right) \frac{1}{4x} + \phi \quad (2.92)$$

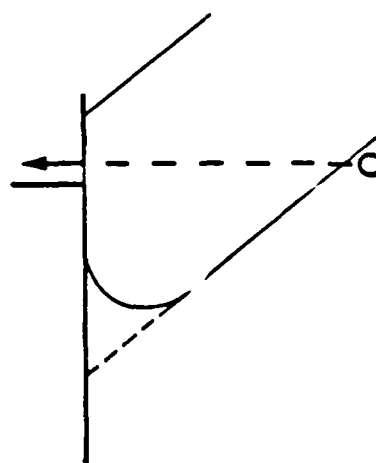
The constant of integration ϕ is chosen so that $W=\phi$ at large distances from the electrode under zero applied field. The problem of $F \rightarrow -\infty$ when $x \rightarrow 0$ is ignored. For non-zero fields, W reaches a maximum value of ϕ_{app} at the point where $F=0$. The distance, x_m , is on the order of several nanometers, and



(a)



(b)



(c)

Figure 2.30. High Field Effects at the Contacts: (a) Schottky Emission; (b) Tunneling; and (c) Tunneling Out From Valence Band.

$$\phi_{app} = \phi - \beta_s E^{1/2} \quad (2.93)$$

where

$$\beta_s = \left(\frac{e^3}{4\pi\epsilon_0\epsilon} \right)^{1/2} \quad (2.94)$$

The current density thus drawn over the barrier is

$$J = AT^2 \exp\left(-\frac{\phi}{k_B T}\right) \exp\left(\frac{\beta_s E^{1/2}}{k_B T}\right) \quad (2.95)$$

where A is the Richardson-Dushman constant. Currents which obey this expression will appear as straight lines on a Schottky plot of J versus $E^{1/2}$.

This equation does not include any backflow of charge from the insulator. At low fields, the reverse flow may be significant¹¹³ and leads to ohmic contact at fields below 10^4 V/cm. Two factors which lead to modifications of this simple model are the presence of surface states and/or space charge. Space charge storage changes the field--band bonding occurs.

Tunneling

As the strength of the field is increased to values greater than 10^6 V/cm at room temperature, tunneling through the barrier becomes the more probable mechanism. As shown in Figure 2.30(b), a particle impinging from the metal encounters an almost triangular barrier. This barrier has been modified by the image force and any space charge that

may be present. The current passing through the barrier is the product of the flux of electrons of a particular energy approaching the barrier from the metal and the transmission probability, integrated over all available energies. The result is the Fowler-Nordheim equation¹¹⁴

$$J = \frac{e^3 E^2}{8\pi h \phi} \exp\left(-\frac{4\sqrt{2m} \phi^{3/2}}{3\hbar e E}\right) \quad (2.96)$$

Tunneling of electrons from the valence band can lead to hole injection, as shown in Figure 2.30(c).

2.3.5 Steady-State Behavior: A Perspective

Ohmic dependence is observed at low field values and a linear response of current versus applied voltage is expected. This behavior can be explained by a number of mechanisms, both ionic and electronic. Nonlinear response is observed upon increasing the field to higher values. Once again, several different mechanisms can be invoked to describe the behavior. The problem of selecting the proper conduction mechanism is further complicated in that it is very hard to analyze mobility and conductivity measurements as functions of field and temperature because the information gained often is not definitive. For example,⁷⁵ several conduction mechanisms may be operating at the same time--a particular specimen may inject by the Schottky mechanism, conduct by the Poole-Frenkel mechanism, while storing charge at the same time. The net effect is that

field is everywhere different and (except for one coordinate) not equal to (V_{app1}/b) . The Schottky plots of the observed data will possess slopes that correspond to neither β_{BF} nor β_s and may show some curvature.¹¹⁵

Each case must therefore be considered on its own merits. There exists no well defined set--nor is there likely to be--of criteria by which particular conduction models can be identified unambiguously for a given case.

2.4 Generalized Theory of Conductivity in Organic Polymers (Cotts and Reyes)

Introduction to Model

Cotts and Reyes³¹ have developed a model of conductivity in organic polymers that hopefully accounts for a wide range of properties within polymers for the degree of structural order encountered. This model attempts to evaluate the conductivity by separately estimating the number, charge and mobility of charge carriers. The following list represents a summary of key features of the Cotts and Reyes model for conductivity (For specific details of the model, see Reference 31).

- (1) Macroscopic charge transport occurs via hopping of charges between adjacent localized electronic states. As the volume and number fraction of localized states increases, the macroscopic conductivity increases as a continuous percolation

network, allowing the formation of long-range transport.

- (2) Localized electronic states serving as lattice sites in the percolation network may be unimolecular (e.g., TNF-doped polycarbonate), intramolecular backbone segments (e.g., undoped polyvinyl carbazole or pyrolyzed Kapton), or intermolecular ordered dopant-repeat unit aggregates (e.g., AsF₅-doped polyphenylene sulfide or polyacetylene). Volume and relative electronic energy of the localized states determine the critical number of localized, charged states necessary for the formation of the percolation network.
- (3) Hop length depends on the extent of long-range periodic order. For disordered systems where long-range order is absent, hops occur between adjacent sites. If superlattice structures are formed, long-range tunneling can occur.

Model for Conductivity

The basic conceptual element of the model is the localized, inter- or intramolecular charge-stabilizing site which is idealized as a simple potential well of finite depth. The potential well corresponds to a single molecular dopant in an inert matrix or a three dimensional assembly of an inorganic dopant with unsaturated repeat units from the backbone of several different polymer molecules. Three

properties characterize the basic operational unit--(1) the volume V , (2) the well depth, or barrier height, V_0 , and (3) the energy E of the charge carrier. The energy E corresponds to the highest energy electron in the potential well and is analogous to the energy of the highest occupied molecular orbital in molecular orbital theory.

Calculating localized electronic state volumes is difficult except when the state is well defined with a simple geometry. One example of a well defined state is that of a dopant molecule embedded in an inert matrix. There are several ways of arriving at the localized state volume. For example, in doped polyacetylene, polypyrrole or polyphenylene sulfide, the onset of conductivity occurs when the total volume fraction of polymer-dopant aggregates exceeds the percolation threshold, ϕ_c . Thus

$$V = \phi_c \equiv \frac{\text{volume of system}}{\text{number of dopant molecules}}$$

Additionally, the localized state volume may also be represented in terms of the number of polymer repeat units with respect to the number of dopant molecules.

$$V = \phi_c \equiv \frac{\text{molar volume}}{\text{repeat unit}} \times \frac{\text{repeat unit}}{\text{dopant molecule}}$$

The most readily applied method of calculating the energy required to remove an electron from a localized state is to calculate the activation energy based on the temperature dependence of conductivity. The particle-in-a-box is a theoretical method of calculating the energy. The

energy of n quantized orbitals is calculated by filling each orbital with two electrons per bond and then estimating the energy of the highest occupied molecular orbital. Then the barrier height V_0 is assumed to be equal to twice the estimated value.

Functional Dependence of Conductivity

To arrive at an expression for conductivity, one can apply the mobility concepts as well as definitions of molecular structure properties. The number density of carriers, the charge per carrier, and the mobility applicable to its motion from site to site are all quantities which must be calculated or estimated in order to arrive at a value of conductivity for a polymer in a given environment.

The number of carriers is equal to the number of localized electronic states formed. For doped polymers (for example, with I_3^- , AsF_6^- , BF_4^-), the number of localized states is proportional to the dopant concentration. Charge transfer complexes produce one localized state per charge transfer pair. For partially oxidized cofacial polyphthalocyanes, a localized state exists for every metal atom-phthalocyanane dopant assembly. This type of investigation is necessary for the particular polymer-dopant system.

Mobility calculations are very critical to the model and two mobility states, one above and one below the percolation threshold, ϕ_c , are determined. Below the

percolation threshold, the mobility is given by $\mu = |e|D/k_B T$ for nearest neighbor hopping with $D = \Gamma \ell^2/6$ for the isotropic three-dimensional case. There are two methods of arriving at a meaningful hop length ℓ . A hop length, based on geometric considerations, is the average distance between localized states or it may be taken as the average cluster radius used in the percolation approach. Calculation of the hop frequency (i.e., number of hops per unit time Γ) depends on the transmission coefficient of an electron with frequency ν escaping the localized state (i.e., potential well). The frequency with which an electron impinges upon the wall, for those systems where the mean free path is comparable to the localized state dimension, is inversely proportional to the distance the electron travels before it encounters a barrier--therefore $s \approx v^{1/3}$. This is a weak dependence and thus s is sensitive to the local atomic structure. To simplify calculations, the frequency ν is set equal to unity. Additionally, the probability of a hop is hypothesized to be the same as the probability of transmission out of the potential well.

For cases well below the percolation threshold, the energy difference between barrier height and particle energy is very important. The functional form of the conductivity is given as

$$\sigma \sim \Phi^* \exp\left(\frac{V_0 - E}{k_B T}\right) \quad (2.97)$$

where ϕ^* includes the frequency of an electron impinging upon the potential barrier and its probability of escape. At low dopant levels, only small clusters are found. As ϕ_c is approached, the size of the localized states (equivalent to the hop length) increases exponentially, while there is only a slow variation in ϕ^* . The exponentially increasing hop length influences greatly the dependence of the mobility on dopant concentration. Phenomenologically, this introduces a variable-range hopping mechanism and the concomitant fractional temperature exponent. The functional form for conductivity becomes

$$\sigma \sim \exp \left[\left(\frac{V_0 - E}{k_B T} \right)^y \right] [(\phi - \phi_c)^{-\xi}] \quad (2.98)$$

where ξ is equal to 6.3. Thus the conductivity is dominated by the $(\phi - \phi_c)$ term and the fractional temperature exponent. In this instance, ϕ is the volume fraction of occupied sites.

Above ϕ_c , there are large extended delocalized regions through which electrons travel freely. Structural order is not really long range and macroscopic transport is limited by thermally activated variable-range hopping. Mobilities are increased by the extended, although localized, charge states. Conductivity takes the functional form

$$\sigma \sim \exp \left[\left(\frac{\theta}{T} \right)^{1/y} \right] \quad (2.99)$$

where θ is a constant and y varies between 2 and 4, depending upon whether ϕ is greater than ϕ_c .

This model is phenomenological in nature and is an *ab initio* quantum mechanical calculation of transport in disordered systems. It succeeds in phenomenologically modeling electronic conduction in polymers in a general sense and rationalize diverse temperature and dopant dependencies of the conductivity.

CHAPTER III

EXPERIMENTAL CONSIDERATIONS

3.1 Introduction

A great deal of experimental work in measuring the resistivity, ρ , or its reciprocal, the conductivity σ , of polymers has been done over the years. In industry, where plastics are used for a variety of purposes, but mainly as insulating materials, the standard test is modeled on ASTM D257.¹⁹ This allows bulk sheet samples of thicknesses up to 7 mm to be tested when an HP 16008A Resistivity Cell¹¹⁶ is used. However, the need for innovative cell design arises when sample geometry or dimensions cannot be accommodated with the standard test procedure.

In this research, new cells had to be designed to measure the conductivity of thin films and sheets and also of very small diameter fibers. Several cells were designed which allowed the measurement of the desired conductivities for the particular polymer geometry under controlled conditions of humidity and temperature.

Due to the combination of low conductivity and small sample cross-section, a very high degree of current sensitivity was needed. This need was met by the use of a very sensitive electrometer (the Keithley 642). Because of the extreme sensitivity of various components of the apparatus, it was necessary to take systematic precautions

to provide electrostatic shielding and proper grounding. This was accomplished by constructing a Faraday cage around the important components of the measuring system. This setup provided more consistent results, especially when testing lower conductivity polymers.

3.2 Formalism for Describing the Conductivity Measurements

The operational definition of the volume, or bulk, resistivity ρ_v (Ωm), of an isotropic material is based on the resistance, as determined in accordance with Ohm's law, between opposite faces of a unit cube. Thus, the longitudinal resistance R of a block of material of length l and cross-section A can be written as

$$R = \frac{\rho_v l}{A} \quad (3.1)$$

This is shown in Figure 3.1. Alternatively, volume resistivity can also be expressed by a generalized form of Ohm's law

$$E = \rho_v J \quad (3.2)$$

where E and J are scalar quantities representing the magnitudes of the electric field and current density, respectively, at any point in the material. For anisotropic materials, the resistivity can be written in general form as a second rank tensor which relates the vector quantities of field and current density

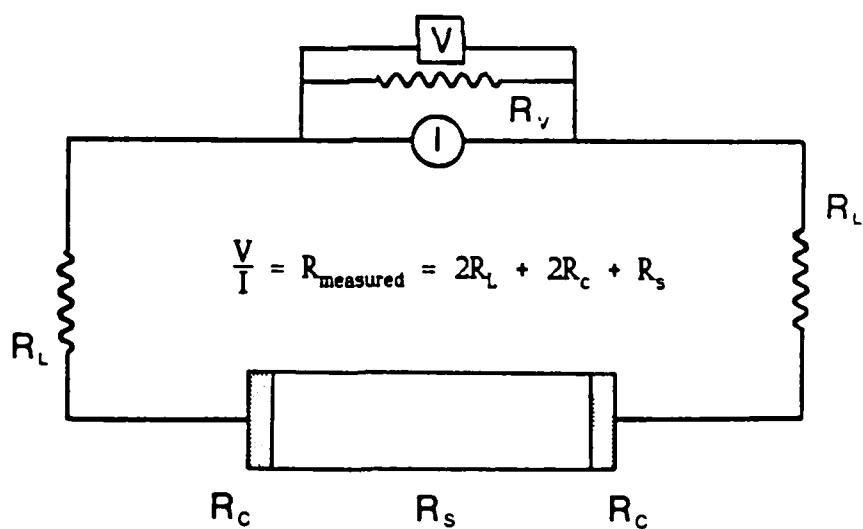
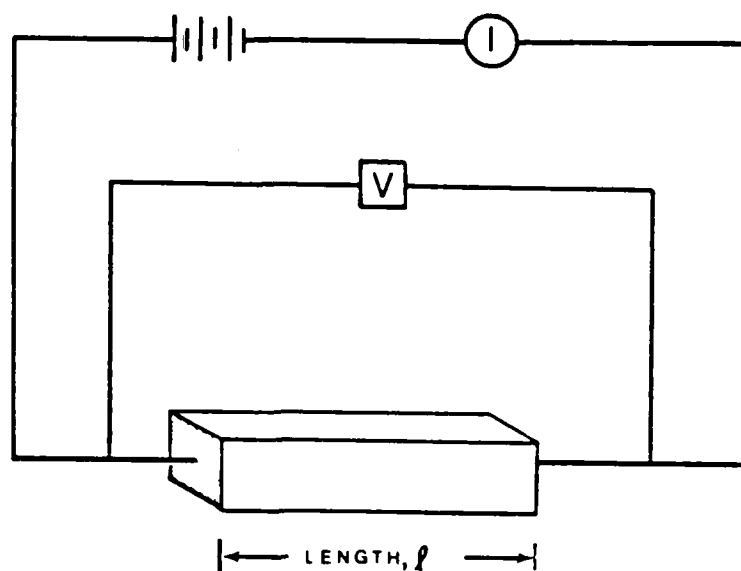


Figure 3.1. (a) Schematic Representation of Two Probe Resistivity Measurement; (b) Circuit Diagram of Two Probe Method.

$$\vec{E} = \rho_v \cdot \vec{J} \quad (3.3)$$

Another way of expressing the relationship between the electric field and current density is through volume conductivity

$$\sigma = \frac{1}{\rho_v} \quad (3.4)$$

in units of S/m or S/cm. In the general tensor notation form, conductivity is written as

$$\vec{J} = \sigma_v \cdot \vec{E} \quad (3.5)$$

When the current flow is confined to a surface, it is convenient to define an analogous surface resistivity, ρ_s in (Ω), as the resistance between opposite edges in a square. For a medium with a linear electrical response, the resistance across a square is independent of the size of the square, so that the unit surface resistivity is properly called the ohm and often is written as ohm per square (Ω/\square). In real terms, a conducting surface must be a layer with a finite thickness δ . Thus, an effective surface resistivity is measured which is related to the effective volume resistivity of the layer by

$$\rho_s = \frac{\rho_v}{\delta} \quad (3.6)$$

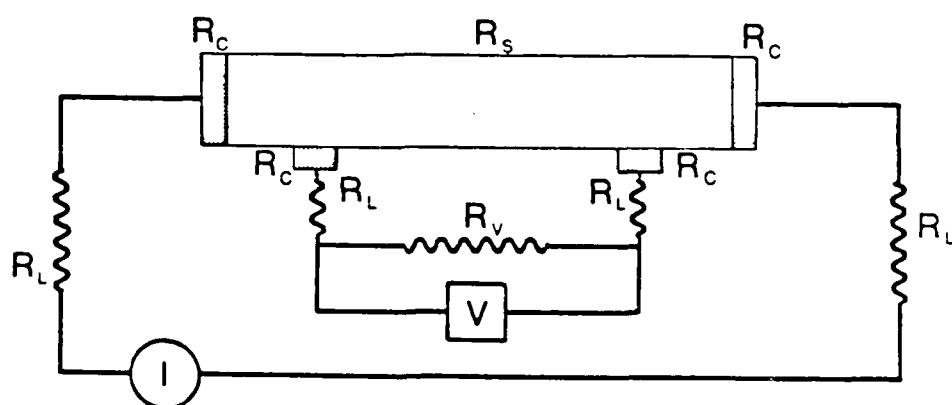
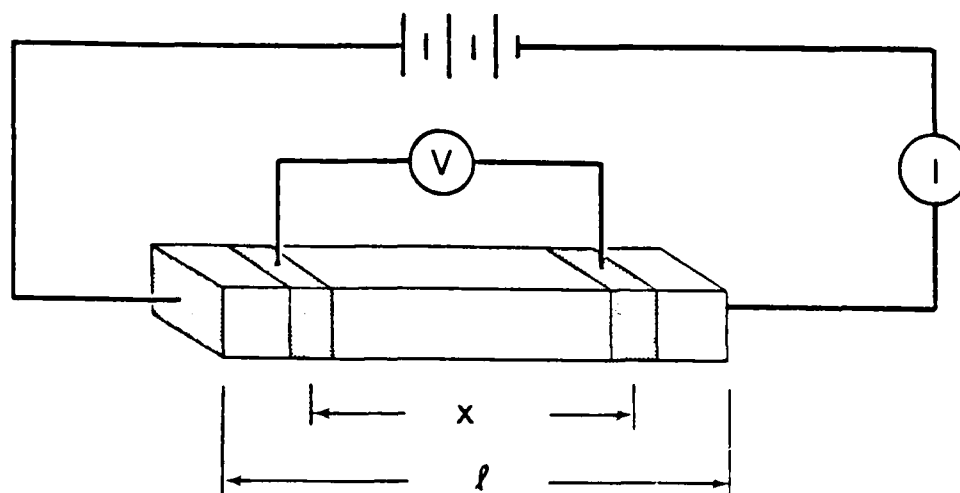
It is apparent that the simple appearance of Eq. (3.6) is deceptive because for real materials, the morphology and specific properties of the surface layer, and even its

composition, may be considerably different than for the bulk material.

3.3 General Principles of Electrode Geometry^{30,117}

The simplest electrical resistivity measuring arrangement consists of a rectangular or cylindrical block with two electrodes applied, at opposite ends (see Figure 3.1). The resistance then becomes the ratio of the applied voltage to the series current. The difficulty in making accurate measurements lies in the uncertainty of the contact resistances between the specimen and electrodes. Thus, pressure resistance as utilized by the standard resistivity cells must be augmented by painting or evaporating conductive electrodes onto the polymer surface. This allows more uniform and continuous contact between the polymer and the electrode. One method of circumventing some of the contact problems is to use a four-terminal method. This is shown schematically in Figure 3.2. A current density, J , is established in the central region (of cross-sectional area, A) by passing a known current, I , between the outer electrodes. The electric field, E , is determined by measuring the potential drop ΔV across the two inner probes which are separated by a known distance (x in this case). The resistivity is then given as:

$$\rho_v = \frac{E}{J} = \frac{\Delta V/x}{I/A} \quad (3.7)$$



$$V = IR_s - 2I_v R_c - 2I_v R_L$$

$$I_v R_v = IR_s - 2I_v R_c - 2I_v R_L$$

$$\text{as } R_v \rightarrow \infty \quad I_v \rightarrow 0$$

$$V = IR_s$$

$$R_{\text{measured}} = \frac{V}{I} \rightarrow R_s$$

Figure 3.2. (a) Schematic Representation of Four Probe Resistivity Measurement; (b) Circuit Diagram of Four Probe Method.

The effects of contact resistance are thus avoided, provided that the contact resistances of the voltage electrodes are much smaller than the input resistance of the voltmeter. This method is usually restricted to resistivities below $10^6 \Omega\text{m}$; otherwise currents become too small to measure accurately and voltmeter resistances become significant. Thus, the four-point probe method is used primarily in semiconductor research, but is not generally used for polymers where resistivities of $10^{15} \Omega\text{m}$ are not unusual.

When measuring high resistivity materials, e.g., polyethylene, polypropylene), thin sheet specimens are used, thereby reducing the specimen thickness between the conducting electrodes. The problem now becomes one of current leakage from the high voltage source to the ammeter via routes other than the intended one through the specimen. A major problem area is leakage along the specimen surface, which in many instances, provides a lower resistance path than the intended one through the bulk of the specimen. This path along the surface is enhanced by the accumulation of adsorbed moisture and stray ions. This has led to the development of the three electrode system, shown in Figure 3.3. The extra electrode in this system is designated as a guard electrode and is applied to the side with the low voltage electrode and its connection to the ammeter. This electrode is grounded so that it can intercept and prevent current from leaking to the ammeter.

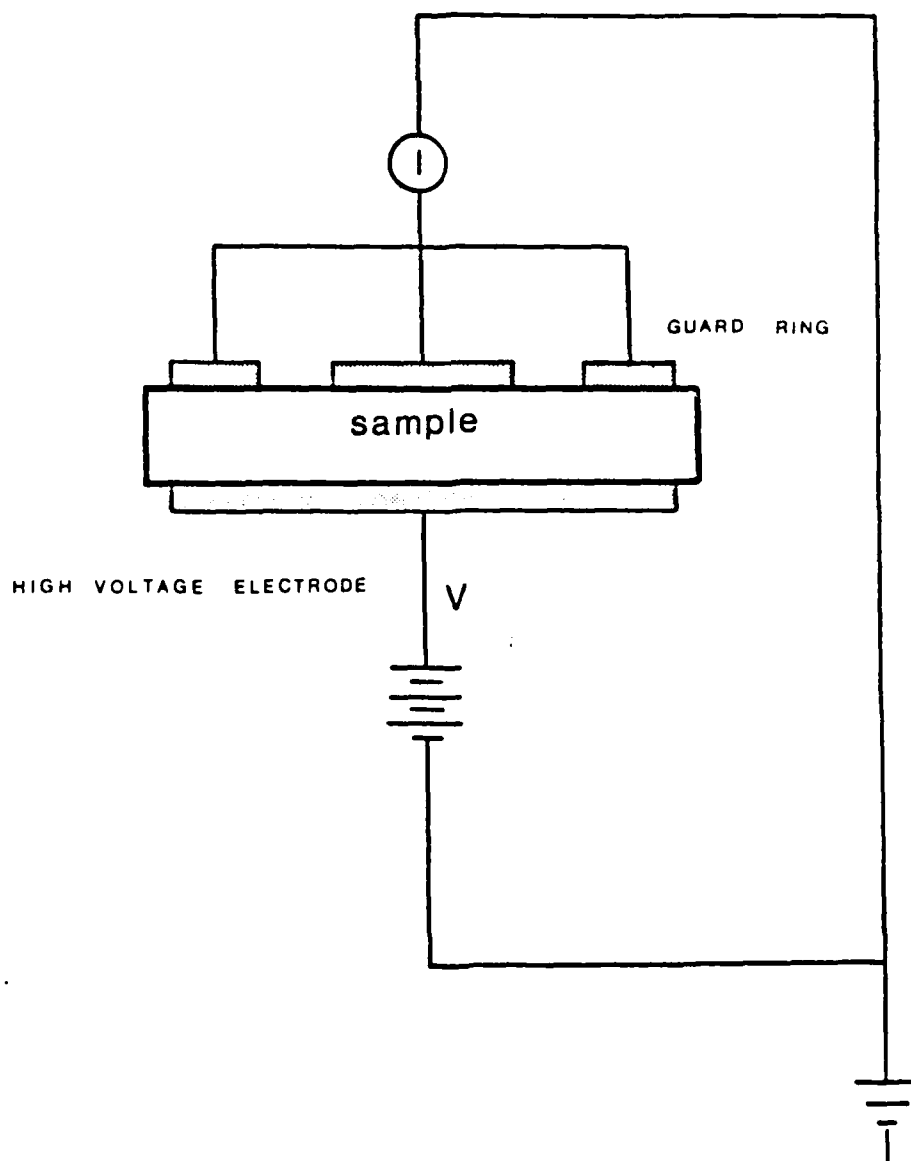


Figure 3.3. Measurement of High Volume Resistivity: Three Terminal or Guarded Electrode System.

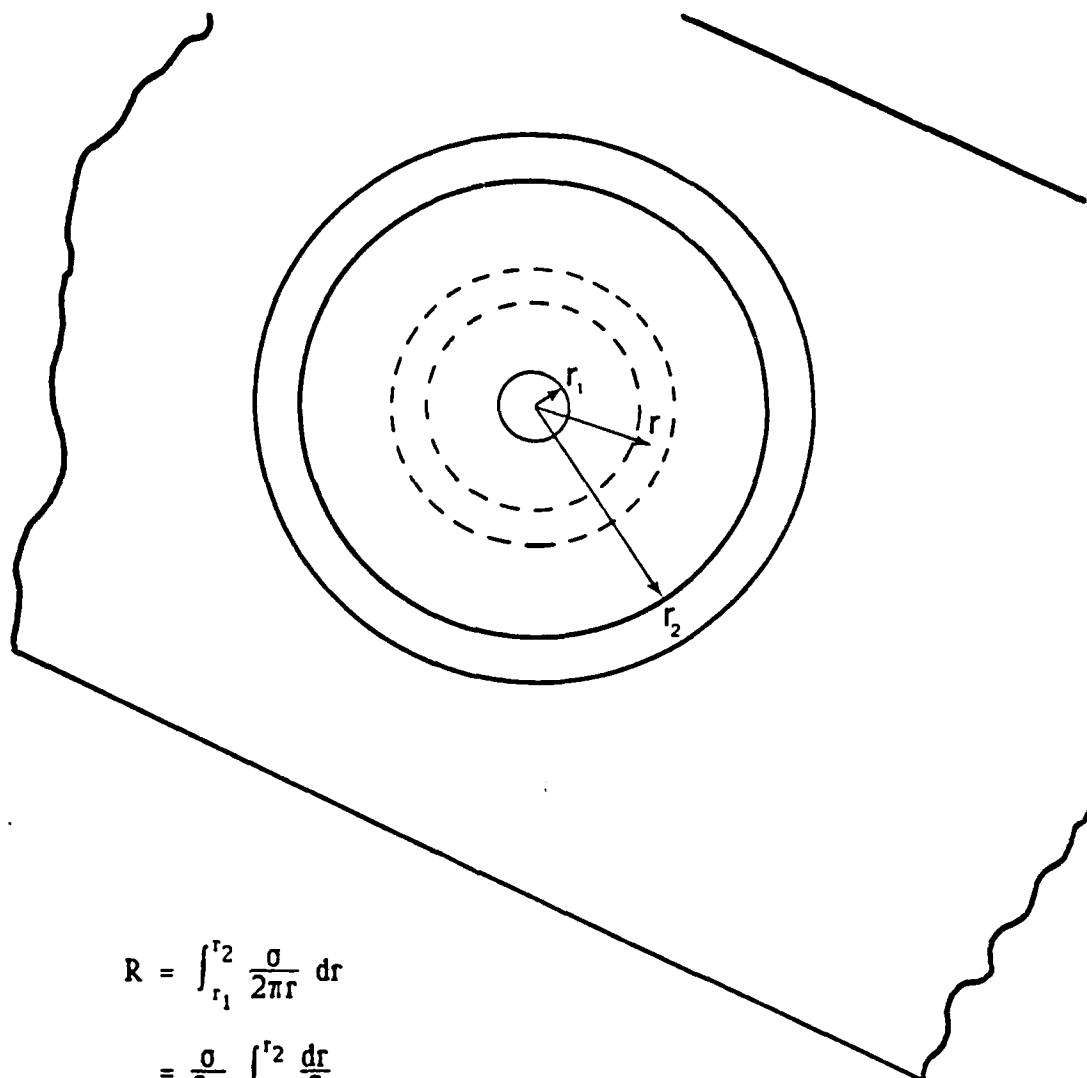
In making reliable surface conductivity measurements, the humidity must be strictly controlled. Concentric ring electrodes are the easiest to use when making measurements of surface conductivity. This arrangement is shown in Figure 3.4. The resistance R between the electrodes is the sum of the resistances of the elemental annuli, of mean radius r , in series and can be written as:

$$R = \int_{r_1}^{r_2} \frac{\rho_s}{2\pi r} dr \quad (3.8)$$

where r_1 and r_2 are the radii of the inner and outer electrodes respectively. Hence,

$$\rho_s = 2\pi R \ln\left(\frac{r_1}{r_2}\right). \quad (3.9)$$

Generally speaking, if the polymer surface is flat and not too hard, good contact between the polymer and the electrodes can be achieved with knife-edge metal electrodes, where the question of non-ohmic (i.e., non-linear) processes may need to be considered. Otherwise, it may once again be necessary to paint or evaporate conducting electrodes onto the surface. A significant portion of the surface conductivity can be attributed to ions associated with the surface zone, therefore experimental conditions must be regulated so that these effects can be taken into account in the analysis of the data. As previously mentioned, the humidity must be closely monitored and controlled if the results of surface conductivity experiments are to be meaningful. It must also be realized that a surface



$$\begin{aligned} R &= \int_{r_1}^{r_2} \frac{\sigma}{2\pi r} dr \\ &= \frac{\sigma}{2\pi} \int_{r_1}^{r_2} \frac{dr}{r} \\ &= \frac{\sigma}{2\pi} \ln\left(\frac{r_2}{r_1}\right) \end{aligned}$$

Figure 3.4. Schematic Representation of System for Measuring Surface Resistivity.

conductivity measurement not only includes the surface component of the conductivity, but also an inseparable volume component which flows through the bulk of the material just below the surface and is influenced greatly by the electrode geometry.

3.4 Experiments Performed and Selection of Materials

Previously, Barker^{64,65} has carried out research into the ionic nature of conductivity in polymers. Significant advances into the understanding of the interaction between diffusant ions and the structure of the polymer was achieved.²⁰ Other researchers^{58,60-64,76,77,81,118} have also examined various aspects of ionic conductivity in polymers, but few of these investigations have examined conduction in fibers.

Fibers, by their very nature, are both easy and extremely difficult with which to work. An idealized fiber would be a circular cylinder. Measurement of this type of structure, in principle, should be easy--paint electrodes on the ends of the cylinder, apply a voltage and either measure the current flow through the circuit or the voltage drop across the specimen. The surface component can easily be eliminated by applying a conductive strip around the circumference of the cylinder and grounding it. Imagine, however, reducing the diameter of the cylinder from millimeters to just tens of microns. The length of the specimen is reduced to just a few millimeters. Therefore,

working with cylindrical fibers is easy in principle, but their small size presents both handling and measurement problems.

The main reason for working with fibers is that a number of new and interesting polymers developed for the U.S. Air Force are in this form. These polymers are poly p-phenylene bensobisthiazole (PPBT) and benzimidazo-benzophenanthrolin (BBL). Both of these polymers are characterized as quasi-planar with rigid backbones.^{119,120} The Air Force is interested in a number of properties, including electrical, thermal and diffusional. However, out of this initial interest came some interesting questions--one being the role of surface conductivity in the overall conduction process. Additionally, the change in conductivity due to various organic and metal-salt diffusants was considered to be important in conjunction with the effect that diffusing moisture had on the electrical conductivity, and its variation with time. Temperature versus current measurements yielding values for the activation energy of conduction are also necessary for an adequate evaluation of the effects of the various diffusants.

Thus, a number of different types of experiments were performed on the polymer fibers. These experiments can be summarized as

- (a) current versus time measurements
 - doped and undoped samples


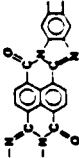
- dry and humid atmosphere
- differing temperatures
- (b) current versus temperature measurements
 - dry atmosphere for doped and undoped samples
- (c) current versus voltage (or field strength)
- (d) current versus change in specimen length/diameter.

Not all of these experiments were performed on each polymer fiber. Some polymers were more suited than others to a particular measurement procedure.

A number of different polymers were studied, in addition to those of interest to the Air Force. Since these experiments were performed on fibers, a number of well-studied polymers (e.g., polyethylene (PE), polypropylene (PP), and polyamides--trade name, nylon) were chosen as some information on the conductivity of these fibers is available. The selection of these materials allowed a comparison between the measured values of conductivity for the fiber and values found in the literature. This gave a way of interpreting the data from the less well studied materials, i.e., PPBT and BBL.

Structurally, PPBT and BBL are rigid backbone, almost planar type polymers, whereas the other polymer fibers are more flexible and less ordered in nature. Table 3.1 summarizes information on the polymers used in this research.

Table 3.1
Properties of Selected Polymers

Polymer	Structure	$\rho_{\text{volume}} \text{ (g/cm}^3\text{)}$	$\rho_{\text{surface}} \text{ (S)}$	Water uptake	Fiber diameter (d)
PPBT poly(p-phenylene- benzobisthiazole)		10^{-13}	---	---	20-95
BBL benzimidazo- benzophenanthrolin		---	---	---	70
Nylon 6 poly(caprolactam)	$[\text{NH}(\text{CH}_2)_5\text{C}(=\text{O})]_n$	10^{-12}	---	1.3-1.9	150
Nylon 6,6 poly(hexamethylene adipamide)	$[\text{NH}(\text{CH}_2)_4\text{C}(=\text{O})\text{NH}(\text{CH}_2)_6\text{C}(=\text{O})]_n$	10^{-12}	10^{-10}	1.3-1.9	310
PE polyethylene	$[\text{CH}_2]_n$	10^{-17}	10^{-13}	0.03	270
PP polypropylene	$[\text{CH}_2-\text{CH}(\text{CH}_3)]_n$	10^{-16}	10^{-13}	0.05	500 (unstretched) 240 (stretched)

3.5 Doping of Polymer Samples

The objective of doping polymers is to significantly affect the overall electrical properties of that particular polymer. The term doping usually means the addition of some species that will aid in electronic conduction by introducing charge transfer sites along the polymer chain. Doping can also refer to additives which will enhance ionic conductivity. Dopants may increase the overall conductivity by several orders of magnitude (i.e., an increase of 10^5 S/m is seen in some cases over the initially observed conductivity of the undoped state).²³ This type of doping is routinely performed on polyacetylene with either electron acceptors (e.g., I_2 , AsF_5 or H_2SO_4)^{16,123} or transition metal salts (e.g., iridium and osmium salts) which oxidize the π -bonds in polyacetylene.^{124,125}

The purpose of introducing various organic molecules, acids, and metal-salt ions into the polymer is to observe their effect on the electrical conductivity and to gain some insight into the particular conduction mechanism for the polymer/dopant system of interest. Additionally, the effect of moisture on the conduction process is of interest as well as changes in the activation energy for conduction with doping species.

The usual doping medium was a solution, usually a metal-salt dissolved in distilled water, into which the polymer fiber is placed. The amount of time a polymer fiber was allowed to soak in the doping solution varied, but it

was not less than twenty-four hours and sometimes as long as a week. In some instances the temperature of the solution was raised to aid in the diffusion process. The time allowed for diffusion is sufficient for equilibrium conditions to be reached and a uniform distribution of dopant within the polymer fiber is obtained. The samples are then removed from solution and quickly rinsed and allowed to dry (e.g., in the case of metal-salt solutions) or just allowed to dry (e.g., in the case of formaldehyde, n-pentane, etc.). The purpose of rinsing in distilled water is to remove excess salt deposits from the surface of the polymer. Rinsing the polymer entails the rapid agitation of the fiber in a beaker of distilled water for several seconds. At no time were the fibers allowed to just soak in the distilled water. Upon removal, the polymers were then placed in desiccators to dry until their use in an experiment. Optical examination of the various fibers, especially the nylons, revealed that color changes occurred in the polymer after doping. For example, the nylon 6 fiber soaked in CuCl_2 turned a light green color. This provides some evidence that the Cu^{2+} ions are indeed being absorbed into the polymer. This change in color was observed in other polymers where colored cations were present in the doping medium. Unfortunately, the PPBT and BBL, being opaque, did not exhibit color changes, although it was assumed that some metal salt ions were absorbed since the doping conditions did not vary from polymer to polymer.

Previous work by Chen¹⁸ showed that soaking PPBT in ethyl alcohol reduced the conductivity (see Figure 3.5) by a factor of 4. Therefore, some of the fibers were given ethyl alcohol pre-treatments before being doped in other solutions. This washing in ethyl alcohol is assumed to clean the fiber.

Only in the case of iodine (I_2) doping was the procedure different from that outlined above. In doping the various fibers with iodine, the first step was to suspend the fibers separately in a closed jar. Iodine crystals were placed in the jar and the jar was then heated to increase the iodine vapor pressure. The iodine vapor was allowed to diffuse into the fibers at the elevated temperature between 2 and 4 hours. The jar was allowed to cool overnight. The PE, PP, and nylon fibers turned a deep orange color, thus indicating some iodine absorption. These fibers were then rinsed to remove the iodine which crystallized on the surface and allowed to dry in a desiccator until needed.

Table 3.2 shows the diffusants used in this research. Not all diffusants were used with each polymer. In fact, only BBL, and to some extent PPBT, were doped extensively.

3.6 Instrumentation

The extremely low currents found to flow in polymeric materials demand the use of super-sensitive measuring devices. As such, a Keithley 642 electrometer was chosen as the current measuring device. It has the capability of

		<u>Currents</u>	
<u>PBT Samples</u>		<u>Untreated (i_u)</u>	<u>Ethyl Alcohol Treated (i_t)</u>
28555-19-2	Fiber	2.20×10^{-14} A	4.7×10^{-15} A
29022-14-3	Fiber	2.08×10^{-14} A	4.0×10^{-15} A
27554-48-6	Fiber	4.03×10^{-14} A	1.0×10^{-15} A
27554-48-13	Fiber	2.57×10^{-14} A	6.5×10^{-15} A
28555-25-6	Film	8.00×10^{-15} A	2.2×10^{-15} A

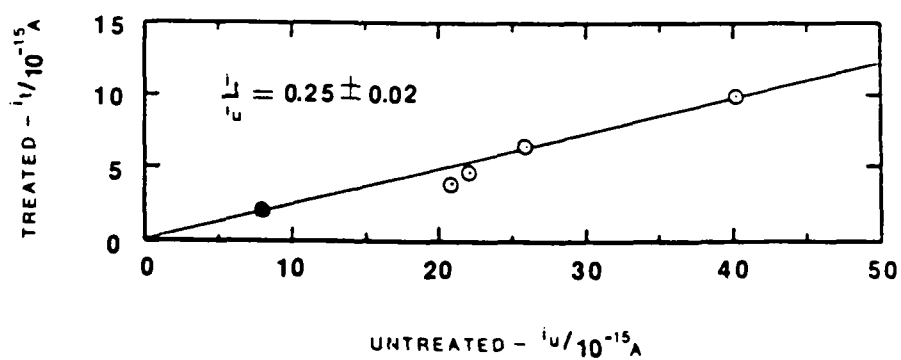


Figure 3.5. Comparison of Observed Current Levels Before and After Washing PPBT Samples in Ethyl Alcohol.¹⁸

Table 3.2
Diffusants Used in Doping
Polymer Fibers

I. Charge Transfer Forming Dopants

A. I_2

B. H_2SO_4

II. Metal-salt Dopants

A. $NaCl$, $LiCl$, $CaCl_2$, $CuCl_2$

B. KI , NaI

C. $Fe(NO_3)_3$, $Co(NO_3)_2$, $Ni(NO_3)_2$

III. Organics

A. Formaldehyde

B. n-pentane

C. Nitrobenzene

D. Ethyl Alcohol

E. Acetone

F. Phenol and Phenol/Water Solution

G. Indigo/Water Solution

H. Dimethyl Sulfoxide

IV. Miscellaneous

A. Distilled Water

reading 10 attoamperes full scale when switched to its most sensitive current scale.

The ability to measure very small currents accurately means that the noise in the high resistance circuits must be kept to a minimum. Coaxial cables, metal shielding and common ground loops are necessary to intercept and reduce stray noise from auxiliary electrical equipment and fluorescent lighting. This led to the construction of a large (i.e., 1.25 m x 0.50 m x 0.50 m) Faraday cage which encloses all current measuring circuitry.

The need for controlled conditions of temperature and humidity led to the design and construction of special conductivity cells. Cell design also provided additional shielding of the polymer sample.

Electrical Instrumentation

The major instrumentation for the research was needed for current measurement, temperature registering and voltage application and measurement. Of the three, current measurement is the most important in that this is the most difficult aspect of the research to control effectively.

The Keithley 642 digital electrometer was selected as the current measuring device. The 642 is a refined direct-current multimeter with input characteristics that allow a wider range of current, voltage, charge and resistance measurement than one normally obtains with multimeters.

In simplified form, the Model 642 is divided into a measurement mainframe and a remote head. A command from the

mainframe (situated outside of the Faraday cage) configures the remote head for current, charge, voltage or resistance measurements at a specified level. One feature of the 642 is that all components whose performance would be affected by dust, moisture, or other contaminants are sealed inside the remote head. The only exception is the sapphire-insulated input connector which is protected by the input slide cover. Avoiding contact of contaminants with the sapphire-insulated input connector is of prime importance.

The Keithley 642 uses a specially packaged dual monolithic MOSFET with compensated temperature coefficient in a guarded package. Ambient temperature variations do not produce significant errors because the circuitry is individually compensated and adjusted for each FET to give a voltage coefficient of only $30 \mu\text{V}/^\circ\text{C}$.

The design of the remote head minimizes the active input volume. Less than 15 ionization current pulses are observed per hour of operation. The remote head is sealed and contains desiccant paper to maintain low internal humidity. In addition, the remote head has been isolated inside the Faraday cage in a specially sealed compartment where the humidity is controlled. Coaxial cables from the conductivity cell to the remote head are shielded by the Faraday cage and clamped at various points to prevent movement. Thus, the 642 is capable of monitoring current levels down to the theoretical limits imposed by the level of the input offset current.

The Keithley 642 has an input resistance greater than $10^{16} \Omega$ which allows it to measure current as low as 10^{-17} amperes. This is satisfactory in most instances. One drawback to the 642 is the 30 volt limitation on the maximum allowable dc input voltage. This limits the electric field that can be applied to a particular sample. More detailed information on the Keithley Model 642 can be found in product information and special publications.^{126,127}

In order to record the temperature in the conductivity cell, a type T (copper vs. constantan) thermocouple was used with an ice reference junction. The thermo-electric voltage is displayed on a Keithley 195A digital multimeter.

A step voltage is provided by a Hewlett Packard 6115A precision power supply, capable of delivering 0-50 dc voltages at up to 0.8 amperes, or 50-100 dc volts at up to 0.4 amperes.

Conductivity Cell Design

The concept of measuring the electrical conductivity of small diameter fibers is analogous to the method used for measuring thin films. In this case, the lateral dimensions (i.e., radius) is much smaller than the distance between the electrodes. The cell design is simple--suspend a fiber between two metal electrodes and apply the voltage (V). The current (I) is measured and by knowing the length of the fiber (l) and its cross-sectional area (A), the conductivity (σ) can be calculated in the usual way, i.e., $\sigma = (l/VA)I$.

Figure 3.6 shows schematically the design of the measuring cell. No current path other than through the fiber exists. The teflon blocks are purposely separated and grounded to the Faraday cage so that there is no alternative path through which the current can flow. The electrode material is either copper or platinum wire, which is mounted to the teflon blocks by metal set screws. It is from these wires that the polymer fiber is suspended.

The polymer fiber is attached to the wire electrodes by means of colloidal silver paste/paint. The colloidal silver was used because it was a good conducting medium, and it provided mechanical stability and support. One problem in using silver paste/paint is the unknown effect on the fiber by the solvent. In all cases, the solvent is allowed to evaporate before any measurements are made.

This assembly fits into a desiccant chamber. Mounted inside the desiccant chamber is a light bulb assembly which serves as the heat source for moderating the temperature. The intensity of the light bulbs is controlled by a Variac, allowing the temperature to be controlled to within 0.25°C . The light bulb assembly is shielded from the fiber measuring assembly and grounded, thus preventing stray electromagnetic interference. With a 300 watt light bulb, a temperature in excess of 100°C can easily be reached inside the desiccant chamber. By including desiccant to the chamber, the relative humidity is kept to near zero values.

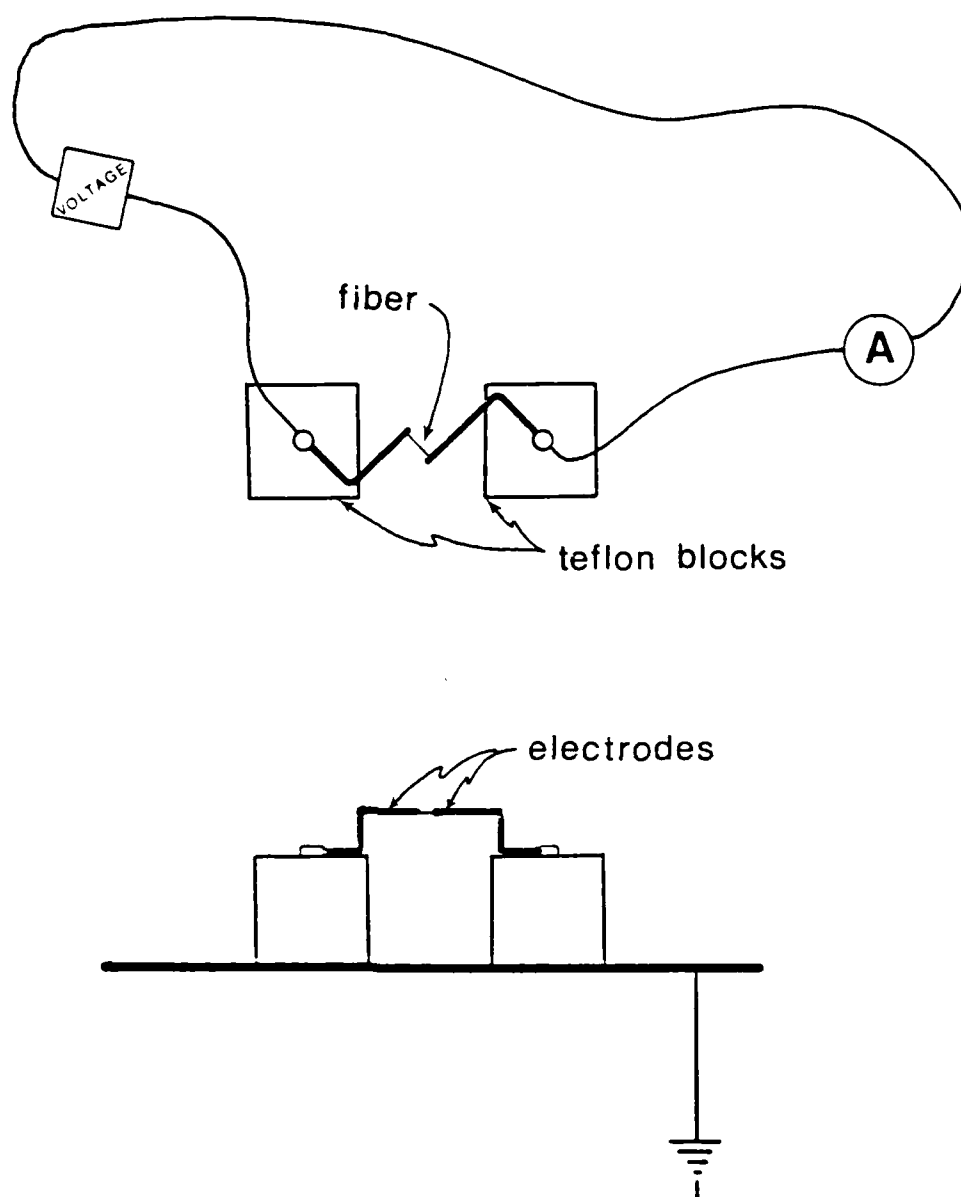


Figure 3.6. Schematic Representation of Conductivity Cell Used in Fiber Research.

3.7 Separation of Surface and Volume Conductivity in Fibers

One way of determining the surface and volume conductivities from the total observed conductivity in a polymer fiber is to measure the current for a series of fibers of differing radii.¹⁸ Assuming that the total current is just the sum of the surface and volume components, the equation can be written as

$$I_{\text{total}} = I_{\text{volume}} + I_{\text{surface}} \quad (3.10)$$

If the volume of the fiber dominates the current flow, then

$$\sigma_{\text{volume}} = \frac{l I_{\text{volume}}}{V A} \approx \frac{l I_{\text{volume}}}{V \pi r^2} \quad (3.11)$$

where r is the fiber radius. In the case where surface conduction dominates the overall measurement, the cross-sectional area becomes $2\pi r\delta$, where δ is the thickness of the conducting layer. Thus

$$\sigma_{\text{surface}} = \frac{l I_{\text{surface}}}{V A} = \frac{l I_{\text{surface}}}{V 2\pi r \delta} \quad (3.12)$$

By convention, surface conductivities are measured in ohm^{-1} , so a rearrangement of the equation is necessary. The surface conductivity will be redefined in terms of

$$\sigma'_{\text{surface}} = \delta \sigma_{\text{surface}} = \frac{l I_{\text{surface}}}{V 2\pi r} \quad (3.13)$$

where σ'_{surface} is the surface conductivity as defined in the conventional way. In a numerical sense, one has the effect of replacing δ by one unit in Eq. (3.12). As a means of

trying to determine which mode dominates, an apparent conductivity is defined:

$$\sigma_{\text{apparent}} = \frac{l I_{\text{total}}}{V \pi r^2} \quad (3.14)$$

and for the case where fiber length and voltage are constant

$$\pi r^2 \sigma_{\text{app}} = \pi r^2 \sigma_{\text{vol}} + 2 \pi r \sigma'_{\text{sur}} \quad (3.15)$$

or,

$$\sigma_{\text{app}} = \sigma_{\text{vol}} + \frac{2}{r} \sigma'_{\text{sur}} \quad (3.16)$$

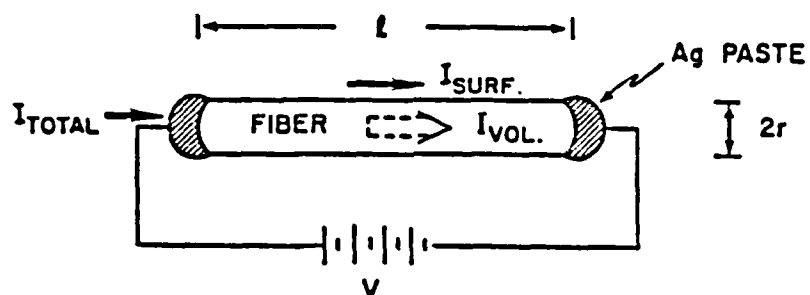
from which a graph of σ_{app} versus $1/r$ yields a linear plot with a slope equal to two times σ'_{surface} . This is shown in Figure 3.7(b). This is an obvious result because as r becomes larger $1/r$ approaches zero in the limit. Physically, increasing the radius of the fiber to infinity, i.e., essentially modeling an infinite solid, reduces the surface component of conductivity to zero. When the condition $r \rightarrow \infty$, leading to $1/r \rightarrow 0$, is approached, $\sigma_{\text{app}} \approx \sigma_{\text{volume}}$.

The possibility remains that in small diameter fibers, the majority of the current is carried by a thin surface layer. Thus, the apparent conductivity can be modeled as

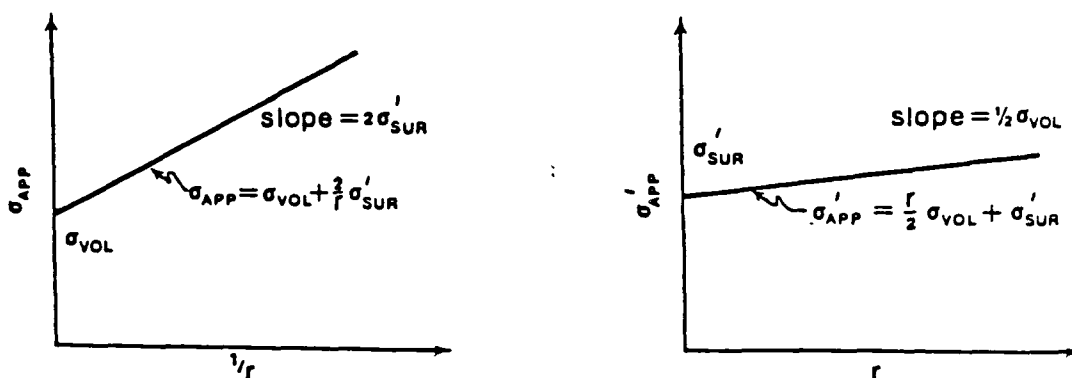
$$\sigma'_{\text{apparent}} \equiv \delta \sigma_{\text{apparent}} = \frac{l I_{\text{total}}}{V 2 \pi r} \quad (3.17)$$

and is subject to the same initial conditions of voltage and specimen length. Thus, the equation now becomes

(a) EXPERIMENTAL TECHNIQUE



(b) DATA ANALYSIS



(c) ADVANTAGES & DISADVANTAGES

- | | |
|---|--|
| <ul style="list-style-type: none"> • SIMPLE IN CONCEPT • INDIVIDUAL MEASUREMENTS EASY | <ul style="list-style-type: none"> • NEED MANY DATA POINTS • VERY UNIFORM DIAMETER SAMPLES NEEDED • NEED HIGHLY REPRODUCIBLE CONTROLLED ENVIRONMENT |
|---|--|

Figure 3.7. Theoretical Technique to Separate σ_{VOL} and σ_{SUR} . (a) Experimental Technique; (b) Case Where $\sigma_{VOL} \gg \sigma_{SUR}$ and Case Where $\sigma_{SUR} \gg \sigma_{VOL}$; (c) Advantages and Disadvantages of Method.

$$\sigma'_{app} = \frac{f}{2} \sigma_{vol} + \sigma'_{sur} . \quad (3.18)$$

In this case, a graph can be plotted of σ'_{app} versus r . This is illustrated in Figure 3.7(b). As r goes towards zero, $\sigma'_{app} \approx \sigma'_{sur}$ and the slope of the straight line yields a value of one-half the volume conductivity.

Unfortunately, this type of analysis is difficult to perform because in some instances, a wide variety of fiber diameters for a particular polymer is not readily available. This difficulty has forced a re-evaluation of the problem, and as such, the following model was developed. This model requires a minimum of only two measurements being made on a fiber in order to separate the bulk and surface conductivities.

The rationale behind this model can be seen qualitatively by examining an idealized representation of a fiber using an equivalent circuit model. This situation is depicted schematically in Figure 3.8. The polymer fiber is idealized as a finite, but large bundle of parallel resistors, completing a circuit between two electrodes. This is a fairly realistic model for PPBT and BBL fibers, as they are essentially linear, rigid rod-type polymers. This model is not applicable (although it may be suitable from a continuum point of view) for PE, PP or nylon fibers where the chains are tangled. In any case, significant reduction in fiber length between the electrodes, brought about by the application of silver paint around the surface of the fiber,

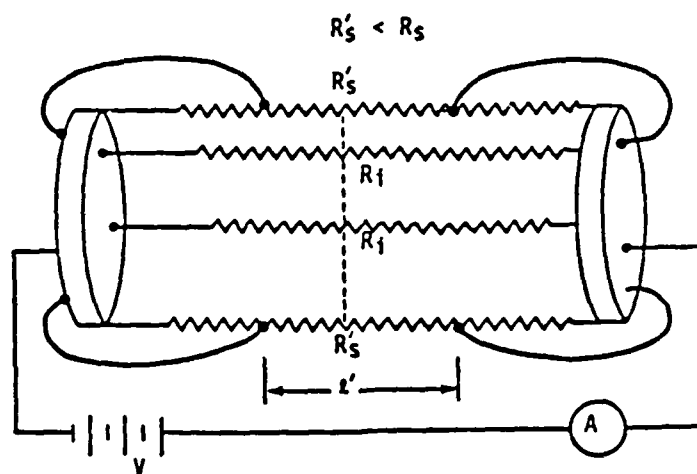
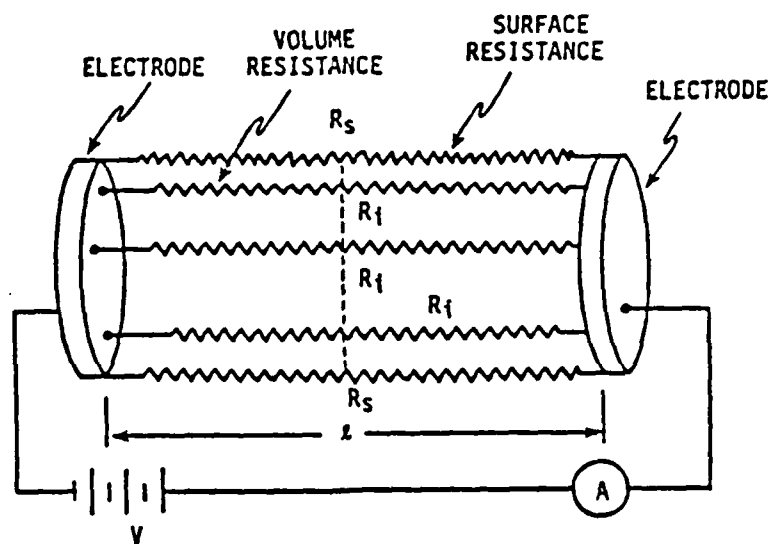
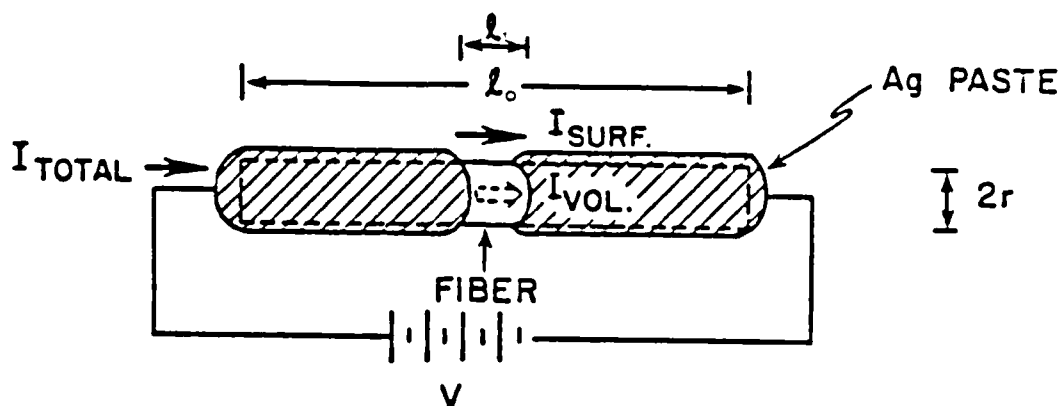


Figure 3.8. Equivalent Circuit Model for Determining Surface and Bulk Conductivity by Making Two Measurements on a Single Fiber.¹⁸

is viewed as being analogous to a partial shorting of R_s (surface resistance) to give a new value of resistance, R'_s . In this model, only the surface resistance of the total resistance is assumed to change.

Thus, the first measurement is made when the effective length of the fiber is ℓ_0 . The second measurement is made after the original length is reduced to a value of ℓ_1 by the application of silver conducting paste as shown in Figure 3.9. Once again, two possible cases of describing the conductivity are possible--either the volume conductivity dominates the total conduction or the surface region is the primary current carrier. When the volume of the fiber is the main conducting region, advancing the silver paint along the surface should have a minimal effect on the total current flow. This is analogous to the expression $R_{\text{surface}} \gg R_{\text{volume}}$. However, if the surface is the more highly conductive region, then decreasing the length between the electrodes should increase the observed current significantly. This situation corresponds to $R_{\text{surface}} \ll R_{\text{volume}}$.

In either case, changing the length of the fiber for a given voltage should yield a direct inverse (i.e., linear plot with negative slope) relationship with current. If the volume dominates, the slope should not vary much from zero. However, if the surface is the dominant conducting region, then the slope of the line should be -1, i.e., a direct inverse proportionality between I and ℓ . Depending on the



IF

$$(\sigma_{VOL.})_{||} \gg (\sigma_{VOL.})_{\perp} , \quad (\sigma_{SURF.})_{||} \gg (\sigma_{SURF.})_{\perp} ,$$

AND $\sigma_{APP.}(l)$ & $\sigma_{APP.}(l_0)$ ARE KNOWN,

THEN $(\sigma_{SURF.})_{||}$ AND $(\sigma_{VOL.})_{||}$ CAN BE CALCULATED.

Figure 3.9. Special Technique to Separate σ_{vol} and σ_{sur} by Varying Effective Length of Fiber.¹⁸

relative contributions of the surface and bulk, intermediate values of slope are possible.

Making measurements at the two lengths leads to two equations which must be solved simultaneously. The first equation is the apparent conductivity (for both surface and volume) that were derived previously.

- volume dominating conduction yields

$$(a) \quad \sigma'_{app}(l_0) = \sigma_{vol} + \left(\frac{2}{l}\right)\sigma'_{sur} \quad (3.18a)$$

- surface dominating conduction yields

$$(b) \quad \sigma'_{app}(l_0) = \left(\frac{l}{2}\right)\sigma_{vol} + \sigma'_{sur} \quad (3.18b)$$

The second pair of equations is constructed for the case where l_0 is reduced in length to a value l_1 . From the equivalent circuit diagram, if conduction dominates, the effective length of those resistors remains unchanged. The surface resistance changes by the ratio l_0/l_1 , i.e., $R'_S = (l_0/l_1)R_S$, thus leading to

$$\sigma_{app}(l_1) = \sigma_{vol} + \frac{l_1}{l_0} \left(\frac{2}{l}\right)\sigma'_{sur} \quad (3.19)$$

Solving Equations (3.18a) and (3.19) allow σ_{vol} to be calculated (remembering that the effective length of the volume resistors remains unchanged):

$$\left[\sigma_{app}(l_0) - \left(\frac{l_0}{l_1}\right)\sigma_{app}(l_1) \right] = \left[1 - \frac{l_0}{l_1} \right] \sigma_{vol} \quad (3.20)$$

All values of the variables are known or can be

measured. Then σ'_{sur} can be calculated, and ideally, the contribution of σ'_{sur} to the total conduction will be small.

When the surface layer provides the primary means of current flow, then l_1 becomes the effective length of the equivalent circuit and any change in specimen length should produce measurable and significant changes in current. Thus, a new equation may be written for this case.

$$\sigma'_{\text{app}}(l_1) = \left(\frac{l_1}{l_0} \right) \left(\frac{r}{2} \right) \sigma_{\text{vol}} + \sigma'_{\text{sur}} \quad (3.21)$$

Solving Equations (3.18a) and (3.21) simultaneously gives the result:

$$\left[\sigma'_{\text{app}}(l_0) - \left(\frac{l_0}{l_1} \right) \sigma'_{\text{app}}(l_1) \right] = \left[1 - \frac{l_0}{l_1} \right] \sigma'_{\text{sur}} \quad (3.22)$$

3.8 Conduction by Thin Surface Layers

In working out the models by which volume and surface components of conductivity can be calculated for polymer fibers, it was realized that thin surface layers may indeed be important in the conduction process. As an example,¹²⁸ consider the case where it is assumed that all of the observed current I , in a given experiment on the longitudinal conduction of a fiber, is due to a relatively thin surface layer of thickness δ . Suppose that the insulating core fiber is elliptical in cross-section, with semi-major and semi-minor axes a and b , respectively, and of length l between electrodes to which a voltage V is applied. The current I is given by

$$I = \frac{\pi \sigma V}{l} [(a+b)\delta + \delta^2] \quad (3.23)$$

and the thickness δ needed to produce the observed current under the imposed condition is

$$\delta = \frac{a+b}{2} \left[\sqrt{1 + \frac{4Il}{\pi(a+b)^2 \sigma V}} - 1 \right] \quad (3.24)$$

If the fiber in question is cylindrical in shape with a circular cross-section, the equations simplify to (when $\delta \geq r_0$)

$$I = \frac{\pi \sigma V}{l} [2r_0\delta + \delta^2] \quad (3.25)$$

and

$$\delta = r_0 \left[\sqrt{1 + \frac{l I}{\pi r_0^2 \sigma V}} - 1 \right] \quad (3.26)$$

Figure 3.10 shows a schematic representation of the second case of a fiber with a circular cross-section.

For cases when $\delta \ll r_0$, the square of δ can be discarded as contributing little to the total current. Thus, an approximate expression becomes

$$I \approx \left(\frac{2\pi r_0 \sigma}{l} V \right) \delta \quad (3.27)$$

and the conducting layer is of the order

$$\delta \approx \frac{I l}{2\pi r_0 \sigma V} \quad (3.28)$$

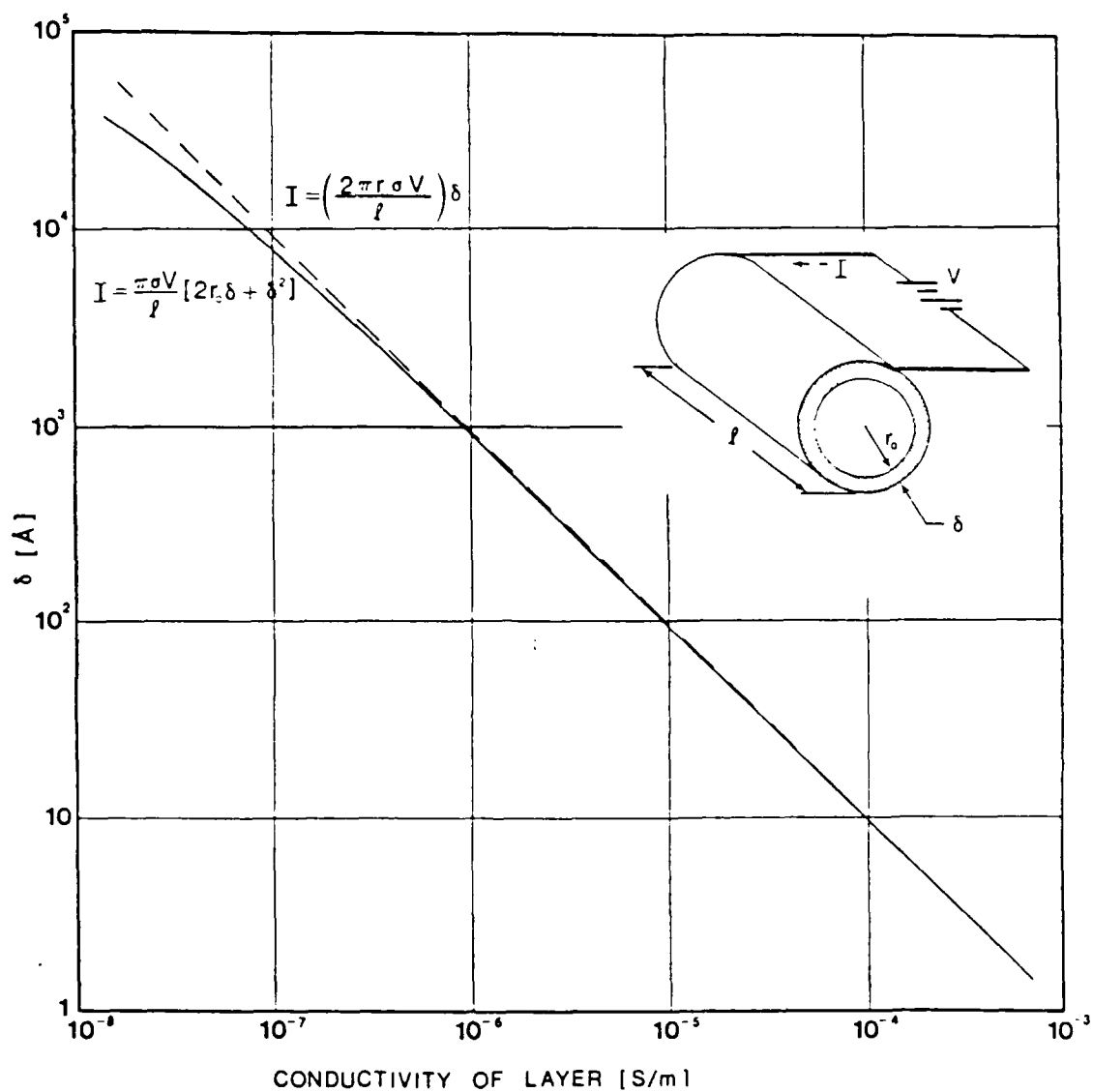


Figure 3.10. Schematic Representation of Conduction by a Surface Layer of Thickness δ .

In order to get a perspective of the size of surface layer necessary to conduct a specific current, some calculations are included in the following table.

Table 3.3
Calculation of δ Based on Model
for PPBT at Typical Room Conditions¹²⁸

<u>Conduction Data</u>	<u>Assumed σ (S/m)</u>	<u>Calculated Layer δ (nm)</u>
V = 22 Volts	4×10^{-8}	2760
I = 3×10^{-14} A		
l = 6 mm	4×10^{-6}	32
r _o = 10 μ m	4×10^{-4}	0.32

The calculation with $\sigma = 4 \times 10^{-4}$ S/m gives a value of 0.32 mm for δ and thus it would correspond to a monolayer of H₂O on the surface if this model were true.

3.9 Current Transients in Dielectrics

Applying a step voltage to a dielectric produces immediate charge transfer in the external circuit due to the charging up of the specimen capacitance. The electric field interaction with the dielectric causes the bound and free charges to move. The current, in general, depends on the elapsed time after voltage application to the specimen electrodes. Figure 3.11 is a schematic representation of current-versus time showing the regime of transient current phenomena. The current falls off very rapidly at first (it is often termed polarization, absorption or anomalous charging current), but it eventually reaches a quasi-steady-state level with time. The steady-state current may be many

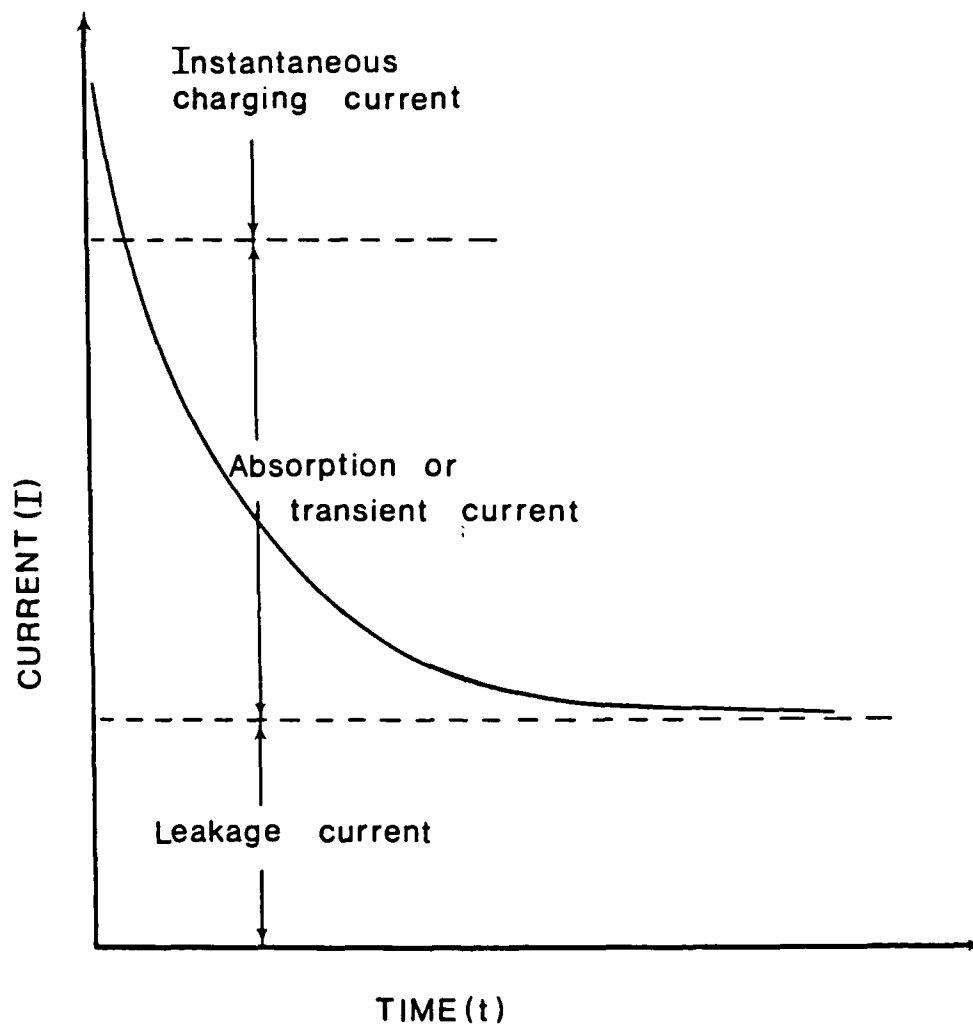


Figure 3.11. Schematic Representation of Current Versus Elapsed Time Showing Transient Current Regimes.

orders of magnitude lower than the initial value of the transient current. The discharge current that is registered upon removal of the voltage is usually the mirror image of the charging current (i.e., if the steady-state current is subtracted from the charging current, then both size and shape of the charging and discharging currents are identical). Of course, the discharge current will not exhibit a steady-state current level and will go to zero with increasing time.^{50,75,129-133} This follows directly from the linearity of the dipolar response which ensures that the superposition theorem will be obeyed.⁹¹

The decay of the transient current sometimes can be described by the Curie-Von Schweidler law^{129,134}

$$I(t) = A(T) t^{-n} \quad (3.29)$$

where I is the observed current, t is the time after application or removal of the external voltage, $A(T)$ is a temperature-dependent factor and n is a constant often observed to be close to unity. This expression can be rewritten in terms of the effective conductivity of the material. The decay function, which can usually be approximated over several decades of time, is written as¹³²

$$\sigma(t) = \sigma(t_0)(t/t_0)^{-n} \quad (3.30)$$

where t_0 is usually chosen as one second, thus making the equation

$$\sigma(t) = \sigma_1 [t]^{-n} \quad (3.31)$$

where σ_1 is numerically equal to the conductivity 1 second after voltage application.

A number of mechanisms have been proposed to explain the occurrence of these absorption and resorption currents. At low fields, the following processes may take place:

- (1) electrode polarization (due to complete or partial electrode blocking),
- (2) dipole orientation (fast types--e.g., resonance and some types of dipole orientation polarizations and slow types--e.g., dipole relaxation orientation),
- (3) charge injection leading to trapped space charge effects,
- (4) tunneling of charge from the electrodes to fill empty traps,
- (5) hopping of charge carriers from one localized state to another,
- (6) relaxation polarization of the Maxwell-Wagner type (caused by micro- or macro-heterogeneities of a continuous or discrete nature).

Table 3.4⁷⁵ is an outline of transient current behavior. The following discussion augments the table by providing short explanations of each process.

Dipolar relaxation can account for the t^{-n} absorption current if a sufficiently wide range of relaxation times exists in the material.^{90,139} The primary characteristic of the process is that the relaxations are thermally activated.

Table 3.4
Outline of Transient Current Behavior

Process	Field Dependence of Isochronal Current	Thickness Dependence of Isochronal Current at Constant Field	Electrode Material Dependence	Temperature Dependence	Time Dependence ($I \propto t^{-n}$)	Relationship Between Charge and Discharge Transients
Dipole orientation (dipoles uniformly distributed through bulk of material)	proportional to ϵ	independent	independent	thermally activated	$0 \leq n \leq 2$	mirror images
Maxwell-Wagner inhomogeneities, dipolar surface layers	proportional to ϵ	L^{-1}	none	related to conductance dependence	exponential	mirror images
Electrode polarization	proportional to ϵ	not specified	strongly dependent through blocking parameter	thermally activated	initially $n \approx 0.5$ followed by $n > 1$	not clear
Charge injection forming trapped space charge	related to mechanism controlling charge injection	independent	related to mechanism controlling charge injection	related to mechanism controlling charge injection	$0 \leq n \leq 1$	dissimilar
Tunneling Hopping	proportional to ϵ	L^{-1}	strongly dependent independent	independent thermally activated	$0 \leq n \leq 2$ $0 \leq n \leq 2$	not clear mirror images

If $t/\tau \ll 1$, where τ is the relaxation time, current temperature curves taken at a fixed polarization time (isochrones) yield an apparent activation energy $E(1-\alpha)$. The thermal activation energy is given by E while α is the distribution parameter. When $t/\tau \gg 1$ as is the case for absorption currents, the current decreases with increasing temperature. The activation energy is apparently negative and is given by $E(\alpha-1)$. These features are illustrated in Figure 3.12. Since dipolar orientation occurs deep within the material, there should be no effects from the electrode contacts. For homogeneous materials, the current at constant field is independent of specimen thickness. If the surface region contains the majority of the dipoles (if the majority of the dipoles were to arise from oxidation), then current will decrease with thickness in an inverse manner. Current should be proportional to the field. This model does present a conceptual difficulty. It is not obvious what microscopic physical model permits the requisite wide distribution of activation entropies necessary to reproduce the experimental observations. For non-polar polymers the model envisages an adequate concentration of adventitious polar groups. Since current levels are usually small, on the order of μA (i.e., 10^{-12} A) the concentration of polar groups may well be present in practice.

A simple heterogeneous system displays Maxwell-Wagner effects with charging up of the internal interfaces. This system exhibits a Debye-like behavior at its terminals.¹⁴⁰

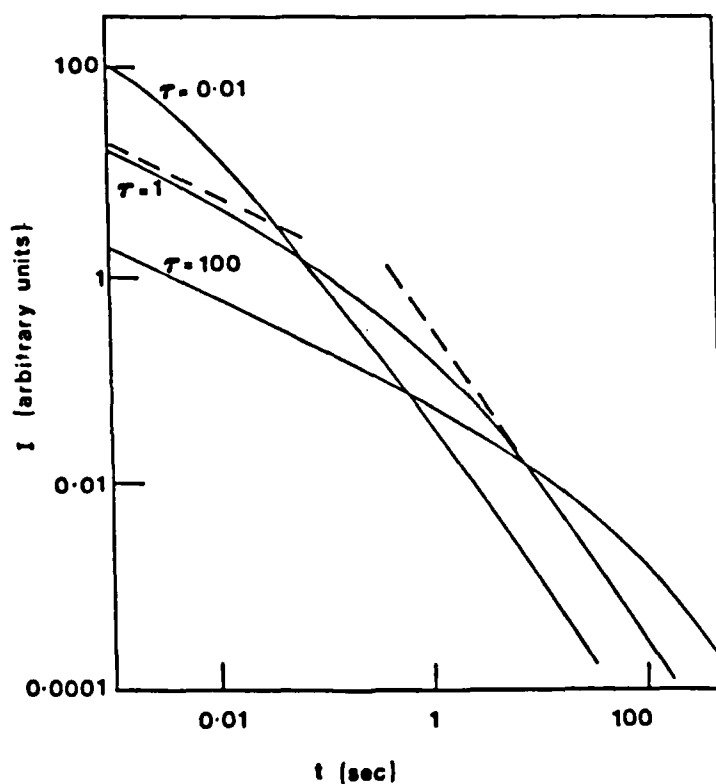


Figure 3.12. Cole-Cole Plots of Current Versus Time With $\alpha = \frac{1}{2}$. The Values of $\tau = 0.01$, 1 and 100 Correspond to High, Intermediate and Low Temperatures Respectively. At Long Times, the Apparent Activation Energy is Negative. Asymptotic Limits for $\tau=1$ are Shown as Dashed Lines.¹²⁹

To a first approximation, the charge current is composed of a number of overlapping, decaying exponentials and is linear in the field. Appendix F discusses the Maxwell-Wagner model for a two-layer dielectric specimen. Also included in this appendix is an expression for conductivity for the case of blocking electrodes.

Electrode polarization (or blocking mechanism) is another process by which current is observed to decrease with time. The charge carriers of one or both signs are prevented from leaving the specimen and as a result, they pile up in front of the drain electrode. A reverse field is established due to the resulting space charge and this tends to inhibit further charge flow. All this leads to a current that exhibits a wide variety of time dependence that depends directly upon the precise conditions at the electrodes. The time dependence appears to be initially $t^{-1/2}$, but then increases abruptly to a value of n greater than 1. The polarization phenomenon is also accompanied by a larger increase in low frequency capacitance.

The space charge model, related to charge injection, assumes an adequate concentration of deep trapping levels. An induced field gradient is established (through Poisson's equation) as the charge carriers enter the material. This results in a reduction of field at the source and an enhancement of the field at the drain electrode. The model proceeds thusly: the rate of supply of carriers depends on the field, while some significant trapping occurs in the

bulk. The particle current density decreases at the source electrode with time as the electric field there falls. The measured current, i.e., the sum of particle and displacement currents, falls like t^{-n} ($n \leq 1$) regardless of the injection mechanism. The field dependence of the current at fixed times is thus related to the field dependence of the injection mechanism.^{129,134} Whether the trapping of charge occurs adjacent to the electrode or in the volume of the dielectric materials is not important.¹⁴¹

Tunneling to traps assumes the presence of a trap level or levels in the dielectric. A general trap distribution may be present in the dielectric, but the current versus time curve is dominated by those traps lying closest to the Fermi-level of the injecting electrode prior to application of the field.¹⁴² The current falls inversely with time for traps located at a single energy level. Preferential concentration close to the surface leads to a sharper fall off with time because of the more rapid filling of the traps. A slower time dependence occurs if there are more traps situated in the bulk than near the surface. A comparison of calculations with experiments reveals that a trap concentration of $N_t = 10^{22} \text{ cm}^{-3}$ is needed to account for the absorption current.⁷⁵ This concentration of traps is not likely to be found in polymers. In general, the tunneling current should be independent of temperature and proportional to field at levels approaching 10^5 V/cm . The current should vary inversely with specimen thickness.

Contact material also should influence greatly the observed current.

The last mechanism to explain transient current phenomena is due to hopping conduction. Phonon-assisted tunneling between impurity states gives rise to a-c conductivity that is frequency-dependent, $\sigma_{ac} \propto \omega^\nu$. The exponent ν is close to 0.8 and arises from the fact that at low frequencies, the carriers can follow the field without phase delay. This limits the amount of loss. This behavior is not possible at higher frequencies.^{147,148}

It is just as difficult to make unambiguous decisions as to the origin of the transient current as to the mechanism of charge transport leading to steady-state currents. As can be seen from Table 3.4, most of the processes are linear in applied field and several are thermally activated. As such, the observed time dependencies does not allow any discrimination to be made between the various models. To be able to narrow the choice of mechanism responsible for the transient current phenomenon, careful studies on different materials must be performed by varying the experimental parameters (e.g., temperature, field strength, electrode material, sample thickness and thermal or electrical history).

From a more practical point of view, the absorption current may be used to obtain information on the frequency dependence of its loss of factor ϵ'' . The Hamon

approximation¹⁴⁹ has been used for this purpose, and is given by

$$\epsilon''(f) = \frac{I(t)}{2\pi f C_a V} = \frac{I(0.1/f)}{2\pi f C_a V} \quad (3.32)$$

where $I(t)$ is the magnitude of the transient current at time t , C_a is the geometric capacitance of the electrode assembly without the sample, V is the magnitude of the step voltage applied, and f is the Hamon frequency, equal to $0.1/t$. This method, even though it is an approximation, provides reasonable accuracy in the calculation of dielectric loss as long as there exists a broad distribution of relaxation times.¹⁵⁰

CHAPTER IV

RESULTS AND DISCUSSION

4.1 Introduction

This section presents the results of the electrical conductivity experiments on the various polymer fibers. In performing the research, certain measurement techniques were more conducive to a particular polymer; for example, BBL was one polymer where suitable values of current versus voltage could be obtained easily at room temperature. The main difficulty in performing current versus voltage measurements with the Keithley 642 is that it is limited to a maximum dc voltage input of 30 volts. The other more insulating polymers, e.g., PE and PP, exhibit such low values of current (i.e., on the order of 10^{-15} A or less at 25 volts) that there is insufficient resolution with the Keithley 642 with which to perform these experiments. A second type of experiment limited to a particular polymer was the separation of surface and volume conductivities. PPBT was used for the variable radius method, because this polymer was the only one where a wide range of fiber radii was available.

From a practical point of view, the bulk of the research centered on BBL. PPBT was also studied in some detail, as it also is considered an important polymer by the Air Force. Subsequent results for nylon 6, nylon 6,6,

polyethylene and polypropylene are intended to round out the research. As such, not as many experiments were performed, on the second group of polymers. They do, however, serve as a means of verifying whether or not the results of the research are reasonable, based on values obtained from the literature.

Each section focuses on the type of experiment performed giving brief details of the procedure. Results and a short discussion are also included. As an example, the section on the effect that humidity has on the conductivity will include data from each polymer tested, both in the undoped and doped state. Thus, comparisons as to the effect of humidity on the conductivity in each polymer can easily be made. The last section will contain a summary of the information contained in the previous sections.

4.2 Current Versus Time Measurements

The current versus time measurements were divided into two parts--transient current behavior and steady-state conduction. The transient current behavior focuses on the first 100 seconds of current response after the application of a step voltage. The steady-state behavior investigates the long time current response of the polymer.

Transient currents arise after the application of the step voltage and decay with time until a quasi-steady-state current is reached. The quasi-steady-state current defines

that region where the drop in current during a specified time interval is small in comparison to the total observed initial transient current. Hereafter, steady-state current is used to mean the quasi-steady-state current. Thus, the steady-state current may be several orders of magnitude lower in value than the initial transient current value. A typical transient current curve is shown in Figure 4.1 for a stretched polypropylene fiber. This figure also shows another important feature of transient current phenomena--the mirror image discharge curve. Transient currents exhibit a charging and discharging curve that are mirror images of one another, except that the discharge curves goes to zero with time while the charging current reaches a steady-state value, I_0 . Subtracting I_0 from the observed charging current gives values that are identical to the discharging curve. Figure 4.2 shows this effect for nylon 6,6 soaked in NaI; this same response was also noted for PE, nylon 6 and PPBT. One aspect of the transient current behavior is the length of time needed to reach a steady-state value decreases markedly in the higher conductivity polymers such as the nylons. As can be seen in Figure 4.1, it takes approximately 300 seconds for the PP to reach the beginning stages of steady-state current response while nylon 6,6 begins to display steady-state response between 50 to 100 seconds.

BBL, the most conductive polymer studied in this research, exhibits almost no transient behavior. It is true

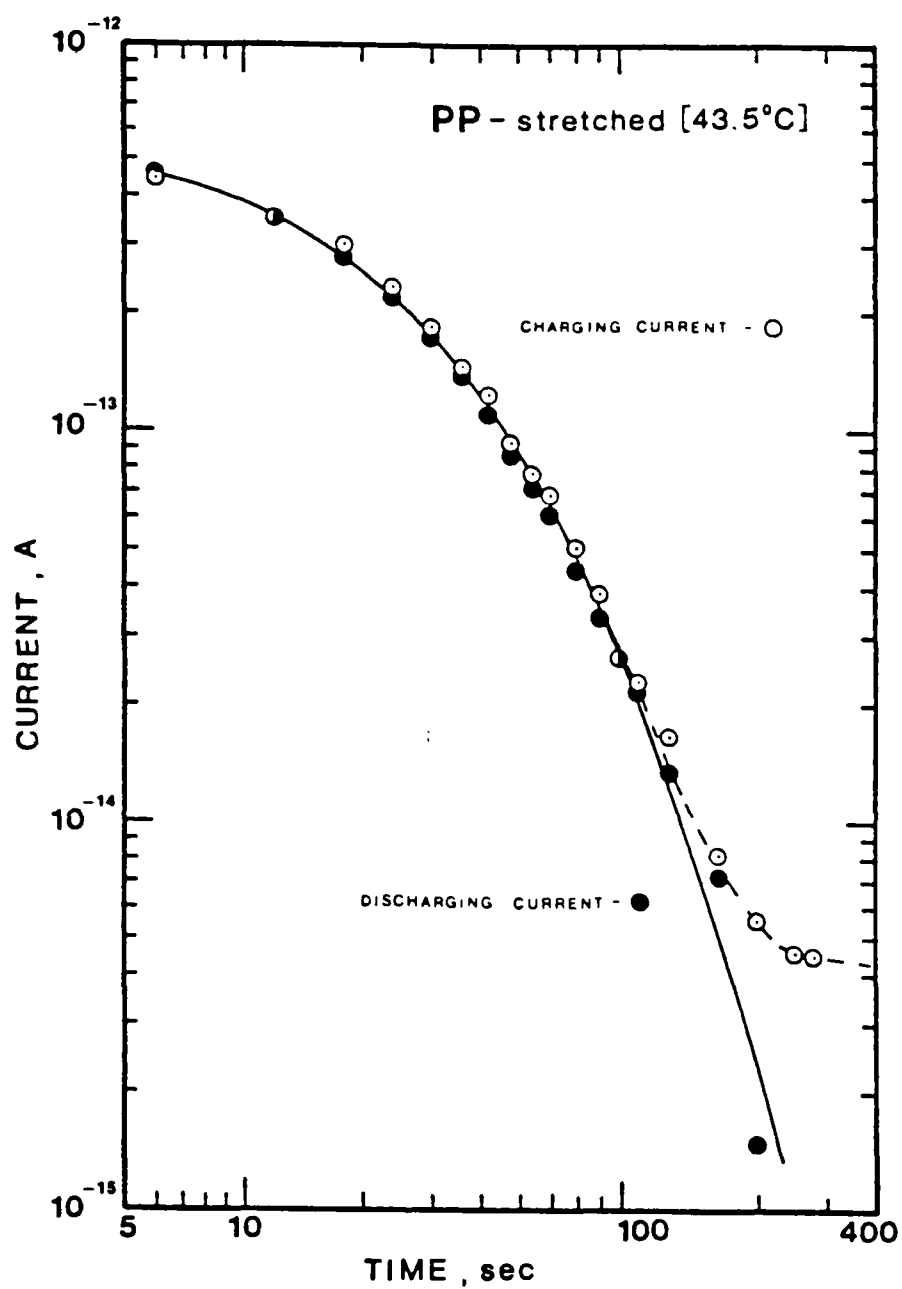


Figure 4.1. Transient Charge and Discharge Curves for Undoped, Stretched Polypropylene Fiber.

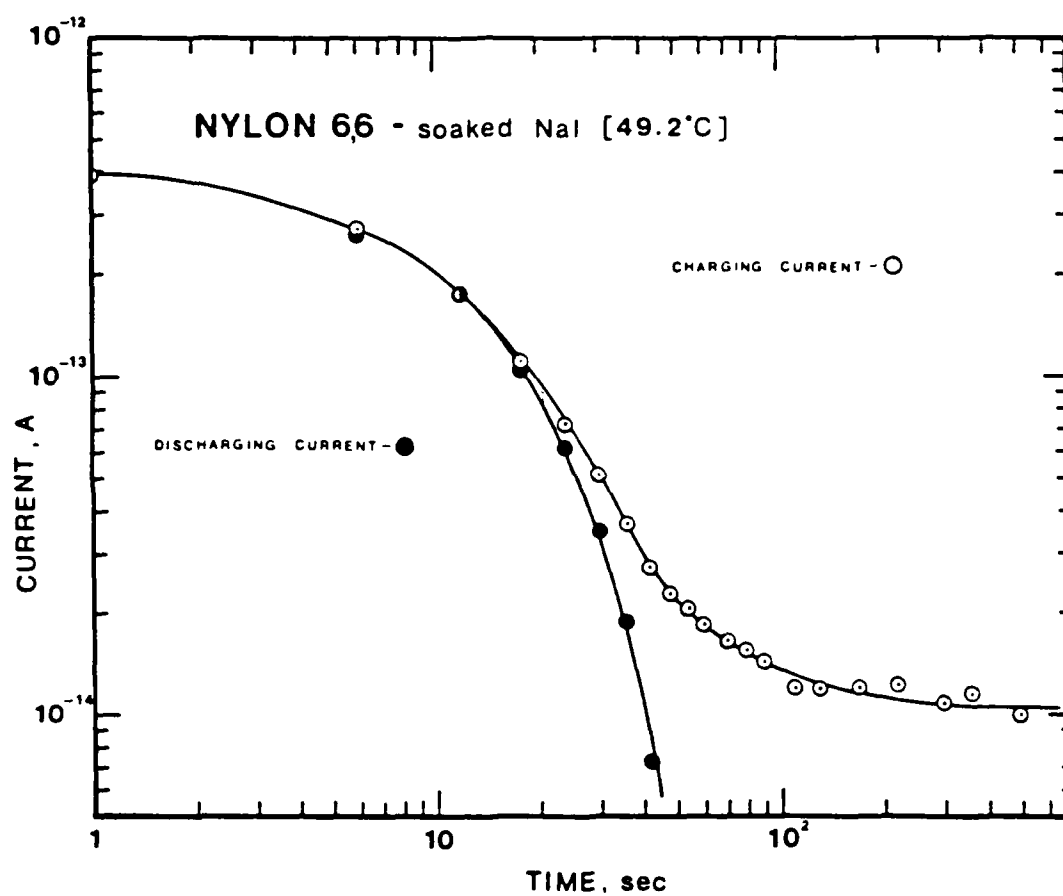


Figure 4.2. Transient Charge and Discharge Curves for Nylon 6,6 Fiber Soaked in NaI Solution.

that BBL does experience a transient response, but it is very short in duration (less than 30 seconds) and the total transient current magnitude is small--less than 2% of its steady-state value. This is compared to nylon 6,6, where at 49°C, the drop in transient current is well over one order of magnitude. The current at 100 seconds is only 4% of the current observed one second after the application of the voltage. For PP, there is almost a two order of magnitude drop in the observed current, and after 300 seconds, the steady-state current is only 1% of the observed maximum transient current.

It is fairly obvious that the proposed mechanisms leading to transient behavior in PE, PP, etc., as mentioned in Section 3.9, are not operating in BBL. This can partly be explained by its rigid, planar structure. However, it would be expected that PPBT, also being planar and more crystalline than PP, PE or nylon, would exhibit a behavior similar to BBL. It did not. Indeed, while the duration of the transient response for PPBT is short, its drop in magnitude is very large. For example, in undoped PPBT (29022-48-4), the steady-state current was reached after about 60 seconds. However, in this instance, the steady-state current level for PPBT is only 2% of the maximum observed transient current value.

The next set of graphs, depicted in Figures 4.3-4.5, shows how increasing the temperature shortens the duration of the transient current phenomena and also increases the

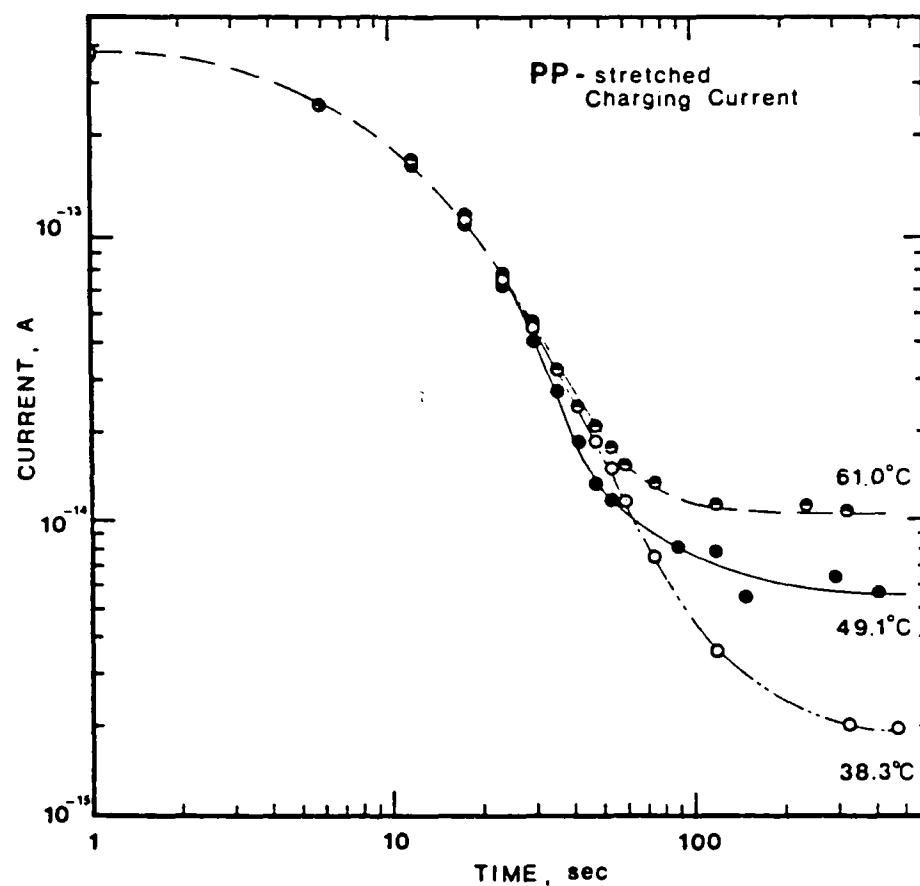


Figure 4.3. Variation in Transient Charging Curves With Temperature for Undoped, Stretched Polypropylene Fiber.

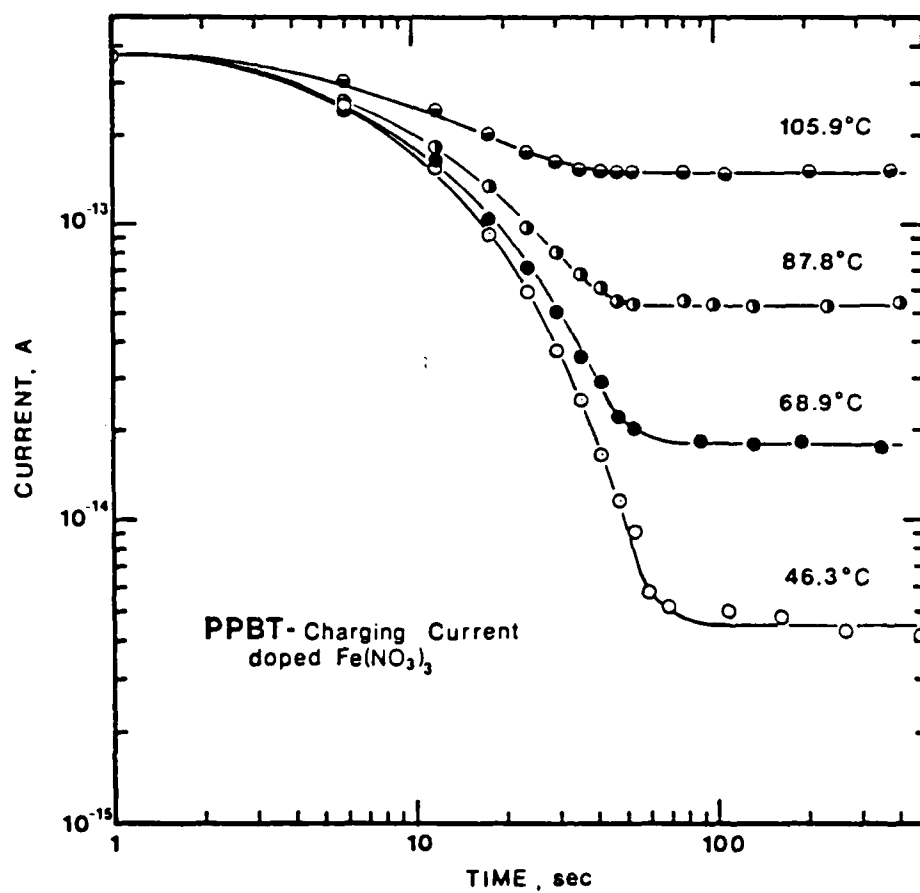


Figure 4.4. Variation in Transient Charging Curves With Temperature for $\text{Fe}(\text{NO}_3)_3$ Doped PPBT (30-1) Fiber.

magnitude of the steady-state current. This is emphasized in Figure 4.5 for nylon 6 soaked in dimethyl sulfoxide. The temperature of the upper curve is about 82°C, and it can be seen that no transient behavior was observed. Figure 4.6 emphasizes this point. This experiment was performed at 97°C, and as can be seen, the initial current level has increased by a factor of 3 over that observed for the curves in Figure 4.5. Also, the current slowly increases with time until the steady-state value is reached. The discharge current exhibits the same general shape as those previously noted, except for two things. First, the discharge curve is not a mirror image of the charging curve, and second, the maximum value of the discharge current corresponds to the value of the observed steady-state current at that temperature.

As can be seen, once a certain temperature is passed, the t^{-n} dependence no longer holds. This depends in part on the polymer. For nylon 6 soaked in dimethyl sulfoxide, this temperature lies somewhere below 80°C. The failure of the t^{-n} relation is probably due to the combined effects of a rapid decrease in relaxation times characteristic of the transient phenomena and to the progressive superposition of a steady-state conduction current growing exponentially with increasing temperature. In other words, all the processes normally leading to the transient current phenomenon are greatly accelerated.

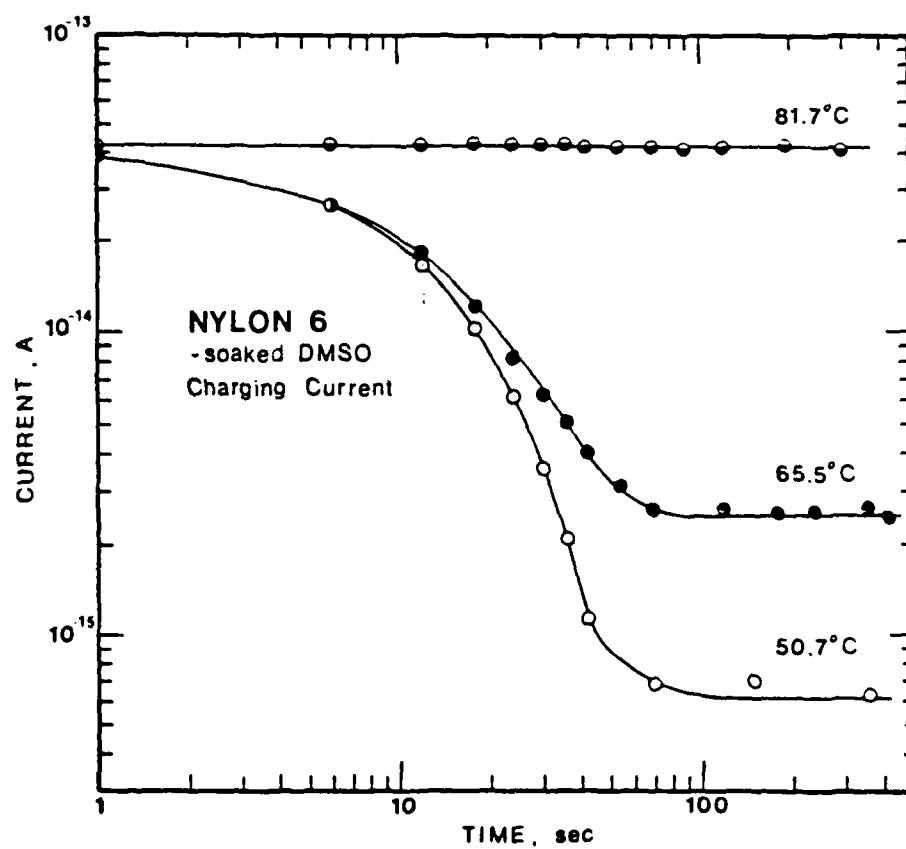


Figure 4.5. Variation in Transient Charging Curves With Temperature for Nylon 6 Fiber Soaked in Dimethyl Sulfoxide.

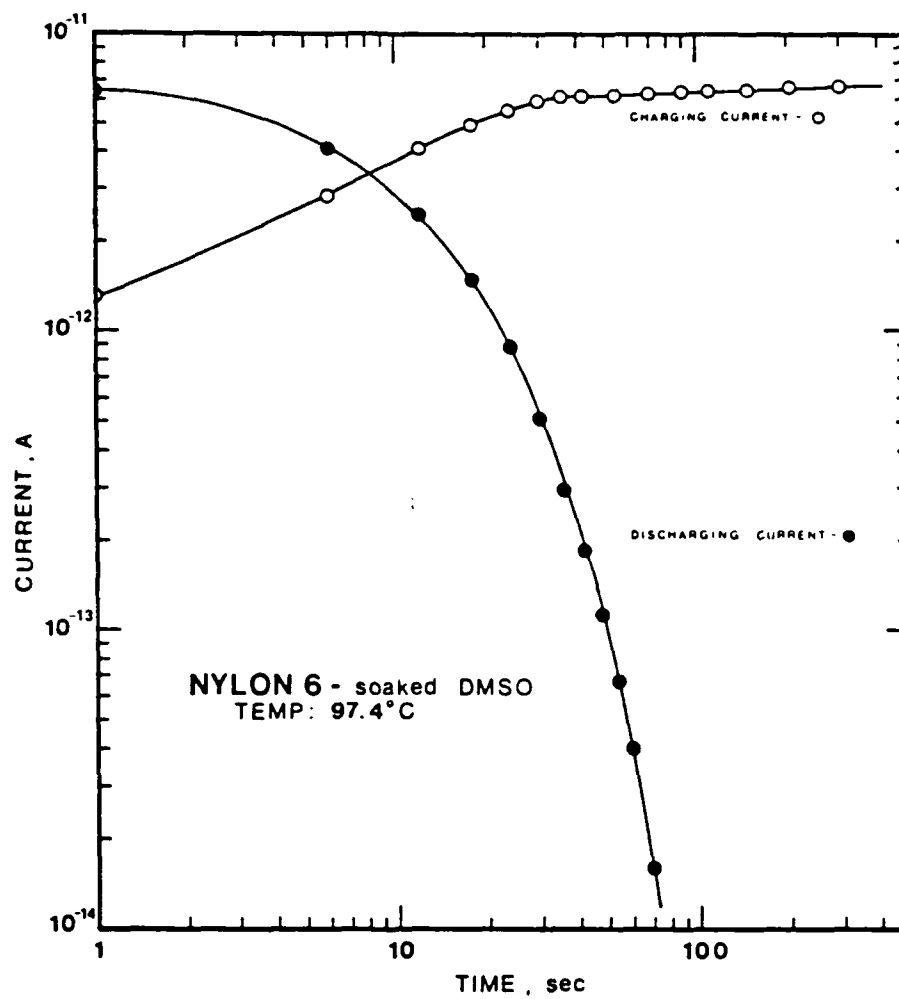


Figure 4.6. Transient Charge and Discharge Curves at High Temperature for Nylon 6 Fiber Soaked in Dimethyl Sulfoxide.

Additional information can be gained by examining the transient current behavior of polymers. Watanabe et al.⁸⁴ have examined ionic conduction in polyester films containing alkali metal thiocyanate (LiSCN, NaSCN and KSCN). From making electrical impedance measurements, graphs of $\log I$ versus time can be generated. Assuming that the time dependence of the current is dominated by the migration of ions, they hypothesize that the current through the polymer with ion blocking electrodes can be expressed by

$$I(t) = \left(\frac{A}{b} \right) V^*(t) \sum_{j=1}^n [n_j(t) e \mu_j] \quad (4.1)$$

where A and b are sample area and thickness, respectively. $V^*(t)$ is an effective voltage across the sample; $n(t)$ is the number of ionic carriers in the bulk, and μ is the ionic mobility. Thus, the profile of the transient ionic current can be explained by the dependence of the terms $V^*(t)$ and $n(t)$. $V^*(t)$ may possibly decrease with time. It may also deviate from the applied voltage, V , because of the formation of space charge in the vicinity of the electrodes. $n(t)$ may also decrease with time because of the cleanup effect of the carrier ions in the bulk.

Now, by assuming that $V^*(t)$ is consistent with V for the initial short time and that there is one kind of mobile species, Eq. (4.1) reduces to

$$I(t) = \frac{A n_0 e \mu V}{b} \exp \left[- \left(\frac{\mu V}{b^2} \right) t \right] \quad (4.2)$$

where n_0 is the number of carrier ions at $t=0$. Thus the ionic mobility, μ_i can be estimated from the initial slope of the transient ionic current.

The data from Figures 4.1-4.4, as well as that for BBL fibers soaked in acetone and doped in LiCl, were replotted in a $\log I$ versus t (measured in minutes). Values of μ_i were thus calculated. The results are given below.

<u>Polymer/ Dopant</u>	<u>T (°C)</u>	<u>μ_i (cm²/V-sec)</u>
Nylon 6,6 (NaI)	49.0	2.8×10^{-4}
Nylon 6,6 (Fe(NO ₃) ₃)	21.3	1.0×10^{-4}
BBL (LiCl)	21.6	1.5×10^{-6}
BBL (acetone)	20.6	2.2×10^{-6}
PPBT (Fe(NO ₃) ₃)	46.3	1.6×10^{-4}
[29022-30-1]	68.9	1.4×10^{-4}
	87.8	1.0×10^{-4}
	105.9	0.7×10^{-4}
PP (stretched)	49.1	5.9×10^{-5}
	61.0	5.4×10^{-5}
	71.7	4.7×10^{-5}
	86.6	4.8×10^{-5}

These results reveal several interesting trends. In the polymers, i.e., nylon 6,6 and PPBT, where ionic conduction is thought to occur and is considered to be significant, the value for μ_i is on the order of 10^{-4} cm²/V-sec. On the other hand, a value of about 5×10^{-5} cm²/V-sec was obtained for stretched, undoped PP fiber. Although no ions were purposely introduced into the PP, the possibility exists that ions from the polymerization process may be found in the fiber. BBL, on the other hand, has mobility values on the order of 10^{-6} cm²/V-sec. It is thus seen, that at least

from this approximate method of determining a mobility value, BBL possesses the lowest value of mobility. This is to be expected in a sense, because the more crystalline the polymer microstructure, the harder it becomes for the ions to migrate through the polymer matrix.

One curious aspect of this analysis must be mentioned--the behavior of PPBT doped with $\text{Fe}(\text{NO}_3)_3$. The results show that as the temperature is increased, the mobility decreases. This seems to contradict what one would expect to see, that is, an increase in mobility with increasing temperature. Indeed, in looking at PP, the trend also appears, but to a somewhat lesser extent. This trend in PP can be explained within the error for the measurement of time and current. The case for PPBT cannot be so easily explained.

The aspect of this analysis that is most disturbing is where to draw the tangent to the curve from which the slope is determined. For the values shown in the table, the part of the curve between 6 and 18 seconds after the application of the voltage was chosen as the region from which the slope is determined. This leads to higher values of mobility than if the slope was determined at 30 seconds after the application of the voltage. For example, if a tangent to the $\log I$ versus t curve is drawn through the point corresponding to 42 seconds after the application of the voltage for PPBT doped with $\text{Fe}(\text{NO}_3)_3$ at 87.8°C , the mobility thus becomes $2.7 \times 10^{-5} \text{ cm}^2/\text{V-sec}$. This is compared to a

value of 10^{-4} cm²/V-sec when a shorter value of time is used. Regardless of the absolute value of the numbers, the calculations do indicate that the polymers expected to exhibit ionic conductivity do indeed have lower mobility values. Additionally, the region of the curve which is selected from which the slope is evaluated, and subsequently the mobility is determined, is important and should be selected in a consistent manner.

The steady-state current is usually observed after all the mechanisms leading to transient current behavior have ceased. Figure 4.7 shows a set of three curves for nylon 6,6 soaked in ethyl alcohol. These tests were performed at room temperature and show a general decrease of current with time. These curves depict the quasi-steady-state current. There is a continuing decrease in current throughout the length of the experiment, but the rate of decrease decreases with increasing time.

Figure 4.7 also shows another interesting result. These experiments, run in a controlled atmosphere near 0% relative humidity, were performed on successive days. The overall level of current was seen to decrease with each run, indicating the real possibility that ions contribute to the overall conductivity. This general trend was also displayed in PPBT fibers. The hypothesis is that with each experiment, impurity ions are swept through the fiber to the appropriate electrode. After the conclusion of the experiment, when the step voltage is removed, the ions are

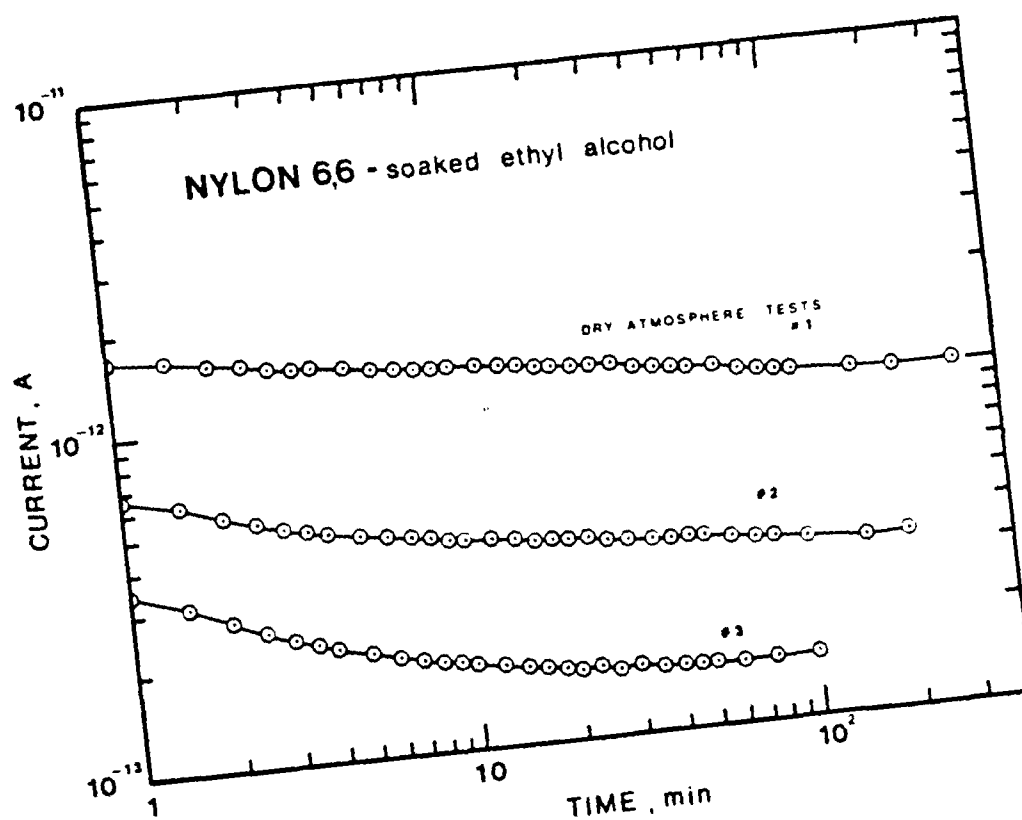


Figure 4.7. Steady-State Current Curves for Nylon 6,6 Fiber Soaked in Ethyl Alcohol. Note Decrease in Observed Current, Possibly Due to the Sweeping Out of Ions.

free to redistribute themselves in the fiber. However, without the advantage of an electric field or thermal energy to aid in a back diffusive process, the ions cannot move far from the electrodes to which they were attracted. Subsequent tests further deplete the polymer of additional ions, thereby lowering the overall conductivity with each test. If this process, were continued, at some point, the curves would become reproducible. At this point, it could be hypothesized that all ions have been swept clean of the polymer and the observed current is due to the transport of electrons alone. This type of behavior was not observed in BBL fibers. The curves were essentially identical in shape and magnitude except for minor variations which are attributed to the differences in temperature of the various experiments. This, and the fact that there is a very small transient current response, points to electronic conduction as opposed to ionic conduction, as the main transport mode in BBL.

Figures 4.8-4.16 show curves of steady-state current behavior for the various polymers studied. The open circles represent the current versus time response for the doped and undoped polymers at room temperature in a dry atmosphere. In all the polymers, except BBL, the current decreases with time, sometimes smoothly as in Figures 4.8, 4.10 and 4.12 and also erratically, as in Figures 4.11 and 4.13. PE doped with iodine shows an initial increase in current for about 8 minutes and then a gradual decrease in current with time.

AD-A173 498

PHYSICAL TECHNIQUES FOR THE STUDY OF SORPTION DIFFUSION

3/4

ELECTRICAL PROPER (U) VIRGINIA UNIV CHARLOTTESVILLE

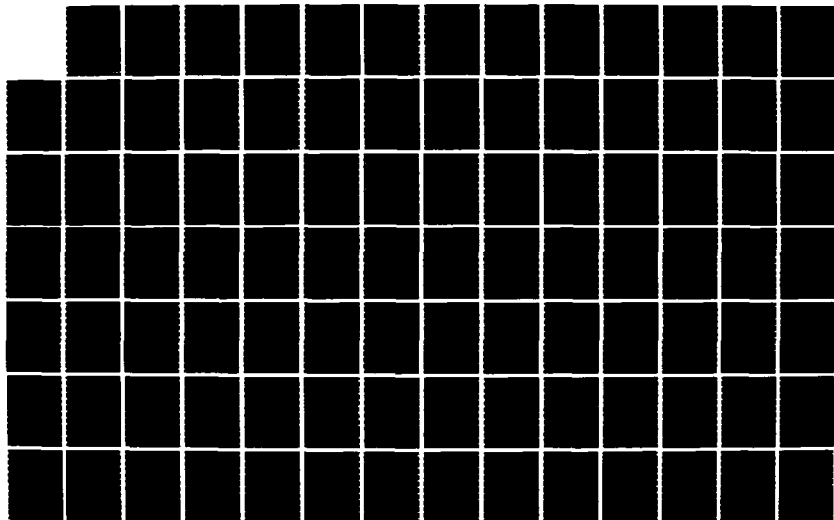
DEPT OF MATERIALS SCIENCE R E BARKER ET AL 26 JUL 86

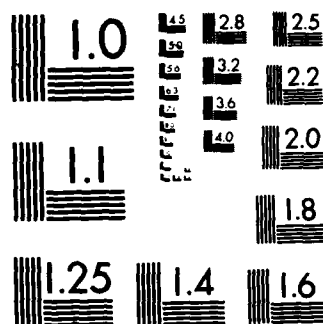
UNCLASSIFIED

UVA/525646/H587/101 AFOSR-TR-86-8831

F/G 11/9

NL





MICROCOPY RESOLUTION TEST CHART
NATIONAL BUREAU OF STANDARDS-1963-A

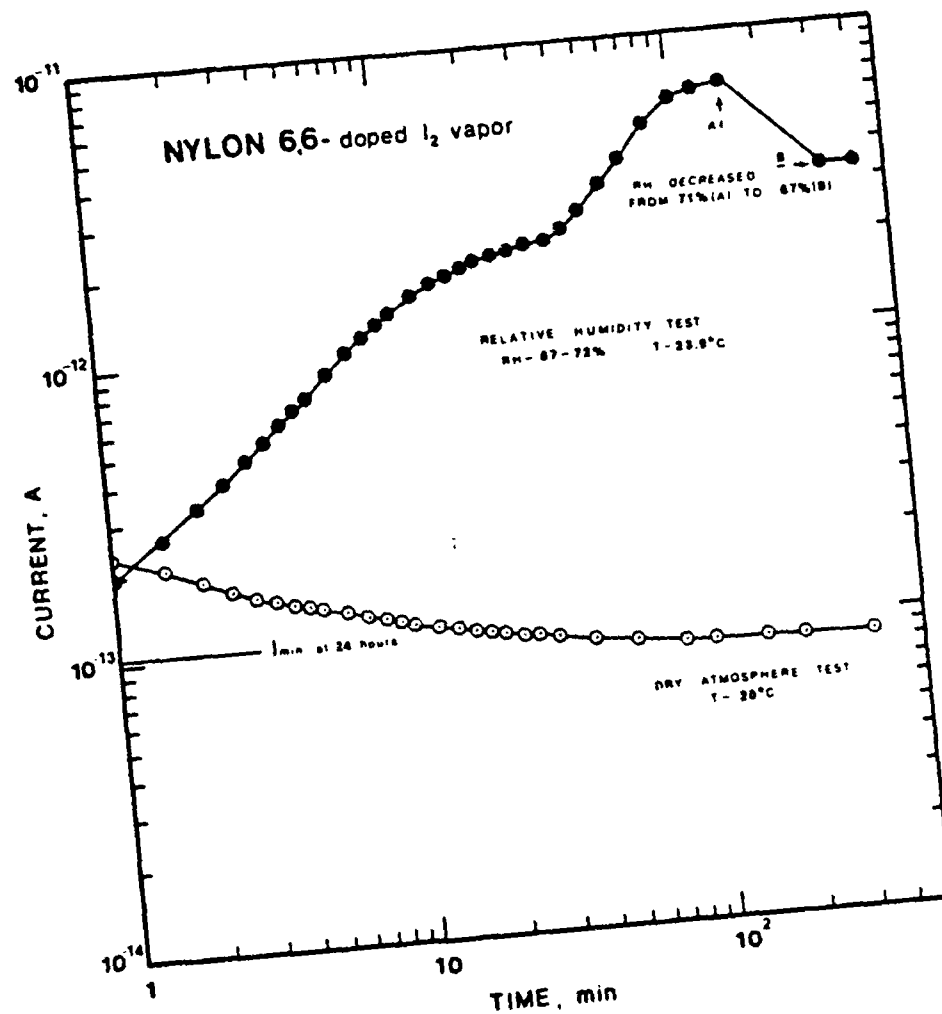


Figure 4.8. Current Versus Time Curves for Nylon 6,6 Fiber Doped With Iodine Vapor (I_2) Showing the Steady-State Current Observed in Dry Atmosphere and Resulting Change in Current From Exposure to a Moist Atmosphere.

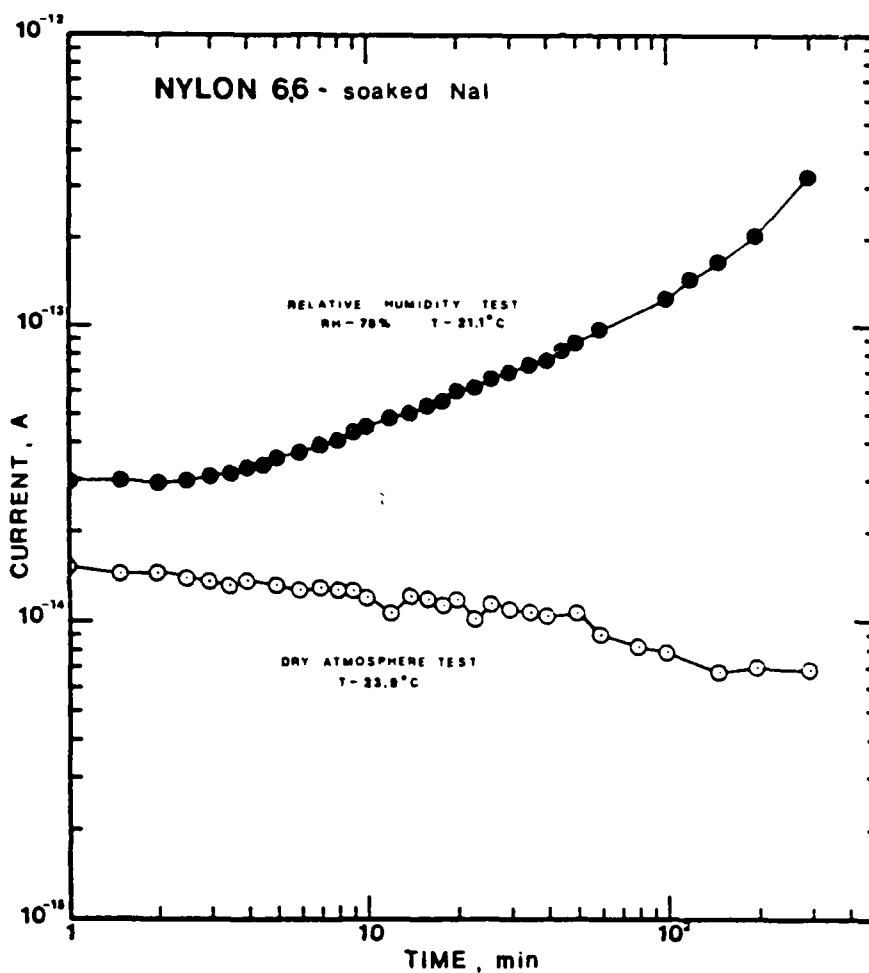


Figure 4.9. Current Versus Time Curves for Nylon 6,6 Fiber Soaked in NaI Solution Showing the Steady-State Current Observed in Dry Atmosphere and Resulting Change From Exposure to a Moist Atmosphere.

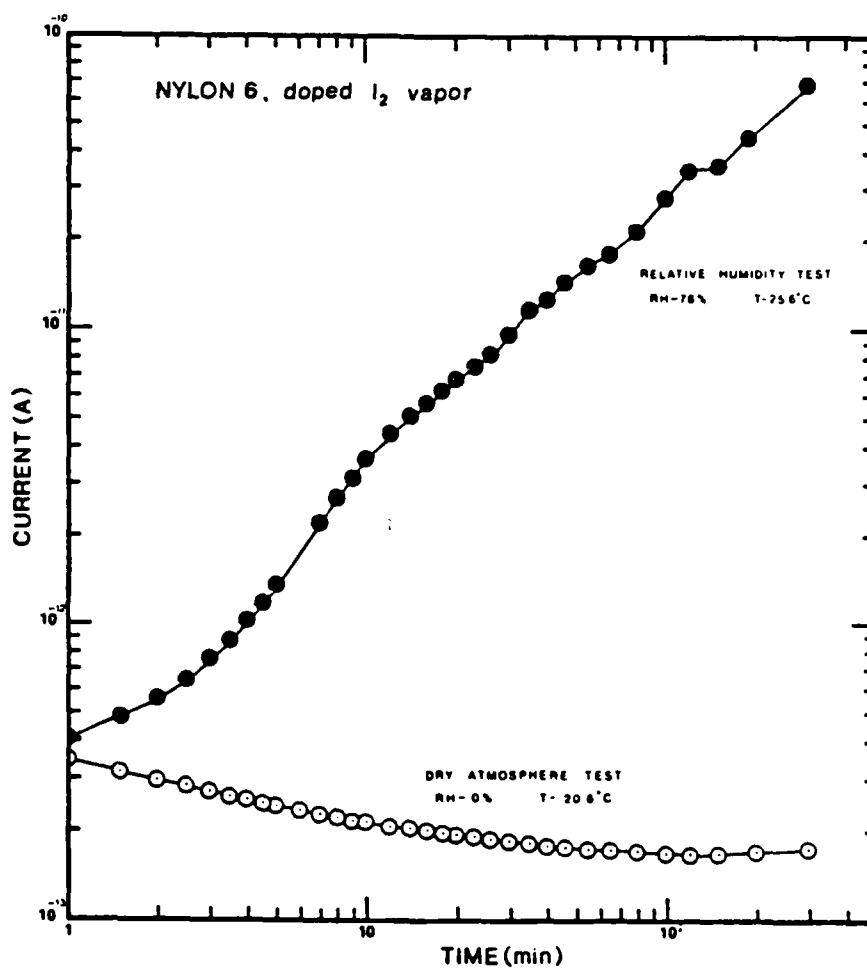


Figure 4.10. Current Versus Time Curves for Nylon 6 Fiber Doped With Iodine Vapor (I_2) Showing the Steady-State Current Observed in Dry Atmosphere and Resulting Change in Current From Exposure to a Moist Atmosphere.

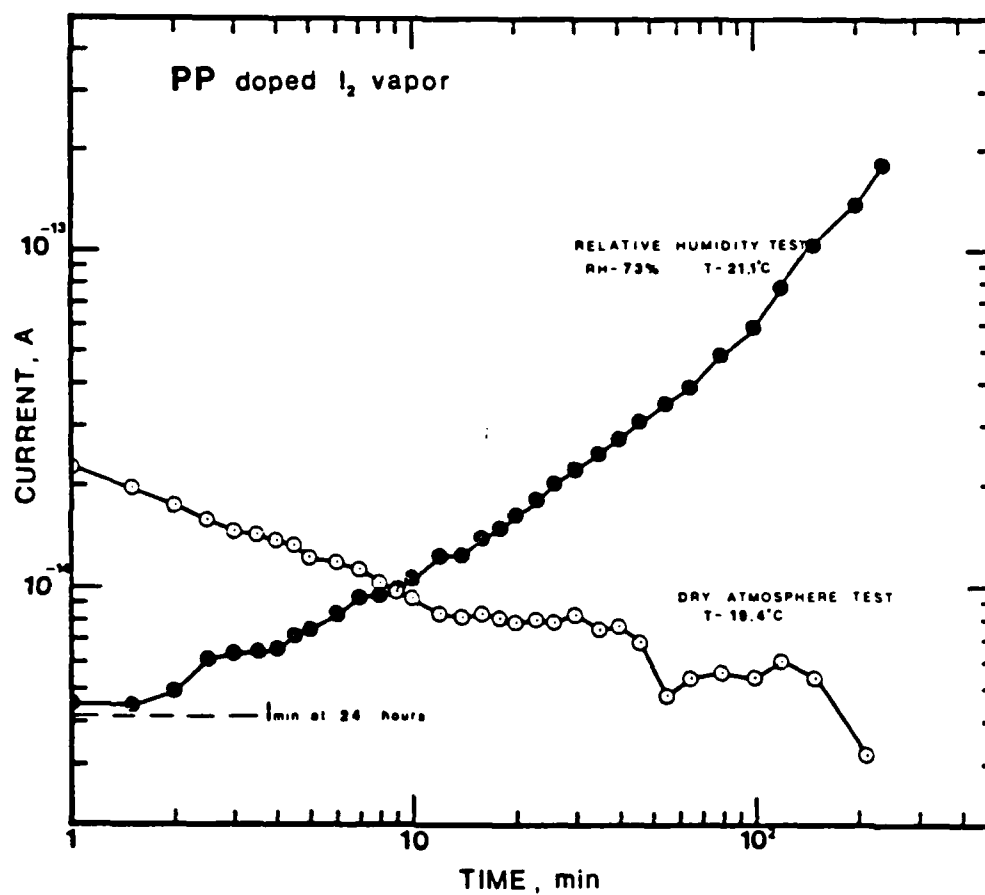


Figure 4.11. Current Versus Time Curves for Polypropylene Fiber doped With Iodine Vapor (I_2) Showing the Steady-State Current Observed in Dry Atmosphere and Resulting Change in Current From Exposure to a Moist Atmosphere.

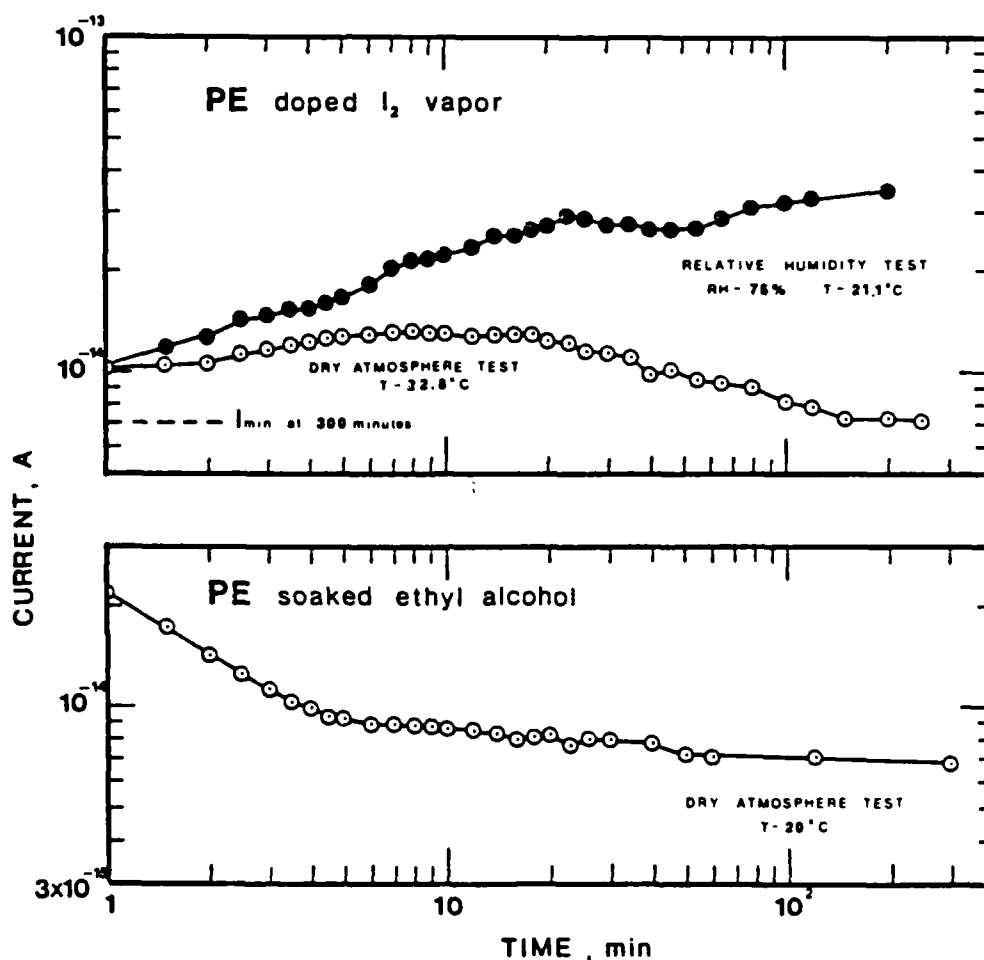


Figure 4.12. Current Versus Time Curves for Polyethylene Fiber Doped With Iodine Vapor (I_2) Showing the Steady-State Current Observed in Dry Atmosphere and Resulting Change in Current From Exposure to a Moist Atmosphere. The Second Graph Shows the Steady-State Current for Polyethylene Soaked in Ethyl Alcohol.

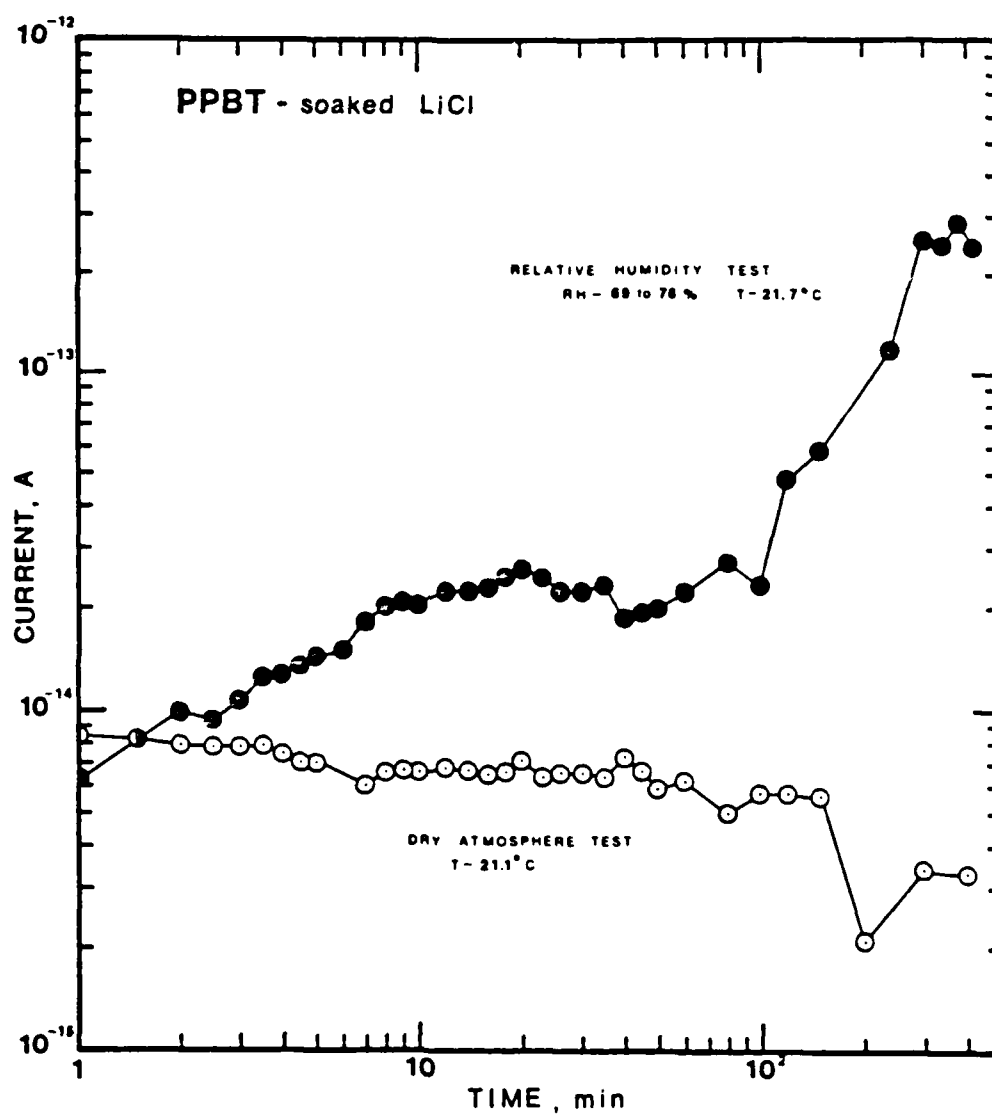


Figure 4.13. Current Versus Time Curves for PPBT (30-1) Fiber Soaked in LiCl Solution Showing the Steady-State Current Observed in Dry Atmosphere and Resulting Change in Current From Exposure to a Moist Atmosphere.

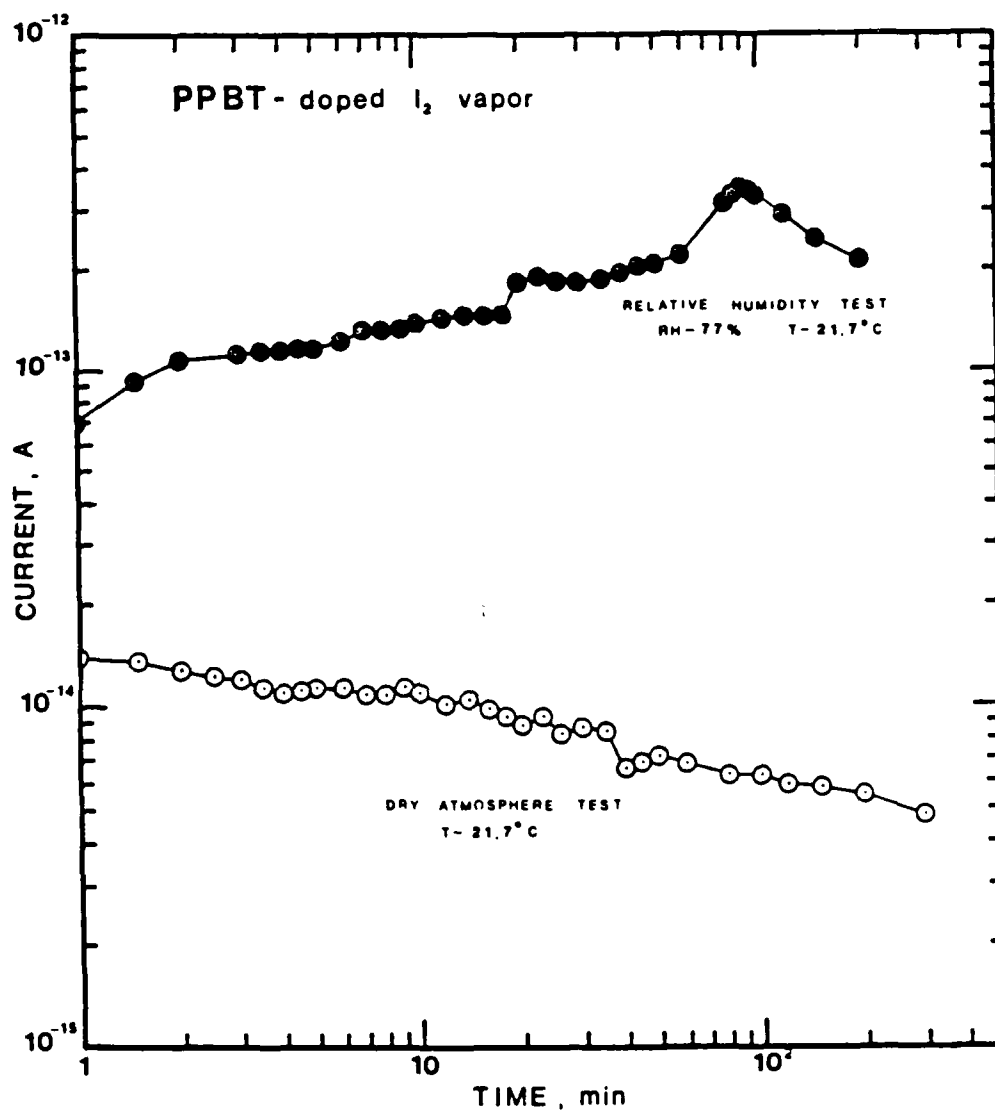


Figure 4.14. Current Versus Time Curves for PPBT (30-1) Fiber Doped With Iodine Vapor (I_2) Showing the Steady-State Current Observed in Dry Atmosphere and Resulting Change in Current From Exposure to a Moist Atmosphere.

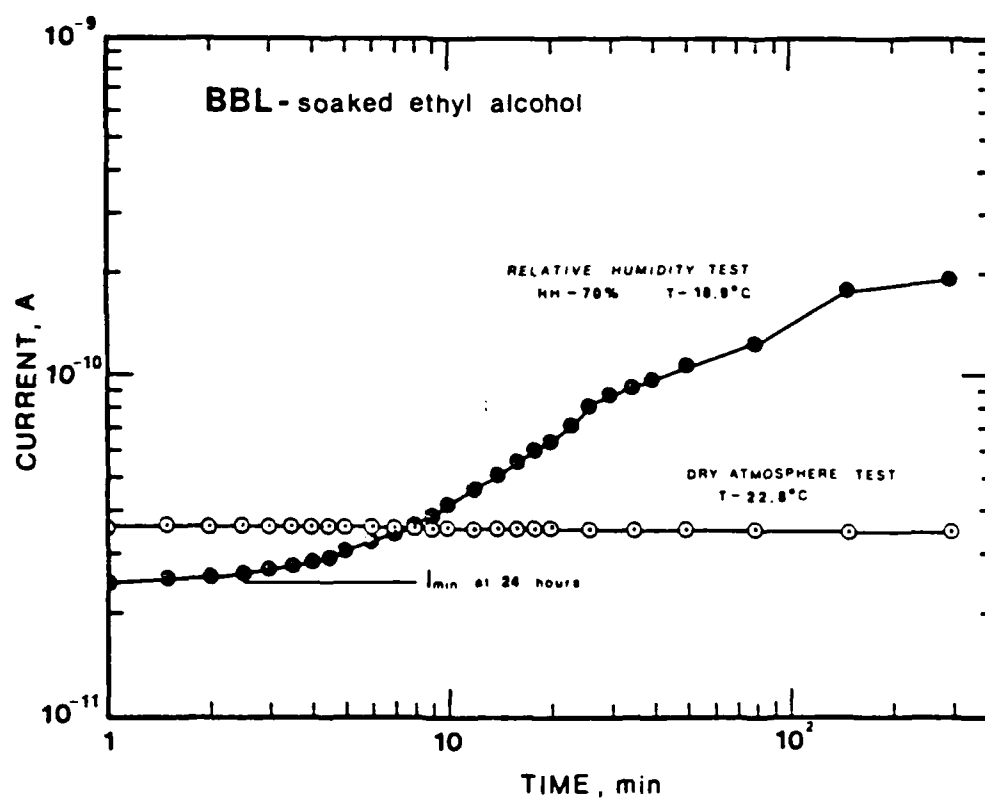


Figure 4.15. Current Versus Time Curves for BBL Fiber Soaked in Ethyl Alcohol Showing the Steady-State Current Observed in Dry Atmosphere and Resulting Change in Current from Exposure to a Moist Atmosphere.

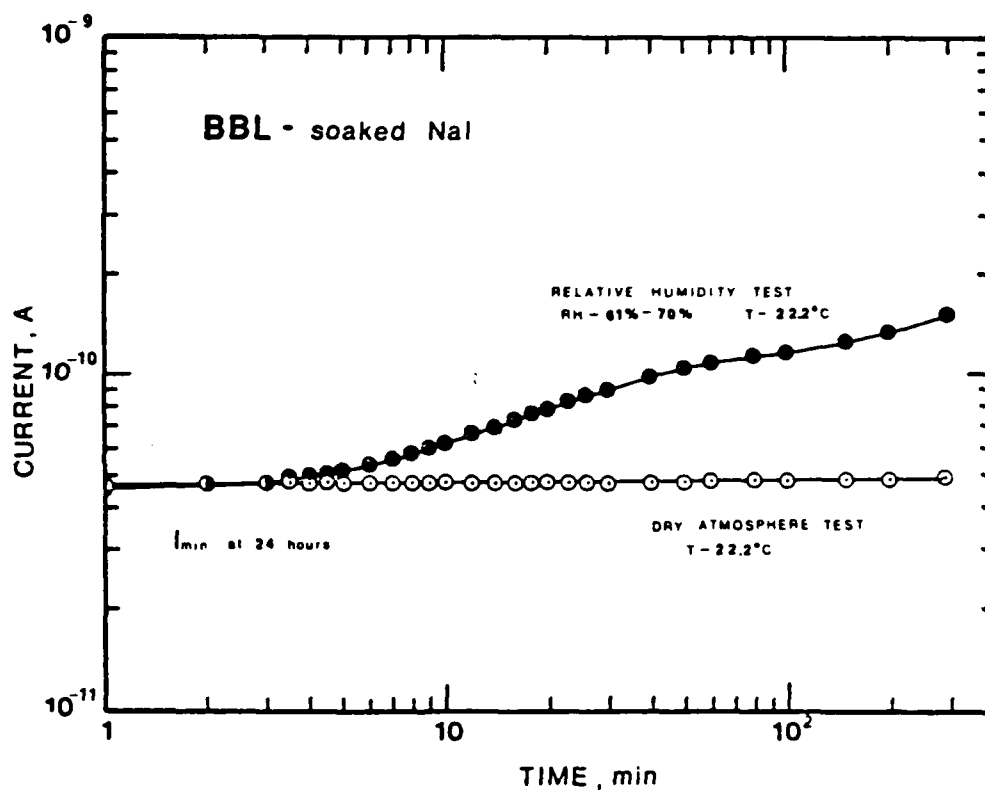


Figure 4.16. Current Versus Time Curves for BBL Fiber Soaked in NaI Solution Showing the Steady-State Current Observed in Dry Atmosphere and Resulting Change in Current From Exposure to a Moist Atmosphere.

BBL in Figures 4.15 and 4.16 shows essentially no decrease in current at all. In fact, the current actually increases with time for BBL in some cases. However, this increase is small in magnitude and is probably due to increases in the room temperature during the course of the experiment.

The second curve on each graph, which are indicated by the solid dark circles, represent the effect on the current due to the moisture in the atmosphere as measured by the relative humidity. The general experimental procedure was to run the polymer in a dry atmosphere for at least 300 minutes and sometimes for as long as 24 hours. This establishes, by definition, a minimum current value, I_{\min} . Then, the specimen chamber is opened to the atmosphere, i.e., to the moisture contained in the air, and the subsequent changes in current are plotted as a function of time. In all instances, moisture enhances the overall conductivity of the polymer fiber.

The effect of water on PE, PP and BBL is small when compared to the nylons and PPBT. This is to be expected as PE and PP are hydrophobic, and as such, not expected to be greatly affected by moisture uptake. On the other hand, nylon is hydrophilic and moisture does greatly affect the conductivity. Thus, by analogy, PPBT can be classified as hydrophilic and BBL as hydrophobic.

Some general comments on the shape of the curves should be made. As can be seen, the conductivity shows a uniform increase with time when the humidity remains constant over

the test period. Fluctuations of the current during these tests can be equated to changes in the relative humidity. For example, in Figure 4.8, the relative humidity started increasing from an initial value of 69% to one of 72% after about 40 minutes. Subsequently, the humidity leveled off at 71% for the next 70 minutes before falling to a final value of 67%. This is reflected by the changes in current shown in Figure 4.8.

Another obvious result is that the higher the relative humidity, the more profound is the increase in current. Also, the initial effect on the current for the nylons and PPBT is greater, the larger the initial values of humidity. At long times, as more moisture is absorbed into the polymers, the current continues to increase at a more rapid rate. Conversely, the effect on PP, PE, and BBL is not as great. Generally speaking, for these polymers, there is a slow, gradual increase in current with time. Then, the current begins to increase more rapidly as water is adsorbed into the surface of the fiber.

4.3 Relative Humidity Experiments

Perhaps a better way of visualizing the effect of water on conduction in these polymers is to plot the differential current versus the logarithm of time. The differential current is defined at $\Delta I/I_{\min}$, where ΔI is the difference between the measured current when subjected to a humid atmosphere and the lowest measured current in a dry

atmosphere. This differential current gives a good idea of the effect that moisture has on the polymer. It is essentially a measure of the increase in current due to water uptake by the polymer over that of the dry state.

A word is in order about the concept of a dry atmosphere and its implied meaning of a dry polymer. Most of the dopants were in solution form, with the metal salts dissolved in distilled water. Once the fiber had soaked in the doping solution, it was dried and stored in a desiccator. Unfortunately, the fibers were not dried under a vacuum, and the possibility exists that deep sorbed water could be present in microvoids within the polymer. However, since the experimental procedure was the same for all polymers, the results will show the same general trends. The dry atmosphere for these tests was achieved by using silica gel as the drying medium. Usually the samples were allowed to sit for at least 12 hours, and sometimes for as long as 24 hours, before the start of the current measuring procedure. Although 0% relative humidity is assumed for the dry atmosphere tests, it is not certain that the polymer itself is free of all water.

Figures 4.17-4.21 are graphs of $\Delta I/I_{\min}$, or the differential current, versus time for various fibers. Figures 4.17 and 4.18 are typical for the case of hydrophobic polymers. In Figures 4.17, the darkened circles correspond to the behavior of BBL soaked in ethyl alcohol. Note the slow increase in current over the dry state. This

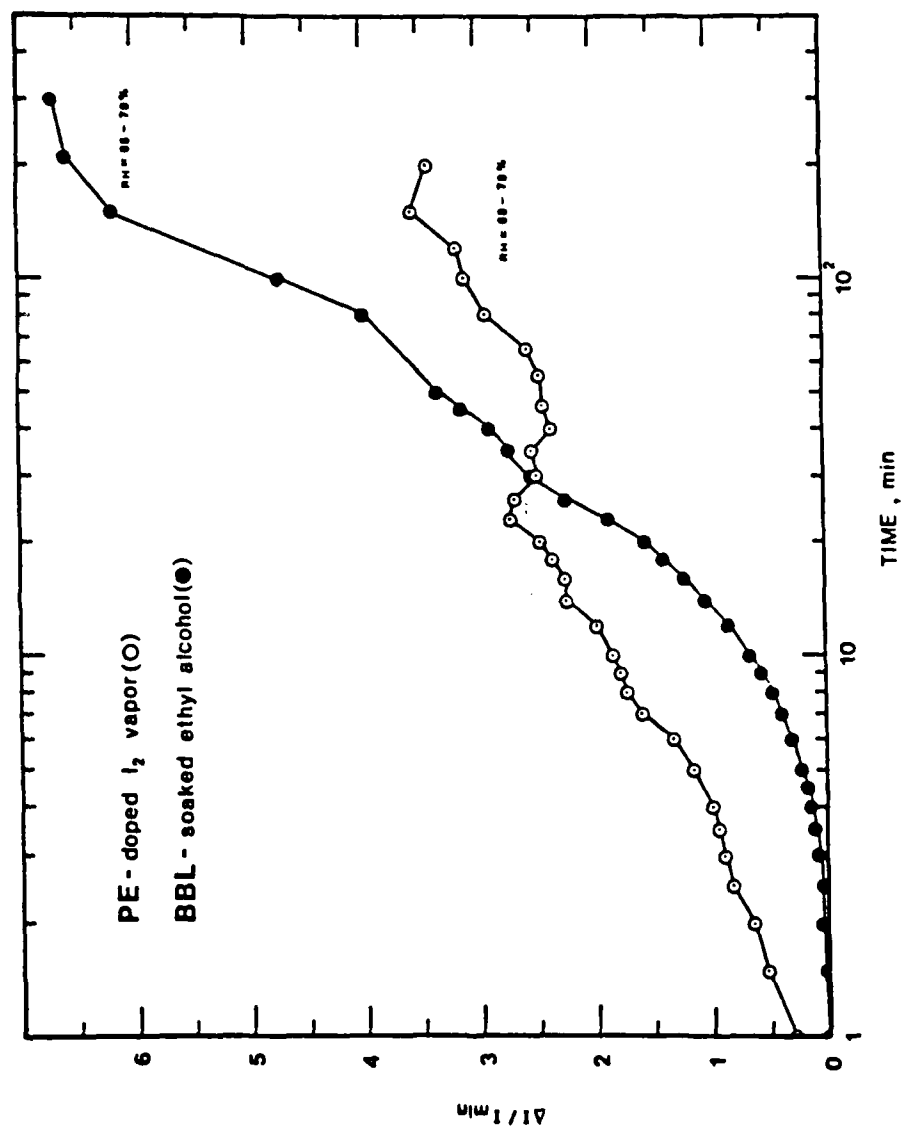


Figure 4.17. Differential Current, $\Delta I/I_{min}$, Versus Time, Showing Relative Current Increase With Moisture Sorption for Various Doped Polymer Fibers.

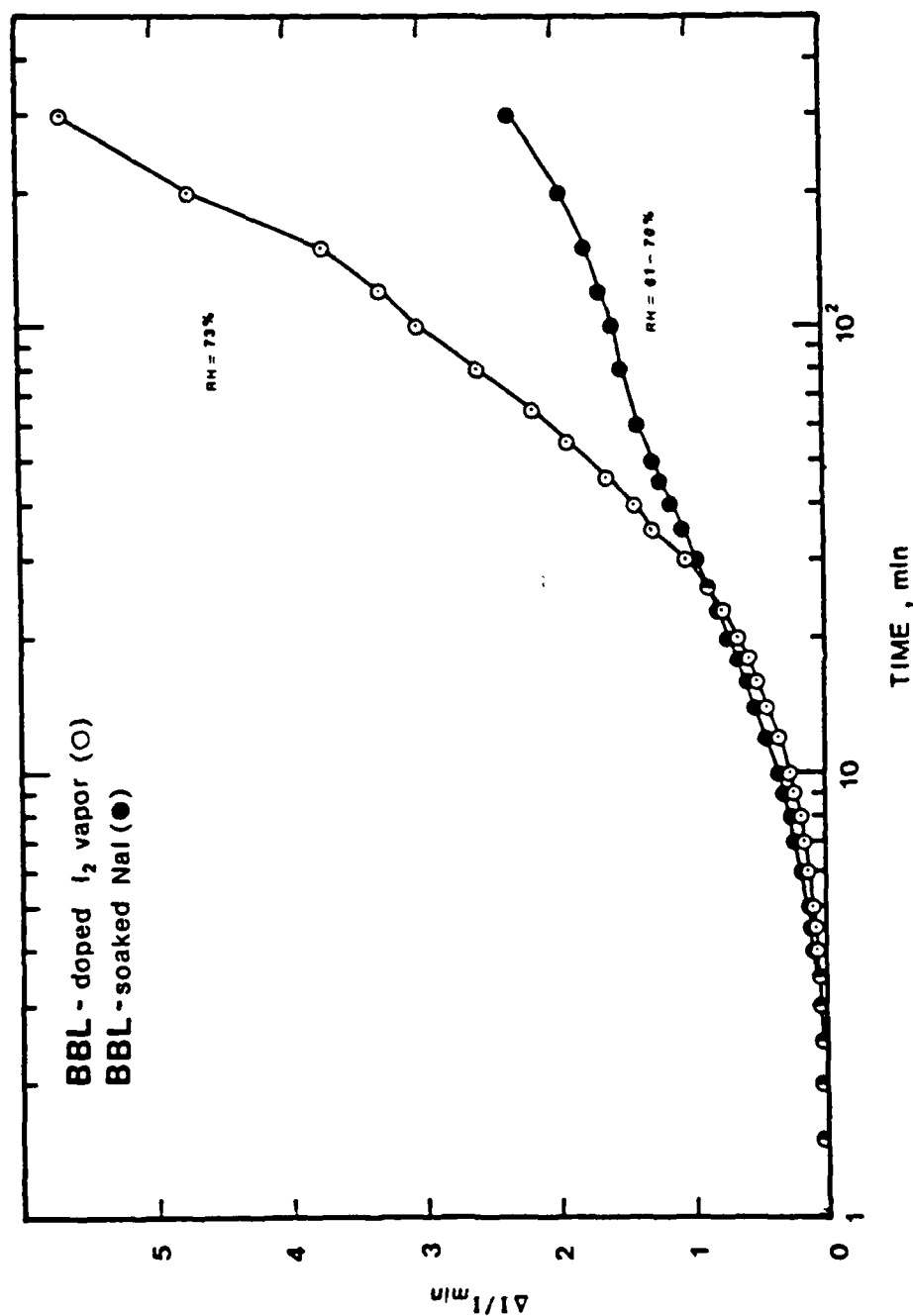


Figure 4.18. Differential Current, $\Delta I/I_{\min}$, Versus Time, Showing Relative Current Increase With Moisture Sorption for Various Doped Polymer Fibers.

would suggest that enhancement of the current is due to an adsorbed water layer on the fiber surface. As the thickness of the layer increases, the current should also increase with the possibility that water is also being absorbed into the polymer fiber at the same time. An alternative explanation is possible. BBL has a significantly higher conductivity, i.e., on the order of 10^{-6} S/m as compared to 10^{-11} S/m for the other polymer fibers, so that the effect of the water is not seen to influence the observed current as soon as it might in the case of the other polymers. For example, in the case of PP, at one minute after exposure to the moist air, there is a discernable increase in the conductivity over that seen in the dry case. This effect is more profound in the case of PPBT and the nylons. These results are shown in Figures 4.19-4.21.

Typically, the overall increase in differential current for BBL ranges from 2.3 times (for fibers treated in NaI solutions) to 6.7 times (for those soaked in ethyl alcohol). PE doped with I_2 increases by 3.4 times while PP doped in I_2 increases by 29.3 times. PPBT fibers exhibit increases ranging from a low of about 12.4 times (for a KI treatment) to a high of 72.9 times (when exposed to I_2 vapor). Nylon 6,6 shows increases in the differential current values of between 50 and 60 times for those samples doped in NaI solutions and exposed I_2 vapor, respectively. Finally, nylon 6 showed the largest overall current increase,

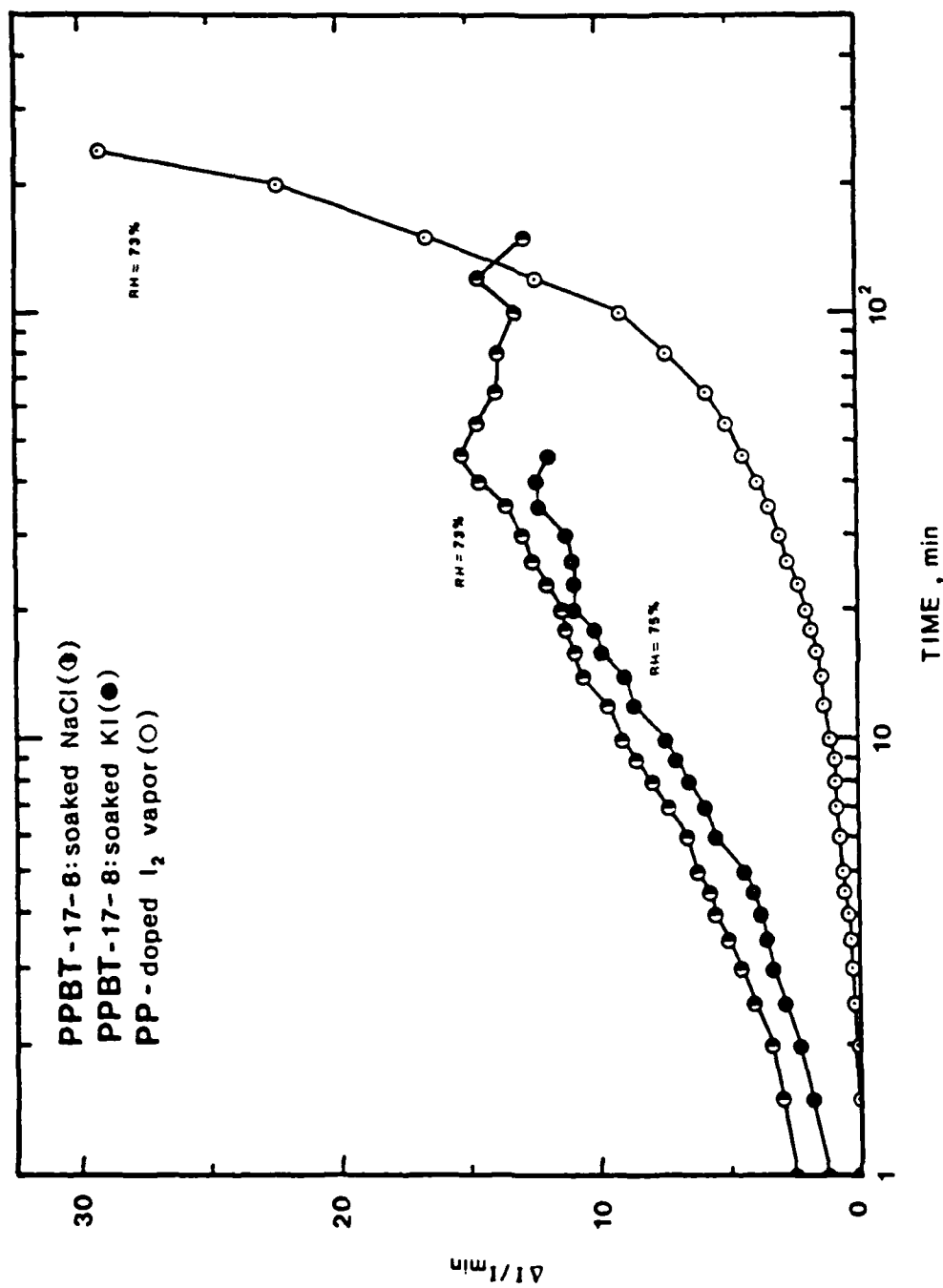


Figure 4.19. Differential Current, $\Delta I/I_{min}$, Versus Time, Showing Relative Current Increase With Moisture Sorption for Various Doped Polymer Fibers.

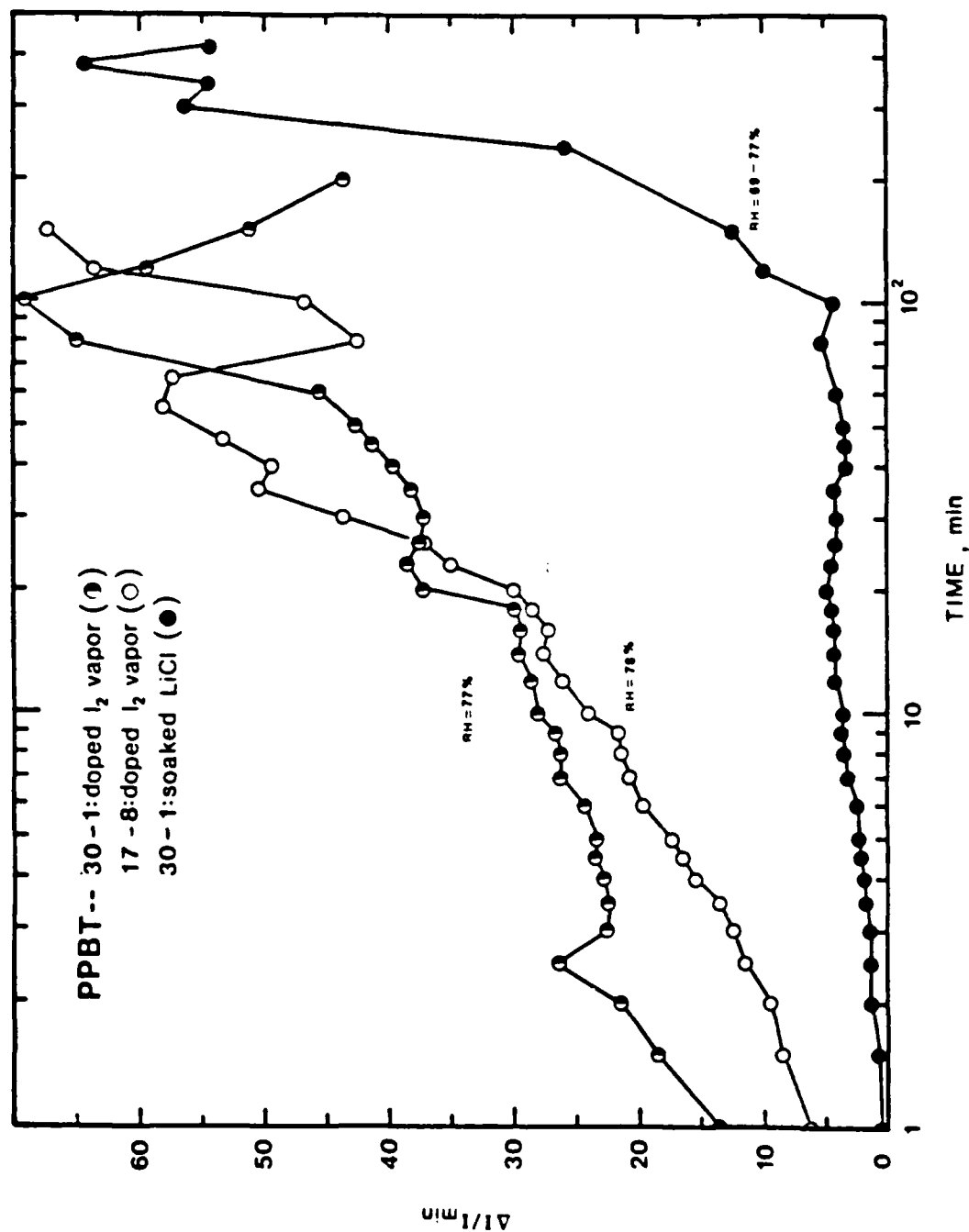


Figure 4.20. Differential Current, $\Delta I/I_{min}$, Versus Time, Showing Relative Current Increase With Moisture Sorption for Various Doped Polymer Fibers.

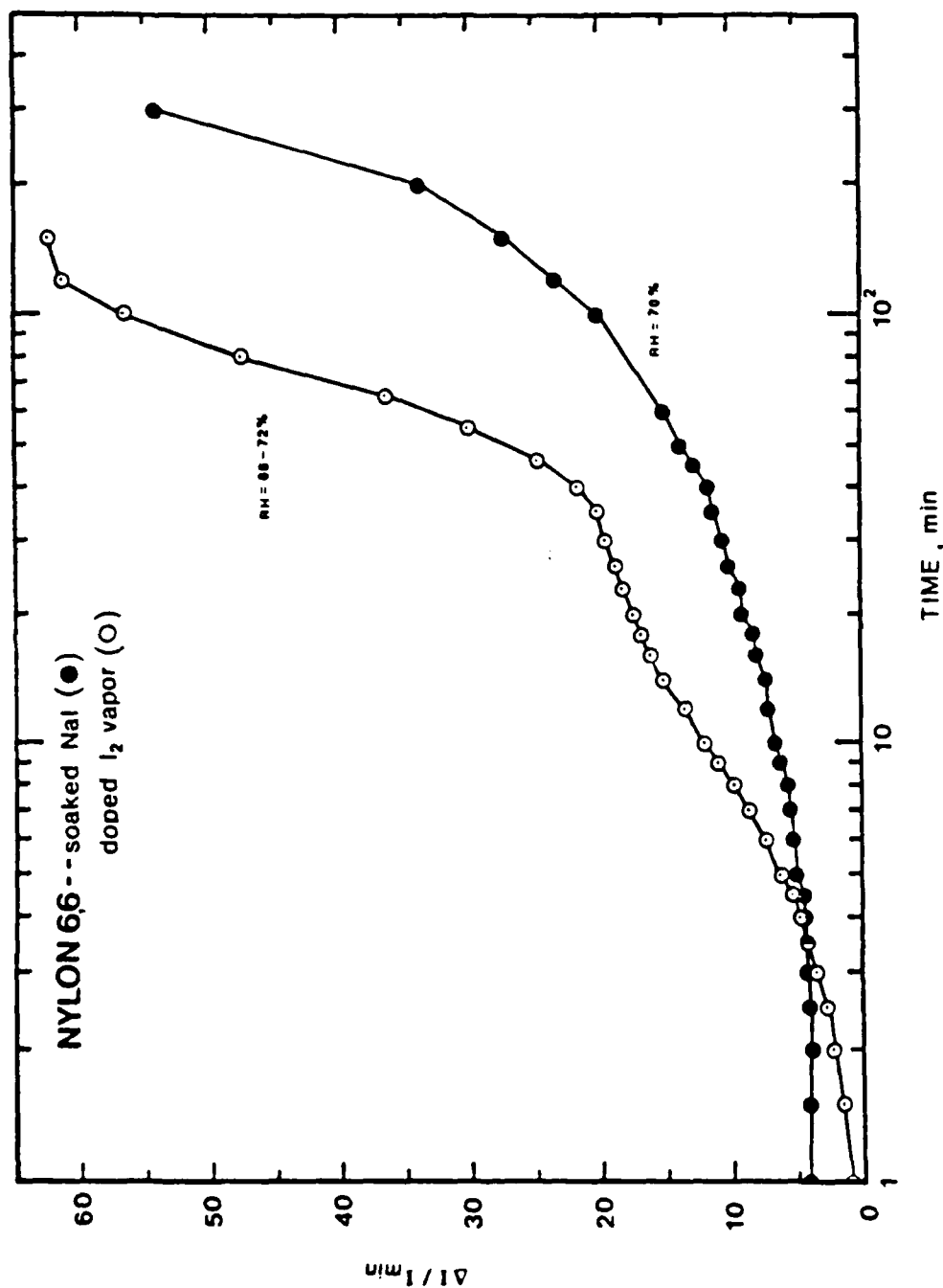


Figure 4.21. Differential Current, $\Delta I / I_{min}$, Versus Time, Showing Relative Current Increase With Moisture Sorption for Various Doped Polymer Fibers.

approximately 400 times that of the dry state recorded minimum current value, for the fiber doped in I_2 .

Irregularities due to changes in the relative humidity show up very well on these plots. In Figure 4.20, the curve for PPBT (29022-17-8) fiber shows a very large decrease in the differential current. The relative humidity during this period decreased from 79% to 75%. The humidity then began to rise once again, reaching a value of 77%. The minimum of the $\Delta I/I_{\min}$ curve at 80 minutes corresponds to 75% relative humidity. As the humidity in the room increased, so did the differential current. It is somewhat surprising that small changes in the relative humidity should cause such significant effects on the current.

4.4 Activation Energy Calculation

The experiments to determine activation energies were structured in such a way so that thermal equilibrium conditions in the fiber could be approached at each temperature for which current measurements were recorded. Each sample was kept at the desired temperature for at least 30 minutes. Additionally, each point on the plot is the averaged value of 10 to 20 minutes of current measurements, usually 20 to 40 data points. In most instances, the amount of scatter about each point is kept to a minimum and the results produce linear plots of current (or conductivity) versus reciprocal temperature. The plot of current versus reciprocal temperature can be used because the value

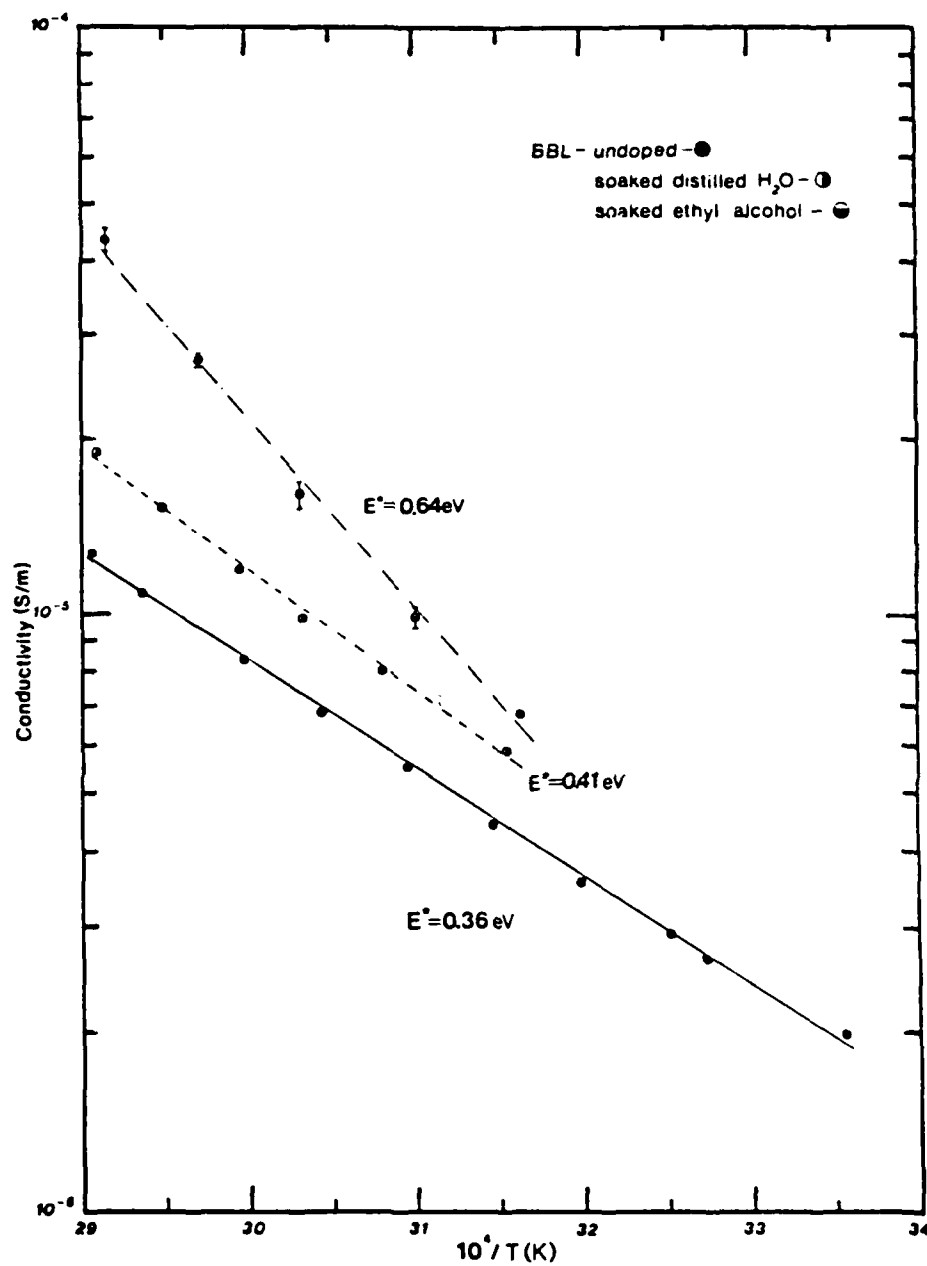


Figure 4.22. Arrhenius Plots of Conductivity Versus $10^4/T$ for BBL Fibers--Untreated and Soaked in Distilled Water and Ethyl Alcohol.

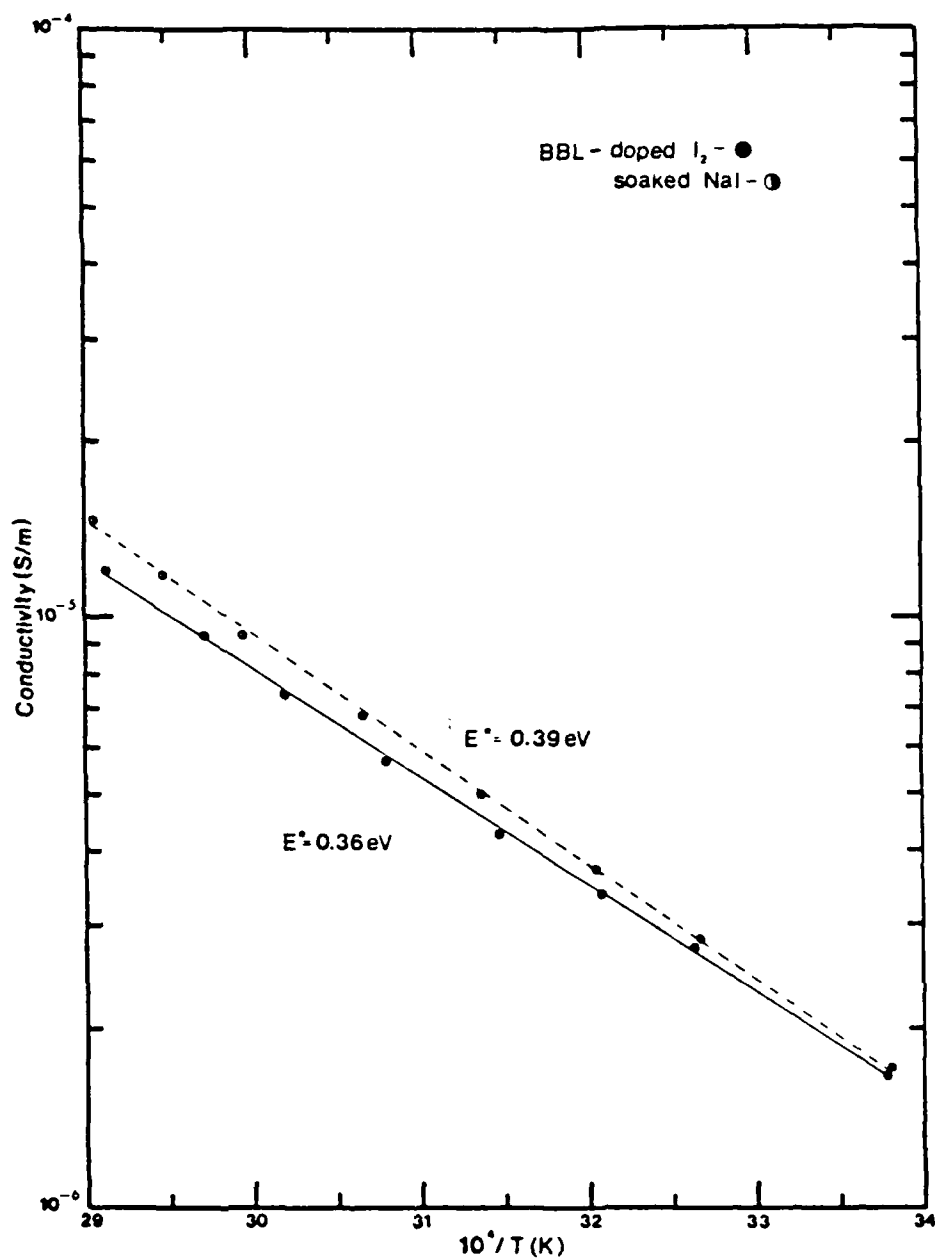


Figure 4.23. Arrhenius Plot of Conductivity Versus $10^4/T$ for BBL Fibers Treated With Iodine Vapor (I_2) and NaI Solution.

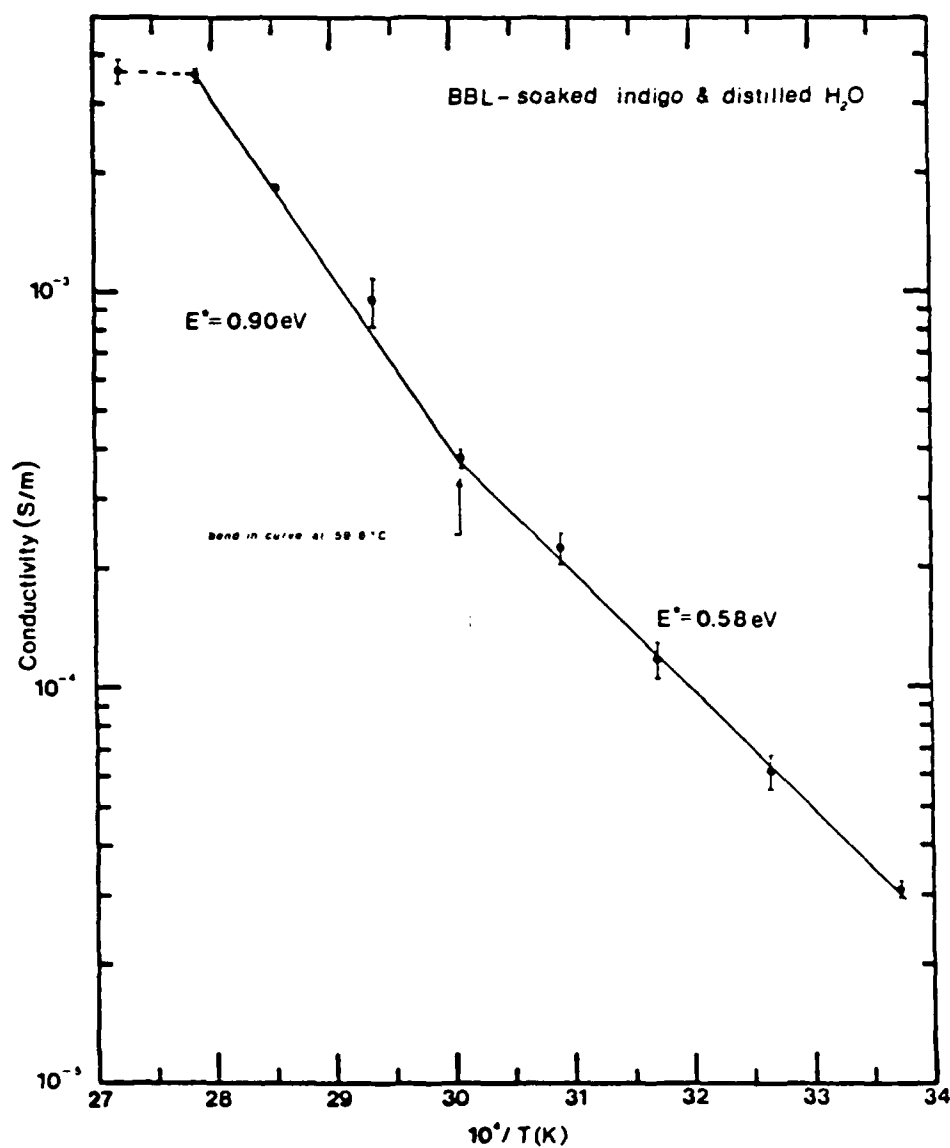


Figure 4.24. Arrhenius Plot of Conductivity Versus $10^4/T$ for BBL Fiber Soaked in an Indigo and Distilled Water Solution (0.2497 gms Indigo in 40 ml of Distilled Water).

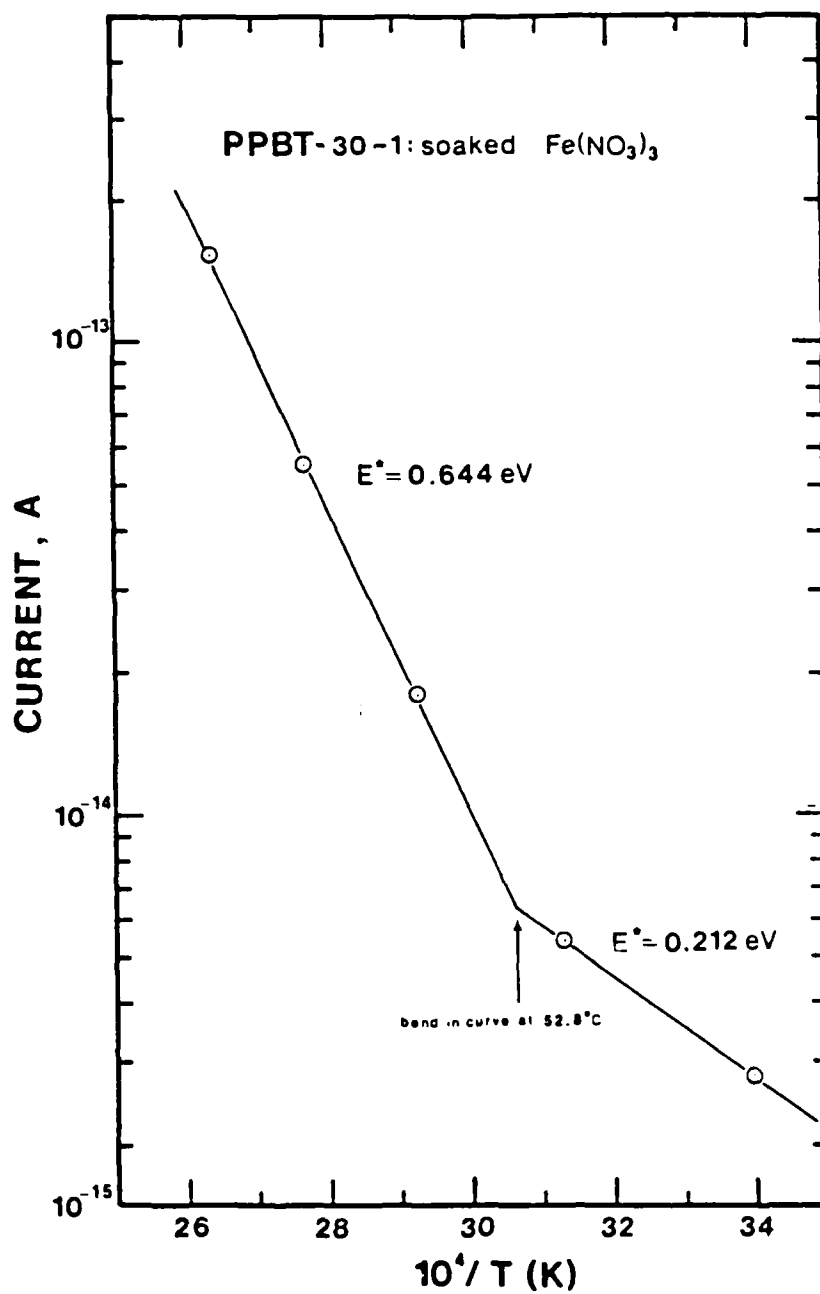


Figure 4.25. Arrhenius Plot of Current Versus $10^4/T$ for PPBT (29022-30-1) Fiber Soaked in $\text{Fe}(\text{NO}_3)_3$ Solution.

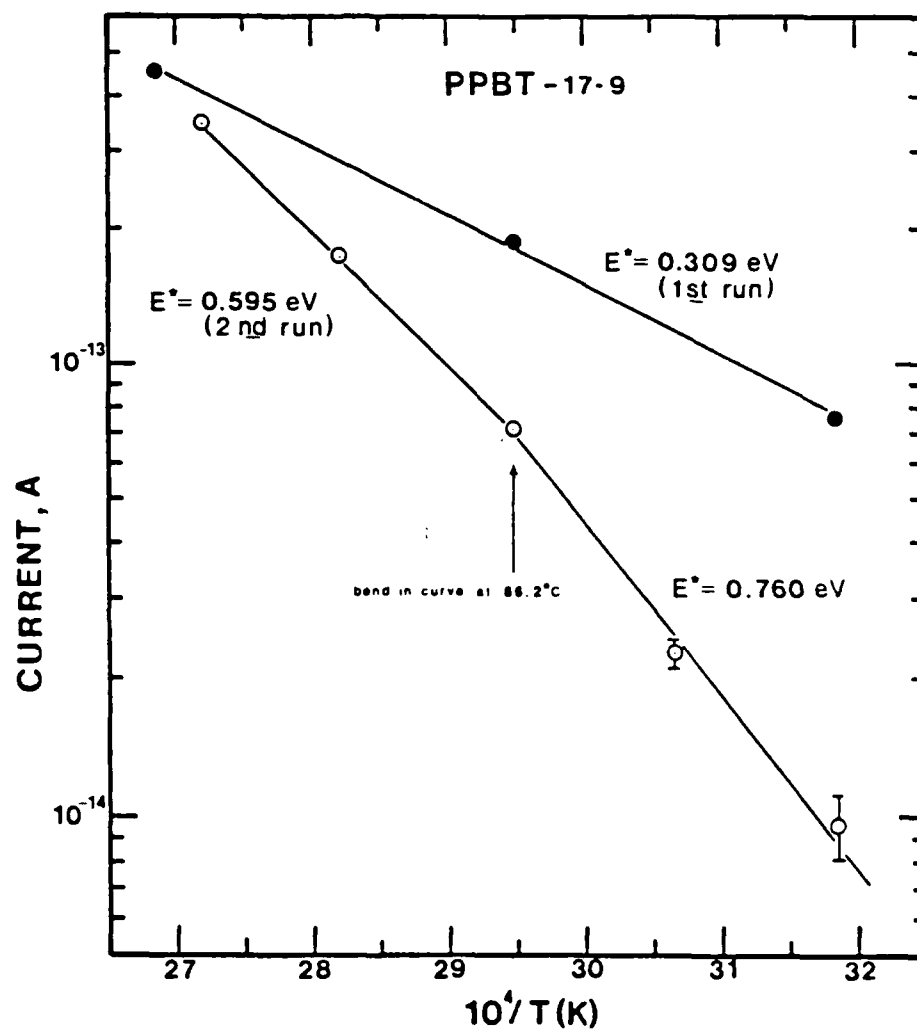


Figure 4.26. Arrhenius Plot of Current Versus $10^4/T$ for Untreated PPBT (29022-17-9) Fiber. Upper Curve is First Test of the Fiber, While Lower Curve was Generated 29 Hours Later.

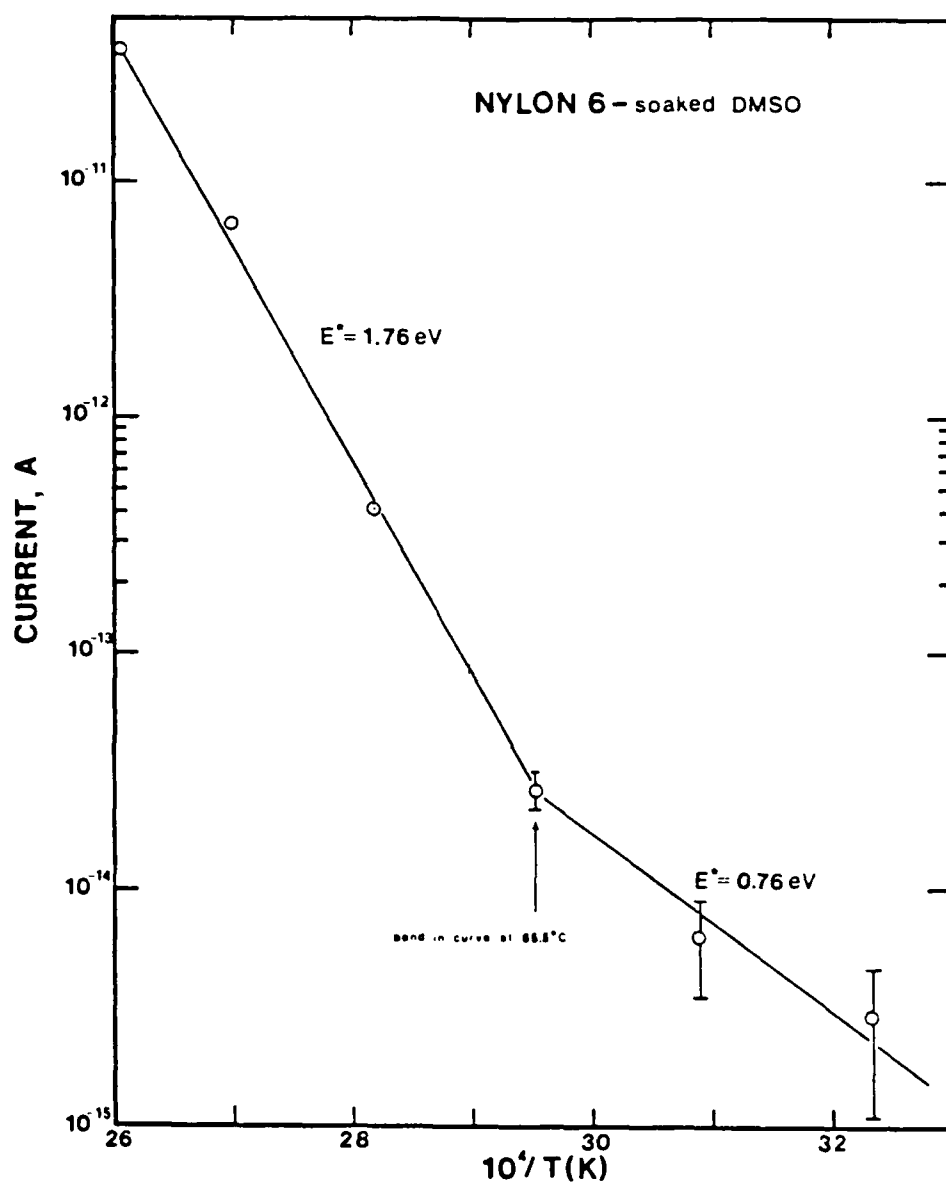


Figure 4.27. Arrhenius Plot of Current Versus $10^4/T$ for Nylon 6 Fiber Soaked in Dimethyl Sulfoxide.

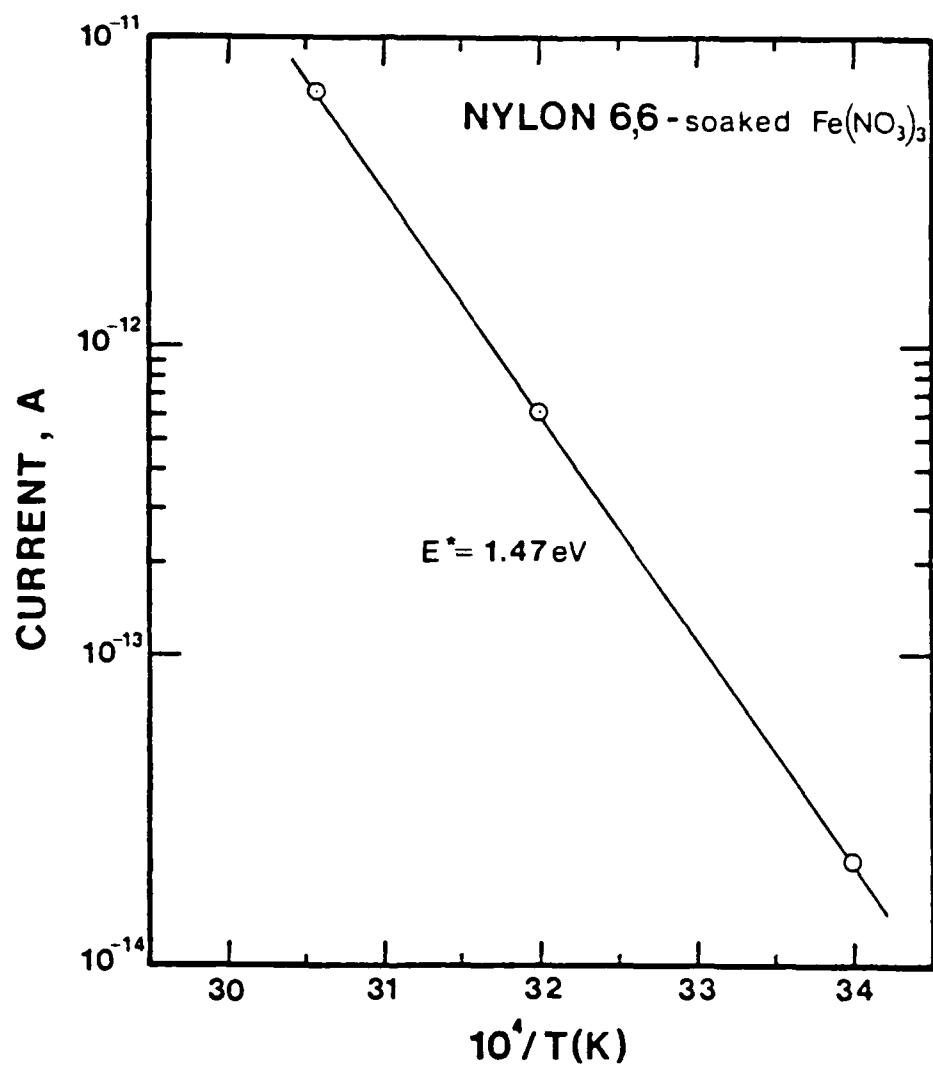


Figure 4.28. Arrhenius Plot of Current Versus $10^4/T$ for Nylon 6 Fiber Soaked in $\text{Fe}(\text{NO}_3)_3$ Solution.

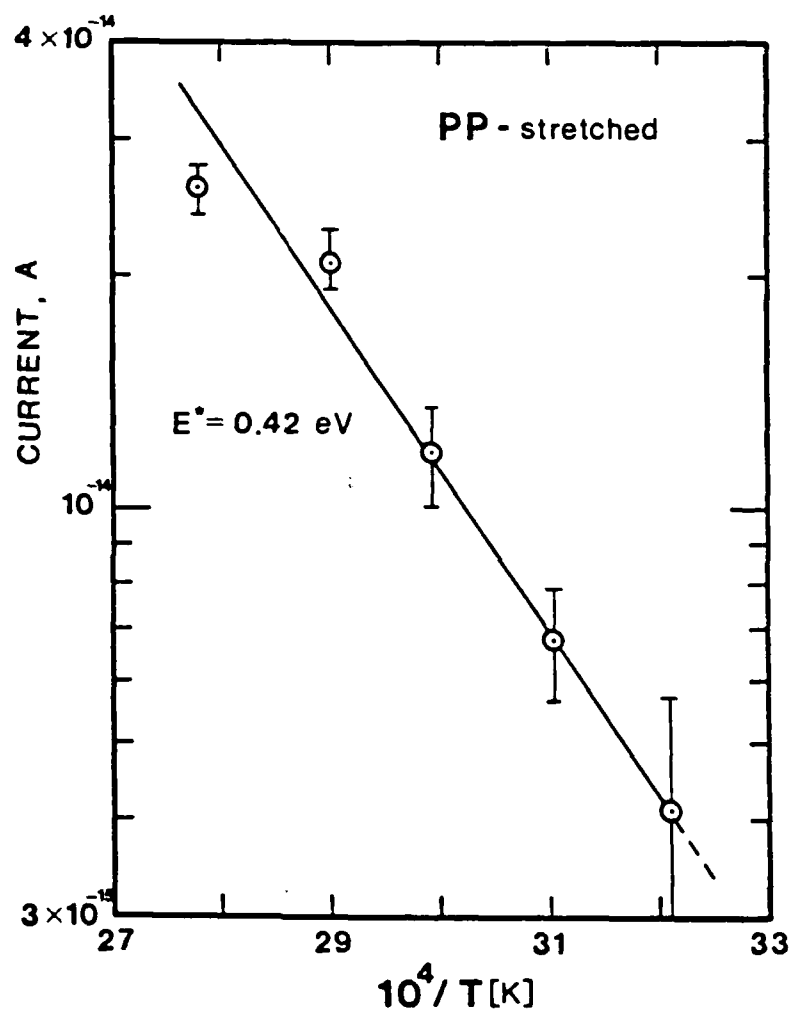


Figure 4.29. Arrhenius Plot of Current Versus $10^4/T$ for Stretched and Untreated Polypropylene Fiber.

equivalent to (l/VA) in the conductivity equation remains constant during the course of the experiment. This allows the relationship between σ and T to be applicable to I and T . Representative graphs are presented in Figures 4.22-4.24 for BBL, Figures 4.25-4.26 for PPBT, Figure 4.27 for nylon 6, Figure 4.28 for nylon 6,6 and Figure 4.29 for stretched PP. Further results are presented in tabular form in the chapter summary.

Very little data exists in the literature for activation energies for PP and nylon. However, Das Gupta and Joyner¹⁵¹ have studied absorption currents in polypropylene and have arrived at some values of activation energies for PP films. The results are listed below for a temperature range of 256K to 393K (-17°C to 120°C):

<u>E* (eV)</u>	<u>Time (sec)</u>
0.48	10
0.50	10^2
0.54	10^3
0.54	10^4

The "time" corresponds to the time after the application of the voltage when the experimental measurement was made. The activation energy arrived at from this research on the PP fibers was 0.42 eV in the range of 38.3°C to 86.6°C . These fibers were stretched, thereby aligning the individual chains. The stretching should aid electronic conduction and hinder ion movement. The agreement between the values for

Das Gupta and the present research is good, considering the different experimental procedures and types of samples used.

In addition, Baird et al.¹⁵² have measured the activation energy for nylon 6,6 in the temperature range of 50°C to 89°C. They arrived at a value of 1.4 eV which corresponds nicely with the value of 1.47 eV obtained in this research for nylon 6,6 doped in an $\text{Fe}(\text{NO}_3)_3$ /distilled water solution. Additionally, Seanor⁵⁸ has studied electronic and ionic conductivity in nylon 6,6. He arrived at the following values of E^* for different nylon 6,6 samples:

<u>E^* (eV)</u>	<u>Temp. Range (°C)</u>
1.85	60-95
2.18	70-120
1.30	> 125

According to the theory of Evans and Gergeley,¹⁵³ referenced by Seanor, the energy gap for conductivity should be about 3.0 eV. Assuming intrinsic conductivity, the observed activation energy should be at least 1.5 eV ($E^* = E_g/2$). The activation energy thus arrived at for nylon 6,6 in this research is at least a reasonable value. However, one fact is troublesome--how much of an effect does the $\text{Fe}(\text{NO}_3)_3$ addition have on the polymer's overall conductivity. The results of the doping of the fibers with various diffusants will be discussed in a later section, but it does appear that not much increase in the overall conductivity is gained

by the doping of the polymers with various metal salts, or organic liquids. However, an effect is seen in the recorded values for activation energies. An estimate as to the width of the energy gap, $E_g = 2E^*$, can be made from thermal activation energies. The following list gives some representative values for the temperature range indicated for E_g in terms of thermal activation energies obtained for the various polymers studied.

<u>Polymer</u>	<u>E^*(eV)</u>	<u>E_g(eV)</u>	<u>Temp. Range(°C)</u>
BBL	0.357	0.72	24.7-70.9
PPBT(48-4)	0.176	0.35	30.7-59.2
(17-9)	0.760	1.52	40.8-66.2
	0.595	1.19	66.2-94.6
PP	0.420	0.84	38.3-86.6
Nylon 6			
(DMSO)	0.760	1.52	36.2-65.5
	1.760	3.52	65.5-110.6
Nylon 6,6			
($\text{Fe}(\text{NO}_3)_3$)	1.470	2.94	21.3-53.9

Although there is no corroborative evidence for activation energies for BBL and PPBT, Bhaumik¹⁵⁴ has calculated a theoretical value for E_g for PPBT of 1.73 eV. The values for E_g obtained in this research are quite scattered and seem to depend more on the processing history of the fiber used. However, the value of $E_g = 1.52$ eV for PPBT (29022-17-9) for a temperature range of 40.8-66.2°C is close to Bhaumik's calculated value.

4.5 Current Versus Voltage Measurements

These measurements were made to show the linear relationship between current and voltage that exists in the ohmic region for both PPBT and BBL fibers. Figure 4.30 shows the field dependence for undoped PPBT while Figures 4.31 and 4.32 show the effect that various dopants have on the field dependence of BBL. Soaking BBL in ethyl alcohol and distilled water produce linear plots with the values of field increasing from 33 V/m to 7 kV/m. These fields are quite low, one would think well within the ohmic region. However, the slope for the PPBT (Fig. 4.30) is close to two, suggesting either a trap limited conduction process or perhaps a space charge limited situation due to electrochemically released charge in the surface region. Soaking BBL in an indigo/water solution produces a curve with a definite bend at about 0.8V, as shown in Figure 4.32. On either side of the bend, the curve is linear. This appears to be unusual in that there is an initially non-ohmic region at a very low field, followed by an almost ohmic one at a somewhat higher field. Again, electrochemical effects in the surface regions are suspected. This effect may be due to the fact that the increase in voltage, even though it is slight, enhances the overall conduction process.

Figure 4.33 depicts the current versus voltage behavior of an acetone soaked BBL fiber at various temperature levels. The upper portion of each curve is linear with a

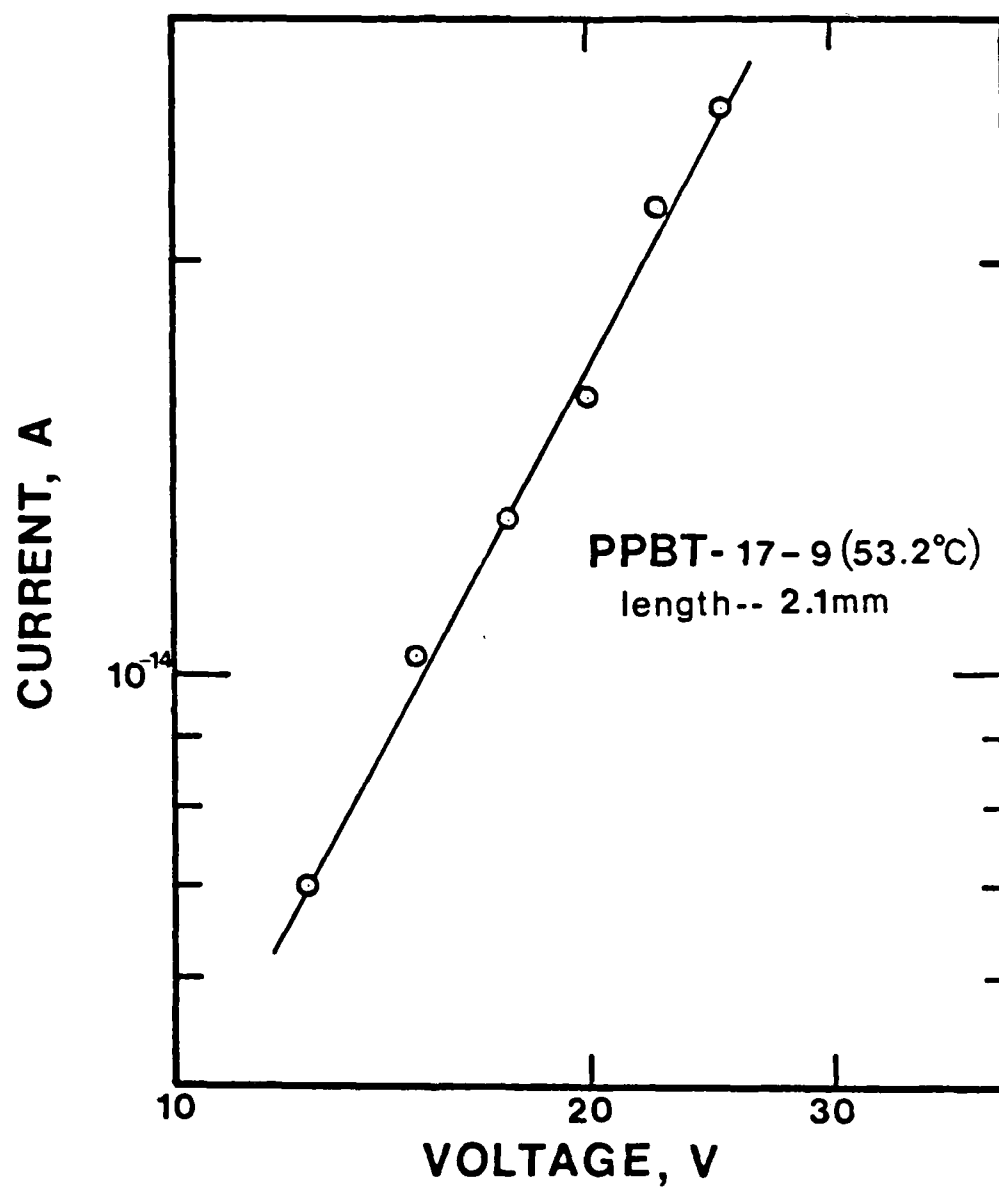


Figure 4.30. Current Versus Voltage Curve Showing Linear Dependence for Untreated PPBT (29022-17-9) Fiber.

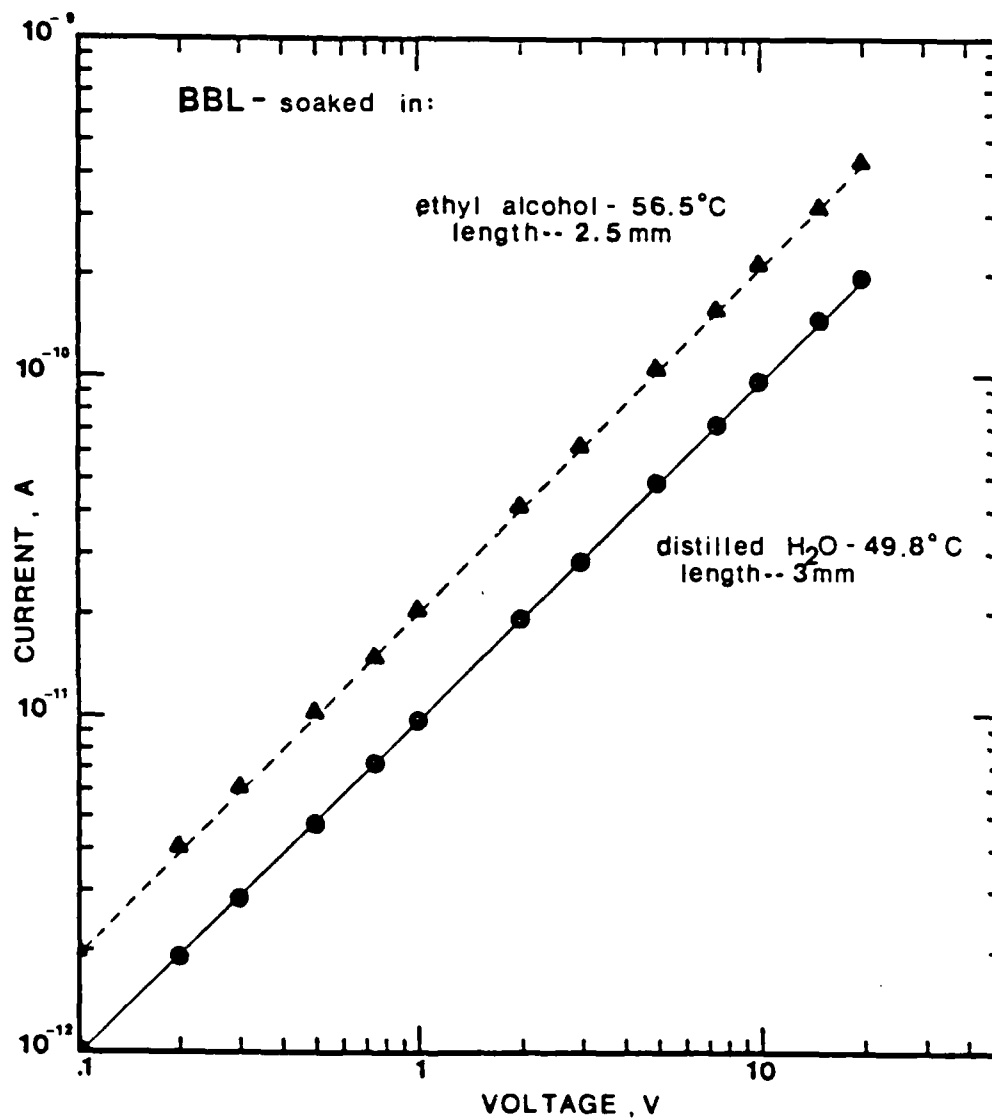


Figure 4.31. Current Versus Voltage Curve Showing Linear Dependence for BBL Fibers Soaked in Ethyl Alcohol and Distilled Water.

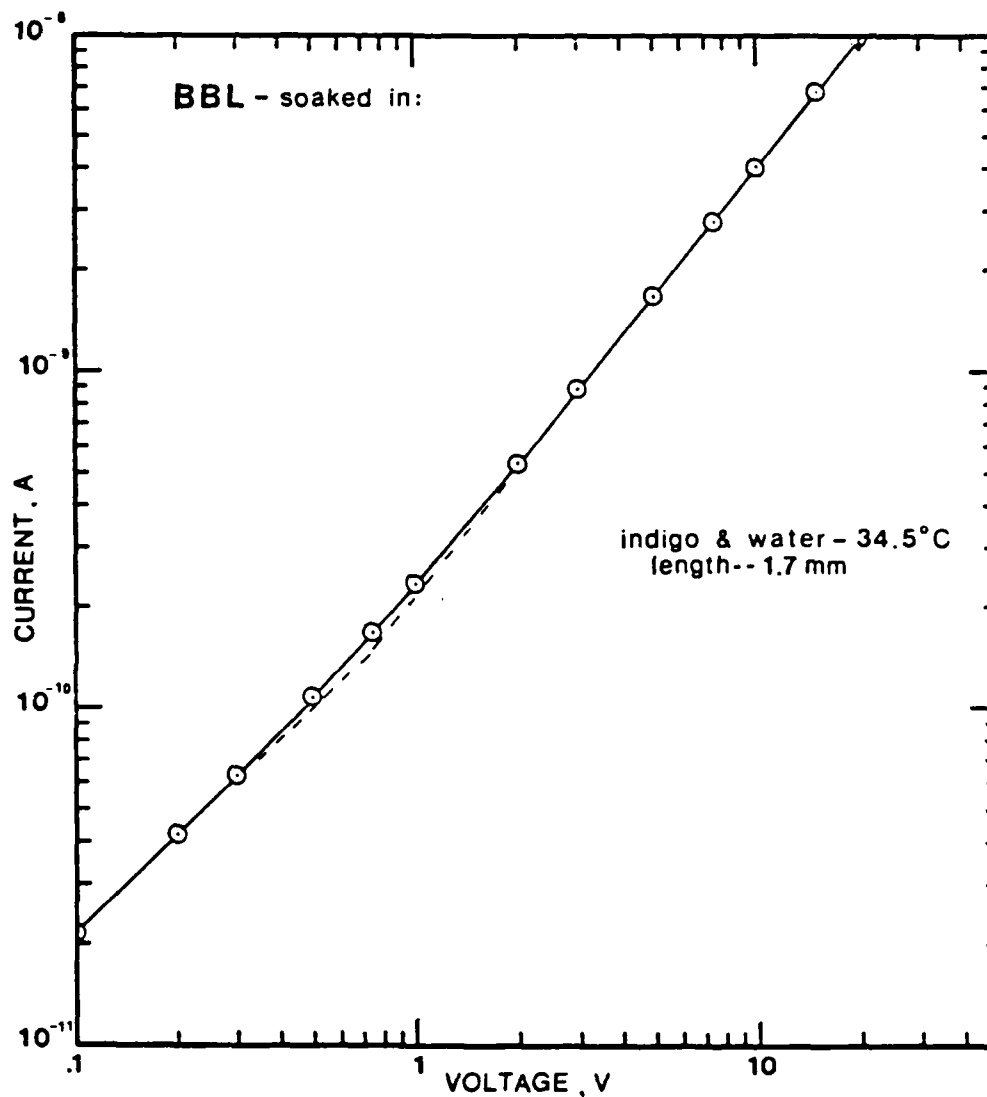


Figure 4.32. Current Versus Voltage Curve for a BBL Fiber Soaked in an Indigo/Water Solution. There is a Bend in the Curve at Around 0.8 Volts.

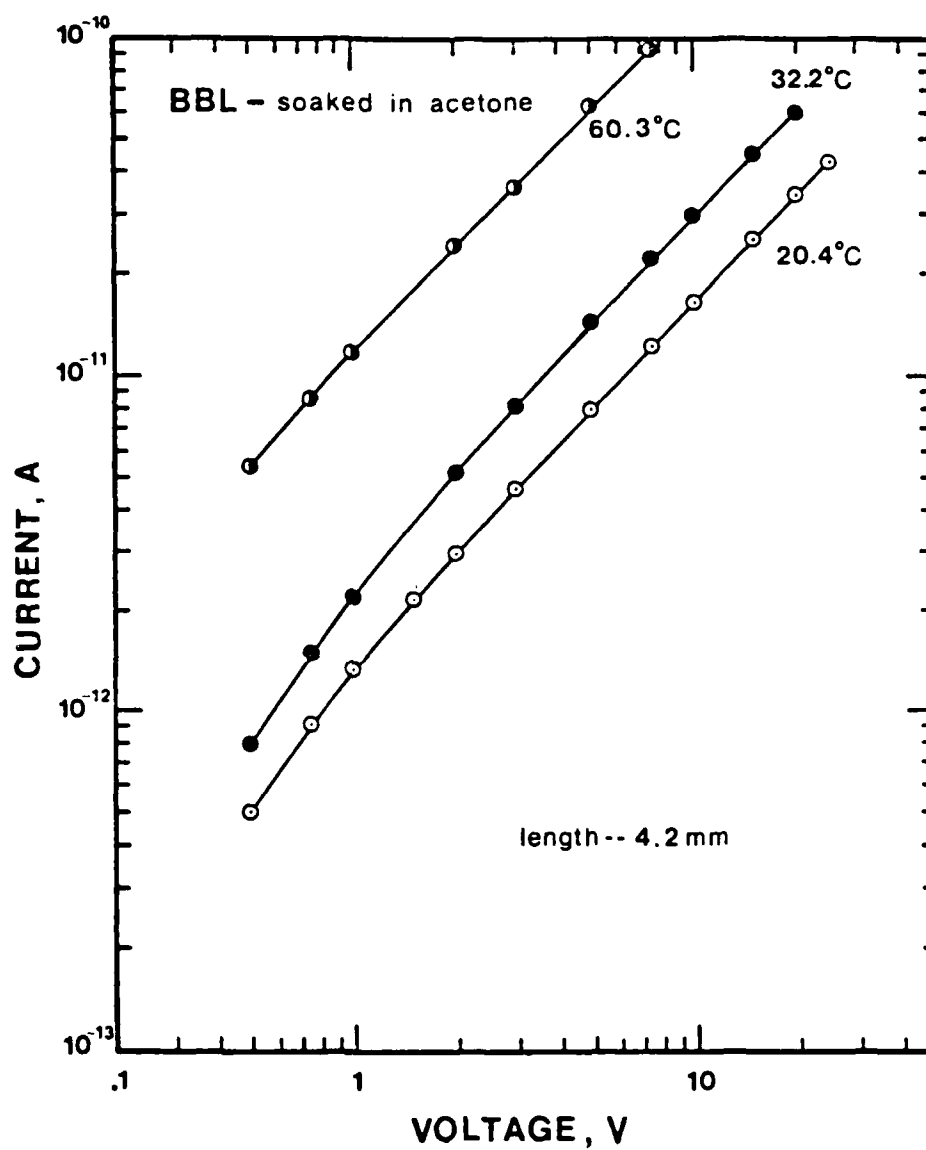


Figure 4.33. Current Versus Voltage Curves at Various Temperatures for a BBL Fiber Soaked in Acetone. A Slight Downward Curvature Exists in the Low Voltage Region.

slope of 1.06 and parallel to the other curves in this region.

If it were possible to increase the field into the non-ohmic region at considerably higher fields, then useful information about the charge carrier could be deduced.²⁰ Figures 4.34 and 4.35 present typical models which can be used to identify both electronic and ionic conduction processes which are non-ohmic. For example, in electronic conductors, the Poole-Frenkel effect is the consequence of a strong applied electric field enhancing the de-trapping of electrons within a semiconductor or insulator. Any high field experimental work on these polymers, probably in thin film form, would yield useful information that cannot readily be obtained through fiber research.

4.6 Surface-to-Volume Conductivity Determination

An attempt was made to separate the surface and volume conductivity for a set of PPBT fibers by varying the fiber diameter. It was not possible to obtain a large number of fibers each of different radii from one processed batch to perform these experiments. As such, two groups of processed undoped PPBT fibers were chosen. The conductivity measurements were made at $66.5 \pm .5^{\circ}\text{C}$ and the specimen length, l , and voltage were kept constant for all experiments. There is an order of magnitude difference between the 29022-17 and 29022-48 series of PPBT fibers and no general trend is established by the data.


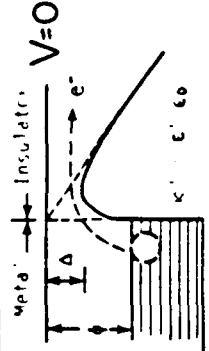

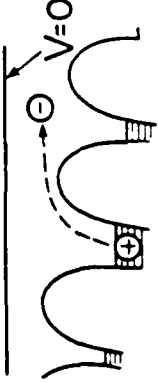

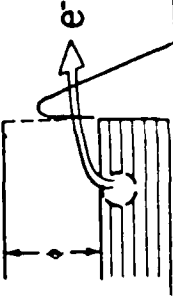
NAME OF EFFECT AND USUAL TEST PLOT	DESCRIPTIVE EQUATIONS	PHYSICAL INTERPRETATION
SCHOTTKY- (RICHARDSON) EMISSION  $E^{1/2}$ $\text{LOG } J$	$\frac{J}{E} = \frac{A_R T^2}{E} \exp \left[\frac{B_S E^{1/2} - \phi}{kT} \right]$ $A_R = 1.2 (10^6 \text{ A/m}^2)$ $B_S / k = 0.44 \text{ } \kappa^{-1/2}$	 FIELD ASSISTED HOPPING OVER IMAGE BARRIER AT CATHODE
POOLE-FRENKEL EFFECT  $E^{1/2}$ $\text{LOG } J$	$\frac{J}{E} = \frac{A_R T^2}{E} \exp \left[\frac{B_P E^{1/2} - \phi}{kT} \right]$ $B_P / k = 0.88 \text{ } \kappa^{-1/2}$ $B_P = 2B_S$	 FIELD ASSISTED ELECTRON-HOLE SEPARATION WITHIN BULK OF SAMPLE
FOWLER-NORDHEIM EMISSION  $1/E$ $\log \frac{J}{E}$	(NO EXPLICIT DEPENDENCE ON TEMPERATURE) $\frac{J}{E} = 1.54 (10^{-6}) \frac{E}{\phi} \exp \left[\frac{-6.8 \phi^{3/2}}{10^9 E} \right]$	 QUANTUM TUNNELING THROUGH IMAGE BARRIER

Figure 4.34. Non-Ohmic Electronic Processes.


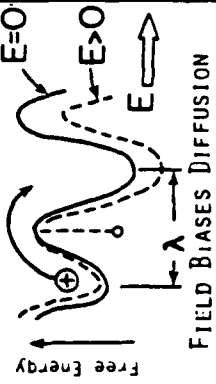

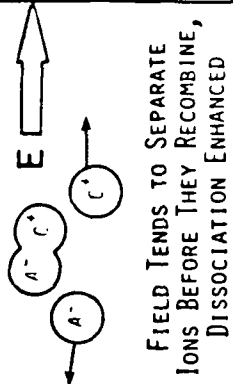
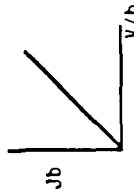
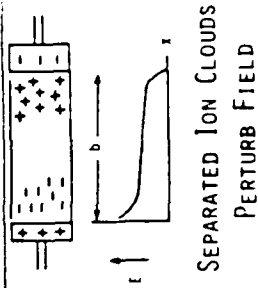
NAME OF EFFECT AND TYPICAL TEST PLOT	DESCRIPTIVE EQUATIONS	PHYSICAL INTERPRETATION
MODIFIED STERN-EYRING RATE THEORY 	$\sigma = \frac{j}{E} = nqu$ $u = \frac{Dq}{kT} \frac{e^{\alpha W} - e^{-(\alpha-1)W}}{W}$ $W = Eq\lambda/kT$	 <p>FIELD BIASES DIFFUSION</p>
ONSAGER THEORY 	$\frac{\sigma(E)}{\sigma(0)} = \left[\frac{-2i J_1(iF)}{F} \right]^{1/2}$ $F = 88.2T(E/\kappa')^{1/2}$ $E \text{ in [V/m]}$	 <p>FIELD TENDS TO SEPARATE IONS BEFORE THEY RECOMBINE, DISSOCIATION ENHANCED</p>
SPACE-CHARGE-LIMITED CONDUCTION 	$IF \quad v = uE$ $\sigma = \frac{j}{E} = \frac{9}{8} \epsilon_0 u \frac{V}{b^2}$	 <p>SEPARATED ION CLOUDS PERTURB FIELD</p>

Figure 4.35. Non-Ohmic Ionic Processes.

<u>Fiber Designation</u>	<u>Diameter (μm)</u>	<u>Conductivity (S/m)</u>
29022-17-2	17.1	2.2×10^{-9}
29022-17-9	38.1	5.3×10^{-9}
29022-48-4	62.9	1.4×10^{-10}
29022-48-2	82.9	2.4×10^{-10}
29022-48-3	94.3	1.1×10^{-10}

It was not possible to graph these results, i.e., σ_{app} versus $1/r$ or σ_{app} versus r , and produce a linear plot. A line may be forced through these points, but more points are necessary if the statistics are to be considered reliable. Of course, if only two points are used, a straight line is obtained; however, the validity of the calculated values for surface and volume conductivity may be questioned. It is hypothesized that differences in the processing history between the 29022-17 series and the 29022-48 series preclude the use of this method to separate the volume and surface components of the conductivity. PPBT also does not lend itself to this method because very uniform diameter samples are needed and this is not the case for PPBT fibers, as previously pointed out by Chen.¹⁸ Thus, this method is enticing in concept, but impractical from the standpoint that a wide variety of fibers of differing diameters processed in exactly the same way are not readily available.

The second method of separating surface and volume conductivity, whereby the effective length of the fiber is varied, proved more successful. In this case, undoped and

ethyl alcohol treated BBL fibers were used. BBL was used for two reasons. First, it exhibited the highest conductivity of the polymers that were studied. This allowed the measurements to be made at room temperature which made for easy control of the environment. Second, the fibers are uniform in their appearance when examined in the optical microscope. The results of these experiments are shown in Figure 4.36. Overall, straight lines were generated with slopes near to or slightly less than -1. This is a desirable result because a direct inverse proportionality between I and ℓ provides evidence that the measured conductance is that of the material and not of the contacts.²⁹ The slope being near -1 is not contradictory to the hypothesis that the surface is the more highly conducting region of the fiber. Equations developed in Section 3.7 were used to determine values of σ'_{sur} for each of the curves in Figure 4.36. These results depend on the points chosen from the curve. For example, for undoped BBL at 32.3°C where,

$$\begin{aligned}\sigma_1 &= 2.67 \times 10^{-6} \text{ S/m}; \ell_1 = 8.04 \times 10^{-3} \text{ m} \\ \sigma_2 &= 2.62 \times 10^{-6} \text{ S/m}; \ell_2 = 3.60 \times 10^{-3} \text{ m} \\ \sigma_3 &= 2.46 \times 10^{-6} \text{ S/m}; \ell_3 = 1.91 \times 10^{-3} \text{ m};\end{aligned}$$

The calculated values for σ'_{sur} become

$$\begin{aligned}(1-2) \sigma'_{\text{sur}} &= 2.58 \times 10^{-6} \text{ S} \\ (1-3) \sigma'_{\text{sur}} &= 2.39 \times 10^{-6} \text{ S} \\ (2-3) \sigma'_{\text{sur}} &= 2.27 \times 10^{-6} \text{ S}.\end{aligned}$$

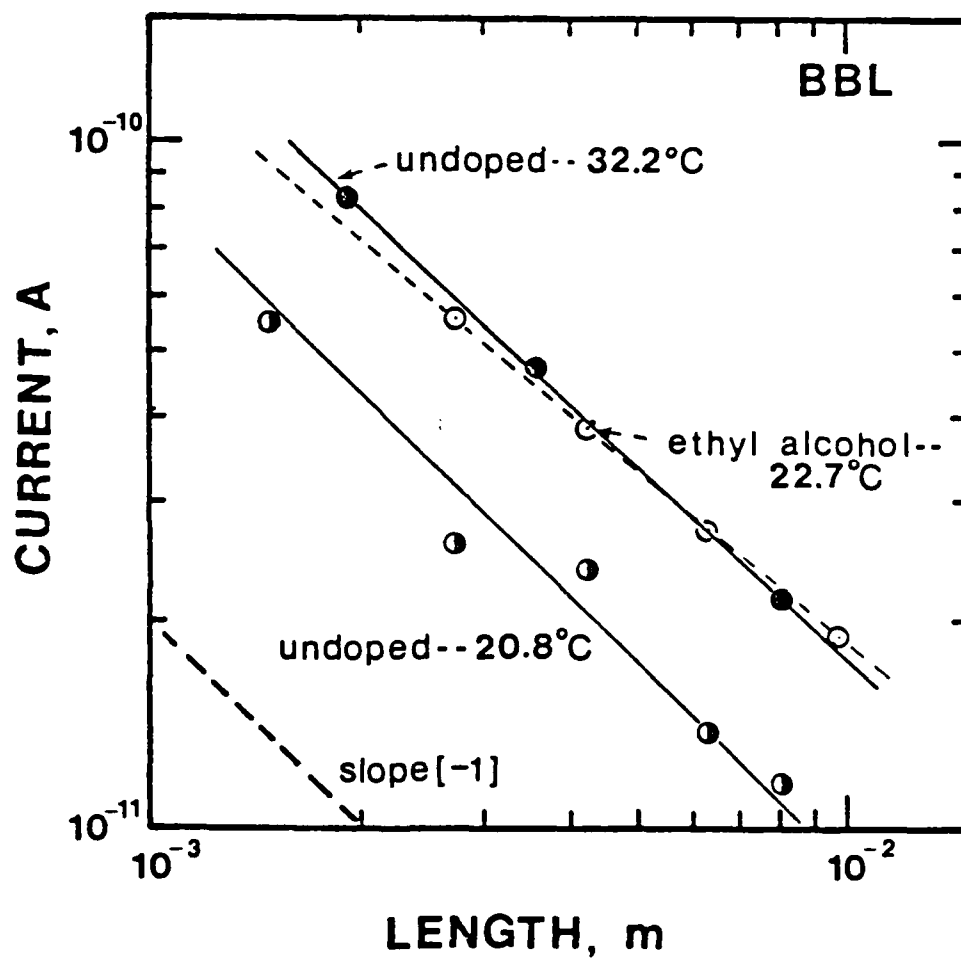


Figure 4.36. Current Versus Length for BBL Fibers Used in Determining the Portion of the Surface or Volume Conductivity of the Total Observed Conductivity.

The percentage of the total conductivity exhibited by σ'_{sur} (1-2) when compared to the average value of conductivity for σ_1 and σ_2 is 97.5%. This value drops to 89.4% when σ'_{sur} (2-3) is compared to the average value of σ_2 and σ_3 .

This comparison procedure takes two adjacent points on the plot for the polymer fiber under consideration. σ'_{sur} is determined using the values of length and conductivity for these two points. Then the average value of conductivity is determined for these two data points and it is against this average value that the calculated value of surface conductivity is compared.

For undoped BBL at 20.9°C, the two points closest to the extrapolated line were used in order to arrive at a value for σ'_{sur} . In this case, σ'_{sur} was found to be equal to 1.37×10^{-6} S. This represents 94.4% of the average value for conductivity of the two points used to determine σ'_{sur} .

BBL soaked in ethyl alcohol at 22.6°C produced a curve with a slope of slightly less than -1. In this instance, the percentage of current calculated to be conducted by the surface layer is only 86.1% of the total average value.

Of the two methods, the one where the length of the fiber is varied is perhaps the easiest to use, as only one fiber is needed. Silver paint is advanced along the fiber, thereby reducing its effective length. The assumption of the model is that electrical contact is made with the ends of the "bulk" fibers, which in turn are not "cross-connected" inside the sample region. The slope of the curve

qualitatively describes the region in the fiber where most of the conduction occurs. When the slope is -1, or close to this value, surface conduction dominates. As the slope becomes less steep, a mixed mode of surface and volume conduction is indicated. As the slope approaches zero, the volume will be the conduction region of importance. It needs to be emphasized that these statements depend on the validity of the model, but that the slope of slightly less than one provides some evidence for this model. Performing these types of experiments on doped fibers, preferably those containing metal salt ions, would be a logical extension of this research.

4.7 Effects of Doping of Polymer Fibers

The primary goal of doping a polymer is to enhance the conductivity by increasing its overall magnitude. The results of this research did not produce any doping medium that consistently and significantly increased the conductivity of the polymer fiber. This was a disappointing result. However, several observations can still be made.

Of primary importance in any doping experiment is making sure that the dopant is indeed introduced into the polymer in the correct way. As an example, Oh-Kil Kim¹⁵⁵ doped BBL film with H_2SO_4 and observed an increase in conductivity from 10^{-12} S/cm to 1 S/cm. However, when doping the BBL fibers in sulfuric acid for this research, a decrease in conductivity was observed. The difference in

these results apparently lies in the method of doping the polymer. Kim placed the film in a vacuum chamber and passed a steady stream of H_2SO_4 over the sample for several days, all the while keeping the system under a vacuum. Kim diffused gaseous H_2SO_4 into the BBL, as opposed to placing the polymer in a sulfuric acid solution.

Another concern in doping experiments is to ensure that the diffusant enters the polymer. Hill¹⁵⁶ has solved the diffusion equation of a long cylindrical fiber of radius r placed in an infinite bath of diffusant at zero time. The uptake of diffusant is then described by Eq. (4.3) given below.

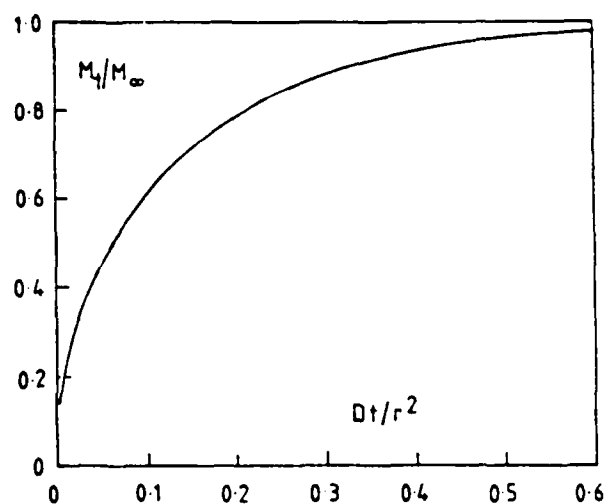
$$\frac{M_t}{M_\infty} = 1 - A \exp\left(\frac{-aDt}{r^2}\right) - B \exp\left(\frac{-bDt}{r^2}\right) - C \exp\left(\frac{-cDt}{r^2}\right) \dots \quad (4.3)$$

where A , B , C and a , b , c , are numerical constants with the following values:

$A = 0.692$	$a = 5.785$
$B = 0.131$	$b = 30.5$
$C = 0.0536$	$c = 74.9$

The higher terms in this equation diminish rapidly. A plot of this equation with some representative values for the times necessary to reach $M_t/M_\infty = 0.8$ for various values of D are given in Figure 4.37 for representative values of fiber radii.

The diffusion coefficient for water in various polymers ranges from 10^{-9} cm^2/sec in nylon 6 to $2.3\text{--}2.4 \times 10^{-7}$ cm^2/sec in PE and PP.¹⁵⁷ From these values in the



$\frac{r}{D}$	10	50	100	200
10^{-6}	0.22 s	5.5 s	22.0 s	88.0 s
10^{-8}	22.00 s	550.0 s (9.2 m)	2.2×10^3 s (0.61 h)	8.8×10^3 s (2.44 h)
10^{-10}	2.2×10^3 s (0.6 h)	5.5×10^4 s (15.3 h)	2.2×10^5 s (2.6 days)	3.8×10^5 s (10.2 days)

Figure. 4.37. Mass Uptake for Long Cylindrical Fibers in an Infinite Bath, From Eq. (4.3).¹⁵⁶ (The Diffusion Coefficient D is Expressed in cm^2/sec and Depth of Penetration r is Expressed in μm .)

literature, it can be seen that for $M_t/M_\infty = 0.8$ when D is approximately 10^{-10} cm²/sec, the amount of time a fiber must spend in the solution ranges from a low of 0.6 hours for a 10 μ m fiber to a high of 10.2 days for a 200 μ m fiber. Thus, it can be seen that in most instances the polymer fibers had sufficient time in solution to absorb a significant amount of diffusant in the form of water. Although absorption of water into the fiber is certain, this does not mean that the metal salt ions diffuse into the polymer.

When various metal salt solutions were used to dope the polymer fibers, color changes were observed. CuCl_2 turned the nylon sample a pale green color. Indigo turned the nylon a deep blue. The iodine vapor turned the nylon a deep orange and the PE and PP a lighter orange. Burford and Harrauer¹⁵⁸ have diffused salt solutions, specifically zinc chloride and lithium bromide, into nylon 6 and nylon 6,6 polymer samples. They measured the ZnCl_2 penetration (in mm) versus time (in days) the polymer spent in the salt solution, using SEM microprobe analysis. After 5 days, the zinc ions had penetrated a distance of 0.35 mm (i.e., 350 μ m) into the nylon 6. Since the nylon 6 and nylon 6,6 fibers used in the research were 150 μ m and 310 μ m in diameter, respectively, it can be assumed that the metal salts used in this research were able to diffuse throughout the fiber. They also found that the amount of zinc absorbed

into the polymer decreased with distance from the solution/polymer interface. These results are shown below.

<u>Distance From Edge(mm)</u>	<u>Zinc Content(w/o)</u>
0.000 - 0.023	10.2
0.023 - 0.131	4.9
0.131 - 0.173	0.3
0.173 - 0.217	0.5
0.217 - 0.283	0.3

This essentially means that the various salt solutions penetrate throughout the fiber. However, the large majority of the metal ions will be found near the outer surface. This supports the hypothesis that the surface region may conduct the majority of the current. It is seen that the surface region of the fiber contains the highest concentration of metal ions in the polymers and thus it is the most likely region for ionic conduction.

Some of the results were interesting and encouraging. Nylon 6 doped with iodine vapor (i.e., I_2) exhibited an increase in conductivity from 7.8×10^{-11} S/m in the undoped state to a value of 2.6×10^{-9} S/m in the doped state. However, BBL exhibited only a very slight increase, from 1.4 to 1.7×10^{-6} S/m. This is statistically insignificant and it is also of interest to note that the activation energies of undoped BBL and BBL containing molecular iodine were very similar--0.357 eV to 0.364 eV, respectively. On this basis,

it must be concluded that I_2 had very little effect on the conductivity of BBL.

One dopant that did affect BBL was the indigo/water solution. This caused an order of magnitude increase in the conductivity. Additionally, the thermal activation energy for conduction was significantly greater for BBL doped in indigo over that observed for the undoped polymer. In fact, if only the activation energy calculations are examined, it is obvious that the various dopants do influence the conductivity of BBL. The conductivity is influenced by an increase in the activation energy for conduction. It is hypothesized that certain of the organic penetrants influence the conductivity as the temperature is raised.

Another interesting effect seen in doped BBL is the change in magnitude of the activation energy. In some of the doped fibers, there is an increase in E^* , usually in the range between 50°C and 65°C. This change in slope of the Arrhenius plot for current versus $1/T$ usually occurs near the glass transition temperature. Since this effect was not observed for undoped BBL, or BBL doped with metal salts, it seems likely that this bend is not related to the glass transition in BBL. Additionally, BBL's glass transition, like PPBT, is not well known, but it is well above 60°C. Since this change in slope was observed for BBL soaked in some form of an organic solution, this effect probably has more to do with the dopant, or dopant/polymer interaction, than with the polymer itself.

4.8 Summary of Results

This section presents in tabular form many of the results discussed in the previous sections. Table 4.1 contains data on the conductivity of undoped polymers at various temperatures. Table 4.2 lists the observed conductivities of polymers doped with iodine in vapor form (I_2). Table 4.3 presents the results on the conductivity measurements of undoped and doped BBL near or at room temperature (i.e., from a low of 20.4°C to a high of 24.5°C).

A comment is in order concerning the conductivity of BBL soaked in distilled water. It appears that this value is an order of magnitude larger than that of the virgin, undoped BBL. The value for BBL soaked in distilled water in Table 4.3 and in Table 4.4 were obtained before the measurement procedure was perfected. For these measurements, Drierite drying compound ($CaSO_4$) was used. This desiccant does not absorb as much moisture as the silica gel, and it is hypothesized that the conductivity cell atmosphere for these tests was not at zero percent relative humidity, but at some higher value. This value is probably less than the room relative humidity. This also applies for the BBL soaked in NaI--the data contained in Table 4.4. This table was included because it shows that the duration of soaking times for BBL fiber in distilled water is relatively unimportant. The conductivity for BBL

Table 4.1
Comparison of Conductivities
of Polymer Fibers in Undoped State

<u>Polymer Fibers</u>	<u>Conductivity (S/m)</u>	<u>Temperature (°C)</u>
BBL	1.4×10^{-6}	23.4
PPBT (30-1)	4.9×10^{-10}	23.3
Nylon 6	7.8×10^{-11}	22.2
PP (stretched)	1.3×10^{-11}	49.1
PPBT (17-2)	2.2×10^{-9}	66.9
(17-9)	5.3×10^{-9}	66.2
(48-2)	2.4×10^{-10}	66.7
(48-3)	1.1×10^{-10}	65.9
(48-4)	1.4×10^{-10}	66.5

Table 4.2
Comparison of Conductivities
of Polymer Fibers in Iodine Vapor

<u>Polymer Fiber</u>	<u>Conductivity</u> <u>(S/m)</u>	<u>Temperature</u> <u>(°C)</u>
BBL	1.7×10^{-6}	22.9
PPBT		
(29022-30-1)	3.3×10^{-10}	21.1
(29022-17-8)	4.1×10^{-10}	20.6
Nylon 6	2.6×10^{-9}	21.1
Nylon 6,6	2.8×10^{-10}	20.6
PE	3.9×10^{-11}	22.8
PP	8.7×10^{-12}	19.4

Table 4.3
Comparison of Conductivities
of Doped and Undoped BBL Fibers

<u>Condition of Fiber</u>	<u>Conductivity (S/m)</u>	<u>Temperature (°C)</u>
Undoped	1.4×10^{-6}	23.4
Distilled H ₂ O	1.0×10^{-5}	22.2
Ethyl Alcohol	2.8×10^{-6}	22.8
NaI	1.7×10^{-6}	22.6
I ₂	1.7×10^{-6}	22.9
Dimethyl Sulfoxide	7.0×10^{-6}	20.6
Formaldehyde*	4.8×10^{-7}	20.4
Conc. Phenol*	5.2×10^{-7}	23.1
Phenol/Water Soln*	2.0×10^{-7}	20.4
Acetone	1.9×10^{-6}	20.6
N-Pentane*	8.9×10^{-7}	21.1
Nitrobenzene*	4.1×10^{-6}	23.1
Sulfuric Acid	9.6×10^{-8}	21.6
Indigo/Water Soln*	3.1×10^{-5}	23.3
LiCl	3.3×10^{-6}	21.6
CaCl ₂	2.7×10^{-6}	20.7
Co(NO ₃) ₂	3.2×10^{-6}	24.5

*pre-soaked in ethyl alcohol.

Table 4.4

Comparison of Conductivity of BBL Fibers
Soaked in Distilled H_2O and NaI (1 molar)
Versus Length of Time in Soaking Medium

<u>Distilled H_2O</u>		
<u>Length of Time (hrs)</u>	<u>Conductivity (10^{-5} S/m)</u>	<u>Temperature ($^{\circ}C$)</u>
24	1.10	22.2
48	1.05	22.2
96	0.98	21.1
144	1.10	22.2
240	1.06	22.2

<u>NaI</u>		
<u>Length of Time (hrs)</u>	<u>Conductivity (10^{-5} S/m)</u>	<u>Temperature ($^{\circ}C$)</u>
24	2.70	21.1
48	3.90	24.4
96	1.50	23.7
144	1.70	23.1
240	1.10	20.0

fibers soaked in water from 1 to 10 days appear to reach a maximum, of about three times the initial value, after 2 days and then to approach a level near the initial value. A similar situation seems to exist for BBL soaked in an aqueous NaI solution. In fact, it appears as if soaking the fiber longer actually lowers its conductivity. This may be somewhat deceiving as the BBL/NaI system experiences greater fluctuations in temperature between the various tests than does the BBL/H₂O system.

Table 4.5 compares the various conductivities for doped and undoped PPBT fibers at room temperature. Table 4.6 presents some data for doped and undoped nylon 6 and nylon 6,6 fibers, respectively.

Table 4.7 is a tabulation of the effect that relative humidity has on the various doped and undoped polymers.

Finally, Tables 4.8 and 4.9 display activation energy data for the BBL doped and undoped systems and the other polymers, respectively.

Generally, BBL exhibits the highest conductivity of the fibers tested. It was also affected less by moisture than all the other fibers, except PE. The addition of the various dopants, with the exception of the indigo/water solution, had small effects. Some of the dopants, such as formaldehyde, phenol, n-pentane, and sulfuric acid, lowered the overall conductivity. Other dopants produced minor increases in the conductivity; for example, dimethyl sulfoxide increased the conductivity from 1.4 to 7.0 ($\times 10^{-6}$

Table 4.5
Comparison of Conductivities
of Doped and Undoped PPBT Fibers

<u>Condition of Fiber</u>	<u>Conductivity (S/m)</u>	<u>Temperature (°C)</u>
Undoped (30-1)	4.9×10^{-10}	23.3
I ₂ (30-1)	3.3×10^{-10}	21.1
I ₂ (17-8)	4.1×10^{-10}	20.6
NaI (17-8)	2.8×10^{-10}	21.7
KI (17-8)	1.3×10^{-10}	22.2
LiCl (30-1)	2.1×10^{-10}	20.6
NaCl (17-8)	2.2×10^{-10}	22.2
Ni(NO ₃) ₂ (30-1)	4.1×10^{-10}	23.3
Fe(NO ₃) ₃ (30-1)	7.8×10^{-11}	21.3

Table 4.6
Comparison of Conductivities
of Doped and Undoped Nylon Fibers

<u>Condition of Fiber</u>	<u>Conductivity (S/m)</u>	<u>Temperature (°C)</u>
<u>Nylon</u>		
Undoped	7.8×10^{-11}	22.2
I ₂	2.6×10^{-9}	21.1
<u>Nylon 6,6</u>		
Ethyl Alcohol	6.4×10^{-9}	22.8
I ₂	2.8×10^{-10}	20.6
NaI	2.4×10^{-11}	23.3
CaCl ₂	2.3×10^{-11}	23.9
Fe(NO ₃) ₃	3.0×10^{-11}	21.3

Table 4.7

Comparison of Differential Current ($\Delta I/I_{\min}$)
for Various Doped and Undoped Polymer Fibers

Polymer/Dopant System	Initial Value $\Delta I/I_{\min}$	Maximum Value $\Delta I/I_{\min}$	Temp/RH of Max
BBL (H ₂ O)	0.01 (1)	0.57 (300)	22.2°C (68%)
BBL (ethyl alcohol)	0.00 (1)	6.71 (300)	21.1°C (68%)
BBL (NaI)	0.01 (1)	2.32 (300)	22.8°C (61%)
BBL (I ₂)	0.02 (1)	5.68 (300)	23.3°C (73%)
PPBT-17-8 (NaCl)	2.51 (1)	15.23 (46)	22.2°C (74%)
PPBT-17-8 (KI)	1.21 (1)	12.30 (35)	22.2°C (72%)
PPBT-17-8 (NaI)	47.73 (1)	81.73 (150)	21.7°C (77%)
PPBT-17-8 (I ₂)	6.39 (1)	67.39 (150)	21.1°C (77%)
PPBT-30-1 (LiCl)	0.46 (1)	64.34 (380)	22.2°C (77%)
PPBT-30-1 (I ₂)	13.69 (1)	72.88 (90)	21.7°C (77%)
PP (ethyl alcohol)	----	29.44 (300)	22.8°C (75%)
PP (I ₂)	0.07 (1)	29.33 (240)	22.2°C (75%)
PE (I ₂)	0.30 (1)	3.58 (150)	24.4°C (69%)
Nylon 6,6 (ethyl alcohol)	----	31.69 (330)	24.4°C (60%)
Nylon 6,6 (CaCl ₂)	----	14.52 (500)	22.8°C (66%)
Nylon 6,6 (NaI)	4.03 (1)	54.12 (300)	22.2°C (70%)
Nylon 6,6 (I ₂)	0.92 (1)	62.34 (150)	23.9°C (71%)
Nylon 6	----	15.36 (200)	22.2°C (71%)
Nylon 6 (I ₂)	1.39 (1)	396.00 (300)	23.3°C (79%)

Table 4.8
Activation Energies for
Doped and Undoped BBL Fibers

<u>Condition</u>	<u>Activation Energy (eV)</u>	<u>Temperature Range (°C)</u>
Undoped	0.357	24.7 - 70.9
Distilled H ₂ O	0.410	44.0 - 70.7
Ethyl Alcohol	0.640	43.1 - 70.0
NaI	0.390	22.6 - 71.0
I ₂	0.364	22.9 - 70.1
Dimethyl Sulfoxide	0.490	20.6 - 67.7
Dimethyl Sulfoxide*	0.420	22.6 - 70.8
Formaldehyde*	0.530 0.780	24.4 - 54.5 54.5 - 60.2
Conc. Phenol*	0.640	23.1 - 70.7
Phenol/Water Soln*	0.490 0.920	20.4 - 64.1 64.1 - 96.5
Acetone	0.430 0.630	20.6 - 60.3 60.3 - 95.8
N-Pentane*	0.410 0.590	31.3 - 54.5 54.5 - 70.5
Nitrobenzene	0.530 0.810	23.1 - 49.8 49.8 - 66.2
Sulfuric Acid	0.480 0.770	21.6 - 64.5 64.5 - 105.5
Indigo/Water Soln*	0.580 0.900	23.3 - 59.6 59.6 - 94.4
LiCl	0.410	21.6 - 90.8
CaCl ₂	0.420	20.7 - 99.6
Co(NO ₃) ₂	0.390	24.5 - 96.0

*pre-soaked in ethyl alcohol

Table 4.9
Activation Energies for Other Polymer
Fibers: Doped and Undoped

<u>Polymer and Condition</u>	<u>Activation Energy (eV)</u>	<u>Temperature Range (°C)</u>
<u>PPBT</u>		
Undoped (17-9) (run #1)	0.309	40.9 - 99.1
Undoped (17-9) (run #2)	0.760 0.595	40.8 - 66.2 66.2 - 94.6
Undoped (48-4)	0.176	30.7 - 59.2
$\text{Fe}(\text{NO}_3)_3$ (30-1)	0.212 0.644	21.2 - 52.8 52.8 - 105.9
<u>Nylon 6</u>		
Dimethyl Sulfoxide	0.760 1.760	36.2 - 65.5 65.5 - 110.6
<u>Nylon 6,6</u>		
$\text{Fe}(\text{NO}_3)_3$	1.470	21.3 - 53.9
<u>PP</u>		
Undoped (stretched)	0.420	38.3 - 86.6

S/m). NaI and I₂ had small effects on the observed conductivity, and indeed, on the activation energy.

The effect of moisture on nylons was expected, as they do sorb significant amounts of water. However, the effect of water on PPBT was unexpected as it has been hypothesized that PPBT is not water-sensitive. However, the change in conductivity in a moist atmosphere approaches that exhibited by nylon 6,6. It may be hypothesized that this increase in current arises from ion liberation through the interaction with water sorbed into the polymer.

The processing history also seems to influence the conductivity in the PPBT fibers, as the (29022-17) type fibers exhibited an order of magnitude (i.e., 10^{-9} S/m as opposed to 10^{-10} S/m) increase in conductivity than do the (29022-48) type PPBT fibers.

Values of conductivity for nylon 6 and nylon 6,6 as found in the literature were corroborated in this research. For example, at room temperature, a conductivity of approximately 8×10^{-13} S/cm was measured for an untreated nylon 6 fiber. This compares to a value of 10^{-12} S/cm found in the literature. The agreement in conductivity for PE and PP was not as good. Measured values for stretched PP approach 10^{-13} S/cm. This compares to values of 10^{-16} S/cm for volume conductivity found in the literature. However, the surface conductivity for PP is 10^{-13} S, which corresponds well to the measured value. This leads to the conclusion that in the very good insulating polymers, of

which PP is a member, surface conduction plays an important role. In cases where a guard electrode is impractical, surface conduction must then play an important role.

This hypothesis is supported by the work on BBL, which determined that the surface was the major current-carrying region of the fiber. This is probably the case for all fibers. Further research needs to be done on the role of surfaces in the conduction process in polymer fibers.

CHAPTER V

CONCLUSIONS

A good deal of useful information on conduction in polymer fibers was obtained in this research, especially values of activation energies, E^* , for conduction of the various BBL/dopant combinations. A model was also developed to investigate the role that a surface layer of thickness δ had on a polymer fiber's conductivity. The effect of moisture on conductivity in these polymers was also clarified.

The role of dopants on a polymer's electrical properties is complex. Doping of the polymer fibers promoted substantial changes in E^* while producing only minor variations in the observed conductivity of the polymer. This tends to support Barker's local structure hypothesis, whereby changes in the polymer's local structure are produced by the addition of impurity ions.

Water in the form of moisture in the atmosphere, as measured by the relative humidity, produced substantial changes in the differential current for nylon and PPBT. PP exhibited a moderate increase in differential current, while BBL and PE produced only small increases. It is concluded that water aids the ionic conduction process, especially for the more hydrophilic polymers and this effect can be further enhanced when additional impurity or dopant ions are present. The effect of moisture on the conductivity of BBL

is minor, leading one to the conclusion that BBL does not have a great affinity for water uptake.

The surface region of a polymer fiber, as hypothesized in the model, does indeed seem to pass the majority of the current in the conduction process. In making measurements of current versus length for BBL fiber slopes near (-1) were obtained, adding further evidence in support of this hypothesis.

It was concluded that the conduction mechanism in BBL is primarily electronic, while that for PPBT and nylon is a combination of electronic and ionic.

Care must be taken when doping polymer fibers and further quantitative work is needed on the specific sorption characteristics, e.g., shape of sorption curve and speed of moisture uptake, of fibers in general. This will enable a more definitive relationship between the specific features of electrical conduction and water sorption to be made.

There is also a need to perform high field measurements on the fibers to complete the research on ionic contributions to the overall conductivity.

Finally, care is needed in developing the instrumentation for polymer research. Proper shielding and grounding techniques are essential in making accurate and reproducible measurements.

REFERENCES

1. Greene, R. L. and G. B. Street. Science, 226, 651 (Nov. 1984).
2. Physics Today, 32(9), 19 (Sept. 1979).
3. Street, G. B. and T. C. Clark. IBM J. Res. Develop., 25, 51 (1981).
4. DeYoung, H. G. High Technology, 3(1), 65 (Jan. 1983).
5. Chemical and Engineering News, 61(21), 27 (May 23, 1983).
6. Chemical and Engineering News, 60(16), 29 (April 19, 1982).
7. Chemical and Engineering News, 58(13), 36 (March 31, 1980).
8. Duke, C. B. and H. W. Gibson. "Polymers, Conductive" in Kirk-Othmer: Encyclopedia of Chemical Technology, V18, 3rd ed., John Wiley, New York, 1982.
9. Fox, L. RCA Review, 39, 116 (1978).
10. Davenport, D. E. Org. Coat. Plast. Chem., 43, 740 (1980).
11. Duke, C. B. and L. B. Schein. Physics Today, 33(2), 42 (Feb. 1980).
12. Conductive Polymers, (ed. R. B. Seymour), Plenum Press, New York, 1981.
13. Baughman, R. H., R. R. Chance, R. L. Elsenbaumer, D. M. Ivory, G. G. Miller, A. F. Preziosi, and L. W. Shacklette. Org. Coat. Plast. Chem., 43, 762 (1980).
14. Street, G. B. and T. C. Clark. Adv. Chem. Ser., 186, 177, (1980).
15. Shirakawa, H. and S. Skeda. Polym. J., 2, 231 (1971).
16. Chiang, C. K., C. R. Fincher, Y. W. Park, A. J. Heeger, H. Shirakawa, E. J. Lewis, S. J. Gau, and A. G. MacDiarmid. Phys. Rev. Lett., 39, 1089 (1977).

17. Münstedt, H. in Electronic Properties of Polymers and Related Compounds. (ed. H. Kuzmany, M. Mehring and S. Roth), Part I, p. 8, Springer-Verlag, 1982.
18. Chen, D. Y. Ph.D. Dissertation, University of Virginia, 1982.
19. American Society for Testing Materials (ASTM), ANSI/ASTM D 257-76, p. 114.
20. Barker, R. E. Pure Appl. Chem., 46, 157 (1976).
21. Vogel, F. L. J. Mater. Sci., 12, 982 (1977).
22. Kronik, P. L., H. Kaye, E. Chapman, S. B. Maintha, and M. M. Labes. J. Chem. Phys., 36, 2235 (1962).
23. MacDiarmid, A. G. and A. J. Heeger. Synthetic Metals, 1, 101 (1980).
24. Shirakawa, H., E. J. Louis, A. G. MacDiarmid, C. K. Chaing, and A. J. Heeger. J. C. S. Chem. Commun., No. 16, 578 (17 Aug. 1977).
25. Seanor, D. A. in Electrical Properties of Polymers (ed. D. A. Seanor), Chapter 1, p. 1, Academic Press, New York, 1982.
26. Ziman, J. M. Principles of the Theory of Solids, 2nd ed., Cambridge University Press, Cambridge, 1972.
27. Adler, D. Scientific American, 236(5), 36 (May 1977).
28. Kommandeur, J. in Physics and Chemistry of the Organic Solid State, Vol. II (ed. D. Fox, M. M. Labes and A. Weissberger), Chapter 1, p. 3, John Wiley, New York, 1965.
29. Gutman, F. and L. E. Lyons. Organic Semiconductors, Part A, John Wiley, New York, 1967.
30. Blythe, A. R. Electrical Properties of Polymers, Cambridge University Press, Cambridge, 1979.
31. Cotts, D. B. and Z. Reyes. SRI International Final Report No. RADC-TR-85-129 (July 1985).
32. Frenkel, J. Physik. Z. Sowjetunion, 9, 158 (1936).
33. Frenkel, J. Phys. Rev., 37, 17 (1931).
34. Frenkel, J. Phys. Rev., 37, 1276 (1931).

35. Lyons, L. E. J. Chem. Soc. (London), Part 4, 5001 (1957).
36. Partridge, R. H. J. Chem. Phys., 52, 2485 (1970).
37. Philpott, M. R. J. Chem. Phys., 63, 485 (1975).
38. Vlanski, J. Poly. Plast. Tech. Eng., 17, 139 (1982).
39. Mort, J. and G. Pfister. Poly. Plast. Tech. Eng., 12, 89 (1979).
40. Pohl, H. J. Polym. Sci. Sym. Ed., 17, 13 (1967).
41. Scott, A. C., F. Y. F. Chu and D. W. McLaughlin. Proc. IEEE, 61, 1443 (1973).
42. Su, W. P., J. R. Schrieffer and A. J. Heeger. Phys. Rev. Lett., 42, 1698 (1979).
43. Tomkiewicz, Y., T. D. Schultz, H. B. Broom, T. C. Clark, and G. B. Street. Phys. Rev. Lett., 43, 1532 (1979).
44. Fox, K. and J. E. Turner. J. Chem. Phys., 45, 1142 (1966).
45. Flory, P. J. Principles of Polymer Chemistry, Cornell University Press, Ithaca, 1953.
46. Maxwell, J. C. Electricity and Magnetism, Vol. I, University of Oxford Press (Clarendon), Oxford, 1872.
47. Wagner, K. W. Archiv. für Electrotechnik, 2, 371 (1914).
48. Sillars, R. W. J. Inst. Elect. Eng., 80, 378 (1937).
49. Daniel, V. V. Dielectric Relaxation, Academic Press, London and New York, 1967.
50. McCrum, N. G., B. E. Read and A. Williams. Anelastic and Dielectric Effects in Polymeric Solids, John Wiley, New York, 1967.
51. Schatzki, T. F. J. Polym. Sci., 57, 496 (1962).
52. Mott, N. F. Adv. Phys., 16, 49 (1967).
53. Mott, N. F. Contemp. Phys., 10, 125 (1969).
54. Mott, N. F. and E. A. Davis. Electronic Processes in Non-Crystalline Materials, Oxford University Press (Clarendon), London and New York, 1971.

55. Duke, C. B. and T. J. Fabish. Phys. Rev. Lett., 37, 1075 (1976).
56. Duke, C. B. Surf. Sci., 70, 674 (1978).
57. Bartnikas, R. in Engineering Dielectrics, Vol. IIA (ed. R. Bartnikas and R. M. Eichhorn). Chapter 1, p. 1, ASTM, Baltimore, 1983.
58. Seanor, D. A. J. Polym. Sci. A-2, 6, 463 (1968).
59. Hoover, M. F. and H. E. Carr. Tappi, 51, 552 (1968).
60. Crowley, J. L., R. A. Wallace and R. H. Bube. J. Polym. Sci. Polym. Phys. Ed., 14, 1769 (1976).
61. Sodolski, H., phys. stat. sol.(a), 89, 647 (1985).
62. Sodolski, H. Proc. 5th Inter. Symp. Electrics, (Heidelberg, 1985), p. 238.
63. Wallace, R. A. J. Appl. Phys., 42, 3121 (1971).
64. Wallace, R. A. J. Appl. Polym. Sci., 18, 2855 (1974).
65. Barker, R. E. and C. R. Thomas. J. Appl. Phys., 35, 87 (1964).
66. Barker, R. E. and C. R. Thomas. J. Appl. Phys., 35, 3203 (1964).
67. Thomas, C. R. and R. E. Barker. J. Appl. Polym. Sci., 7, 1933 (1963).
68. Barker, R. E. J. Appl. Polym. Sci., 9, 1197 (1965).
69. Rosenberg, B. J. Chem. Phys., 36, 816 (1962).
70. Rancourt, J. D., J. L. Swartzentruber, and L. T. Taylor. American Laboratory, 18(3), 75 (March 1986).
71. Barker, R. E. and A. H. Sharbaugh. J. Polym. Sci., C10, 139 (1965).
72. Sharbaugh, A. H. and R. E. Barker in Phénomènes de Conduction dans les Liquids Isolants. Edition du Centre National de la Recherche Scientifique, Paris, No. 179, 349 (1970).
73. Link, G. L. 1980 Ann. Rept. Conf. Electr. Insul. Dielectr. Phenom., Natl. Aca. Sci., Washington, D.C., p. 183.

74. Mott, N. F. and R. W. Gurney. Electronic Processes in Ionic Crystals, Oxford University Press, London, 1948.
75. Wintle, H. J. in Engineering Dielectrics, Vol. IIA (ed. R. Bartnikas and R. M. Eichhorn), Chapter 3, p. 239, ASTM, Baltimore, 1983.
76. Kosaki, M., K. Sugiyama, and M. Ieda. J. Appl. Phys., 42, 3388 (1971).
77. Miyamoto, T. and K. Shibayama. Kobunshi Kagaku, 29, 301 (1972).
78. Miyamoto, T. and K. Shibayama. J. Appl. Phys., 44, 5372 (1973).
79. Miyamoto, T. and K. Shibayama. 1973 Ann. Rept. Conf. Electr. Insul. Dielectr. Phenom., Natl. Aca. Sci., Washington, D.C., p. 431.
80. Cohen, M. H. and T. Turnbull. J. Chem. Phys., 31, 1164 (1959).
81. Watanabe, M., K. Sanui, N. Ogata, T. Kobayashi and Z. Ohtaki. J. Appl. Phys., 57, 123 (1985).
82. Watanabe, M., M. Kanba, K. Nagaoka, and I. Shinohara. J. Polym. Sci. Polym. Phys. Ed., 21, 939 (1983).
83. Watanabe, M., M. Rikukawa, K. Sanui, and N. Ogata. J. Appl. Phys., 58, 736 (1985).
84. Watanabe, M., M. Rikukawa, K. Sanui, and N. Ogata. Macromolecules, 19, 188 (1986).
85. Williams, M. L., R. F. Landel and J. D. Ferry. J. Amer. Chem. Soc., 77, 3701 (1955).
86. Bässler, H. Phil. Mag. B, 50, 347 (1984).
87. Bässler, H. phys. stat. sol (b), 107, 9 (1981).
88. Lange, J. and H. Bässler. phys. stat. sol (b), 114, 561 (1982).
89. Zbonski, Z. J. Chem. Phys., 75, 297 (1983).
90. Scher, H. and E. W. Montroll. Phys. Rev. B, 12, 2455 (1975).
91. O'Dwyer, J. J. The Theory of Electrical Conduction and Breakdown in Solid Dielectrics, Oxford University Press, London, 1973.

92. Amos, A. T. and R. J. Crispin. J. Chem. Phys., 63, 1890 (1975).
93. Lampert, M. A. and P. Mark. Current Injection in Solids, Academic Press, New York, 1970.
94. Kittel, C. Introduction to Solid State Physics, 5th ed., John Wiley, New York, 1976.
95. Spear, W. E. Adv. Phys., 23, 523 (1974).
96. Paul, W. Thin Solid Films, 33, 381 (1976).
97. Ambegaokar, V., B. I. Halperin and J. S. Langer. Phys. Rev. B, 4, 2612 (1971).
98. Many, A. and G. Rakavy. Phys. Rev., 126, 1980 (1962).
99. Lindmayer, J., J. Reynolds and C. Wrigley. J. Appl. Phys., 34, 809 (1963).
100. Lampert, M. A. and F. Edelman. J. Appl. Phys., 35, 2971 (1964).
101. Mehl, W., J. M. Hale and F. Lohmann. Electrochem. Soc., 113, 1166 (1966).
102. Mark, P. and W. Helfrich. J. Appl. Phys., 33, 205 (1962).
103. Rosental, A. and A. Sapor. J. Appl. Phys., 45, 2787 (1974).
104. Mort, J. and P. Nielsen. Phys. Rev. B, 5, 3336 (1972).
105. Murgatroyd, P. N. phys. stat. sol. (a), 8, 259 (1971).
106. Barbe, D. F. J. Phys. D., 4, 1812 (1971).
107. Poole, H. H. Phil. Mag., 34, 195 (1917).
108. Adamec, V. and J. H. Calderwood. J. Phys. D., 8, 551 (1975).
109. Pai, D. M. J. Appl. Phys., 46, 5122 (1975).
110. Teubner, W. and B. Fromm. phys. stat. sol. (a), 41, K47 (1977).
111. Reehal, H. S. phys. stat. sol. (b), 80, K63 (1977).

112. Nottingham, W. B. in Handbuch der Physik, Vol. 21 (ed. S. Flugge), p. 1, Springer-Verlag, Berlin, 1956.
113. Murgatroyd, P. N. phys. stat. sol. (a), 6, 217 (1971).
114. Good, R. H. and E. W. Muller in Handbuch der Physik, Vol. 21 (ed. S. Flügge), p. 176, Springer-Verlag, Berlin, 1956.
115. Pulfrey, D. L., A. H. M. Shousha and L. Young. J. Appl. Phys., 41, 2838 (1970).
116. Hewlett-Packard 16008A Resistivity Cell Operation Manual, January 1980.
117. Blythe, A. R. in "Measurement Techniques for Polymeric Solids," (ed. R. P. Brown and B. E. Read), Elsevier Applied Science Publishers, London, 1984.
118. Kaneko, F. and T. Hino. Elect. Engr. Jpn, 101, 35 (1981).
119. Wolfe, J. E., B. H. Loo and F. E. Arnold. Polym. Prepr., Am. Chem. Soc., Div. Polym Chem., 19, 1 (1978).
120. Berry, G. C. in Rigid Chain Polymers: Synthesis and Properties (ed. G. C. Berry and C. E. Scroog), J. Polym. Sci. Polym. Symp. Ed. No. 65, J. Wiley, New York, 1978, p. 143.
121. Modern Plastics Encyclopedia, McGraw-Hill, New York, 1985.
122. Wunderlich, Bernhard. Macromolecular Physics, Vol. 1, Academic Press, London and New York, 1973.
123. Watanabe, A., M. Tanaka and J. Tanaka. Chemistry Letters, 575 (1980).
124. Pron, A., I. Lulshewicz, D. Billaud and J. Przyluski. J. Chem. Soc., Chem. Commun., 554, 783 (1981).
125. Rubner, M., J. Georges, Jr., and E. Sichel. Polym. Prepr., V, Am. Chem. Soc., Div. Polym. Chem., 23, 96 (1982).
126. "Low Level Measurements," Keithley Instruments, Inc., Cleveland, 1984.
127. Keithley 642 Electrometer Operations Manual, March 1980.

128. Barker, R. E. "Physical Techniques for the Study of Sorption, Diffusion, Electrical Properties and Interfacial Effects in Ordered Polymers," U.Va. Proposal No. MS-AFOSR-2633-83 (May 1983), p. 14.
129. Wintle, H. J. J. Non-Cryst. Solids, 15, 471 (1974).
130. Wintle, H. J. Solid State Elect., 18, 1039 (1975).
131. Das Gupta, D. K. and K. Joyner. J. Phys. D., 9, 829 (1976).
132. Adamec, V. and J.H. Calderwood. J. Phys. D., 11, 781 (1978).
133. Vanderschuren, J. and A. Linkins. J. Appl. Phys., 49, 4195 (1978).
134. Walden, R. H. J. Appl. Phys., 43, 1178 (1972).
135. Lindmayer, J. J. Appl. Phys., 36, 196 (1965).
136. Adamec, V. Koll. Z. Z. Polymere, 237, 219 (1970).
137. Taylor, D. M. and T. J. Lewis. J Phys. D., 4, 1346 (1971).
138. Wintle, H. J. J. Appl. Phys., 42, 4724 (1971).
139. Cole, K. S. and R. H. Cole. J. Chem. Phys., 10, 98 (1942).
140. van Belk, L. K. H. in Progres in Dielectrics, Vol. 7 (ed. J. B. Birks), CRC Press, Cleveland, 1967.
141. Wintle, H. J. IEEE Trans. Electr. Insul., EI-12, 424 (1977).
142. Wintle, H. J. J. Appl. Phys., 44, 2514 (1973).
143. Pike, G. E. Phys. Rev. B., 6, 1572 (1972).
144. Brenig, W. in Amorphous and Liquid Semiconductors (ed. J. Stuke and W. Brenigh), p. 31, Taylor and Francis Press, London, 1974.
145. Kumar, N. and J. Heinrichs. J. Phys. C., 9, 2331 (1976).
146. Hill, R. M. phys. stat. sol. (a), 39, 615 (1977).
147. Johnscher, A. K. Nature, 267, 673 (1977).

148. Dissado, L. A. and R. M. Hill. *Nature*, 279, 685 (1979).
149. Harmon, B. V. *Proc. IEEE (London)*, 99, 151 (1952).
150. Baird, M. E. *Rev. Mod. Phys.*, 40, 219 (1968).
151. Das Gupta, D. K. and K. Joyner. *J. Phys. D.*, 9, 2041 (1976).
152. Baird, M. E., G. T. Goldworthy, and C. J. Creasy. *Polymer*, 12, 159 (1971).
153. Evans, M. G. and J. Gergeley. *Biochem. Biophys. Acta.*, 3, 188 (1949).
154. Bhaumik, D. and J. E. Mark. *Polym. Preprints*, 23, 105 (1982).
155. Kim, Oh-Kil. *J. Polym. Sci. Polym. Letters Ed.*, 20, 663 (1982).
156. Hill, A. V. *Proc. Roy. Soc. B.*, 104, 39 (1928).
157. Barrie, J. A. in Diffusion in Polymers (ed. J. Crank and G. S. Park), Academic Press, London and New York, 1968, p. 274.
158. Burford, R. P. and E. Harrauer. *Polymer*, 24, 1001 (1983).
159. Kallweit, J. H. *J. Polym. Sci.*, A1, 337 (1966).
160. Foss, R. A. and W. Dannhauser. *J. Appl. Polym. Sci.*, 7, 1015 (1963).
161. Shockley, W. and W. J. Read. *Phys. Rev.*, 87, 835 (1952).
162. Schottky, W. *Z. Phys.*, 15, 872 (1914).
163. Frenkel, J. *Phys. Rev.*, 54, 647 (1938).
164. Frenkel, J. Kinetic Theory of Liquids, Dover, New York, 1955.
165. Mead, C. A. *Phys. Rev.*, 128, 2088 (1962).
166. Johnscher, A. K. *Thin Solid Films*, 1, 213 (1967).
167. Hartke, J. L. *J. Appl. Phys.*, 39, 4871 (1968).
168. Adamec, V. and J. H. Calderwood. *J. Phys. D.*, 11, 781 (1978).

169. Omar, M. A. Elementary Solid State Physics, Addison-Wesley, Reading, 1975.

APPENDIX A

WALDEN'S RULE AND ITS FAILURE (PARTIAL) FOR POLYMERS

In ionic conduction in polymers, a simple theoretical analysis is not always applicable. Walden's rule relating charge mobility to viscosity is not followed. This was pointed out by Kallweit¹⁵⁹ explicitly and also by others.^{20,82,160}

Walden's rule relates the viscous drag on an ion to the accelerating force of an applied electric field. At equilibrium, $F_a = F_v$ where the viscous force acting on the ion is given by Stokes' law

$$F_v = 6\pi\eta r_s v \quad (A.1)$$

In this equation, η is the viscosity, v is the mean drift velocity in the direction of the electric field and r_s is the effective radius of an ion of spherical shape. The electric force can be written as

$$F_e = z e E \quad (A.2)$$

where z is the valence of the ion in solution. Assuming a one-dimensional case, Equations (A.1) and (A.2) can be equated to give

$$zeE = 6\pi\eta r_s v \quad (A.3)$$

The mean drift velocity v can be replaced by μE and the conductivity included by making a substitution of $zen\mu$. Thus,

$$\sigma\eta = \frac{z^2 e^2 \eta}{6\pi r_s} = \text{constant (T)} \quad (\text{A.4})$$

This means that the product $(\sigma\eta)$ for a particular electrolyte at a given temperature should be a constant.

However, Kallweit did not find that Eq. (A.4) was not correct for polymers and it was slightly modified from experimental data in the following manner

$$\log \eta = m \log(\sigma\eta) + \text{constant} \quad (\text{A.5})$$

or

$$\sigma\eta^{m-1/m} = \text{constant} \quad (\text{A.6})$$

Kallweit concluded that Stokes' law was too crude an approximation in the case of polymers. Also, the viscosity in Stokes' law is not identical to the viscosity η obtained by retardation experiments, i.e., a macroviscosity. In the case of polymers, it is necessary to use an effective local viscosity, η' , i.e., a microviscosity because the local environment of the ion in the polymer affects its mobility in the polymer. Kallweit concluded that only in fluids is $\eta \approx \eta'$. This changes the equations slightly, whereby

$$F_v = 6\pi r_s \eta' v \quad (\text{A.1a})$$

and thus

$$\sigma\eta' = \text{constant}(T) \quad (\text{A.4b})$$

Thus, a relation between η and η' can be made,

$$|\eta^{m-1/m}| = |\eta'|. \quad (\text{A.7})$$

and when $m \approx 1$, η' is low.

Equation (A.3) can be modified in a different way, using the Einstein relation

$$zeD = \mu k_B T. \quad (\text{A.8})$$

Equation (A.3) can then be written as

$$zeE = 6\pi\eta r_s v. \quad (\text{A.3b})$$

Upon replacing v by μE , or $zeDE/k_B T$,

$$k_B T = 6\pi\eta r_s D \quad (\text{A.9})$$

or

$$D = \frac{k_B T}{6\pi\eta r_s} \quad (\text{A.10})$$

which is the Stokes-Einstein relation.

The substitution of $\sigma = zen\mu$ can also be made to Eq. (A.8), so that

$$zeD = \frac{\sigma}{zen} k_B T \quad (\text{A.11})$$

or

$$\frac{\sigma}{D} = \frac{nz^2e^2}{k_B T}. \quad (\text{A.12})$$

These equations are useful in obtaining estimates of the mobilities in the polymers studied by making conductivity measurements.

APPENDIX B

THE FERMI LEVEL

The thermal equilibrium of a system can be explained by the Fermi Level, E_F , the energy at which the electron states are half filled on the average. It also be interpreted as the chemical potential of the conduction electrons. The occupancy of a state is given by

$$f(E) = \left\{ \exp \left[\frac{E - E_F}{k_B T} \right] + 1 \right\}^{-1}. \quad (B.1)$$

For $(E - E_F) \gg k_B T$, this can be approximated by the Boltzmann distribution

$$\exp \left[- \frac{(E - E_F)}{k_B T} \right]$$

and by unit for $E \ll E_F$. A material in thermodynamic equilibrium must be macroscopically neutral, so the number of electrons per unit volume are equal to both the number of positive nuclear charges and the number of occupied states. The neutrality condition is written in terms of the free electron concentration, n , the free hole concentration, p , and the corresponding trapped concentrations, n_t and p_t , of electrons and holes. Referring to Figure B.1, n and p are obtained by integrating over the density of states in the conduction and valence bands respectively

$$n = \int_{E_c}^{\infty} f(E) N(E) dE \quad (B.2)$$

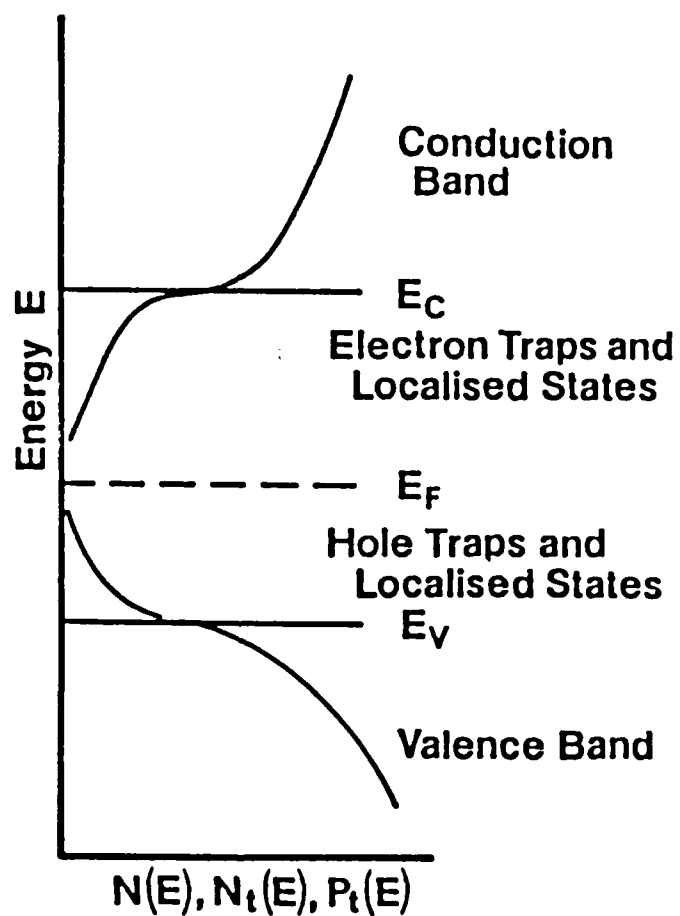


Figure B.1. Densities of States for Free Electrons and Free Holes, $N(E)$, and Densities of Electron Traps, $N_t(E)$, and Hole Traps, $P_t(E)$, as a Function of Energy.⁷⁵

and

$$p = \int_{-\infty}^{E_v} [1 - f(E)] N(E) dE \quad (B.3)$$

Electron traps are centers that have an available level within the band gap. They are uncharged at absolute zero and have a density of states $N_t(E)$. The hole traps have a density of states $P_t(E)$. Thus

$$n_t = \int_{E_v}^{E_c} f(E) N_t(E) dE \quad (B.4)$$

and

$$p_t = \int_{E_v}^{E_c} [1 - f(E)] P_t(E) dE \quad (B.5)$$

and the neutrality equation becomes

$$n + n_t = p + p_t. \quad (B.6)$$

The valence and conduction bands can be replaced by effective densities of states N_v and N_c located at their respective band edges (as long as the Boltzmann approximation is used). This gives

$$n = N_c \exp\left[-\frac{(E_c - E_F)}{k_B T}\right], \text{ for } (E_c - E_F) > k_B T \quad (B.7)$$

and

$$p = N_v \exp\left[-\frac{(E_F - E_v)}{k_B T}\right], \text{ for } (E_F - E_v) > k_B T \quad (B.8)$$

where

$$N_c = \int_{E_c}^{\infty} N(E) \exp\left[-\frac{(E - E_c)}{k_B T}\right] dE \quad (B.9)$$

and

$$N_v = \int_{-\infty}^{E_v} N(E) \exp\left[-\frac{(E_v - E)}{k_B T}\right] dE. \quad (\text{B.10})$$

It is likely that there is a sufficiently large trap density in polymeric solids so that E_F always lies inside the forbidden gap, so the conditions of Eqs. (B.7) and (B.8) are always satisfied.

APPENDIX C

DERIVATION OF CHILD'S LAW

Child's law, already given in Eq. (2.72), can be derived from basic concepts in the following manner. Assume that the number of charge carriers and the local electric field are functions of location in the sample and in the one-dimensional case are represented by the terms $n(x)$ and $E(x)$, where x is the distance from a reference electrode.

The steady-state current density J is not a function of position, i.e.,

$$J = q n(x) \mu E(x) \neq f(x) \quad (C.1)$$

and thus the charge flux is constant across the sample.

The relationship between the electric field gradients and the number of charge carriers is defined by Poisson's equation:

$$\frac{dE(x)}{dx} = \frac{q n(x)}{\epsilon} \quad (C.3)$$

where $\epsilon = \epsilon' \epsilon_0$.

The integral of the local electric field across the sample is the applied potential, i.e.,

$$\int_0^x E(x) dx = V. \quad (C.3)$$

These three equations, in combination with any set of boundary conditions, define the current-voltage relationships.

In the simplest case, $n(x)$ is independent of position and constant across the sample. In this case, $E(x)$ is not a function of position, $dE/dx = 0$, and

$$J = q n \mu E \quad (C.4)$$

For an ohmic electrode which has no potential barrier to injection and which, in theory, is capable of providing an infinite supply of charge carriers, the electric field adjacent to the electrode is zero. Thus, the boundary conditions are:

$$n(0) = \infty \quad \text{and} \quad E(0) = 0$$

Substituting Eq. (C.2) into Eq. (C.1),

$$J = \epsilon \mu E(x) \frac{dE(x)}{dx} \quad (C.5)$$

which upon integration, yields

$$J_x = \frac{\epsilon \mu}{2} E(x)^2 \quad (C.6)$$

and solving for $E(x)$ and substituting into Eq. (C.3) gives

$$V = \int_0^b \left(\frac{2J}{\epsilon \mu} \right)^{1/2} x^{1/2} dx \quad (C.7)$$

Integrating and rearranging terms yields

$$J = \frac{9\epsilon \mu V^2}{8b^3} \quad (C.8)$$

which is Child's law for a trap-free insulator. As mentioned previously, deviations from Ohm's law arise because the solid is unable to transport all the injected

charge. A space charge subsequently builds up adjacent to the electrode, changing the field distribution. Thus, $n(x)$ and $E(x)$ become

$$n(x) = \frac{3\epsilon V}{4qb^{3/2}x^{1/2}} \quad (C.9)$$

$$E(x) = \frac{3V_x^{1/2}}{2b^{3/2}} \quad (C.10)$$

For low applied potentials, conduction is ohmic. At a higher potential, the solid is unable to transport all the charge and the current becomes non-linear in voltage. At a potential V_x , the mobility and the voltage can be calculated from the cross-over current J_x , i.e.,

$$J_x = \frac{qn\mu V_x}{b} = \frac{9\epsilon\mu V_x^2}{8b^3} \quad (C.11)$$

$$V_x = \frac{8qb^2n}{9\epsilon} \quad (C.12)$$

$$n = \frac{9V_x\epsilon}{8qb^2} \quad (C.13)$$

$$\mu = \frac{8J_x b^3}{9V_x^2\epsilon} \quad (C.14)$$

Alternatively, μ can be obtained from the slope of the $J - V_2$ curve, i.e., $dJ/d(V^2)$:

$$\mu = \frac{8b^3}{9\epsilon} \frac{dJ}{d(V^2)} \quad (C.15)$$

APPENDIX D

TRAPPING AND DETRAPPING:
CHARACTERISTICS OF RATE EQUATIONS

Charge carriers in insulators can be trapped at impurity atoms, physical defects, etc. The immobilization of a carrier causes a reduction in the conductivity. The capture rate for free electrons by a single trapping level can be written in general terms with a time constant, τ

$$\left(\frac{dn}{dt} \right)_{\text{capture}} = - \frac{n}{\tau} . \quad (\text{D.1})$$

This lifetime toward trapping can be regarded as a constant for a given material. Thus, by analogy to a simple kinetic theory gas, the mean free time, τ , can be expressed as

$$\tau = \frac{1}{N_t \Lambda v} \quad (\text{D.2})$$

where v is the mean velocity of the free electrons, N_t is the trap concentration, and Λ is the capture cross-section. For insulators, some typical values are $v \approx 10^7$ cm/s, N_t can be as high as 10^{19} cm $^{-3}$ (corresponding to one trapping center per 1000 repeat units), and a range of values for Λ , 10^{-12} - 10^{-15} cm 2 .

Equation (D.1) should be written in a reaction kinetics formulation, with a rate constant A_1 ,

$$\left(\frac{dn}{dt} \right)_{\text{capture}} = A_1 n (N_t - n_t) \quad (\text{D.3})$$

where n_t is the concentration of filled traps. This is illustrated below. Equations (D.1) and (D.2) apply to the limiting case of $n_t \ll N_t$, but more generally $A_1 = \Lambda v$. Detrapping takes place with a rate constant of A_2 , at a rate given by

$$\left(\frac{dn_t}{dt} \right)_{\text{excitation}} = -A_2 n_t (N_c - n) \quad (\text{D.4})$$

Inserting the thermal equilibrium conditions of Fermi statistics and detailed balancing, it follows that¹⁶¹

$$A_2 = A_1 \exp \left[- \frac{(E_c - E_t)}{k_B T} \right] \quad (\text{D.5})$$

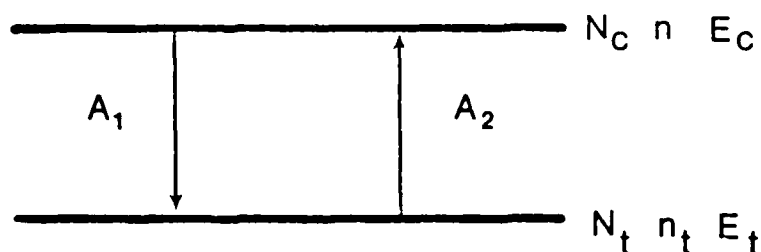


Figure D.1. Capture (A_1 Process) and Excitation (A_2 Process) of an Electron at a Trap Site.

The trap depth ($E_c - E_t$) is simply the binding energy of the charge in the center. In theory, this energy can be calculated if the Schrödinger equation can be solved for the particular combination of impurity and matrix being considered. The energy is normally determined by experimental procedures.

APPENDIX E

CURRENT-VOLTAGE DEPENDENCE

In Section 2.3, a discussion of current-voltage dependence was given for a certain set of conditions. This appendix is presented as a means of gathering other equations that model this type of behavior. Most models presented are based on the ideas of Schottky¹⁶² and Frenkel¹⁶³. The general problems with this approach and subsequent equations are: (a) the derived relationships do not fit satisfactorily over the whole range of the measured current-voltage dependence and can only be applied asymptotically to the high field region, and (b) in the case of those relationships which give the best fit, the resulting value for permittivity cannot be considered reasonable.

The following list of the relative conductivity (σ/σ_0) over a range of field strengths is presented without any details. A reference to the literature is given for each model and details as to derivation and range of applicability will be found in the original article.

$$(1) \quad \frac{\sigma}{\sigma_0} = \frac{2k_b T}{eE\delta} \sinh\left(\frac{eE\delta}{2k_b T}\right) \quad (\text{Frenkel 1955-F}\delta)^{164}$$

$$(2) \quad \frac{\sigma}{\sigma_0} = \frac{K}{E} \exp\left(\frac{\beta_s E^{1/2}}{k_b T}\right), \quad \beta_s = \left(\frac{e^3}{4\pi\epsilon_0\epsilon}\right)^{1/2} \quad (\text{Schottky 1914-S})^{162}$$

$$(3) \quad \frac{\sigma}{\sigma_0} = \exp\left(\frac{\beta_F E^{1/2}}{2k_B T}\right) \cdot \beta_F = \left(\frac{e^3}{\pi \epsilon_0 \epsilon}\right)^{1/2} \quad (\text{Frenkel 1938-F})^{163}$$

$$(4) \quad \frac{\sigma}{\sigma_0} = \exp\left(\frac{\beta_F E^{1/2}}{k_B T}\right) \quad (\text{Mead 1962-M})^{165}$$

$$(5) \quad \frac{\sigma}{\sigma_0} = \left(\frac{k_B T}{\beta_F E^{1/2}}\right)^2 \left[\left(\frac{\beta_F E^{1/2}}{k_B T} - 1\right) \exp\left(\frac{\beta_F E^{1/2}}{k_B T}\right) + 1 \right] \quad (\text{Johnscher 1967-J})^{166}$$

$$(6) \quad \frac{\sigma}{\sigma_0} = \left(\frac{k_B T}{\beta_F E^{1/2}}\right)^2 \left[\left(\frac{\beta_F E^{1/2}}{k_B T} - 1\right) \exp\left(\frac{\beta_F E^{1/2}}{k_B T}\right) + 1 \right] + \frac{1}{2} \quad (\text{Hartke 1968-H})^{167}$$

$$(7) \quad \frac{\sigma}{\sigma_0} = \frac{1}{3} \left[2 + \cosh\left(\frac{\beta_F E^{1/2}}{2k_B T}\right) \right] \quad (\text{Adamec and Calderwood 1975-AC})^{108}$$

When (σ/σ_0) over a range of field strengths using the above equations is plotted against the measured ratio $(\sigma/\sigma_0)_{\text{meas}}$, a good fit should be a straight line with a slope of +1. Figure E.1 presents some data assembled by Adamec and Calderwood¹⁰⁸ to show how the various equations fit the data.

APPENDIX F

MAXWELL-WAGNER MODEL FOR BLOCKING ELECTRODES¹⁶⁸

The Maxwell-Wagner model for a two-layer dielectric specimen is shown below in Figure F.1. It is assumed that the conductivity of the air gaps is zero, the inherent conductivity of the solid dielectric is σ and its permittivity is ϵ .

The permittivity changes with time due to the slow polarization process in accordance with the relationship

$$\epsilon_0 \frac{d\epsilon}{dt} = \sigma_p \quad (F.1)$$

where σ_p is the effective conductivity corresponding to the operative polarization processes. The current is given by

$$I = VA \left\{ \frac{d}{[\epsilon(d_0 - d) + d]^2} \right\} (\sigma_p + \sigma) \exp \left[- \int \frac{(d_0 - d)(\sigma_p + \sigma)}{[\epsilon(d_0 - d) + d]\epsilon_0} dt \right] \quad (F.2)$$

Since ϵ changes very little with time, the following term, $\int \{(d_0 - d)\sigma_p / [\epsilon(d_0 - d) + d]\epsilon_0\} dt$ is always less than unity. Additionally, the denominator essentially acts as a constant and can be removed from under the integration sign. This gives an approximate current-time relationship

$$I = VA \left\{ \frac{d}{[\epsilon(d_0 - d) + d]^2} \right\} (\sigma_p + \sigma) \exp \left[- \frac{(d_0 - d)\sigma}{[\epsilon(d_0 - d) + d]\epsilon_0} t \right] \quad (F.3)$$

For times where $t < \tau$, where τ is given by

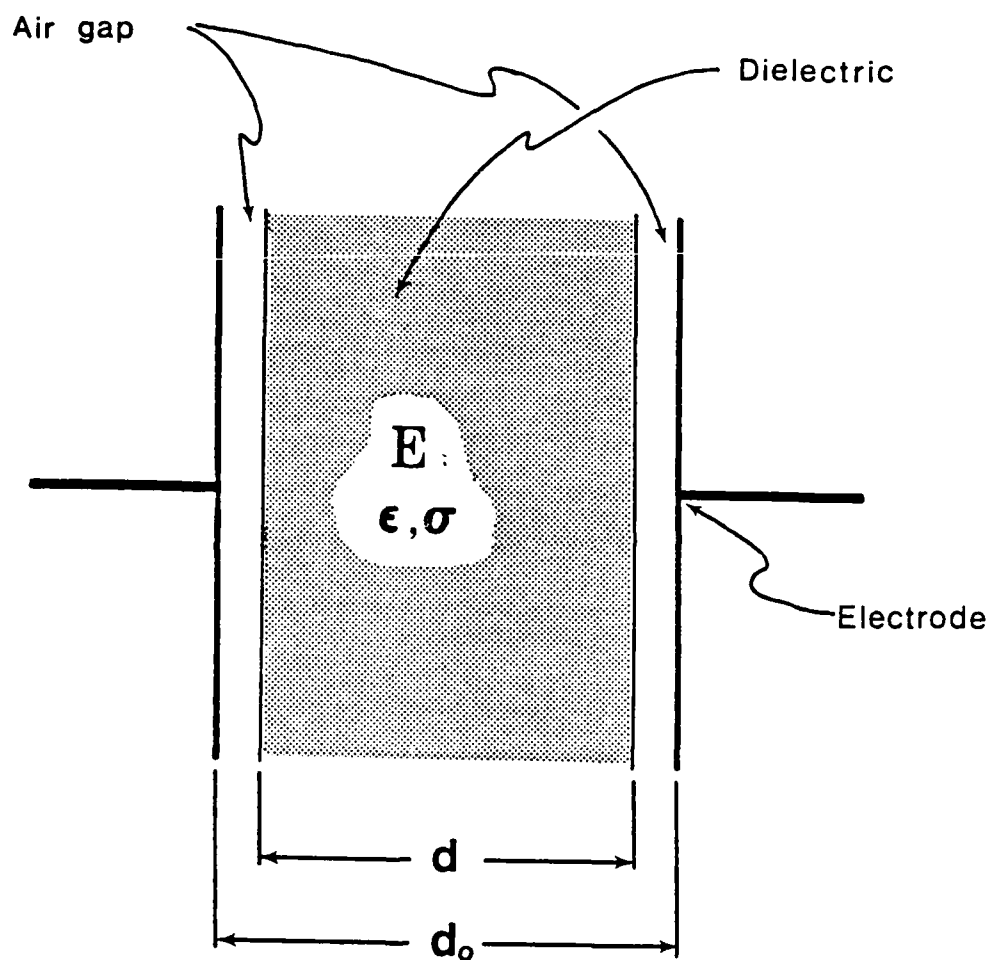


Figure F.1. Contactless Electrodes.

$$\tau = \frac{\epsilon(d_0 - d) + d}{\sigma} \frac{\epsilon_0}{\sigma} \quad (F.4)$$

the current is determined mainly by the pre-exponential term. At low temperatures, σ_p dominates while at higher temperatures σ is the more controlling factor. In the timeframe of interest, the field strength E is very nearly steady in the dielectric and it is given by

$$E = \frac{V}{\epsilon(d_0 - d) + d} \quad (F.5)$$

The time τ , when the current starts to fall off due to the rising counterfield, is determined by the conductivity σ .

When conduction occurs, the problem of free, or partially or totally hindered, charge transfer from the electrode to dielectric or from the dielectric into the electrode is encountered. For the case where there is partial or total charge transfer hindrance, some of the transported charge will accumulate at one of both electrodes.

For the case of fully blocked electrodes, the current falls to zero with time. For the case of partially blocked, i.e., semi-transparent, electrodes, the measured current falls to a lower, but definite value. the Maxwell-Wagner model is used to describe the case of totally blocking electrodes. To reiterate the details of the model, there exists a uniform layer adjacent to each electrode of zero conductivity, usually an air gap. The permittivity of the layer adjacent to the electrode is ϵ and the combined

thickness of the layer is d_e (i.e., $d_e = d_0 - d$). The value of thickness d_e is much less than the overall thickness of the dielectric with the bulk properties ϵ and σ . The effective conductivity from the measured current may be given by

$$\sigma_{\text{eff}} = \sigma \exp\left(-\frac{\sigma}{\epsilon\epsilon_0} \frac{d_e}{d} t\right) \quad (\text{F.6})$$

Thus, the initial value of effective conductivity is equal to the bulk conductivity of the dielectric. It then falls exponentially with a time constant τ given by

$$\tau = \frac{\epsilon\epsilon_0}{\sigma} \frac{d}{d_e} \quad (\text{F.7})$$

When the current flow has all but vanished after an elapsed period of time, the whole of the applied voltage appears across the blocking layers. This results in an apparent or effective permittivity of

$$\epsilon_{\text{eff}} \propto \frac{d}{d_e} \quad (\text{F.8})$$

Since--as previously stated-- $d \gg d_e$, the apparent permittivity is much larger than the real permittivity of the bulk dielectric. Experimental observations of large permittivity values may be strong evidence for electrode polarization. Polarization of this type features a decrease in field strength in the bulk of the specimen.

APPENDIX G

THE HALL EFFECT¹⁶⁹

Figure G.1 illustrates the physical process underlying the Hall effect. Suppose an electric current J_x is flowing in the solid in the x-direction, and a magnetic field B_z is applied normal to the solid in the z-direction. This subsequently leads to an additional electric field, normal to both J_x and B_z in the y-direction.

Before the magnetic field is introduced, an electric current flows in the x-direction, which means that conduction electrons drift with a velocity in the negative x-direction. When the magnetic field is introduced, the Lorentz force

$$\vec{F}_L = e(\vec{v} \times \vec{B}) \quad (G.1)$$

causes the electrons to bend downward. As a result, electrons accumulate on the lower surface, producing a net negative charge there. Simultaneously, a net positive charge appears on the upper surface because of the deficiency of electrons there. The combination of positive and negative surface charges creates a downward electric field, which is called the Hall field.

The Lorentz force producing the charge accumulation is in the negative y-direction, and it has the value

$$F_L = e v_x B \quad (G.2)$$

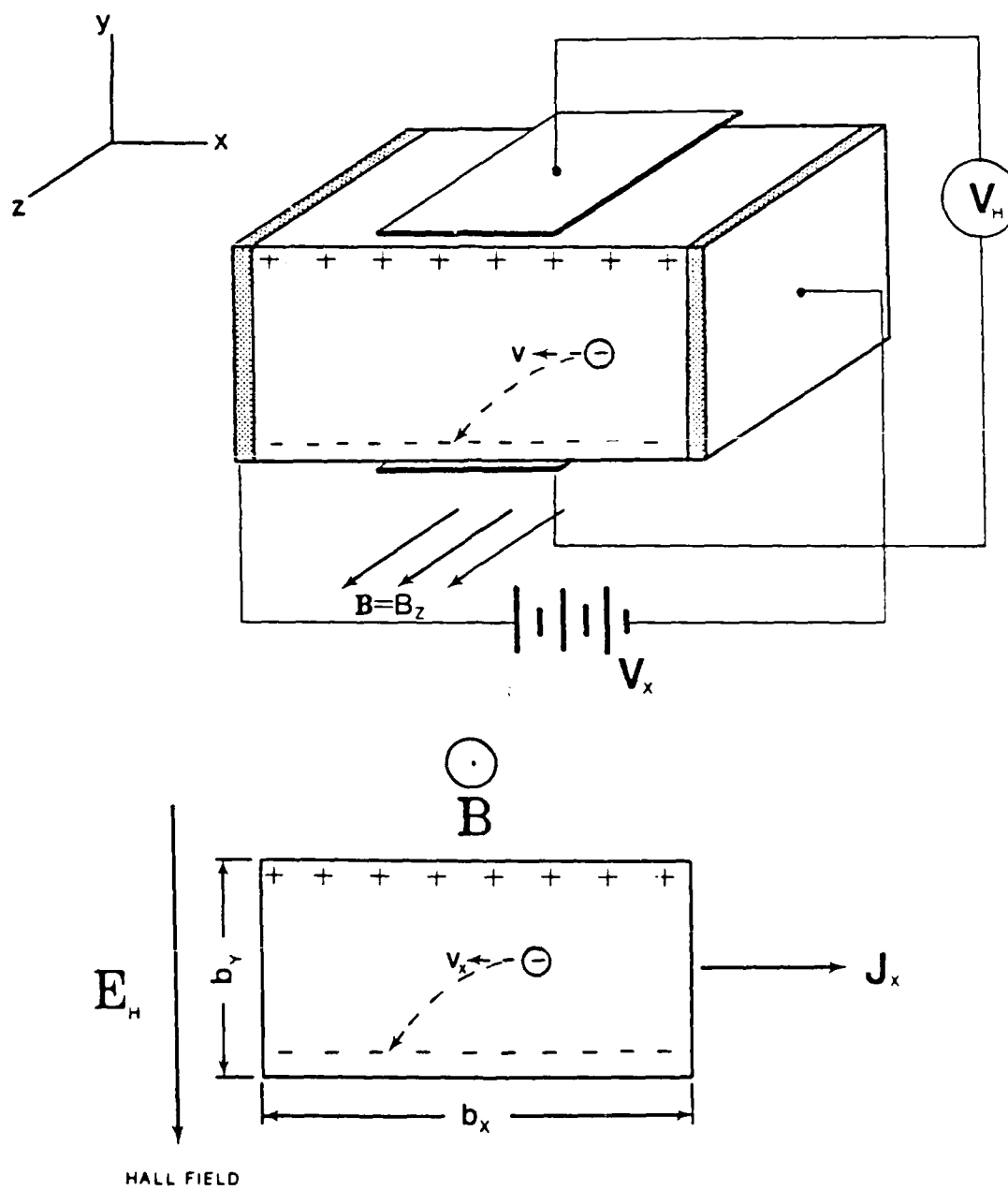


Figure G.1. Origin of Hall Field and Hall Effect.

AD-A173 498

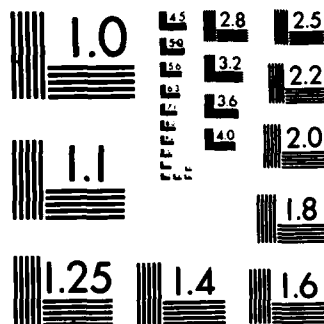
PHYSICAL TECHNIQUES FOR THE STUDY OF SORPTION DIFFUSION
ELECTRICAL PROPER (U) VIRGINIA UNIV CHARLOTTESVILLE
DEPT OF MATERIALS SCIENCE R E BARKER ET AL 26 JUL 86
UVA/525646/MS87/101 AFOSR-TR-86-0831 F/G 11/9

4/4

UNCLASSIFIED

NL





MICROCOPY RESOLUTION TEST CHART
NATIONAL BUREAU OF STANDARDS-1963-A

where the sign is adjusted so that F_L is negative in accordance with the figure (recall that V_x , being to the left is negative). The field created by the surface charges produces a force which opposes the Lorentz force. The accumulation process continues until the Hall force completely cancels the Lorentz force. Thus, in the steady state, $F_H = F_L$:

$$-e E_H = -e v_x B \quad (G.3a)$$

which becomes

$$E_H = v_x B \quad (G.3b)$$

which is the Hall field.

To see what this Hall field would be for the case of some of the polymers studied, the equation is rearranged in terms of the measurable physical parameters of the system. Thus

$$\frac{V_H}{b_y} = \mu \frac{V_x}{b_x} B \quad (G.4)$$

where E_H has been replaced by V_H/b_y and V_x has been replaced by $\mu V_x/b_x$, where μ is the mobility of the charge carrier. Rearranging the equation to get an estimate of the Hall voltage yields

$$V_H = \mu V_x \frac{b_y}{b_x} B \quad (G.5)$$

The fibers used in this research ranged from 20-500 μm in diameter (i.e., 2×10^{-5} to 5×10^{-4} m). The effective length

of the fiber in the x-direction is approximately 2.5 mm (i.e., 2.5×10^{-3} m). The mobility can be assumed to lie between 10^0 and 10^{-10} $\text{m}^2/\text{V-sec}$, depending on the type of carrier, polymer and temperature of the test. If a value of magnetic field, $B \approx 0.5 \text{ Wb/m}^2$, is used, values for V_H are shown in Table G.1 for various values of mobilities when b_y/b_x is 4×10^{-2} . The voltage V_x is limited to a value of 30 volts for the Keithley 642 electrometer.

Table G.1

Value of Hall Voltage for
Different Values of Mobility

$\mu (\text{m}^2\text{V-sec})$	$V_H (\text{volts})$
1	6×10^{-1}
10^{-2}	6×10^{-3}
10^{-4}	6×10^{-5}
10^{-6}	6×10^{-7}
10^{-8}	6×10^{-9}
10^{-10}	6×10^{-11}

By increasing voltage in the x-direction, larger values for V_H can be obtained. However, too high a voltage in the x-direction would present breakdown problems in the polymer. Likewise, by adjusting the ratio of b_y/b_x , i.e., making b_y larger than b_x , the Hall voltage also increases. Unfortunately, this latter procedure is not practical for the polymer fibers used in the research. Another factor complicating the process is the fact that the mobility μ is

not well known for a wide range of polymers, although it can be estimated. Making Hall effect measurements in this research is not practical, although the addition of this information would be extremely useful for a number of reasons. As examples, this information could be used to:

- (a) determine that the conductor is electronic and not ionic;
- (b) determine the sign and the (Hall) mobility of the majority carrier; and
- (c) determine the concentration of carriers.

DISTRIBUTION LIST

Copy No.

1 - 6	U.S. Air Force Office of Scientific Research Bolling Air Force Base Washington, D. C. 20332-6448 Attention: Dr. Donald R. Ulrich Building 410 NC
7 - 8	Dr. T. E. Helminiak AFWAL/MLBP WPAFB, Ohio 45433-6533
9	Dr. W. W. Adams AFWAL/MLBP WPAFB, Ohio 45433-6533
10	Dr. J. E. Mark Chemistry Department Polymer Research Center University of Cincinnati Cincinnati, Ohio 45221
16 - 17	E. H. Pancake Clark Hall
18 - 19	R. E. Barker, Jr., MS
20	T. C. Courntey, MS
21	SEAS Publications Files

JO#7794:rsr

UNIVERSITY OF VIRGINIA
School of Engineering and Applied Science

The University of Virginia's School of Engineering and Applied Science has an undergraduate enrollment of approximately 1,500 students with a graduate enrollment of approximately 560. There are 150 faculty members, a majority of whom conduct research in addition to teaching.

Research is a vital part of the educational program and interests parallel academic specialties. These range from the classical engineering disciplines of Chemical, Civil, Electrical, and Mechanical and Aerospace to newer, more specialized fields of Biomedical Engineering, Systems Engineering, Materials Science, Nuclear Engineering and Engineering Physics, Applied Mathematics and Computer Science. Within these disciplines there are well equipped laboratories for conducting highly specialized research. All departments offer the doctorate; Biomedical and Materials Science grant only graduate degrees. In addition, courses in the humanities are offered within the School.

The University of Virginia (which includes approximately 2,000 faculty and a total of full-time student enrollment of about 16,400), also offers professional degrees under the schools of Architecture, Law, Medicine, Nursing, Commerce, Business Administration, and Education. In addition, the College of Arts and Sciences houses departments of Mathematics, Physics, Chemistry and others relevant to the engineering research program. The School of Engineering and Applied Science is an integral part of this University community which provides opportunities for interdisciplinary work in pursuit of the basic goals of education, research, and public service.

END

12-86

DTIC